Development of New Conjugated Polymers for Application in Solar Cells

By:

Ahmed Ghaleb Al-Azzawi

A thesis submitted in partial fulfilment of the requirements for the degree
of Doctor of Philosophy

The University of Sheffield

Department of Chemistry

June 2016

Dedication

"A journey of a thousand miles begins with a single step"

Declaration

This thesis is submitted for the degree of doctorate of philosophy (PhD) at the University of Sheffield, having been submitted for no other degree. It records the research carried out at the University of Sheffield from October 2012 to October 2016. It is entirely my original work, unless where referenced.

Signed ....

Date ....

Abstract

Solar radiation can be exploited to generate electricity *via* photovoltaic devices without carbon dioxide emission or any polluting gases. Photovoltaic technology is one of the essential ways to harvest energy from sunlight streams and address global growth needs. The current technology which uses devices based on crystalline silicon dominates the solar cell market. However, it has limitations and drawbacks such as energy and financial costs. Thus, plastic solar cells are being developed by numerous researchers in order to develop their performance as an alternative technology. This new concept is particularly attractive over its inorganic counterpart due to the extraordinary advantages it could offer in the area of solar cells including: increased flexibility, high processability, light weight and potential low cost fabrication in the large scale. Furthermore, organic solar cells have high optical absorption relative to their analogues. Although considerable development has been made in this area, much work is needed to improve the performance of organic semiconductors which are still not as efficient as their inorganic semiconductor counterparts. To optimise the efficiency of this new technology concept, it is crucial to understand the limitations of its performance. Unlike inorganic solar cells, the charge carrier mobility and stability of organic solar cells are generally low which reduces their performance. As a result of these limitations, this technology is still not as competitive for use in electronic applications that require high charge mobility and stable materials. However, organic materials with superior properties and ideal morphology may push plastic solar cell technology to compete with traditional semiconductors in the commercial market for electronic applications.

In the second chapter, the preparation and investigation of the physical properties of a series of low energy bandgap alternating donor-acceptor polymers comprising 4,9-linked di-2-thienyl-2,1,3-naphthothiadiazole units and carbazole, anthracene or fluorene units with alkoxy or alkyl substituents is presented. The influence of replacing 2,1,3-benzothiadiazole (BT) with 2,1,3-naphthothiadiazole (NT) in this series of conjugated polymers is investigated, and the optical, electrochemical and photovoltaic properties of these three polymers are examined. Previous works within the Iraqi group have shown that the benzothiadiazole (BT) counterpart polymers have low solubility and molecular

weight. Replacing BT with NT moieties in the conjugated polymers resulted in materials with increased molecular weights and solubilities. It was hypothesised that this is due to twisting out of planarity of rings adjacent to the naphthothiadiazole repeat units along polymer chains. Surprisingly, the NT-based polymers still displayed lower bandgaps relative to their BT-based analogues despite of this. Photovoltaic devices with an active layer composed of thin films (65-75 nm) of polymer/PC$_{71}$BM blends spin coated from chlorobenzene or a mixture of carbon disulphide and acetone were analysed. Power conversion efficiencies (PCEs) ranging from 1.74 to 2.17%, are obtained with these NT-based polymer systems with PCDTNT-**P2** showing the best performance among this series of polymers.

In the third chapter, the preparation of materials where the thiophene-spacers used in the conjugated polymers discussed in chapter 2, were replaced with either acetylene-spacers or acetylene-thiophene linkers was undertaken. The new series of polymers was prepared through Sonogashira polymerisation conditions. Incorporation of acetylene groups on the polymer chains reduces steric hindrance between donor and acceptor moieties and increase planarity, resulting in decreased molecular weights of the resulting materials. Thus, both ethynylene-based polymers and ethynylene-thiophene based polymers showed red-shifted absorption maxima compared to their counterparts in the second chapter, owing to adoption of more planar structures. We speculate that this is a consequence of enhanced intermolecular interactions brought about by incorporation of ethynylene units in the polymer main chains.

Finally, in chapter 4, the effect of ethtynylene spacers on the bandgap of alternating polymers, comprising 4,7-linked benzothiadiazole units and 2,7-linked fluorene, 2,7-linked carbazole or 2,6-linked anthracene repeat units has been investigated. The three novel ethynylene-based polymers were prepared *via* the Sonogashira coupling reaction. The optical, electrochemical and thermal properties of the resulting polymers were compared and analysed. All polymers displayed low solubility in common organic solvents and have moderate molecular weights. Optical studies revealed that all the new ethynylene-based polymers displayed large bandgaps in excess of 2.1 eV. It is hypothesised that incorporation of acetylene units between the BT units and the other electron donor units over polymer chains leads to a poor electron delocalisation and conjugation length between donor and acceptor moieties; a result of the slight electron

accepting properties of the acetylene units. The HOMO levels of the resulting polymers are unaffected by the different donor moieties. However, varying the electron donor units can perturb the electron accepting ability of the polymers in this series and as a consequence their LUMO levels. Anthracene-based polymer (PPADEBT-**P12**) displayed the lowest LUMO level, while the fluorene-based polymer (PFDEBT-**P10**) displayed the highest LUMO level. All polymers showed good stability to thermal degradation. The amorphous nature of these polymers was confirmed with powder X-ray diffraction studies.

Acknowledgements

xi

List of Figures

List of Tables

List of Schemes

List of Equations

List of Abbreviations

A

AcOH   Acetic acid

AM 1.5   Air Mass

a.u.   Arbitrary Units

B

BHJ   Bulk Heterojunciton

BLA   Bond length alternation

br   Broad peak (NMR)

C

CB   Chlorobenzene

CV   Cyclic Voltammetry

D

d   Doublet (NMR)

dd   Double doublet (NMR)

D-A   Donor-Acceptor

DCM   Dichloromethane

DMF   N,N-Dimethylformamide

E

EDOT   Ethylene dioxide thiophene

E_g (opt)   Optical Bandgap

E_g (elec)   Electrochemical Bandgap

eV   Electron Volt

F

FF   Fill Factor

FET   Field-Effect Transistor

G

GPC   Gel Permeation Chromotography

H

HOMO   Highest Occupied Molecular Orbital

Hz   Hertz

I

ICT   Intramolecular Charge Transfer

ITO   Indium Tin Oxide

J

J_{sc} Short Circuit Current

J-V   Current-Voltage

L

LED   Light-Emitting Diode

LUMO   Lowest Unoccupied Molecular Orbital

λ_{max} Maximum Absorption Wavelength

M

m   Multiplet (NMR)

M_n Number-Average Molecular Weight

M_w Weight-Average Molecular Weight

N

NMR   Nuclear Magnetic Resonance

NBS   N-Bromosuccinimide

O

OFETs   Organic field-effect transistors

OLED   Organic light emitting diode

OLETs   Organic light-emitting transistors

OSC   Organic Solar Cell

OPV   Organic Photovoltaic

P

PA   Polyacetylene

Pd   Palladium

PPV   Poly(*para*-phenylenevinylene)

PSC   Polymer Solar Cell

PT   Poly(thiophene)

PV   Photovoltaic

$PC_{70}BM$ Phenyl-C_{70}-Butyric Acid Methyl Ester

PCE	Power Conversion Efficiency
PDI	Polydispersity Index
PEDOT:PSS	Poly(3,4-ethylenedioxythiophene):Polystyrene Sulfonate
$Pd_2(dba)_3$	Tris(dibenzylidene acetone) palladium (0)
R	
R.T	Room temperature
S	
s	Singlet (NMR)
T	
t	Triplet (NMR)
Td	Decomposition temperature
TGA	Thermogravimetric Analysis
THF	Tetrahydrofuran
TLC	Thin Layer Chromatography
TMS	Tetramethylsilane
U	
UV-vis	Ultraviolet-Visible Spectroscopy
V	
Voc	Open Circuit Voltage
X	
XRD	X-ray Diffraction

Chapter 1

1.1 Introduction

The technology of organic semiconductors has developed and progressed remarkably since the early work on polyacetylene (PA) which emerged in 1976 as the simplest conjugated polymer. The conducting ability of the polymers was discovered by Shirakawa and his talented group when they doped PA with Iodine.[1-4] This discovery opened up a new field of research on the electronic technology that is considered as the first generation semiconducting polymers.[5] The second generation of conjugated polymers was introduced as soluble and stable polymers such as poly(3-alkylthiophenes) (PT) and poly(*p*-phenelene vinylene) (PPV) due to alkyl chains and heteroatom over the polymer chains.[2,5,6] The third generation of organic semiconductors has more complex structures with more atoms in the main chains of the conjugated polymers such as donor-acceptor (D-A) alternating polymers along the main chains. These materials have emerged in the past few years as stable semiconducting materials. The main target of synthesis of D-A conjugated polymers is to attain high efficiency materials due to alternating electron deficient and electron-rich units along the backbones of conjugated polymers which will be discussed later.[5,7]

The prototype of conjugated polymers (PA) was described by Natta *et al.* in 1958 and prepared using a Ziegler-Natta catalyst before the conductivity of this type of polymer was discovered.[1,4,8] Later, it was realised that the main chains of conjugated PA might have various interesting properties, especially optical, electrical and magnetic properties.[1,9] To explain the unique optoelectronic properties and conductivity, it is necessary to demonstrate the electronic structure of the repeat units of the polymer. PA is commonly considered as a model system for describing a prototype conducting polymeric material. Compared with un-saturated molecules, σ-bonded hydrocarbon chains possess large bandgaps and are considered as insulating materials such as polyethylene which has an optical bandgap of around 8 eV.[10-12]

With respect to the conjugated polymer, it is an unsaturated molecule that consists of alternate single and double bond C-C atoms over its main chain. The main backbone of PA has three covalent σ-bonds between adjacent C atoms and H atoms due to

overlapping sp^2 hybrid orbitals in the plane geometry; these bonds hold the main structure chain of the PA together. The π-bonds in the chain of the polymer come from the unhybridized p_z orbital on each carbon or nitrogen atom, which lies perpendicular on the plane structure. The overlaps with the p_z orbital on the neighbouring atom *via* the interaction to form π-bonds result in delocalised π-electrons over the long chains.[1,13,14] In order to understand how the optoelectronic properties of the conjugated polymer in organic photovoltaic devices are modulated, molecular orbital theory (MO) is essential to explain the bond formation and delocalised electrons over the conjugated chains.[15] Generally, the conjugated polymers have σ and π-bonds over the main chains, σ-bonds are formed when two atomic orbitals overlap resulting in two molecular orbitals having different energy level. The low energy molecular orbital, is called the bonding (σ) molecular orbital, which is formed as a result of the in phase atomic orbitals overlap (constructive interference) causing an increase in electron density along the bond axis. The molecular orbital of increased energy is referred to anti-bonding (σ*) orbital due to the out of phase atomic orbitals which interfere destructively resulting in low electron density between the two nuclei[16,17] as shown in Figure 1-1.
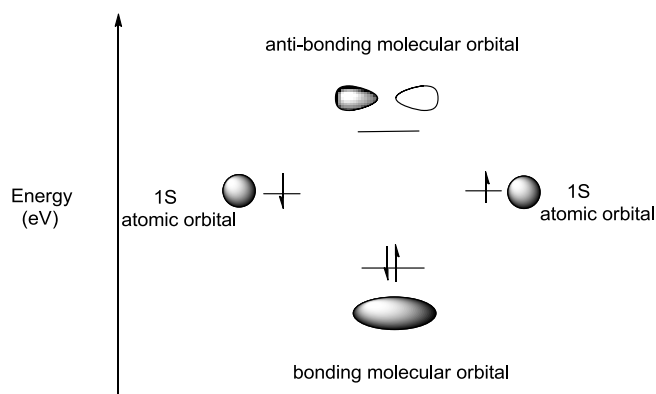
Figure 1-1: Molecular orbital energy levels diagram demonstrating the formation of σ-bonding and σ*-antibonding molecular orbitals.

In terms of energy, the difference energy, commonly known as energy gap or bandgap, is referred to the required energy which excites an electron from the bonding orbital (the valence band) to anti-bonding orbital (the conduction band). As mentioned before, the hydrocarbon molecules containing only σ-bonds are considered as insulators with relative large bandgap resulting in no electrons accommodating the anti-bonding molecular orbital, thus no charge carriers migrate through the alkyl chain structure.[16] π-

Bonds (Figure 1-2) are formed through the overlap of atomic *pz* orbitals that are parallel to each other on carbon atoms and perpendicular to the atom axis. This attraction between atomic orbitals forms a π-molecular orbital which is spread over and below the atomic orbitals with different energy levels. The molecular orbital of reduced energy is termed to as the π-bonding orbital (Highest Occupied Molecular Orbital HOMO), whilst the molecular orbital of increased energy is referred to the π*-bonding orbital (Lowest Unoccupied Molecular Orbital LUMO).[15]
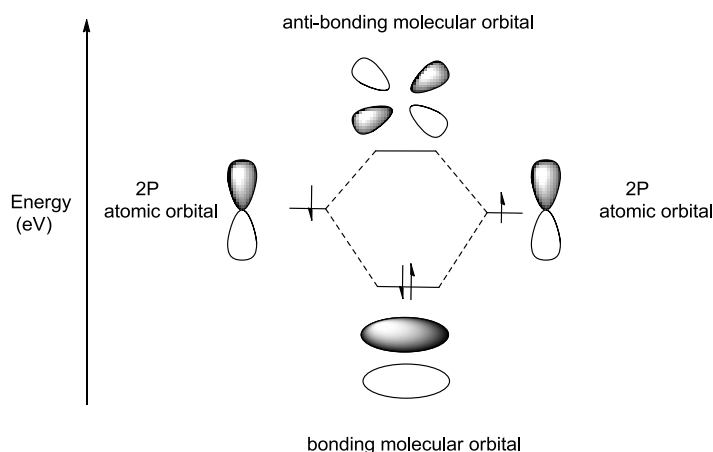
Figure 1-2: The diagram of molecular orbital showing the formation of π and π*bonding orbitals.

Combination of the differences in these energy levels along a polymer chain generates π-bands (difference HOMO vs LUMO). The resulting π-bond is shorter than σ-bond due to the effect of pulling carbon atoms closer to each other, resulting in narrow bandgap.[15] The energy bandgaps of organic molecules are the origin of intrinsic properties that characterise conjugated polymers as semiconducting materials. In addition, the HOMO-LUMO energy gap is determined by the number of sub-bands in low and high energy levels that are dependent on the number of carbon atoms in the repeat unit of the polyene.[1,13,14] The energy gap (Figure 1-3) between HOMO and LUMO are decreased as a sequence of extended conjugation in the main chain, resulting in more thermodynamically stable molecules when compared to a saturated hydrocarbon chain of the same length.[15] Overall, the bandgap of conjugated polymers containing alternating single and double bonds is smaller than the bandgap of non-conjugated materials and is in the range 1 to 4 eV.[10] The HOMO-LUMO bandgap of organic molecules determines the absorption profile, thus this bandgap illustrates a

3

relation between absorption profile and harvesting ability of the conjugated polymer in an organic device with an increasing number of repeating units in the π-system.[14,18]
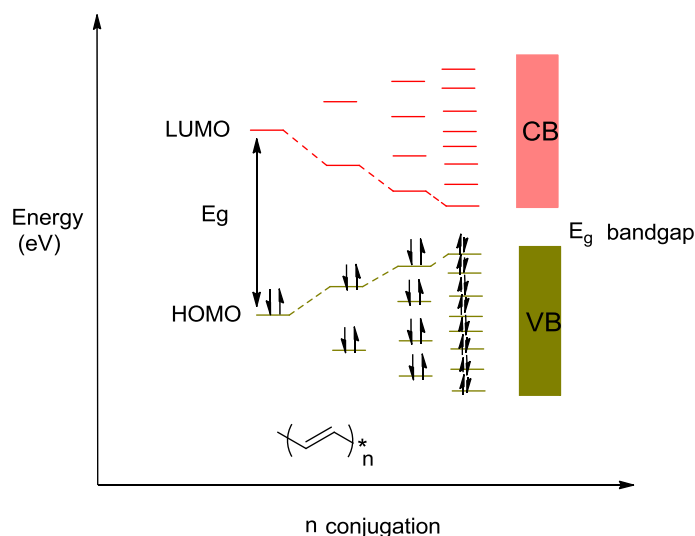
Figure 1-3: Energy diagram profile showing the effect of increasing the number conjugated π-bonds on the magnitude of the bandgap energy of a conjugated polymer.

Generally, this is not the whole picture for conducting conjugated polymers. Most of the conjugated polymers are disordered structures which are termed as amorphous materials. Weak interchain interactions of these molecules are one of the defects of the polymer chains. This weakness [19] causes energy barriers for π-electron delocalisation and reduce the chain packing.[1] In addition, disordered structures result in localisation of the electron-hole pairs which are more strongly bound by Coulomb interaction.[1,10,20] A polymer such as PA, which has a relatively enlarged π-electron system in its backbone, is an insulator (not conductive) in its native state. However, this state can be transformed into a conductive state by doping processes [1] (oxidative dopant or reductive dopant) in order to exhibit metallic and conducting properties for the polymer. This process converts the insulating neutral polymer into (cation or anion) complex that is the reduced or oxidised form of the conducting material. [1,21-23]Although PA is one of the most conducting polymers studied today, its instability in air and the tedious processability are still amongst the challenges [6] that have motivated the research community to develop other stable and easily processable polymeric materials. These materials based on aromatic structures or heterocycles having a five membered ring structure in the main chain. The molecular structures of the second generation of

4

semiconducting polymers[5,6] are depicted in Figure 1-4. For example, polythiophene and poly(phenylene vinylene) were made soluble and processable *via* attaching alkyl or alkoxy side chains.[5] Nevertheless, these species do not possess ideal bandgaps which negatively impacts on their harvesting sunlight ability.[24]

Poly paraphenylene (PPP) Poly paraphenylene vinylene (PPV) Poly (2,5 di alkoxy) paraphenylene vinylene (MEH-PPV)

Polythiophene (PT) Poly 3-alkyl thiophene (P3AT) Poly pyrrole (PPy)
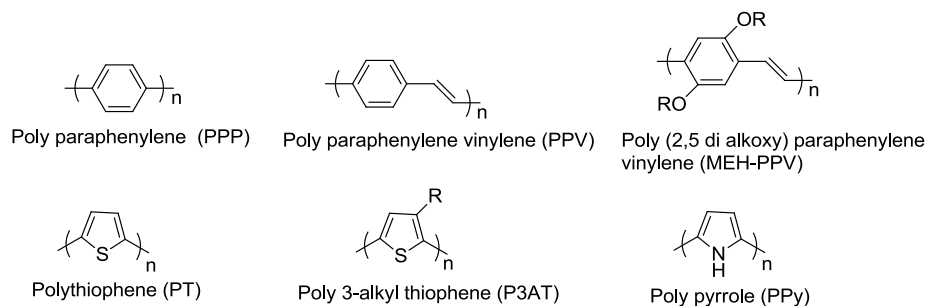
Figure 1-4: Molecular structures of some important heterocyclic polymers (second generation).

The third generation of semiconducting polymers has emerged in the past few years as a result of developments in polymer-based photovoltaic elements. These polymers have more complex molecular structures with different atoms in the repeat units with either heterocycles or benzene rings.[5] Incorporation of alternate electron donor-acceptor units over the polymeric backbone decreases the bandgap of the polymer, resulting in an enhancement of the absorption ability of the organic semiconducting material.[25] During the last few years, remarkable progress has been achieved in this field, and the efficiency of these materials in devices has exceeded 9%.[26] It is well recognized that substantial features and properties of conjugated polymers play crucial roles in the overall performance for organic photovoltaic (OPV) devices.[27] Therefore, an enormous number of conjugated polymers have been reported for application in electronic devices, leading to a wide variety of physical and mechanical properties as a consequence of the various organic syntheses of the conjugated polymers.[7,28] Alternating electron rich and deficient motifs in the main backbone of the polymer results in the tuning of its energy levels and its bandgap.[28,29] The aim of the D-A approach is to obtain a narrow bandgap and a highly ordered chain structure. Moreover, incorporation of alternate donor-acceptor motifs into the polymer chains can facilitate intermolecular interactions.[25,30,31] These interactions can enhance electron transfer in the organic cell.[29] On the other hand, the disordered structure and poor crystallinity of conjugated polymers have considerable influence on charge carrier mobility and

performance. Additionally, large bandgap organic semiconductors limit the absorbing ability of devices compared to traditional crystalline silicon devices which have an efficiency of 25 %. Consequently, the performance of organic devices is greatly limited.[32,33] Nevertheless, the organic photovoltaic devices have received great attention in both research and industrial communities as a consequences of their potential advantages such as, lightweight, affordable costs and ease of manufacture to produce plastic devices for renewable energy.[28,34] Furthermore, the chemical modification and manipulation of synthetic methods of these organic materials introduce various intrinsic and promising properties, which have caught the attention of the research community.[32,34] Despite great progress, organic solar cells have not yet reached the industrial market unlike traditional inorganic solar cells.[35]

1.2 Architecture of organic solar cells

In the history of organic material-based electronic devices, a single layer sandwiched between two electrodes was the first design used for organic solar cells. Then this single layer design has been replaced by a bilayer junction in order to improve the performance of the device. The major breakthrough and rapid development of configuration of these devices have been achieved since the bulk heterojunction (BHJ) concept was introduced. This discovery led to an efficient charge transport in conjugated polymers. Further development of BHJ design was accomplished *via* enhancement of the morphology of the active layer to secure efficient exciton (electron-hole pair) dissociation and charge mobility. Although OPVs have been rapidly improving in terms of their efficiency, there are still challenges that are not fully resolved such as further improvements in device efficiencies, low lifetimes of devices, stability and large scale production.[36]

1.2.1 Single layer device

The earliest organic solar cell (Figure 1-5) was based on a single photoconductive material sandwiched between two metals with different work function electrodes. In an organic single layer device, a photovoltaic effect can arise due to symmetry of organic device,[32,37] which results in formation of a Schottky-barrier. This barrier is formed between the p-type (hole transporter) organic component and the low work function metal as cathode (electron transporter).[32,38] Exciton dissociation occurs at the cathode

interface but excitons are not completely free and tightly bonded. Therefore, only photogenerated excitons that reach the dissociation interface can split and generate free charge carriers. Consequently, as a result of light absorption by the active layer, it is important to highlight that the free charge concentration in the photoactive layer is low. The first fabricated single layer device exhibited low efficiencies in the range of 10^{-3}-10^{-2} %,[32] this can be attributed to a loss mechanism caused by short exciton diffusion lengths in the construction, leading to recombination of the excited charge carriers.[39] However, drastic and rapid progress in single layer device efficiency was achieved (0.7%). In this case, the Schottky-barrier effect was enhanced by constructing organic layers sandwiched between a metal- metal oxide (Metal-Insulator-Semiconductor-MIS-device).[32]
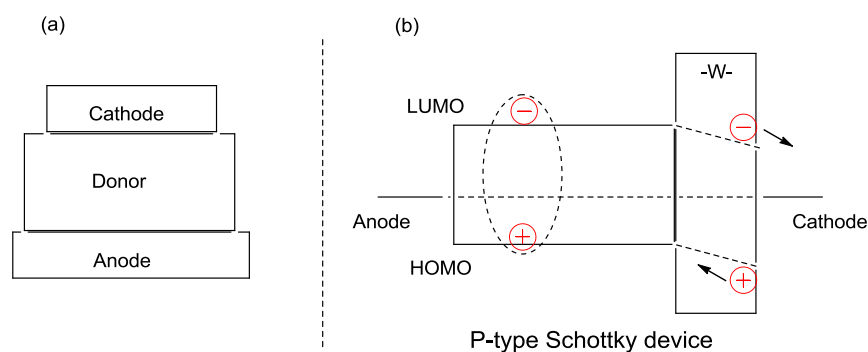
Figure 1-5: (a) Schematic of a single organic device. (b) In a *p*-type Schottcky contact at the metal cathode. Photogenerated excitons are dissociated in a thin depletion region W.

1.2.2 Bilayer device

The introduction of the bilayer concept was considered a major breakthrough in the performance of electronic devices.[32,37] This type of device was introduced by Tang *et al.* in 1986. This structural configuration proved to be the outstanding bench mark in the field of organic solar cells [40] to overcome the above-mentioned serious limitations of a single device.[41] Tang reported a two layer device containing phthalocyanine derivatives as the p-type and perylene derivatives as the n-type components sandwiched between two electrodes as schematically depicted in Figure 1-6. The p-n junction device achieved a power conversion efficiency (PCE) about 1%.[40] In this device, the p and n-type are layered together with a planar interface as phase separation is key [40,42,43]

in controlling the photovoltaic properties of the device.[37] Tang described that excitons generate and diffuse at the D/A interface where excitons are separated to free charge carriers (free hole and electron). The p-type (Donor) carried the holes to the prospective anode (indium tin oxide, ITO) while the n-type (Acceptor) carried the electrons to the respective cathode (Al).[40] A big advantage of this mode of operation and geometry was an efficient exciton dissociation across the interface, resulting in a decrease in recombination losses.[39,40,44] However, a short distance of exciton diffusion into the bilayer was observed due to the excitons' limited lifetimes. This limitation causes decay of excitons to the ground state without reaching the acceptor domain. Moreover, the exciton diffusion length restricts the thickness of the active layer to the range (10-100 nm), resulting in a loss of absorption of photons limiting the performance of the bilayer device.[29,39,45] Therefore, the interfacial area between donor and acceptor material should be as large an area as possible to guarantee better exciton dissociation, hence the invention of the BHJ concept.[37]
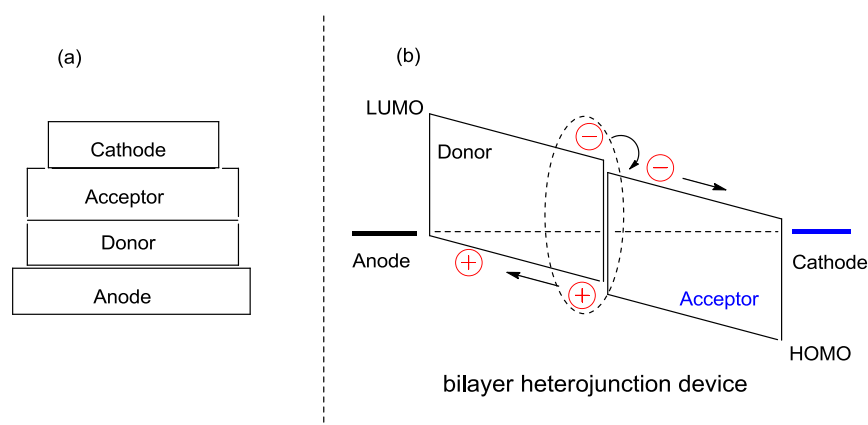
Figure 1-6: (a) Schematic of a bilayer organic structure. (b) Schematic of a phase separation of bilayer device. The donor contacts the higher work function electrode and the acceptor contacts the lower function electrode.

1.2.3 Bulk heterojunction (BHJ) device

Yu *et al.* [29] introduced the concept of the BHJ device, which was constructed by blending two organic materials (donor-conjugated polymer) and (acceptor-fullerene derivatives). Under this concept, the most common method of the formation of the active layer is to disperse the acceptor component in the conjugated polymer. The method is achieved by spin-coating a solution of both components in an organic solvent

to form an interpenetrating network known as a BHJ.[32,46,47] This approach highly distributes and maximises the donor acceptor interfacial area within the active layer ensuring efficient exciton dissociation over the whole extent of the active layer, thus maximising the number of free charge carriers. Moreover, this architecture secures the charge percolated pathways to collect free charge carriers in the donor and acceptor at respective electrodes; completing the conversion photon of energy into electrical energy.[28] A typical dimension of the heterojunction interface must be within the exciton diffusion length (10-20 nm) in order to obtain better exciton dissociation and high free charge concentration. An efficient photoinduced electron transfer in conjugated polymer:fullerene composites can be accomplished by controlling the phase separation between the components using intimate mixing of morphology. This leads to enhancement in the efficiency of exciton splitting and transport and will be discussed further below.[29,34] Concerning BHJ device energy levels, the excited electron shifts from the polymer LUMO to the fullerene LUMO reaching the cathode *via* electron paths, the hole transfers directly from the polymer HOMO to the prospective anode *via* hole paths. The potential difference between the two components at the interfacial area generates a driving force facilitating exciton splitting (bonded electron-hole pair) [48,49] as depicted in Figure 1-7.
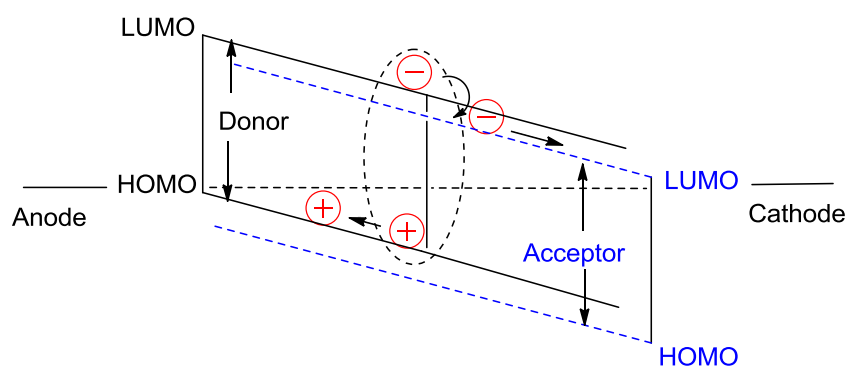
Figure 1-7: Schematic of a bulk heterojunction device. The donor component is blended with the acceptor component throughout the whole film. Consequently, photogenerated excitons can be separated into charge carriers at any place within a thin film.

The architecture of the BHJ has significantly improved the performance of the organic solar cells. However, there are substantial challenges to obtain high efficiency, mainly

because of the difficulty to dissociate the excitons (bonded electron-hole pairs) with the increased disorder of the morphology. Furthermore, inefficient physical mixing might create isolated regions within BHJ layer.[50] The random distribution of electron donating and accepting materials within the single active layer leads to poor charge mobility due to complicated charge carrier paths to the prospective electrodes,[51] resulting in decay and recombination of charge carriers.[39,51]

The layered structure in astandard BHJ device (Figure 1-8) consists of four essential layers: a conductive layer (polymer:fullerene mixture) sandwiched between two electrodes, a transparent ITO coated on a top of a glass substrate is used as anode. It is usually covered with poly(3,4-ethylenedioxythiophene) polystyrene sulfonate (PEDOT:PSS) which is applied between the photoactive layer and the anode, then a metal cathode such as Al is deposited as the top electrode on the OPV device. Both of the electrodes are connected into internal circuit to flow the photocurrent.[28,37]
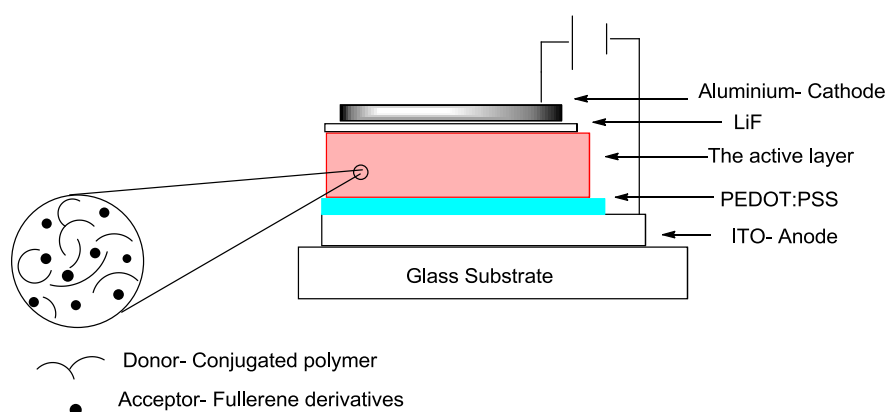
Figure 1-8: Schematic device structure of the OPV (glass/ITO/PEDOT: PSS/ active layer (polymer-fullerene bulk)/ Li/Al).

Employing the conjugated polymer:fullerene derivatives in a bilayer structure achieved highly increased photoconductivity. Recently, Seok *et al.* reported highly efficient devices using a carbazole-based polymer)/fullerene $PC_{70}BM$. The device achieved a PCE of 7.12%.[52] Regarding the BHJ device components, Buckminster fullerene C_{60} and its derivatives such as [6,6]-phenyl-C_{61}-butyric acid methyl ester $PC_{61}BM$ have been intensively used as a standard acceptor in a BHJ solar cell along with the conjugated polymer as typical donor.[29] The exciton dissociation rate of the photoinduced electron transfer takes place rapidly, facilitating the charge splitting at the

10

donor acceptor interfacial area as shown in Figure 1-9. Other fullerene derivatives such as C_{70} and its counterpart C_{71} are the new standard n-type materials within the active layer due to their solubility in organic solvents and absorption ability in the visible area.[28] There is still need to further enhance the p-type material toward an ideal donor; various conjugated polymers have been employed to fabricate the active layer for electronic applications. Using different kinds of conjugated polymers allowed the design of polymers with promising properties in devices.[29] Sprau *et al.* developed co-polymers with alternating benzodithiophene-thienothiophene and achieved a BHJ solar cell with a high performance of 9.5%, using the fullerene ($PC_{71}BM$) as acceptor into the active layer.[53]
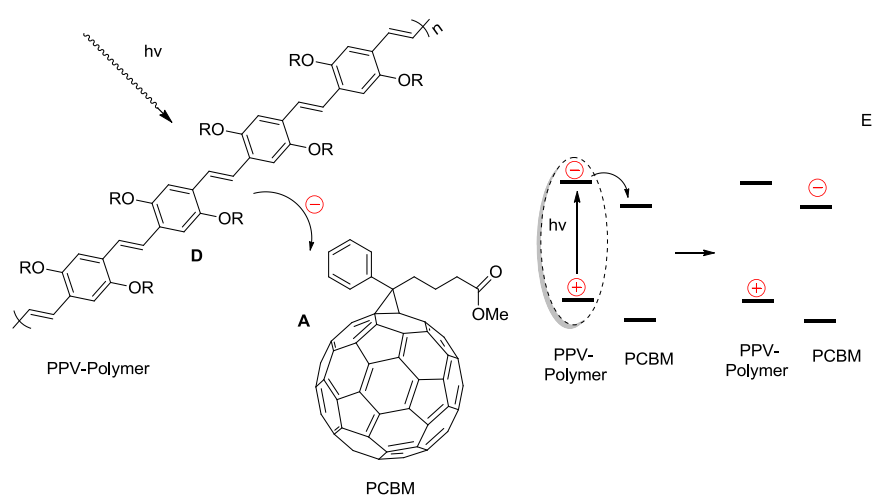
Figure 1-9: Illustration of the main process of photoinduced electron transfer from the donor (RO-PPV) to the acceptor (PCBM) as well as the energy level diagram of the working process for D-A heterojunction solar cell.

1.3   Basic operating principles of organic solar cells

Commonly, the organic photovoltaic device is not able to generate free carrier charges (holes and electrons), unlike the inorganic semiconductors such as silicon solar cells.[54] Photoexcitation process in organic photovoltaic devices (Figure 1-10) generates excitons (a coulomb-correlated electron-hole pair). Therefore, the organic semiconductors need an additional thermodynamic driving force to overcome the Coulombic attraction and split the excitons into free charges at the interfacial area.[55,56] It is well known that the organic photoconversion system consists of two different

potential semiconducting materials, that are blended together to secure the driving forces for exciton splitting as a result of different electron affinities.[57]

The operating principle of an organic photovoltaic device for completing the conversion of a photon of light into electrical energy is outlined in Figure 1-10. The main mechanism of operation of an organic device comprises several steps including: photoexcitation of the conjugated polymer (primary absorber) to generate excitons (electrostatically coupled electron-hole pairs). An electron can be excited from a low energy level to a high energy level in the donor domain of the light capturing film in order to form the exciton due to photoabsorption. The photogenerated exciton then moves to a region where exciton dissociation takes place at an interfacial area as a result of a chemical potential gradient.[58] Previous literature has shown the photogenerated excitons possess a short life time and a diffusion length (10-20 nm).[59] The formation of a charge transfer (CT) complex is preferred to take place at hetero-interface when the binding energy of the complex is less than the energy differences between the LUMO energy levels of the conjugated polymer-fullerene.[58] However, the overall mobility of electron-hole pairs is limited to a few nm owing to the very small lifetime of excitons.[60]
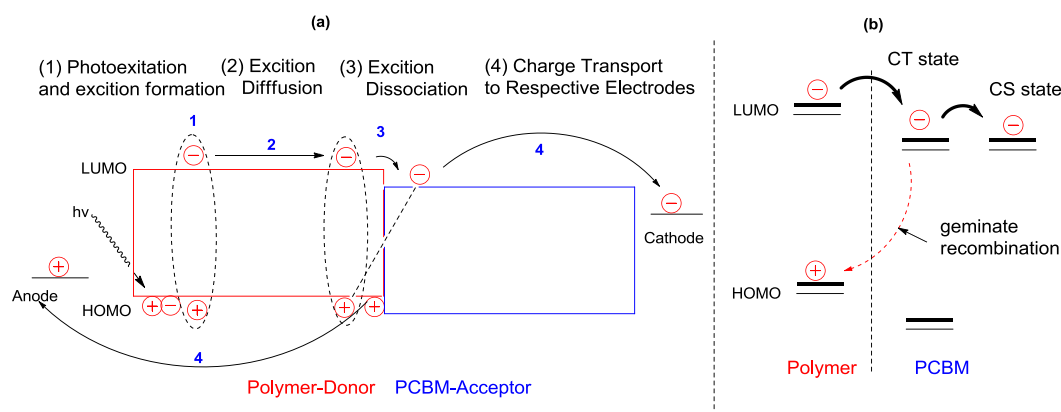
Figure 1-10: (a) Schematic diagram demonstrating the operating mechanism of donor-acceptor BHJ device. (b) Basic energy level diagram for the photovoltaic process.

The CT state energy relies on the Coulombic attraction of the exciton that formed across the donor-acceptor interface when the electron is transferred to the acceptor. The CT complex can convert to a charge separated state (CS) or free charge carriers *via* exciton dissociation.[58,61,62] Generally, the exciton dissociation is highly dependent on

12

the presence of a potential difference between p-type and n-type domains, it is desirable for the electron donor to have a high ionization potential (I_P), while the electron acceptor has strong electron affinity (E_A). This difference can generate the driving force for the dissociation of the photogenerated excitons.[60,62,63] Furthermore, exciton dissociation can be enhanced by maximising the polymer-fullerene interfacial area, resulting in maximising the number of the free charges. Optimising the morphology of the device also enhance the exciton splitting in the organic device.[28] However, the recombination of geminate pairs across a hetero-interface area is assumed to occur as an undesirable outcome in the organic photovoltaic device. This can be attributed to failing to reach the exciton at the interfacial area within its lifetime therefore it will be considered as a loss mechanism and loss in efficiency as radiative decay.[60,62,63] Once the photogenerated excitons have reached the interfacial area, they are dissociated to generate the free charge carriers as a sequence of electron transfer from the LUMO of the polymer (p-type) to the LUMO of the fullerene (n-type), whilst the holes are localised in the polymer component.[55] The transportation of free charge carriers through p and n-type components to prospective electrodes for collection is essential to allow current extraction; both electrodes are connected with an external circuit to transport the free charges after migration through the materials of the active layer.[60,62,63] It is worth mentioning that intramolecular charge transfer (ICT) over the backbone of the polymer induces the charge to migrate through the polymer area.[64] In the BHJ configuration, interpenetrated pathways are important for charge transport. The efficiency of charge transport can be considerably affected by molecular orientation, packing structure and the degree of structure ordered.[58] An internal structure and material design are the key features that determine photovoltaic performance of Polymer Solar Cell (PSC) through minimisation of energy required and charge loss mechanisms.[58,63]

1.4   Characterisation of organic solar cell

Solar cell performance can be evaluated by *J-V* curves. A typical of *J-V* characteristics for a solar cell in the dark and illumination is depicted in Figure 1-11. Commonly, Power Conversion Efficiency (PCE) represents the integrated evaluation of the performance for an electronic device.[65] This measurement is strongly dependent on key parameters including the short circuit current density (J_{sc}), open circuit voltage (V_{oc})

13

and fill factor (FF).[62,65] The *J-V* characteristics are carried out under dark and illumination conditions with standard test condition (STC) as laboratory testing. The STC is accompanied with solar spectrum intensity at 100 W/cm^2 as well as an air mass (AM 1.5) at an incident spectral angle of about 48° and constant room temperature 25 C°.[34,37,63] Importantly, the standardised measurement condition used for organic solar cells is essential to be able to compare the parameters measured for the performance of devices and unify the measurement across the world.[32,34,37,66] The graph can provide intrinsic information on how the OPV works and if the energy levels match with the organic material of the active layer. All these parameters will be helpful in the design of new materials.[66]
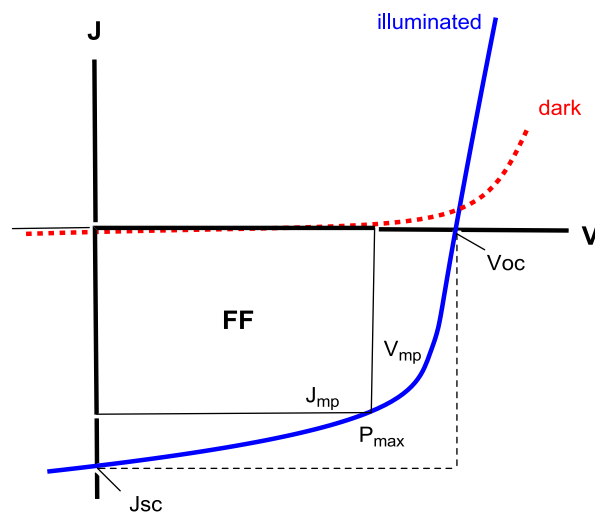
Figure 1-11: Common current density-voltage (*J-V*) curve under dark and illumination for a typical organic solar cell.

The following critical parameters are used to determine the performance of organic solar cells.

Open circuit voltage (V_{oc}): This parameter represents the maximum excluded voltage across the device when there is no current flow, it is highly dependent on the difference between the HOMO of the p-type material and the LUMO of the n-type material[58,63,65] as illustrated in equation (1).[65]

$$Voc = (1/e) \left(\mid E^{Donor} HOMO \mid - \mid E^{Acceptor} LUMO \mid - 0.3\,V \right) \quad (1)$$

Where e is the elementary charge, a minimum energy difference of roughly 0.3 eV between the LUMOs of the conjugated polymer and fullerene is required to facilitate exciton dissociation and formation of free charge carriers.[65] Theoretically, a polymer with low lying HOMO level introduces a high value of V_{oc}. Nevertheless, continuously dropping the HOMO level of polymer would inevitably increase the bandgap of the conjugated polymer, resulting in a low J_{sc} value which is attributed to diminishing the absorption ability of the donor. Furthermore, the morphology of the active layer of devices has a noticeable influence on the V_{oc} value.[28]

Short-circuit current density (J_{sc}): It is defined as the maximum current flow from a photovoltaic device when there is no applied voltage between the electrodes. [58,63,65] The J_{sc} value can be affected by different factors including the amount of the generation and collection of photogenerated charge carriers. Moreover, it is highly sensitive to the morphology of the active layer in devices, which affects exciton diffusion, dissociation efficiency and charge splitting ability.[34,58,63] Therefore, optimisation of photovoltaic devices is required through the choice of casting solvent, additives and deposition method.[32,37,67] The J_{sc} is correlated with the amount of light absorbed, hence the absorption of the active layer especially that of the conjugated polymer should overlap with the solar spectrum in the visible area; where most of the spectrum energy (almost 70%) is distributed. Ideally, the conjugated polymer should absorb over a wide spectrum and have a good harvesting ability which is achieved by designing low bandgap polymers.[28]

Fill Factor (FF): It is defined according to equation (2) as the ratio of maximum actual power output (J_{mp}, V_{mp}) of the cell to its theoretical power output depended on J_{sc} and V_{oc}. This parameter represents the squareness of the *J-V* curve. It provides a good indication of how easy or difficult the charge carriers amount to be excluded out of a photovoltaic device to the electrodes. [63,66,68] The parameter is sensitively affected by the charge mobility, the active layer thickness and morphology.[65]

$$FF = \frac{P_{max}}{J_{sc}V_{oc}} = \frac{J_{mp}V_{mp}}{J_{sc}V_{oc}} \qquad (2)$$

Understanding of FF and the fourth quadrant *J-V* curve are important to probe what is happening inside the cell and how the device works especially associated the efficiency of lifetime and mobility of charge carriers.[66]

Power conversion efficiency (PCE): It is described as the percentage associated with the ratio of maximum produced power output (P_{max}) by an organic cell to the power input (P_{in}) which is available in the incident light. This quantity measures the efficiency of OPV under standardised conditions.[37,58] Once the parameters have been identified, the PCE can be calculated using the following:

$$PCE = \frac{J_{mp}V_{mp}}{P_{in}} = \frac{FF\,J_{sc}V_{oc}}{P_{in}} \tag{3}$$

Over the past few years, the power conversion efficiency (PCE) for BHJ organic solar cells has been steadily improved.[66] Recent theoretical calculations show that it is possible to achieve a PCE for BHJ solar cells over 12%, if the optimum polymer is available within the active layer [28,29] as a result of optimisation of the nanoscale morphology of the active layer in a photovoltaic device.[69] It is required to obtain and combine all the important values such as J_{sc}, V_{oc} and FF in one conjugated polymer in order for achieving the highest possible performance.[28] Recently, interesting studies were achieved by Zang *et al.* where they synthesised and designed a novel conjugated polymer that displayed a high PCE of 9.0 %.[70] Another study by Kim *et al.* achieved a high PCE of 9.21% using a PT-ttTPD/fullerene as BHJ device.[71]

1.5 Molecular engineering of conjugated polymers

Design and synthesis of conjugated polymers toward ideal p-type materials are the most critical challenges in order to obtain the most desirable characteristics. The harvest absorption qualities of the polymer in the visible area, high charge mobility, its HOMO and LUMO positions can be considerably influenced by the make-up of the conjugated polymer. Understanding of molecular design by using various materials and different synthesis methods allows improvement of intrinsic photovoltaic properties of conjugated polymers; hence optimisation of the overall PCE of organic devices. The chemical properties and optoelectronic of the conjugated polymer are dictated by the molecular structure. Thus, tailoring of the molecular structure of the p-type material is

fundamental. Furthermore, controlling of morphology in BHJ devices is another parameter associated that contributes to film-forming properties, excitation diffusion length and charge transportation. All these factors are altered by the design of organic semiconductors. Both design and synthesis parameters are linked as depicted in Scheme 1-1.[29,72]

```
┌─────────────────────┐        ┌─────────────────────┐
│ Control of morphology│        │ Molecular structure │
└─────────────────────┘        └─────────────────────┘

control the charge                    adjust the molecular
separation and transport              energetics and absorption
charcteristics
                 ┌─────────────────────┐
                 │ Devic properties and│
                 │    performance      │
                 └─────────────────────┘
```
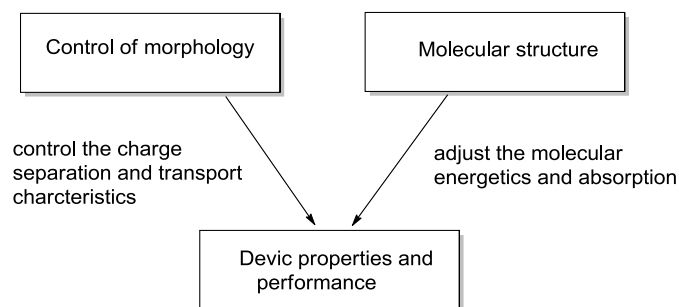
Scheme 1-1: The main factors which improve the performance of PV device.

1.5.1 Requirement of bandgap and energy levels

The magnitude of the energy gap and energy level positions of HOMO and LUMO in the conjugated system of a polymer dictate the optical and electronic properties, hence influence on the ultimate photovoltaic performance of PSC. To fully exploit the sunlight energy, the conjugated polymer in the active layer should be compatible with the incident solar spectrum. Introduction of low bandgap polymers is required for efficient harvesting of the photo flux of sunlight,[32,73] thus the amount of absorbed photons is determined by the size of the optical bandgap of the polymer.[74] Therefore, development of narrow bandgap conjugated polymers for electronic applications is highly needed to absorb the greater part of the terrestrial solar spectrum in the visible region and maximise the exciton generation.[28] Numerous chemical structures, with structural modifications and manipulations, have widely been studied in order to achieve low bandgap systems without the need of doping these materials.[29] The main motivation for the elimination of the doping process for the preparation of organic semiconductors is due to the poor solubility and infusibility of a given doped polymer for electronic applications.[75] A reduction of bandgap of conjugated polymers is obtained by either lifting the HOMO energy level, lowering its LUMO level or compressing both of them simultaneously.[29] In the case of BHJ solar cells, the polymeric material (p-type) acts as the main light absorber in the D/A blend of the

17

active layer.[28] Nevertheless, the properties of the n-type fullerene materials are still under consideration in order to increase their absorption ability and enhance their charge separation at the interfacial region upon replacing C_{60} with PCBM in the resulting active layer.[1,29,76] It has been mentioned above that V_{oc} is theoretically linked to the difference in energy between the polymer HOMO level and the fullerene LUMO level in BHJ cells. This parameter is linearly based on the magnitude of the built-in potential as a result of the differences of energy levels in polymer/fullerene active layer as shown in the energy diagram (Scheme 1-2). [29]
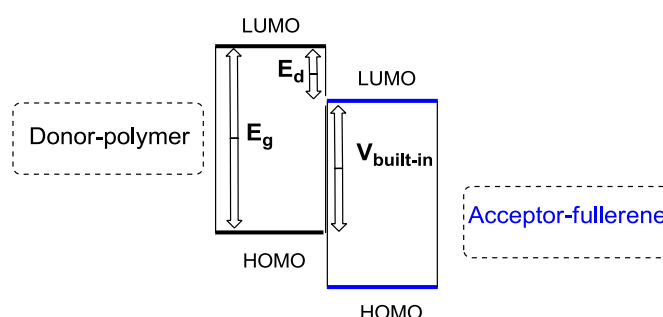
Scheme 1-2: Schematic energy-band diagram of the simple BHJ solar cells consisting of polymer/fullerene derivatives.

In terms of energy, lowering the polymer HOMO level would inevitably achieve high V_{oc} and enlarge the bandgap of the polymer, leading to decreased J_{sc} values because of diminishing of light harvesting ability of the polymer. Whilst an increase of the polymer HOMO level would lead to decreased bandgap of the polymer, resulting in a broad absorption spectrum resulting in reduced V_{oc}. Essentially the difference between the polymer LUMO and the fullerene LUMO must be ~0.3 eV in order to facilitate exciton dissociation, thus, this guarantees the downhill driving force between both of the components of the active layer.[28,77] Lowering the polymer LUMO level for constructing a narrow bandgap would significantly affect the efficiency of exciton splitting and charge transport, this eventually impedes the driving force at D/A interface. Consequently, substantial efforts are being directed to balance the trade-off between bandgap and energy levels of polymer/fullerene mixture, by manipulation the molecular structures of the polymer and using a variety of materials, in order to obtain desirable performance in devices.[77]

1.5.2   Bandgap engineering of conjugated polymer

Intensive research has concentrated on the synthesise and design of conjugated polymers for fine tuning energy levels and bandgap in order to obtain desirable photovoltaic performance for integral success of PSC. Desired properties of the conjugated polymer can be fulfilled by minimisation of bandgap and optimisation of processability. The most important parameters, which play a crucial role in the control of bandgap polymers, are: (i) resonance effect, (ii) bond length alternation (BLA), (iii) substitution/fusion effect, (iv) D–A alternation.[29,75] Apparently, the electronic applications of π-conjugated systems require a special combination of properties *via* a variety of materials. Regarding to bandgap engineering, it does not only require low potential bandgap energy as the main target, but more complex prerequisites are needed that can be under consideration. Generally, most of the skeletons of conjugated polymers are derived from aromatic and heteroaromatic units such as PP, PPV and PT respectively. These structures show two types of resonance forms: aromatic and quinoidal forms. The quinoidal structure is energetically less stable than the aromatic form and hence has a lower energy and low bandgap, resulting in its delocalisation feature destroying aromaticity and thus contributing to decreased bandgap energy ΔE, whilst the stability of aromatic structures tends to confine the π-electronic delocalisation along polymeric chain within aromatic rings due to resonance effect and hence reduce the delocalisation. It is important to understand how synthetic strategies used affect the resulting low bandgap systems.[29,78,79]

The BLA parameter presents the fundamental contribution to determine the magnitude of the energy gap of polymers such as polyene species. Additionally, inserting vinylene groups between adjacent units (Figure 1-12) over the chains of the polymer such as PT exhibits a useful strategy for reduction of the bandgap of the system due to dilution of the aromaticity.[75,78] This molecular manipulation used in the polymeric chains results in red-shifted absorption owing to an extension of π-conjugated system.[29,78]

19

Absorption max= 440   Absorption max= 490
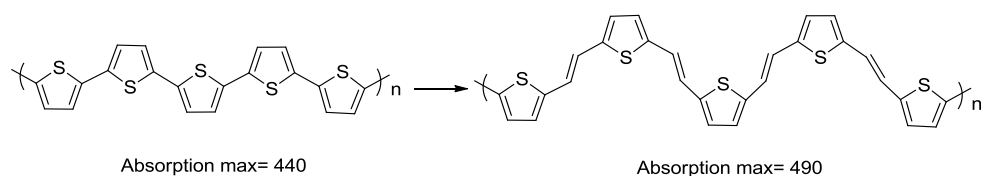
Figure 1-12: The chemical structure of PT polymers, showing the effect of adding ethylene bonds between the thiophene units in the molecular chain.

The introduction of electron-deficient or electron-rich substituent is another way for tuning the HOMO and LUMO energy levels and bandgap of a polymer. This approach (Figure 1-13) is beneficial in designing low bandgap polymers as well as to improve the internal interaction in the molecule such as ethylene dioxy thiophene (EDOT), resulting in enhanced planarity of the main structure owing to extension of the π-conjugated system and reduction of BLA.[29,75,78]

E_g=2.0 eV E_g=1.5 eV
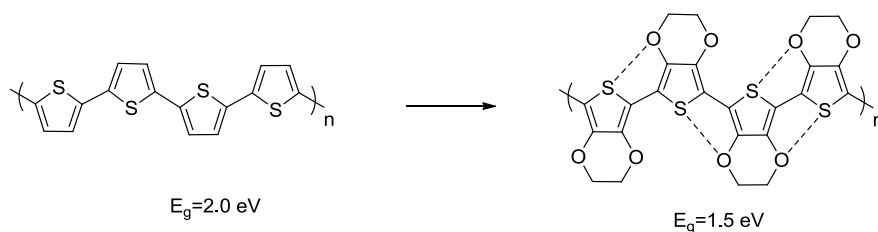
Figure 1-13: Intermolecular interactions between EDOT molecules.

Furthermore, a conjugated polymer (PT), containing electron donor and acceptor moieties as alternate repeat units (Figure 1-14) exhibits a significant low bandgap of 1.1 eV. This can be attributed to an increase of the quinoid character and rigidity of the resulting polymeric chain.[29]

E_g=1.1 eV
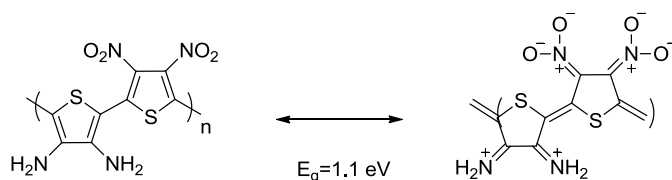
Figure 1-14: Incorporation of electron donor on the thiophene molecules exhibits quinoid structures.

The effect of extended aromatic π-conjugation using fused rings is an effective strategy to decrease the bandgap of semiconducting polymers. This method would be helpful to

increase the quinoid population over the main chain of polymers. In the case of PT, the fusion of benzene rings at the 3,4-positions of thiophene rings such as poly(benzo[c]thiophene) (Figure 1-15) introduces a low bandgap of 1.1 eV instead of 2.0 eV for PT. The decrease in bandgap arises from the consequence of direct of de-aromatisation of the thiophene ring and adoption of the quinoidal structure. [78]

E_g=2.0 eV

E_g=1.1 eV
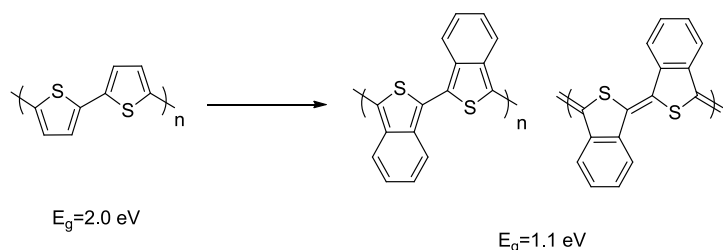
Figure 1-15: The molecular structure of incorporating fused ring in the thiophene system.

1.5.3 Donor-Acceptor alternation approach in conjugated polymer

This approach necessitates copolymerising alternating strong electron-donor monomers with electron acceptor monomers along the same π-conjugated system of polymeric chain in a so-called (D-A).[65] It became clear that alternate donor–acceptor segments contribute to push-pull driving force between adjacent units, in order to facilitate π-electron delocalisation and the formation of a quinoid mesomeric structure (D-A↔D$^+$=A$^-$) over the polymer main backbones, resulting in reduced optical bandgap.[29] Moreover, it is assumed that ICT between the donor-HOMO and acceptor-LUMO reduces the energy bandgap of the polymer, leading to significant reduction in the energy bandgap owing to improved interchain delocalisation. The decreased bandgap energy can be rationalised and explained *via* Molecular Orbital Theory (MO). The HOMOs of the donor and acceptor segments (Figure 1-16) produce two new HOMOs due to the interaction of energy levels.[29] The interaction between low energy levels leads to broadening of the valence band. Similarly, the LUMOs of donor and acceptor moieties overlap to generate two new LUMOs of D-A conjugated polymer, resulting in increasing the magnitude of the conduction band after dispersing electrons to the new hybridized molecular orbitals. These energy levels can be modulated by various combinations of donor and acceptor segments into conjugated polymer in order to tailor the polymeric characteristics for electronic application.[74,75]

21

LUMO

LUMO

E_g

HOMO

HOMO

Donor

D-A
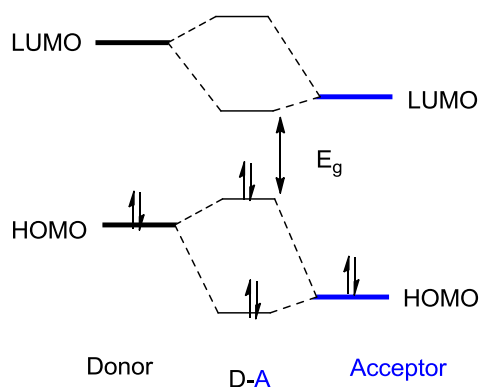
Acceptor

Figure 1-16: The energy diagram demonstrates the effect of polymerising electron-rich donor segments and electron-deficient acceptor moieties on the size of bandgap polymer

This synthetic route allows for obtaining well-engineered bandgap conjugated polymers.[75] Numerous novel low bandgap alternating D-A conjugated polymers have been reported and afford high performance of over 5% as polymer/PCBM from their BHJ solar cells. However, there are still challenges how to obtain desirable energy levels and decent bandgap conjugated polymers with various structures used in repeating units.[65]

1.5.4 Morphology of active layers in organic solar cell

Optimising the active layer morphology is one of the most essential if high performance of the polymer is to be obtained. The nanoscale morphology ensures nanometre phase separation between donor and acceptor components in the active layer that enhance the exciton diffusion, dissociation and charge transport.[32,63,80] Commonly, the ideal active layer morphology in BHJ devices should possess an interpenetrated network between polymer and PCBM with small domain size (10 nm), which is comparable the exciton diffusion length and lifetime.[63] Previous study has shown that the short lifetime of the exciton requires short distances of diffusion between (10-20 nm),[59] this would facilitate all photogenerated excitons to reach interfacial area where they could dissociate into free charge carriers.[32] Maximising of interfacial area between donor and acceptor within active layer is as pre-requisite to optimise the dissociation of photogenerated excitons, as to maintain bicontinuous phases in order to create charge pathways into donor and acceptor domains to the contact electrodes.[28,34,63] It is clear that the active layer morphology plays an important role in determining device

performance and hence has a strong impact over device performance.[37,62] The microstructure and morphology of blends of polymer and fullerenes are directly affected by the processing steps, which include different parameters such as the casting solvent used, polymer/fullerene concentration and ratio, thermal and solvent annealing approaches and additives. All these parameters manipulate and modify the active layer morphology in order to achieve better performance of device. Spin coating is widely used a method in laboratory as a solution phase deposition.[63] Solvent choice is the most critical factor for film-forming properties of the resulting morphology. A proper solvent for processing allows diffusion of the fullerene (acceptor) component into the polymer matrix and increase the roughness of the separation of phases in smaller fullerene domains.[32,37] Many studies investigated the effect of concentration and ratio contents on device performances; the researchers found that high fullerene load with good solvent for polymer/PCBM system is needed for an efficient charge carrier transport. An intimate inter-mixing of the active layer for BHJ solar cells is required for nanomorphology, allowing more diffusion and miscibility of fullerene clusters within the polymer matrix.[32] The optimal morphology of the active layer presents a balance between promoting exciton dissociation at the D/A interface and transport of free charge carriers to the electrodes.[63]

1.6   Application of conjugated polymers

The novelty of conjugated polymers as semiconducting materials is employed in a broad spectrum of applications, as they could combine excellent optical and electronic properties as well as good thermal and chemical stability. Furthermore, these materials contribute to a wide range of applications such as electroluminescent diodes, and field-effect transistors besides plastic solar cells which was discussed above.[29] All these applications have produced several products that are commercially available in global markets.[81,82] Many conjugated polymers have been intensively investigated and applied for these applications.[29]

1.6.1   Light-emitting diodes

The tremendous research efforts after discovering electroluminescence (EL) in conjugated polymers has led to wide innovations and developments in OLEDs. The potential for cheap, easy manufacturing and incorporation into devices of conjugated

polymers has attracted considerable interest for their application in light emitting devices.[83,84] It is important to report that EL products such as digital cameras and mobile phones are some of the kinds of flat display panels that are already commercialised. However, this technology still faces big challenges with regards to the upgrade of performance and solidity of OLEDs for lighting and displays. The basic principle mechanism of OLEDs is the opposite principle to that in organic solar cells (OSCs). Basically the organic emissive and conductive layers are sandwiched between a transparent anode (high-work function electrode) and cathode (low-work function electrode).[85] Injection of holes and electrons from opposite sides of the device and migration of these into the films and their recombination generates excitons (Figure 1-17), which can then decay and radiate visible light.[85,86]
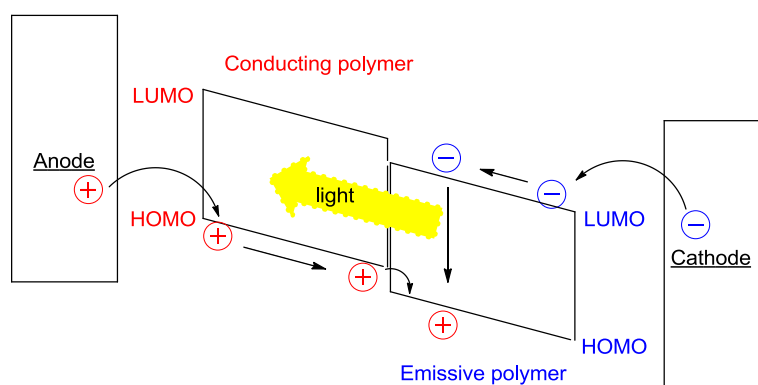
Figure 1-17: Essential parts of a PLED.

The wavelength of the light emission depends on the bandgap of the conjugated polymer used in this application, while the intensity and brightness of the emitted light is proportional to injected current in the device. This is the basic principle of the functioning of the technology.[85] It is hard to implement highly efficient OLEDs with the single emissive layer configuration, as it gives low efficiency and brightness. The performance of OLEDs can be improved by using two or more different materials that help to promote the required function of efficient light emission and create a good hole-electron junction in an organic emitter layer.[84,85]

1.6.2 Field Effect Transistors (FET)

Organic semiconductors had been used in field effect transistors in 1970. From that time, tremendous efforts were devoted in developing this type of transistors for

electronic applications.[87] Conjugated polymers display promising properties such as low cost, flexibility and high mobility which makes them good candidates for use in transistors. Hence, OFETs are preferred to amorphous silicon, which is considered as conventional crystalline silicon. Basically, an OFET is comprised of a thin film of an organic material as given in Figure 1-18. This is applied between two ohmic contacts (source and drain) as well as the third electrode (insulted gate electrode), which is used to change the conductivity of the contacts to control the amount of current flow between ohmic contacts. [88,89]
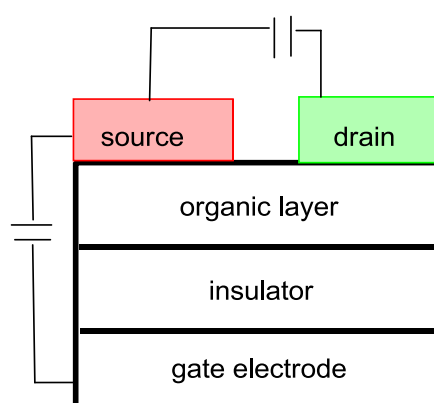
Figure 1-18: Schematic diagram of the device configuration of an OFET.

Organic semiconductors play a crucial role in determining the device performance. Therefore, high carrier mobility polymers are required in these applications. The high carrier mobility polymers have generally linear fused ring structures such as benzene and thiophene molecules, these molecules are common conjugated polymers for this application. There are many requirements of the polymers in order to be appropriate for the OFET industry, for example they should have high charge carrier mobility, good solubility and be synthetically inexpensive. OFETs are the essential part in different industrial applications such as modern circuitry, single amplifiers and electrical switches.[89]

1.7   Synthesis of alternating D-A copolymers

It is important to focus on synthetic approaches that are used to produce conjugated polymers for photovoltaic applications besides highlighting the important building

structure units that construct the necessary monomers.[29] Pd-mediated cross-coupling reactions for organo compounds have been widely used as synthetic common routes for preparing some new efficient conjugated D-A polymers. They are various metal-catalysed routes, including Stille, Suzuki, Sonogashira and Heck coupling. Most high efficient conjugated copolymers used in BHJ devices are being synthesised *via* Suzuki and Stille coupling reactions using Pd catalysts. Notably other reactions such as Sonogashira and Heck are seldom employed to prepare polymers with high efficiencies for organic solar cell applications.

1.7.1 Stille coupling reaction

The Stille coupling reaction is an efficient way that offers both high selectivity and versatility, it is tolerant reaction towards most high functionalised molecules to form C-C bonds molecule as result of coupling between halides and organostannanes. It is known that this reaction belongs to a family of palladium-catalysed cross-coupling reactions. This reaction takes place under neutral reaction conditions in the presence a palladium catalyst. However, one of the main drawbacks associated in this reaction is the high toxicity of organostannane compounds.[90,91] The suggested mechanism of this reaction is presented in Scheme 1-3. According to the proposed catalytic cycle, the oxidative addition of the aryl halide is the rate determining step of the catalytic cycle to produce a cis-palladium complex, this intermediate product is subjected to cis/trans isomerisation to produce more stable trans-intermediate product, followed by trans-metallation step which involves reaction between organo stannane reagent and Pd-complex to yield cis-complex containing new aryl. The last step is reductive elimination of the latter compound that yields the target product and regenerates the Pd-catalyst again.[92]

R¹, R² =allyl, aryl   X = Cl, Br, I   L = phosphine   R³ = methyl, butyle.
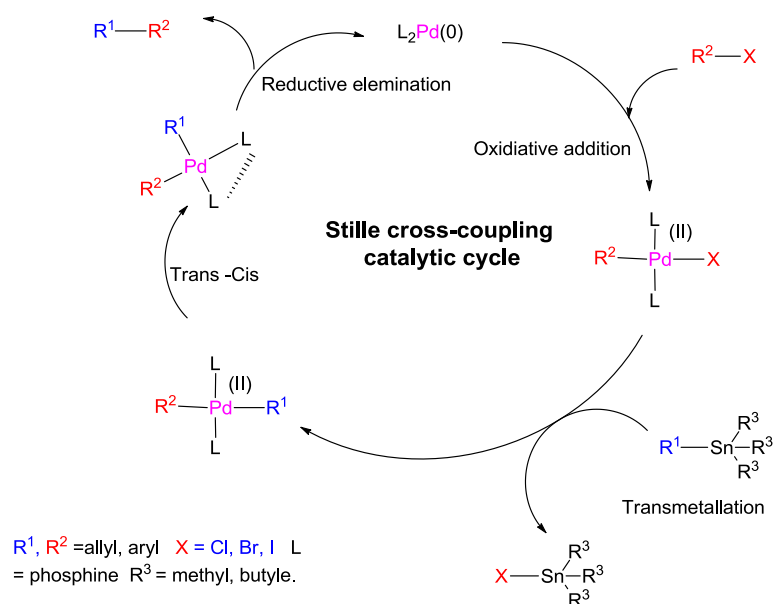
Scheme 1-3: The suggested catalytic cycle mechanism for Stille coupling reaction.

1.7.2   Suzuki coupling reaction

The Suzuki coupling process was first described in 1979 by Akira Suzuki and his group.[93] It is the palladium-catalysed cross-coupling reaction between organoboronic acids or esters and halides in the presence of a base to form C-C bond as outlined in the proposed mechanism (Scheme 1-4). In fact, the chemistry of Stille coupling is less complicated than the Suzuki reaction because this latter reaction requires a base in order to create an intermediate product between the oxidative addition stage and the transmetallation step.[91,94,95] It is clear that the base plays a crucial role for the reaction to proceed forward and form intermediates compounds through the reaction including, formation of palladium complex, activation the boronate reagent and the acceleration of the reductive elimination step.[96] However, boronic acids and their derivatives are less toxic compared to organostannane compounds. Furthermore, it is easy to remove unwanted by-products of boron compounds from the reaction mixture. Consequently, it is very common to perform this reaction on a large-scale with mild conditions.[91,95]

L$_2$Pd(II)

Activation

Reductive
elimination

R^1—R^2

L$_2$Pd(0)

1

Oxidiative
addition

R^2—X

**Suzuki cross-coupling
catalytic cycle**

R^1
R^2—Pd—L
L

Trans -cis
isomerization

R^2—Pd—R^1 **4**
(II)
L
L

Transmetallation

L (II)
2 R^2—Pd—X
L

NaO^{t}Bu

L (II)
R^2—Pd—O^{t}Bu
L

3

NaX

Y Na$^\oplus$
^{t}BuO—B—O^{t}Bu$^\ominus$
Y

R^1
B
Y   Y

NaO^{t}Bu

R^1-B—O^{t}Bu$^\ominus$
Y   Na$^\oplus$
Y

R^1, R^2 =allyl, alkenyle, aryl X =
Cl, Br, I L = phosphine Y= OR
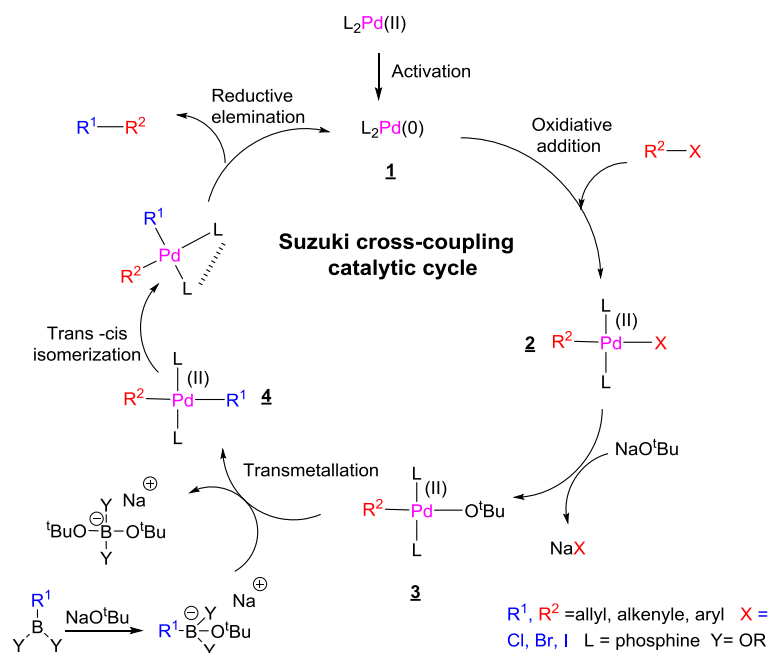
Scheme 1-4: The proposed catalytic cycle for Suzuki cross-coupling reaction.

The first step is the oxidative addition of the palladium catalyst to the halide to generate an organo palladium complex (**2**), followed by reaction with the base to produce intermediate product (**3**). During the transmetallation step of the catalytic cycle, the ligands are transferred from the activated organoborane reagent to the Pd(II)-complex formed to give the new Pd(II)-complex (**4**). Reductive elimination is the final step, in the reduction state the latter complex formed expels the desired product and the Pd(0) catalyst is regenerated.[97]

1.7.3 Sonogashira coupling reaction

Sonogashira coupling reaction is the palladium-catalysed cross-coupling reaction between a terminal sp hybridized carbon of an alkyne and an sp^2 carbon of a halide to yield a variety of synthetic and natural products and bioactive compounds.[98] The resulting products are employed in different applications such as the synthesis of oligomeric and polymeric materials. These materials are considered as functionalised components for electronic and optical applications.[99]

This reaction can be conducted easily under mild reaction conditions and treatment with base that acts as solvent in the presence of Pd/CuI as catalysts. The co-catalyst in this coupling reaction increases the reactivity of the catalytic system. There is,

however, one main complication associated with this type of cross-coupling reaction; the formation of homocoupling alkyne is an undesired product through copper as co-catalyst in the presence of oxygen. To overcome this issue, it is essential to carry out the reaction under degassed an inert conditions to avoid acetylene dimers being formed.[98] It is best to contemplate the catalytic cycle of the Sonogashira coupling reaction from the standpoint of the palladium catalyst as presented in Scheme 1-5.

The initial step is the oxidative addition of the halide to the Pd catalyst to produce a trans-intermediate (**B**); this step is the rate-limiting step of the catalytic cycle **A**. During this step the oxidation state of the palladium catalyst changes form Pd(0) to Pd(II). The second step is transmetallation step, in this step copper acetylide species (**E**), which is generated *via* copper cycle **B** in the presence of the base, reacts with the Pd(II) complex formed to yield the ethynylene-based Pd(II) complex (**C**). During transmetallation, the acetylene groups are transferred from the copper acetylide species to give the Pd(II) complex (**C**). Prior to the reductive step the trans-alkyne species is subject to trans-cis isomerisation to yield cis-intermediate (**D**). The final step is reductive elimination to obtain the desirable alkyne and Pd(0) catalyst is regenerated. Cycle **B** is less well known and under debate. It is hypothesised that the presence of base helps the formation of the copper acetylide species which is involves in transmetallation step of (Cycle **A**) with expulsion of the copper halide (**G**) to (Cycle **B**) again, followed by addition of acetylene reagent to yield π-actylene complex (**F**).[98]
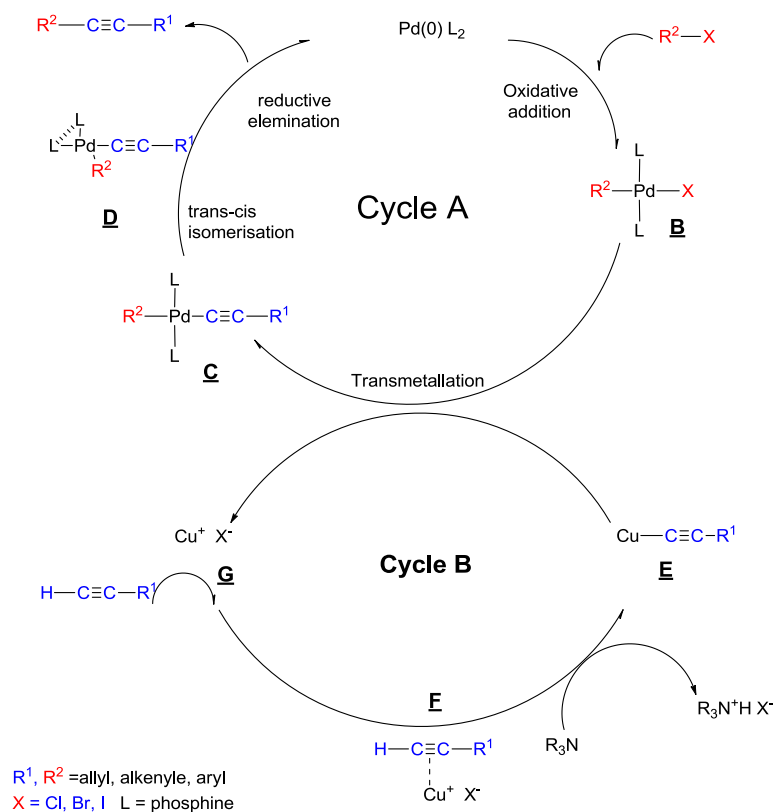
Scheme 1-5: The general mechanism suggested for Sonogashira cross-coupling reaction.

1.8 The use of fused rings as electron donor and acceptor units in conjugated polymers

The aim of using a few single aromatic units in new D-A polymers is to control the electron donating ability of these units, which has influence on the HOMO energy levels and the bandgap of the resulting conjugated polymers. Obviously, fused conjugated units such as fused three rings are employed to tune electronic properties and impact charge mobility. In addition, it is more likely to improve the intermolecular interactions of the main backbone of the polymers,[28] resulting in improved hole-mobility in polymers as a consequence of adopting more ordered structures.[100] The electron accepting units are of equal importance in controlling the energy levels and bandgaps of conjugated polymers as that of donor units. Notably, the acceptor unit plays a critical role in determining the electronic structure of the semiconducting material according to the strategy of alternating D-A polymers. Desirable narrow bandgap polymers require deep LUMO energy level below -4 eV to ensure electron

transport that is considerably influenced by the nature and structure of the acceptor unit.[25,28]

1.8.1 Fluorene as donor unit in conjugated polymers

The fluorene unit is one of the most important polycyclic aromatic hydrocarbons that has been intensively studied as an electron rich unit for electronic applications.[101] Its derivatives are commonly used to form either homopolymers (polyfluorene) or alternating copolymers. Utilisation of fluorene moieties in D-A systems enhances push-pull force in alternating polymers which demonstrated promising performance in organic photovoltaic devices. Furthermore, these species are useful due to unique features, such as high thermal, chemical stability and accessibility of synthesis and alkylation as well as favourable charge (hole) carrier mobility. The chemical structure of fluorene presents a central heterocyclic ring that would eliminate the further severe steric hindrance of benzene rings. In addition, the side alkyl chains can be attached at the 9-position of the fluorene units in the hope to obtain high molecular weight polymers which can be produced without adding any steric hindrance on polymer chains.[28,101] Wang *et al.* synthesised push-pull alternating polymers of 2,7-silafluorene –SiF-and 4,7-di(2-thienyl)-2,1,3-benzothiadiazole (Figure 1-19-a) that showed high power conversion efficiency of 5.4% when fabricated with $PC_{61}BM$ in BHJ organic photovoltaic devices. Despite possessing a moderate optical bandgap (1.82 eV) in the solid state, this polymer displayed good charge mobility in photovoltaic devices.[102] Another study developed a new push-pull polymer based on 9,9-dioctylfluorene (Figure 1-19-b), this polymer showed excellent charge mobility and a maximum PCE of 6.2% when the polymer is fabricated with $PC_{70}BM$ in photovoltaic devices.[103]
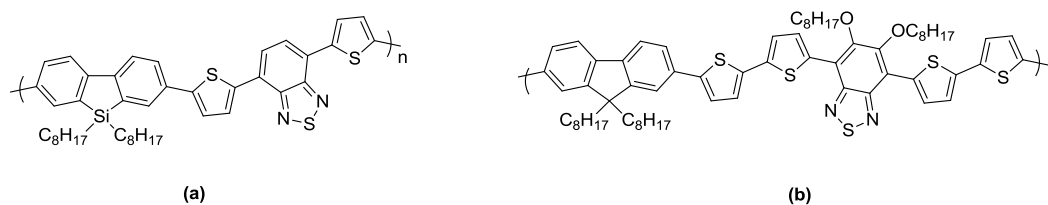
Figure 1-19: Molecular structures of: (a) P Si-FDTBT; (b) PFDT2BT-8

1.8.2 Carbazole as donor unit in conjugated polymers

The carbazole molecule is a structural counterpart to fluorene.[104] The presence of the nitrogen atom in its central fused pyrrole ring improves the donating ability of the unit skeleton, which provides carbazole with desirable properties as result of increased oxidative stability. In addition, functionalising the nitrogen atom in the 9-position can bestow desirable solubility and physical properties of polymer synthesised. Furthermore, the presence of the pyrrole fused ring results in a fully aromatic and electron rich unit.[105] Poly(2,7-carbazole) derivatives have been studied intensively, these polymers displayed high hole mobility and deep HOMO levels, resulting in promising photovoltaic performance. It is well known that an ideal polymer for solar application devices should possess narrow bandgap and tuning energy levels in order to broaden visible absorption is most important. One of the most effective approaches towards an increase of the PCE in BHJ solar cells is to design alternating D-A copolymers in which the tuning of electronic structure and low bandgap polymers can be obtained. The alternating copolymers based on 2,7-carbazoles have been reported as the donor moieties in D-A polymers for photovoltaic devices. It is believed that incorporation of the unique features of the carbazole moiety would present promising p-type material in PSC for high photovoltaic performance.[106] Recently, Chu *et al.* synthesised D-A polymer poly [*N*-heptadecanyl-2,7-carbazole-*alt*-5,5-(4,7-di-2-thienyl-2,1,3-benzothiadiazole)] (PCDTBT) (Figure 1-20). The polymer has demonstrated excellent charge mobility and oxidative stability, as well as high efficiency above 7% which was achieved when the polymer was mixed with fullerene derivatives in BHJ solar cells.[107]
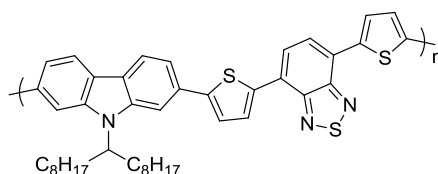
Figure 1-20: Molecular structure of PCDTBT.

1.8.3 Anthracene-based conjugated polymers for application in solar cells

The phenomenon of electroluminescence of anthracene crystals was observed in the 1960s, since then anthracene and its derivatives have been widely studied and

investigated in different applications such as OLEDs and OFETs. Great progress was achieved in the anthracene system applications due to its promising characteristics such as good electrochemical properties and excellent charge carrier transport.[35,108.109] The electronic and photovoltaic properties of D-A polymers based on anthracene are highly dependent on the nature of anthracene units and the positions through which these units are linked with electron acceptor units in D-A polymers. 9,10- and 2,6-linked anthracene units allow quinoid character and extended conjugation system. Some studies revealed that 9,10-linked anthracene in D-A polymers show low performance as a result of the twisting angle between the anthracene rings and the adjacent units, that reduces the length of electronic conjugation over the main polymer backbone. Therefore, it is speculated that incorporation of 2,6-linked anthracene based conjugated polymers would lead to good electrochemical and photovoltaic properties.[110] It is worth mentioning that proper alkyl chains attached on anthracene moieties present strong impact on the π-π stacking over the polymer chains, resulting in excellent charge mobilities and high performance of PV devices.[109] Egbe *et al.* incorporated acetylene spacers in a series of 9,10-linked anthracene polymers. This study revealed that efficiencies ranging from 0.34 to 3.14% were obtained for the resulting polymers.[111] More recently, Jung *et al.* synthesised the push-pull with 2,6-linked anthracene (PTADTDFBT) (Figure 1-21). Despite having medium-bandgaps, the resulting polymers showed a high V_{oc} value of (0.97 V) and J_{sc} higher than 12 mA/cm^2 in BHJ devices. PCE in excess of 8% has been achieved in these devices. This can be explained by the aggregation behaviour of polymer chains in blends with PCBM for the anthracene-based polymers as a sequence of strong π-π stacking, leading to a crystalline form of this polymer.[112]
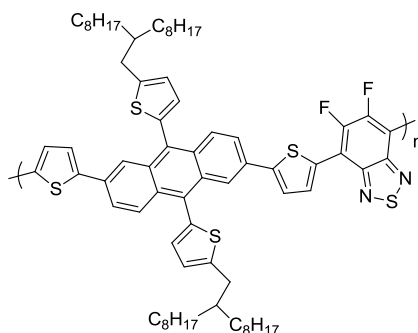
Figure 1-21: Molecular structure of PTADTDFBT.

1.8.4 Benzothiadiazole and naphthothiadiazole units in conjugated polymers

The benzothiadiazole (BT) repeat unit is considered to be one of the classical strong electron acceptor units used in D-A polymers for PV devices. The commercial availability and planarity of BT units serves as a platform to use it in constructing low bandgap D-A copolymers for electronic applications.[28,113] Therefore, these units have attracted much attention in the research community for the development of narrow bandgap polymers in order to obtain promising physical and photovoltaic performance. However, the bandgaps of BT-based conjugated polymers, which range from 1.7 to 1.9 eV, are too high to harvest a large spectral portion of sunlight for PVs applications as a result of the relatively weak electron accepting ability of the BT repeat unit compared to other acceptor units. Moreover, the rigid geometry of BT units without alkyl chains results in limited solubility and low molecular weight of the resulting polymers, resulting in negative impact on the fabrication and performance of the materials in organic electronic devices. Thus, the modification of its molecular structure to obtain stronger electron accepting properties is an attractive way to more efficient polymers for use in bulk heterojunction solar cells using fullerene derivatives as electron acceptors.[113]

There are many approaches for preparing conjugated polymers with low optical bandgap in order to expand the spectrum of their light harvesting of sunlight. One of the methods is to add a fused ring to the BT unit. This modification has been reported by some studies *via* replacing BT with a naphthothiadiazole (NT) unit in an alternating D-A backbone in conjugated polymers. The utilization of NT units into the polymer main chain would extend aromatic π-conjugation of NT. This acceptor unit possesses high electron withdrawing capability that provides deep LUMO levels and broad absorption. The incorporation of NT into the alternating conjugated polymer should lead to lower bandgap and enhance interaction packing and thus promote strong π-π stacking conformations due to more planar structure of NT units. The aim of employing strong electron-affinity (NT) is to build strong π-π stacking backbone in order to facilitate charge carrier mobility over the structure. This can lead to high performance of conjugated polymers for PV devices.[114] Kim *et al.* developed a counterparts of BT-based polymers by replacing BT with NT unit in poly(2,7-carbazole-*alt*-4,7-dithienyl-

2,1,3-benzothiadiazole) PCDTBT (Figure 1-22). The new polymer exhibited the good optical and electrochemical properties *via* low bandgap (1.71 eV), which resulted in a lift of the HOMO energy level compared to its BT polymer analogue. However, the polymer provided a low PCE of 1.31% in BHJ cells using $PC_{71}BM$ as an acceptor, this may be attributed to steric hindrance between NT and adjacent units that affected an intermolecular interaction as well as an unfavourable morphology of devices.[115]
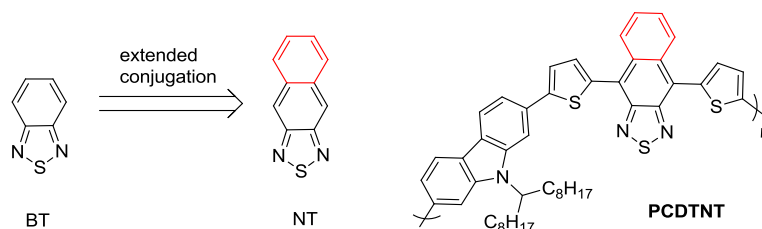
Figure 1-22: Molecular structure of BT and NT monomers as well as molecular structure of PCDTNT.

Wang *et al.* investigated the effects of incorporation NT units instead of BT units on PBTT-DTBT to yield PBDT-DTNT (Figure 1-23). NT-based polymer displayed a narrow bandgap polymer, relative to that of BT-based polymer owing to changing of both HOMO and LUMO levels simultaneously. It can be seen clearly that the NT-copolymer exhibited significantly promising performance in photovoltaic devices with a high PCE of 6% when compared with its counterpart (PBD-DTBT) which provided a PCE of 2.1%.[116]
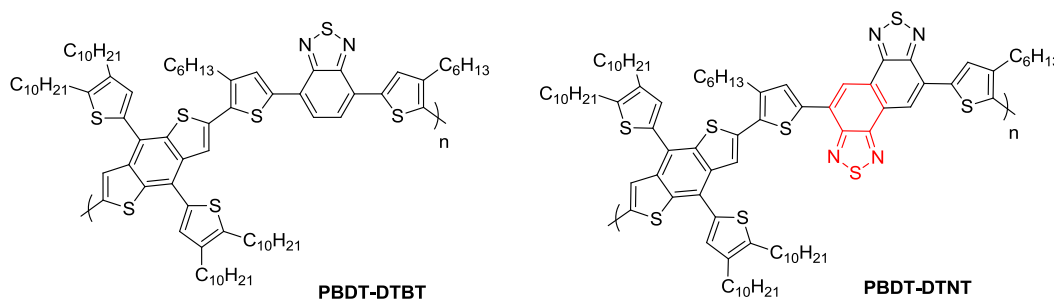
Figure 1-23: Molecular structure of PBDT-DTBT and its counterpart PBDT-DTNT.

1.9 Aims and objectives

In recent years, the growing global energy demand for clean energy resources has led to a spectacular growth in the scientific research and fabrication of solar cells. Currently the established technology uses inorganic semiconductors, such as silicon, in the manufacture of photovoltaic devices in order to produce clean energy and reduce carbon dioxide emission and the greenhouse effect. Current inorganic semiconductors are still leading on the world market of solar cells, with power conversion efficiency reaching to 24% for Si-crystalline devices. However, the manufacturing costs of traditional solar cells are still expensive. Moreover, inorganic solar cells possess low efficiency in low light intensities. To overcome these issues, early studies indicated that utilisation of organic semiconductors in photovoltaic devices could display some positive and advantageous effects. This promising alternative concept has attracted an increasing amount of attention in both industry and academic community due to its ease of processing, increased flexibility, ultralow cost and light weight relative to that of an inorganic counterpart. Additionally, organic materials such as conjugated polymers can be tailored by modifying their chemical structures, resulting in enhanced photovoltaic performance. The major breakthrough in this technology was the innovation of the donor–acceptor concept in BHJ organic photovoltaic devices. This concept has been intensively exploited using various organic materials such as conjugated polymers with different acceptors such as fullerene derivatives. It has enabled an increase in the PCE of devices up to 12%. Although organic solar cells have all these unique features, this technology is still under technological developments. One of the general issues in the design of conjugated polymers is linked to their ability to absorb a sufficient portion of the sunlight spectrum, which affects their overall efficiency in OPV devices. Synthesis of efficient light harvesting organic materials is required in order to harvest a large portion of the terrestrial solar spectrum in which 70% of the sunlight energy is disturbed. Unlike traditional semiconductors, photon energy in organic semiconductors leads to the creation of bonded hole-electron pairs that negatively impacts on the charge carrier mobilities. There are other factors that affect the performance of organic solar cells including processability, molecular weight, morphology of organic layer and the fabrication process. Ideal conjugated polymers and optimised morphological control in devices may push plastic solar cell technology to the market place within a few years.

The motivation of the work conducted within this dissertation is to develop the performance of organic photovoltaic devices, by designing and preparing new families of alternating electron donor-acceptor copolymers for application in this area. The use of naphthothiadiazole (NT) as an alternating electron deficient unit in donor-acceptor conjugated polymers has not been widely explored in the literature. The preparation of a series of NT-based copolymers was targeted in this work in order to explore their physical properties. Previous works in the Iraqi group have been conducted on analogous polymers with benzothiadiazole (BT) units as electron acceptors, yielding materials with low molecular weights and poor solubility but nevertheless with promising efficiencies in solar cells.[117-119] Hence, the NT polymers synthesised will be designed to have extended π-conjugated systems on the acceptor moieties. It is hoped that the NT-based polymers synthesised will possess high molecular weights and higher solubility than the BT-based polymers due to the fused ring on thiadiazole units. The effects of extending π-conjugation on the acceptor units (from benzothiadiazole to naphthothiadiazole) will be investigated. Moreover, the optical, electrochemical and photovoltaic properties of the resulting polymers will be studied to understand the effect of extended π-conjugated NT electron accepting moieties on the performance of the polymers.

In addition to developing NT-based donor-acceptor alternating polymers with thiophene spacers between the donor and acceptor repeat units, this project also aims at preparing a series of analogous polymers. This involves synthesising polymers containing acetylene or thiophene-acetylene spacers between the NT electron accepting units and various electron donating units, such as functionalised 2,7-linked fluorene, 2,7-linked carbazole or 2,6-linked anthracene moieties. The effects of incorporating acetylene or thiophene-acetylene spacers along the main chains of the polymers synthesised in these species will be investigated. Few studies have been conducted on acetylene-based polymers but none have reported any acetylene-based polymers containing NT as electron withdrawing moieties. Given the steric hindrance of the NT electron accepting unit, the use of adjacent acetylene spacers along polymer chains should allow the preparation with very good charge mobilities for use in the area of OPV. The donor moieties (fluorene, carbazole and anthracene) will be substituted with different solubilising chains in order to provide the resulting polymers with good solubilities and high molecular weights. Extended conjugated systems in the donor

moieties flanked by ethynylene or thiophene and ethynylene spacers over the polymer chains of these materials should result in more planar molecules and ordered packing structures. This extension of electronic delocalisation and planarity of polymer chains should lead to materials with high charge mobilities, which should enhance their power conversion efficiencies in solar cell devices. The different electron donor moieties targeted for use in these materials should provide polymers with different physical properties. It will be interesting to understand the impact the various electron donors have upon the optical, electrochemical, thermal and morphological properties of the resulting polymers. Previous investigations showed that incorporation of acetylene units in polymers provided more planar structures and less steric hindrance within repeating units.[120] It is hoped that the polymers synthesised within this project should possess favourable characteristics such as improved intermolecular interactions, resulting in high charge mobilities and a desirable property for BHJ collar cell devices. Comparison of the properties of polymers without acetylene units with those that have acetylene units should ascertain the effects of incorporating unsaturated spacers over the main chains of the polymers. The effects of incorporation acetylene as weak electron-withdrawing units instead of the electron donating thiophene units will also be investigated.

In addition to the preparation and study of NT-based polymers, a series of D-A benzothiadiazole-*alt*-fluorene, carbazole or anthracene polymers containing acetylene units as spacers over the polymer chains will be prepared and their properties compared with those of the NT-based polymers. An evaluation of the use of acetylene spacers as electron withdrawing units and BT electron accepting units in the resulting polymers will be undertaken. These polymers will be substituted with solubilising groups in order to provide the resulting polymers with a good processability. Previous work in Iraqi group has been conducted on D-A benzothiadiazole-*alt*-fluorene, carbazole or anthracene polymers but these polymers were flanked with thiophene units as spacers over the polymeric chains. A comparison of the impact of acetylene units upon solubility and molecular weights as well as optoelectronic properties of this new series of polymers will be undertaken. It is hoped that acetylene-based polymers synthesised within this part of the project possess desirable features for BHJ solar devices.

References

1.   A. J. Heeger, *Angewandte Chemie International Edition*, 2001, **40**, 2591-2611.

2.   D. Bloor and B. Movaghar, *Solid-State and Electron Devices, IEE Proceedings I*, 1983, **130**, 225-232.

3.   C. Chiang, S. Gau, C. Fincher Jr, Y. Park, A. MacDiarmid and A. Heeger, *Applied Physics Letters*, 1978, **33**, 18-20.

4.   G. Wegner, *Angewandte Chemie International Edition in English*, 1981, **20**, 361-381.

5.   A. J. Heeger, *Chemical Society Reviews*, 2010, **39**, 2354-2371.

6.   K. Gurunathan, A. V. Murugan, R. Marimuthu, U. Mulik and D. Amalnerkar, *Materials Chemistry and Physics*, 1999, **61**, 173-191.

7.   A. Pron and P. Rannou, *Progress in Polymer Science*, 2002, **27**, 135-190.

8.   T. Ito, H. Shirakawa and S. Ikeda, *Journal of Polymer Science: Polymer Chemistry Edition*, 1974, **12**, 11-20.

9.   A. G. MacDiarmid, *Angewandte Chemie International Edition*, 2001, **40**, 2581-2590.

10.   W. R. Salaneck, R. H. Friend and J. L. Brédas, *Physics Reports*, 1999, **319**, 231-251.

11.   C. Nicolini, *Nanobiotechnology and Nanobiosciences*, Pan Stanford Publishing, 2009.

12.   W. Salaneck, N. Sato, R. Lazzaroni and M. Lögdlund, *Vacuum*, 1990, **41**, 1648-1650.

13.   P. Chandrasekhar, *Conducting Polymers, Fundamentals and Applications: a practical approach*, Springer Science & Business Media, 2013.

14.   H. Shirakawa, *Angewandte Chemie International Edition*, 2001, **40**, 2574-2580.

15.   J. Cremer, P. Bäuerle, M. M. Wienk and R. A. Janssen, *Chemistry of Materials*, 2006, **18**, 5832-5834.

16.   A. Bar-Lev, *Semiconductors and Electronic Devices*, Prentice-Hall, Inc., 1993.

17.   J. A. Pople and M. Gordon, *Journal of the American Chemical Society*, 1967, **89**, 4253-4261.

18.   D. Dang, W. Chen, R. Yang, W. Zhu, W. Mammo and E. Wang, *Chemical Communications*, 2013, **49**, 9335-9337.

19.   B. J. Schwartz, *Annual Review of Physical Chemistry*, 2003, **54**, 141-172.

20.   J. Halls, J. Cornil, D. Dos Santos, R. Silbey, D.-H. Hwang, A. Holmes, J.-L. Brédas and R. Friend, *Physical Review B*, 1999, **60**, 5721.

21.   a) P. Homyak, Y. Liu, F. Liu, T. P. Russel and E. B. Coughlin, *Macromolecules* **2015**, *48*, 6978-6986; b) E. Zhou, K. Hashimoto and K. Tajima, *Polymer* **2013**, *54*, 6501-6509.

22.   J. Tsukamoto and A. Takahashi, *Synthetic Metals*, 1991, **41**, 7-12.

23.   M. Andersson, K. Väkiparta, M. Reghu, Y. Cao and D. Moses, *Physical Review B*, 1993, **47**, 9238.

24.   D. Mühlbacher, M. Scharber, M. Morana, Z. Zhu, D. Waller, R. Gaudiana and C. Brabec, *Advanced Materials*, 2006, **18**, 2884-2889.

25.   I. Osaka, *Polymer Journal*, 2015, **47**, 18-25.

26.   T. Xu and L. Yu, *Materials Today*, 2014, **17**, 11-15.

27.   J. Kim, M. H. Yun, G.-H. Kim, J. Lee, S. M. Lee, S.-J. Ko, Y. Kim, G. K. Dutta, M. Moon and S. Y. Park, *ACS Applied Materials & Interfaces*, 2014, **6**, 7523-7534.

28.   H. Zhou, L. Yang and W. You, *Macromolecules*, 2012, **45**, 607-632.

29.   Y.-J. Cheng, S.-H. Yang and C.-S. Hsu, *Chemical Reviews*, 2009, **109**, 5868-5923.

30.   P. Homyak, Y. Liu, F. Liu, T. P. Russel and E. B. Coughlin, *Macromolecules*, 2015, **48**, 6978-6986.

31.   E. Zhou, K. Hashimoto and K. Tajima, *Polymer*, 2013, **54**, 6501-6509.

32.   H. Hoppe and N. S. Sariciftci, *Journal of Materials Research*, 2004, **19**, 1924-1945.

33.   T.-C. Lin, T. Subramani, H.-J. Syu, C.-C. Hsueh, C.-T. Liu, K. Uma and C.-F. Lin, Photovoltaic Specialists Conference (PVSC), 2013 IEEE 39th, 2013.

34.   S. Günes, H. Neugebauer and N. S. Sariciftci, *Chemical Reviews*, 2007, **107**, 1324-1338.

35.   H. Spanggaard and F. C. Krebs, *Solar Energy Materials and Solar Cells*, 2004, **83**, 125-146.

36.   F. C. Krebs, *Polymeric Solar Cells: Materials, Design, Manufacture*, DEStech Publications, Inc, 2010.

37.   T. L. Benanti and D. Venkataraman, *Photosynthesis Research*, 2006, **87**, 73-81.

38.   G. Rikken, D. Braun, E. Staring and R. Demandt, *Applied Physics Letters*, 1994, **65**, 219-221.

39.   M. A. Uddin, H. Chan and B. Rahman, *Reviews on Advanced Materials Science*, 2010, **26**, 58-66.

40.   C. W. Tang, *Applied Physics Letters*, 1986, **48**, 183-185.

41.   M. Uddin, H. Chan and B. Rahman, *Reviews on Advanced Materials Science*, 2010, **26**, 58-66.

42.   P. Peumans, A. Yakimov and S. R. Forrest, *Journal of Applied Physics*, 2003, **93**, 3693-3723.

43.   H. Gommans, D. Cheyns, T. Aernouts, C. Girotto, J. Poortmans and P. Heremans, *Advanced Functional Materials*, 2007, **17**, 2653-2658.

44.   L. A. Pettersson, L. S. Roman and O. Inganäs, *Journal of Applied Physics*, 1999, **86**, 487.

45.   S. R. Forrest, *MRS bulletin*, 2005, **30**, 28-32.

46.   G. Yu, J. Gao, J. C. Hummelen, F. Wudl and A. J. Heeger, *Science-AAAS-Weekly Paper Edition*, 1995, **270**, 1789-1790.

47.   Y. M. Yang, W. Chen, L. Dou, W.-H. Chang, H.-S. Duan, B. Bob, G. Li and Y. Yang, *Nature Photonics*, 2015.

48.   J. Bisquert and G. Garcia-Belmonte, *Journal of Physical Chemistry Letters*, 2011, **2**, 1950-1964.

49.   G. Garcia-Belmonte, A. Munar, E. M. Barea, J. Bisquert, I. Ugarte and R. Pacios, *Organic Electronics*, 2008, **9**, 847-851.

50.   J. K. van Duren, X. Yang, J. Loos, C. W. Bulle-Lieuwma, A. B. Sieval, J. C. Hummelen and R. A. Janssen, *Advanced Functional Materials*, 2004, **14**, 425-434.

51.   K. M. Coakley and M. D. McGehee, *Chemistry of Materials*, 2004, **16**, 4533-4542.

52.   J. Seok, T. J. Shin, S. Park, C. Cho, J.-Y. Lee, D. Y. Ryu, M. H. Kim and K. Kim, *Scientific Reports*, 2015, **5**.

53.   C. Sprau, F. Buss, M. Wagner, D. Landerer, M. Koppitz, A. Schulz, D. Bahro, W. Schabel, P. Scharfer and A. Colsmann, *Energy & Environmental Science*, 2015, **8**, 2744-2752.

54.   B. A. Gregg, *Journal of Physical Chemistry B*, 2003, **107**, 4688-4698.

55.   T. M. Clarke and J. R. Durrant, *Chemical Reviews*, 2010, **110**, 6736-6767.

56.   A. A. Bakulin, A. Rao, V. G. Pavelyev, P. H. van Loosdrecht, M. S. Pshenichnikov, D. Niedzialek, J. Cornil, D. Beljonne and R. H. Friend, *Science*, 2012, **335**, 1340-1344.

57.   H. Kim, C. Gilmore, A. Pique, J. Horwitz, H. Mattoussi, H. Murata, Z. Kafafi and D. Chrisey, *Journal of Applied Physics*, 1999, **86**, 6451-6461.

58.   A. M. Haruk and J. M. Mativetsky, *International Journal of Molecular Sciences*, 2015, **16**, 13381-13406.

59.   H. Hoppe and N. S. Sariciftci, *Journal of Materials Chemistry*, 2006, **16**, 45-61.

60.   K. Vivek and G. Agrawal, *Hypothesis*, 2014, **17**, 18.

61.   C. L. Chochos and S. A. Choulis, *Progress in Polymer Science*, 2011, **36**, 1326-1414.

62.   W. Chen, M. P. Nikiforov and S. B. Darling, *Energy & Environmental Science*, 2012, **5**, 8045-8074.

63.   K. A. Mazzio and C. K. Luscombe, *Chemical Society Reviews*, 2015, **44**, 78-90.

64.   D. Hertel, H. Bässler, U. Scherf and H. Hörhold, *Journal of chemical physics*, 1999, **110**, 9214-9222.

65.   L. Bian, E. Zhu, J. Tang, W. Tang and F. Zhang, *Progress in Polymer Science*, 2012, **37**, 1292-1331.

66.   B. Qi and J. Wang, *Physical Chemistry Chemical Physics*, 2013, **15**, 8972-8982.

67.   N. Zhou, H. Lin, S. J. Lou, X. Yu, P. Guo, E. F. Manley, S. Loser, P. Hartnett, H. Huang and M. R. Wasielewski, *Advanced Energy Materials*, 2014, **4**.

68.   D. Gupta, S. Mukhopadhyay and K. Narayan, *Solar Energy Materials and Solar Cells*, 2010, **94**, 1309-1313.

69.   A. Armin, M. Velusamy, P. Wolfer, Y. Zhang, P. L. Burn, P. Meredith and A. Pivrikas, *Acs Photonics*, 2014, **1**, 173-181.

70.   S. Zhang, L. Ye, W. Zhao, D. Liu, H. Yao and J. Hou, *Macromolecules*, 2014, **47**, 4653-4659.

71.   J.-H. Kim, J. B. Park, I. H. Jung, A. C. Grimsdale, S. C. Yoon, H. Yang and D.-H. Hwang, *Energy & Environmental Science*, 2015, **8**, 2352-2356.

72.   Y. Li, B. Xu, H. Li, W. Cheng, L. Xue, F. Chen, H. Lu and W. Tian, *Journal of Physical Chemistry C*, 2011, **115**, 2386-2397.

73.   R. Kroon, M. Lenes, J. C. Hummelen, P. W. Blom and B. De Boer, *Polymer Reviews*, 2008, **48**, 531-582.

74.   C.-Y. Chao, C.-H. Chao, L.-P. Chen, Y.-C. Hung, S.-T. Lin, W.-F. Su and C.-F. Lin, *Journal of Materials Chemistry*, 2012, **22**, 7331-7341.

75.   A. Bakhshi, A. Kaur and V. Arora, *Indian Journal of Chemistry-Part A Inorganic Physical Theoretical and Analytical*, 2012, **51**, 57.

76.   L.-M. Chen, Z. Xu, Z. Hong and Y. Yang, *Journal of Materials Chemistry*, 2010, **20**, 2575-2598.

77.   M. Scharber and N. Sariciftci, *Progress in Polymer Science*, 2013, **38**, 1929-1940.

78.   J. Roncali, *Macromolecular Rapid Communications*, 2007, **28**, 1761-1775.

79.   T. Tadesse, 2015.

80.   C. J. Brabec, S. Gowrisanker, J. J. Halls, D. Laird, S. Jia and S. P. Williams, *Advanced Materials*, 2010, **22**, 3839-3856.

81.   V. Saxena and B. Malhotra, *Current Applied Physics*, 2003, **3**, 293-305.

82.   R. Friend, R. Gymer, A. Holmes, J. Burroughes, R. Marks, C. Taliani, D. Bradley, D. Dos Santos, J. Bredas and M. Lögdlund, *Nature*, 1999, **397**, 121-128.

83.   J.-H. Jou, S. Kumar, A. Agrawal, T.-H. Li and S. Sahoo, *J. Mater. Chem. C*, 2015, **3**, 2974-3002.

84.   A. P. Kulkarni, C. J. Tonzola, A. Babel and S. A. Jenekhe, *Chemistry of Materials*, 2004, **16**, 4556-4573.

85.   B. Geffroy, P. Le Roy and C. Prat, *Polymer International*, 2006, **55**, 572-582.

86.   S. Kappaun, C. Slugovc and E. J. List, *International Journal of Molecular Sciences*, 2008, **9**, 1527-1547.

87.   G. Horowitz, *Advanced Materials*, 1998, **10**, 365-377.

88.   C.-a. Di, G. Yu, Y. Liu and D. Zhu, *Journal of Physical Chemistry B*, 2007, **111**, 14083-14096.

89.   J. C. Perkinson, in *Book Organic Field-Effect Transistors*, ed., ed. by Editor, City, **2007**.

90.   C. C. Johansson Seechurn, M. O. Kitching, T. J. Colacot and V. Snieckus, *Angewandte Chemie International Edition*, 2012, **51**, 5062-5085.

91.   N. Miyaura and A. Suzuki, *Chemical Reviews*, 1995, **95**, 2457-2483.

92.   P. Espinet and A. M. Echavarren, *Angewandte Chemie International Edition*, 2004, **43**, 4704-4734.

93.   N. Miyaura, K. Yamada and A. Suzuki, *Tetrahedron Letters*, 1979, **20**, 3437-3440.

94.   S. S. Gujral, S. Khatri, P. Riyal and V. Gahlot, *Indo Global J. Pharm. Sci*, 2012, **2**, 351-367.

95.   S. Kotha, K. Lahiri and D. Kashinath, *Tetrahedron*, 2002, **58**, 9633-9695.

96.   C. Amatore, A. Jutand and G. Le Duc, *Chemistry–A European Journal*, 2011, **17**, 2492-2503.

97.   K. Matos and J. A. Soderquist, *Journal of Organic Chemistry*, 1998, **63**, 461-470.

98.   R. Chinchilla and C. Nájera, *Chemical Reviews*, 2007, **107**, 874-922.

99.   T. Fukuyama, M. Shinmen, S. Nishitani, M. Sato and I. Ryu, *Organic letters*, 2002, **4**, 1691-1694.

100. M. Muthukumar, C. Ober and E. Thomas, *Science*, 1997, **277**, 1225-1232.

101. J. Wallace and S. Chen, in *Polyfluorenes*, Springer, 2008, pp. 145-186.

102. E. Wang, L. Wang, L. Lan, C. Luo, W. Zhuang, J. Peng and Y. Cao, *Applied Physics Letters*, 2008, **92**, 33307-33307.

103. D. C. Watters, H. Yi, A. J. Pearson, J. Kingsley, A. Iraqi and D. Lidzey, *Macromolecular Rapid Communications*, 2013, **34**, 1157-1162.

104. E. Zhu, F. Zhang, J. Hai, L. Bian and W. Tang, *Towards High-Efficiency Organic Solar Cells: Polymers and Devices Development*, INTECH Open Access Publisher, 2011.

105. C. Brabec, U. Scherf and V. Dyakonov, *Organic Photovoltaics: Materials, Device Physics, and Manufacturing Technologies*, John Wiley & Sons, 2011.

106. Z.-G. Zhang, Y.-L. Liu, Y. Yang, K. Hou, B. Peng, G. Zhao, M. Zhang, X. Guo, E.-T. Kang and Y. Li, *Macromolecules*, 2010, **43**, 9376-9383.

107. T.-Y. Chu, S. Alem, S.-W. Tsang, S.-C. Tse, S. Wakim, J. Lu, G. Dennler, D. Waller, R. Gaudiana and Y. Tao, *Applied Physics Letters*, 2011, **98**, 253301.

108. W. Cui, Y. Wu, H. Tian, Y. Geng and F. Wang, *Chemical Communications*, 2008, 1017-1019.

109. Ö. Usluer, S. Boudiba, D. A. Egbe, L. Hirsch and M. Abbas, *RSC Advances*, 2015, **5**, 50668-50672.

110. J. Xu, Y. Fang, P. Ren, H. Zhang, E. Guo and W. Yang, *Macromolecular Rapid Communications*, 2008, **29**, 1415-1420.

111. D. A. Egbe, S. Turk, S. Rathgeber, F. Kuhnlenz, R. Jadhav, A. Wild, E. Birckner, G. Adam, A. Pivrikas and V. Cimrova, *Macromolecules*, 2010, **43**, 1261-1269.

112. J. W. Jung, F. Liu, T. P. Russell and W. H. Jo, *Advanced Energy Materials*, 2015, **5**.

113. P. Zhou, Z.-G. Zhang, Y. Li, X. Chen and J. Qin, *Chemistry of Materials*, 2014, **26**, 3495-3501.

114. I. Osaka, M. Shimawaki, H. Mori, I. Doi, E. Miyazaki, T. Koganezawa and K. Takimiya, *Journal of the American Chemical Society*, 2012, **134**, 3498-3507.

115. J. Kim, M. H. Yun, G.-H. Kim, J. Y. Kim and C. Yang, *Polymer Chemistry*, 2012, **3**, 3276-3281.

116. M. Wang, X. Hu, P. Liu, W. Li, X. Gong, F. Huang and Y. Cao, *Journal of the American Chemical Society*, 2011, **133**, 9638-9641.

117. H. Yi, S. Al-Faifi, A. Iraqi, D. C. Watters, J. Kingsley and D. G. Lidzey, *Journal of Materials Chemistry*, 2011, **21**, 13649-13656.

118. A. Abdulaziz, *Chemical Communications*, 2013, **49**, 2252-2254.

119. A. A. Alghamdi, D. C. Watters, H. Yi, S. Al-Faifi, M. S. Almeataq, D. Coles, J. Kingsley, D. G. Lidzey and A. Iraqi, *Journal of Materials Chemistry A*, 2013, **1**, 5165-5171.

120. C. W. Ge, C. Y. Mei, J. Ling, J. T. Wang, F. G. Zhao, L. Liang, H. J. Li, Y. S. Xie and W. S. Li, *Journal of Polymer Science Part A: Polymer Chemistry*, 2014, **52**, 1200-1215.

Chapter 2

Naphthothiadiazole-based donor-acceptor polymers for photovoltaic applications

Chapter 2

2.1 Introduction

Nowadays, the research community is focused on developing polymer-based solar cells due to their potential advantages which include light weight, increased flexibility and cheap production costs. Recently, great progress was achieved in the field of bulk heterojunction (BHJ) solar cells.[1-5] The design of efficient polymers for use in this area requires optimal electronic and physical properties of these materials including the energy levels of their HOMO and LUMO levels, the extent of their absorption of sunlight, as well as the nanoscale morphology of blends of these electron donating polymers with fullerene derivatives in order to achieve good charge extraction and efficient exciton dissociation.[2,6,7]

The bandgap and the energy levels of frontier orbitals of the conjugated polymers used in this area have to be optimised in order to obtain good efficiencies in PSCs.[8,9] The use of donor-acceptor alternating conjugated polymers enables the fine-tuning and adjustment of the bandgap and energy levels of these materials through control of intramolecular charge transfer (ICT) along polymer chains.[10-12]

The benzothiadiazole (BT) repeat unit has been found as an excellent acceptor repeat unit in donor-acceptor conjugated polymers used in this area as a consequence of its strong electron accepting ability. Pairing a strong electron accepting unit such as BT with an alternating electron donating unit leads to low bandgap polymers with very good photovoltaic properties.[2,13-15] The use of an even stronger electron acceptor is an attractive alternative to more efficient polymers for use in BHJ solar cells using fullerene derivatives as electron acceptors. However, care should be taken not to lower the LUMO energy level of the resulting polymer below -3.9 eV, which could result in inefficient exciton dissociation.[16-19] There are many approaches for preparing conjugated polymers with narrow optical bandgaps in order to broaden the spectrum of their light harvesting of sunlight. One of these methods is the replacement of benzothiadiazole (BT) units with naphthothiadiazole (NT) repeat units. One report showed that replacing 2,1,3-benzothiadiazole (BT) with 2,1,3-naphthothiadiazole (NT) in poly(2,7-carbazole-*alt*-4,7-dithienyl-2,1,3-naphthothiadiazole) **PCDTBT** reduces the

optical bandgap of the resulting polymer (**PCDTNT)** from 1.88 eV to 1.71 eV. It also red-shifts its λ_{max} position considerably (30 nm) in relation to its benzothiadiazole counterpart. Furthermore, the new naphthothiadiazole polymer possesses a high solution-processability and has suitable HOMO and LUMO energy levels for application in organic photovoltaic (OPV) device. In spite of a good open circuit voltage (V_{oc} = 0.81 V) the photovoltaic performance of **PCDTNT** in solar cells along with PCBM as an acceptor was low; a result of poor fill-factor FF values in devices.[20]

Promising photovoltaic results have been shown from other classes of alternating copolymers, comprising benzothiadiazole as the electron accepting unit along with anthracene (**PPATBT**), or fluorene (**PFDTBT**) as the electron donating units despite the reduced solubilities and the reduced molar masses of the latter polymers. Power conversion efficiencies of 1.93% and 5.41% were obtained respectively for **PPATBT** [21]and **PFDTBT**.[22] In this work, we present the preparation and characterisation of low bandgap copolymers containing alternating naphthothiadiazole as acceptor units and 2,7-linked fluorene or 2,6-linked anthracene repeat units flanked by thienyl units as the donor units. The electronic, photophysical and photovoltaic properties of these polymers are analysed and compared to those of the corresponding donor-acceptor polymer poly(2,7-carbazole-*alt*-4,7-dithienyl-2,1,3-naphthothiadiazole) (**PCDTNT**).

2.2   Result and discussion

2.2.1   Synthesis and characterisation

(Scheme 2-1) shows the preparation route to the NT-polymers prepared in this study. Monomer **M** was prepared according to an established literature procedure.[20] Reaction of **M** with monomers **S2**, **S6** and **S7** using the Suzuki coupling reactions afforded polymers PFDTNT**-P1,** PCDTNT**-P2** and PPATNT**-P3**, respectively.

Synthetic routes to the monomer --
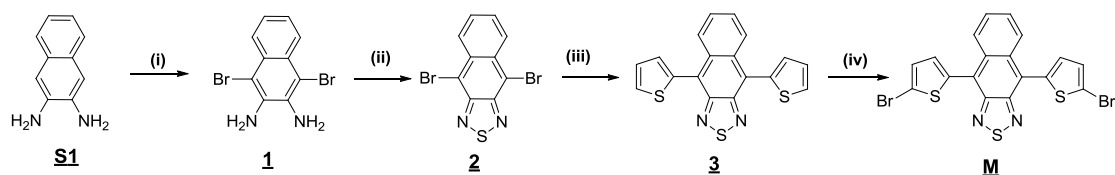
Synthetic routes to the linked polymers (class 1) --

R, R1. C$_8$H$_{17}$

R$_2$. C$_6$H$_4$(OC$_{12}$H$_{25}$)
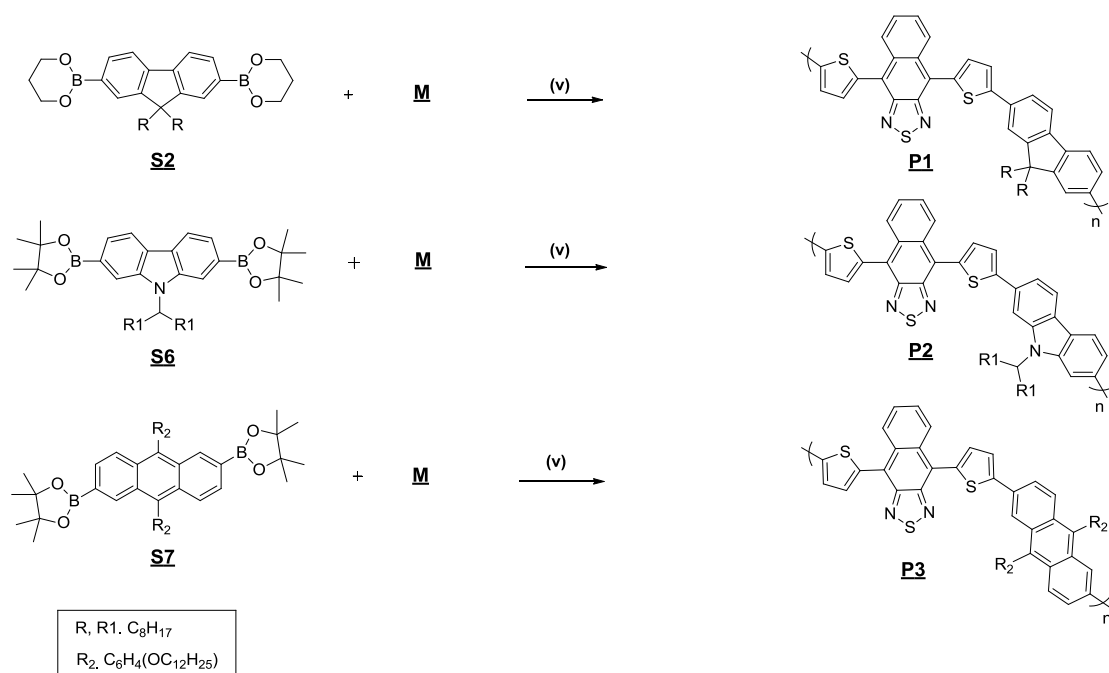
(i) Br$_2$, CHCl$_3$, AcOH. (ii) SnCl$_2$, CHCl$_3$, base, reflux. (iii) Pd$_2$(dba)$_3$, P(o-tolyl)$_3$, C$_{16}$H$_{30}$SSn, DMF, toluene, reflux. (iv) NBS, CB, reflux. (v) Pd(OAc)$_2$, P(o-tolyl)$_3$, base, THF or toluene, reflux.

Scheme 2-1: Synthetic route towards monomer (**M**) and the NT-based polymers

(class 1).

The key monomer **M** was synthesised from 2,3-diaminonaphthalene (**S1**) by bromination with bromine using acetic acid to afford corresponding dibromo compound **1**, followed by ring closure using excess thionyl chloride in basic conditions, generating **2** in a yield of 49% after recrystallization from ethanol. Dithienyl monomer **3** was obtained *via* a Pd-catalysed Stille coupling reaction of **2** and 2-tributylstannylthiophene. Bromination of compound **3** using NBS in chloroform did not

proceed to completion due to insufficient solubility and the low boiling point of chloroform. Chlorobenzene (CB) was used as an alternative solvent to chloroform at reflux temperature to push the reaction to produce the final target monomer **M**. The mechanism of the bromination of diamino naphthalene **S1** proceeds through an electrophilic aromatic substitution reaction as depicted in Scheme 2-2. In this mechanism, activating groups (amino groups) direct electrophilic attack on the 1- or 4- positions on the aromatic ring to yield **1**.
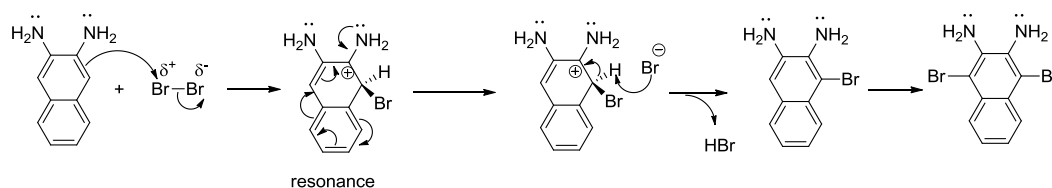
Scheme 2-2: Proposed mechanism for the formation of (**1**).

The mechanism of the cyclization reaction of **2** proceeds through nucleophilic attack as illustrated in Scheme 2-3. The electron donating groups on the amino substituents on the benzene ring act as strong nucleophile groups and attack the sulfur of the thionyl chloride, which is considered to be electrophilic. Thus, ring closure occurs and the target product is formed after a molecule of water is liberated from the product.
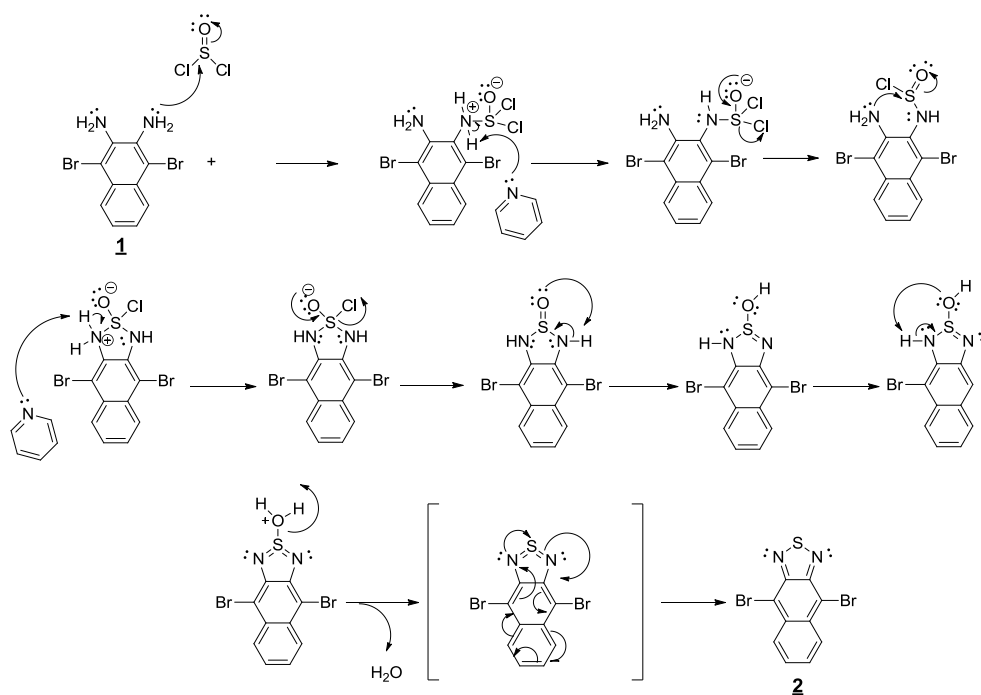
Scheme 2-3: Suggested mechanism for the formation of (**2**).

The Stille coupling reaction was used to prepare compound **3**. The catalytic cycle of this reaction was presented in (Scheme 1-3-Chapter 1). The proposed mechanism of bromination (Scheme 2-4) of dithienyl compound proceeds through an electrophilic aromatic substitution mechanism to produce **M**.
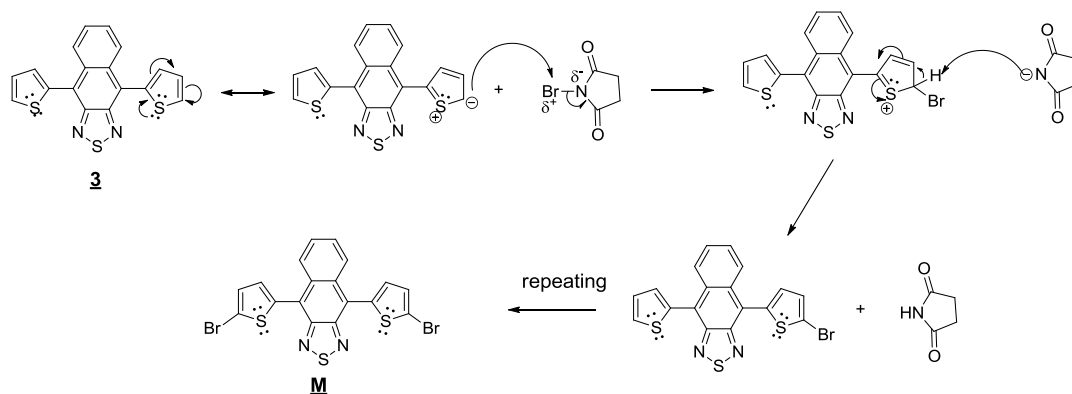
Scheme 2-4: The mechanism of bromination of the final monomer (**M**) using NBS.

The chemical structures of monomers were confirmed by ^{1}H NMR (as depicted in supplementary information section) as well as ^{13}C NMR, mass spectrometry and elemental analysis.

The Suzuki polymerisations were carried out using Pd(OAc)$_2$ as the catalyst and tri(o-tolyl)phosphine as the ligand in alkaline media under an inert atmosphere. All polymerisations were conducted until traces of polymer precipitates started to be observed; the time of polymerisation reactions varied between 24 to 48 hours. The polymers were fractionated *via* Soxhlet extraction using different organic solvents and their toluene and/or chloroform fractions were separated. All of the polymers prepared exhibited high solubility and were easily processable in chloroform as well as in other organic solvents at ambient temperature. The chemical structures of these polymers were confirmed by ^{1}H NMR spectroscopy (supplementary information) and elemental analysis. Results from Gel Permeation Chromatography (GPC) analysis of these polymers are shown in Table 2-1. The analysis was carried out in chloroform as the eluent at 40 °C. Polymer PPATNT-**P3**, which is the naphthothiadiazole counterpart of the known benzothiadiazole polymer **PPATBT**,[21] shows much greater processability. The toluene fraction of this polymer displays an M_n = 10,900 Da, which is three times higher than its analogous benzothiadiazole polymer (M_n = 3,500 Da).[21] Similar results

were obtained for naphthothiadiazole polymer PFDTNT-**P1** for which both of its toluene and chloroform fractions exhibit much higher values of the number-average molecular weight (M_n) and weight-average molecular weight (M_w) compared to its analogous benzothiadiazole polymer **PFDTBT**. The M_n of the chloroform fraction of PFDTNT-**P1** was 41,400 Da while that of the **PFDTBT** analogue which has a much limited solubility was M_n = 5,300 Da.[22] PCDTNT-**P2**, synthesised within this chapter, showed a M_n of 23,100 Da. This value is higher than that reported by Kim *et al.* for **PCDTNT** *(M_n = 12,800 Da),*[20] however, these values are not very different from those generally reported from chloroform fractions of **PCDTBT** [23] (M_n and M_w values of 22,500 and 32,600 Da, respectively). Clearly, apart from the carbazole-based polymers, incorporation of the NT acceptor repeat units along polymer chains instead of the BT repeat unit leads to polymers that have a much greater processability.

Table 2-1: The summary of the GPC analysis of PFDTNT-**P1**, PCDTNT-**P2** and PPADTNT-**P3**.

Polymer	Fraction	Yield %	M_n (Da) [a]	M_w(Da) [a]	PDI [b]
P1	toluene	29	9,900	16,800	1.7
	chloroform	43	41,100	79,500	1.9
P2	chloroform	67	23,100	89,600	3.8
P3	toluene	32	10,900	23,100	2.1

[a] Measurements conducted on the toluene and chloroform fractions of polymers using a differential refractive index (DRI) detection method. [b] Polydispersity index.

2.2.2 Optical properties

(Figure 2-1) shows the absorption spectra of the polymers both in chloroform solutions and as thin films. The values of the absorption maxima are shown in Table 2-2 along with their optical bandgaps as determined from the onset of their absorption in films.

UV-vis spectra of the polymers display two main absorption bands for PFDTNT-**P1** and PCDTNT-**P2** in both chloroform solutions and in thin films with additional absorption bands at 413 nm in solution and around 425 nm in films for PPATNT-**P3**.

Table 2-2: Summary of optical and electrochemical properties of **P1**-**P3**.

Polymer	λ_{max} solution (nm)	λ_{max} film (nm)	$E_{g\,opt}$ [c] (eV)	HOMO [d] (eV)	LUMO [e] (eV)	$E_{g\,elec}$ [f] (eV)
P1 [a]	554	572	1.76	-5.28	-3.49	1.79
P1 [b]	552	570	1.76	-5.36	-3.50	1.86
P2 [b]	555	582	1.74	-5.34	-3.44	1.90
P3 [a]	546	584	1.75	-5.40	-3.47	1.93

[a] Toluene fraction. [b] Chloroform fraction. [c] ($E_{g\,opt}$) optical bandgap, as calculated from the onset of UV-vis absorption spectra on solid films. [d] HOMO position (*vs. vacuum*) determined from onset of oxidation. [e] LUMO position (*vs. vacuum*) determined from onset of reduction. [f] Electrochemical energy gap of the polymers.

The UV-vis absorption spectra of polymers in films have red-shifted absorption bands relative to their solution spectra. This is due to aggregation of the polymer chains in the solid state,[24-26] which increases the electronic conjugation of the polymers and improves the planarity of polymer chains. Absorption bands at high energy are attributed to π-π* transitions while those at lower energies are attributed to intramolecular charge transfer (ICT). It can be seen in Figure 2-1 that the intensity of the ICT bands are lower in intensity than those of the π-π* absorption bands. This can be attributed to steric hindrance between NT repeat units and adjacent thienyl units along the conjugated polymer backbone, which impede an effective ICT between the alternating units of donors and acceptors.[20] While PPATNT-**P3** showed a slightly higher absorption maximum (584 nm *vs.* 582 and 570 nm for PCDTNT-**P2** and PFDTNT-**P1** respectively), all polymers in this series showed similar optical bandgaps (E_g between 1.74 and 1.76 eV), indicating similar electron donating properties of their electron donating segments. Comparison of the optical properties of the naphthothiadiazole-based polymers synthesised in this chapter with the benzothiadiazole analogous polymers, indicates that their energy bandgaps are lower than those of their counterpart polymers with BT repeat units. PPATNT-**P3** has a λ_{max} of absorption at 584 nm in films while its analogue (**PPATBT**) has a λ_{max} at 563 nm. The optical bandgap of PPATNT-**P3** is 1.75 eV while that of **PPATBT** is 1.84 eV.[21] The same comparison for PCDTNT-**P2** *vs.* **PCDTBT** indicates that the λ_{max} position for PCDTNT-**P2** is red-shifted by 22

nm, resulting in a lower optical bandgap of 1.74 eV for PCDTNT-**P2** compared to 1.88 eV for **PCDTBT**.[23] PFDTNT-**P1** (E_g = 1.76 eV) also displayed similar trends when compared to its benzothiadiazole equivalent **PFDTBT** (E_g = 1.86 eV).[22] The decrease in the bandgaps for NT-based polymers has been attributed to a more extended electronic delocalisation on the NT unit by virtue of an additional fused benzene ring in comparison with the BT unit.[20]
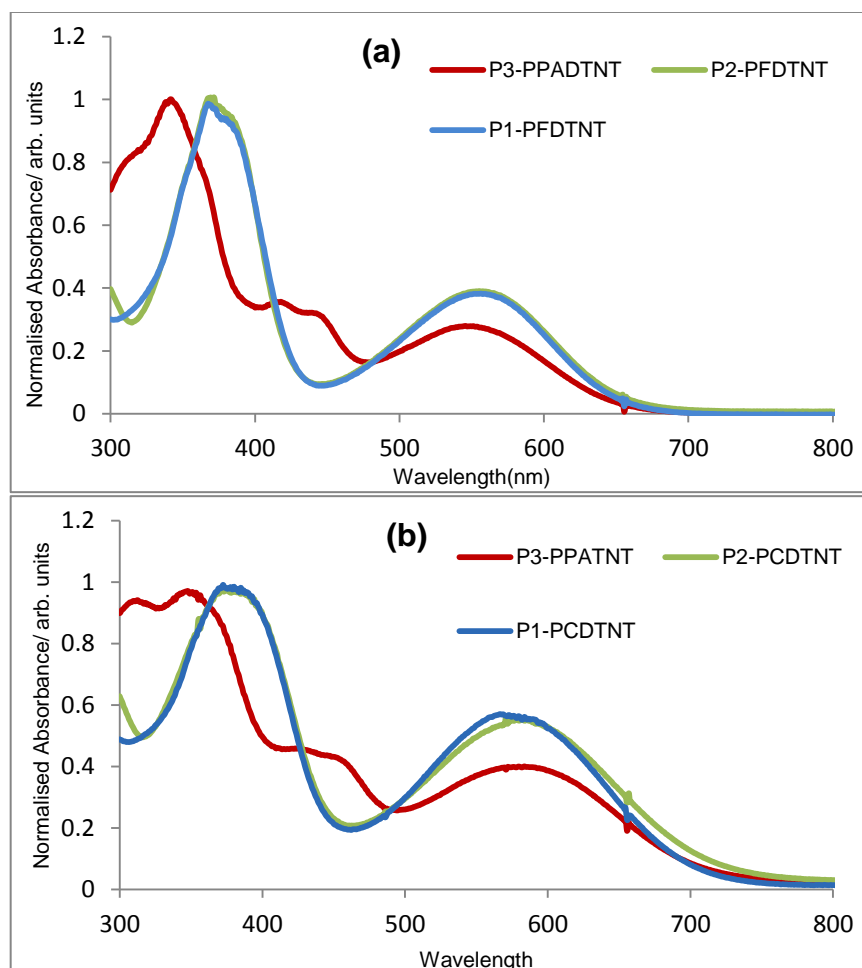
Figure 2-1: Normalised absorption spectra of polymers in $CHCl_3$ solution (a), and thin film (b)

2.2.3 Electrochemical properties

Cyclic voltammetry (CV) studies of the polymers were conducted on drop-cast films in acetonitrile with tetrabutylammonium perchlorate as the electrolyte. The CV measurements of all polymers are shown in Figure 2-2 with their redox potentials, as well as their respective HOMO and LUMO levels (*vs. vacuum*) as determined from the

onsets of oxidation and reduction potentials respectively (Table 2-2). The results show that the HOMO levels of all NT-based polymers presented in this chapter are of similar values to those of the analogous polymers with BT units. The HOMO level of PPATNT-**P3** at **-**5.40 eV is similar to that of **PPATBT** (**-**5.44 eV).[21] The same is observed on comparing the HOMO levels of PCDTNT-**P2** to that of **PCDTBT** (**-**5.34 eV *vs.* **-**5.35 eV[23] respectively) and the HOMO levels of PFDTNT-**P1** with its analogous polymer **PFDTBT** (**-**5.36 *v*s **-**5.34 eV [22] respectively). This trend suggests that a change of BT with NT acceptor units in donor-acceptor polymers has little bearing on the position of the HOMO levels of the resulting polymers. The value of the LUMO level of the NT-based polymer PPATNT-**P3** at **-**3.47 eV (Table 2-2) is deeper than the corresponding BT-based polymer **PPATBT** of (**-**3.21 eV).[21] However, the values of the LUMO levels of the carbazole-based and fluorene-based NT polymers (which have both displayed two reduction waves (Figure 2-2)) are very close to each other. The LUMO level of PCDTNT-**P2** is at -3.44 eV while that of **PCDTBT** is at -3.42 eV.[23] The LUMO of PFDTNT-**P1** is at -3.50 eV while that of the analogous BT polymer **PFDTBT** is at -3.44 eV.[22] The cyclic voltammetry results suggest close similarities in the positions of the HOMO and LUMO levels of the NT-based polymers to those of the corresponding BT-based polymers. While it clear from the electronic spectra that the NT-based polymers have relatively narrower bandgaps than their corresponding BT analogues (~ 0.1 eV lower), the variations of the HOMO and LUMO levels of the two classes of polymers as not obvious from cyclic voltammetric studies. The deviation between optical and electrochemical bandgaps might be caused by the presence of an energy barrier at the interface between the polymer film and the electrode surface during electrochemical measurements.
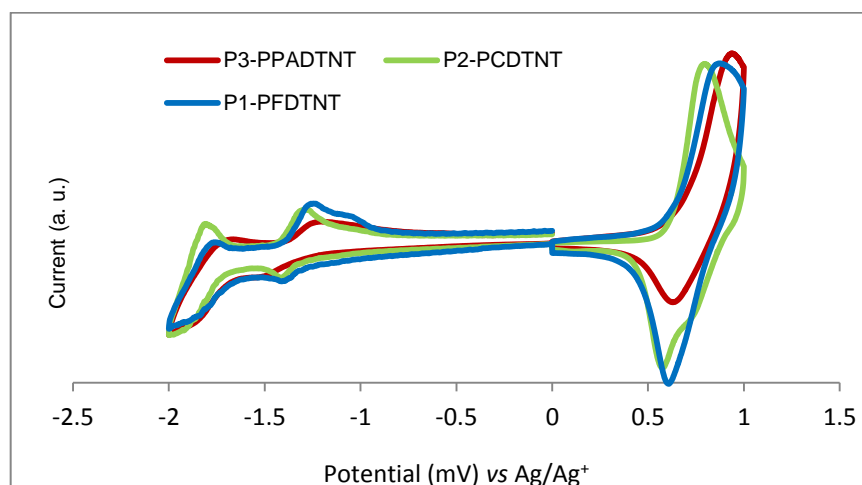
Figure 2-2: Cyclic voltammetry curves of thin polymer films on platinum disc electrodes (area 0.031 cm^2) at a scan rate of 100 mV s^{-1} in acetonitrile/tetrabutyl ammonium perchlorate (0.1 mol.dm^{-3}).

2.2.4 Thermal properties

The thermogravimetric analysis (TGA) studies were carried out on the resulting polymers under a N$_2$ atmosphere at a heating rate of 10 °C/min. The TGA curves reveal that all polymers display excellent thermal stability with initial decomposition temperature (T$_d$, as determined from 5% weight loss) above 400 °C. The TGA plots of the NT-linked polymers exhibits similar thermal decomposition patterns as shown in Figure 2-3, while the TGA data is summarised in Table 2-3.

Table 2-3: Summary of results from TGA of the polymers.

Polymer	1st D/°C[a]	EPL/ (%)[b]	TPL/ (%)[c]	2nd D/°C[d]	R_m/wt %[e]
P1	328-504	27	30	578	5.0
P2	422-523	30	31	591	17.0
P3	313-520	32	35	616	2.0

[a] 1st D is the range of first degradation. [b] EPL is the experimental percentage loss. [c] TPL is the theoretical percentage loss. [d] 2nd. D is the onset of second degradation. [e] R$_m$ is the residual mass after the degradation event.

A similar degradation pattern can be seen for PFDTNT-**P1**, PCDTNT-**P2** and PPADTNT-**P3** although these polymers contain different electron donor repeat units. However, the thermal stabilities of this series of polymers are not considerably affected by incorporation of different electron donor segments. The first step in the degradation appears between 328 and 504°C for PFDTNT-**P1**, between 322 - 523 °C for PCDTNT-**P2** and between 313 - 520 °C for PPADTNT-**P3**. It is likely to be due to loss of alkyl and alkoxy chains for the donor moieties of the polymers. The percentage weight loss recorded experimentally for PFDTNT-**P1**, PCDTNT-**P2** and PPADTNT-**P3** is 27, 30 and 32%, respectively. These values are comparable with theoretical values calculated from the molecular weight of the side chains of the polymers as depicted in Table 2-3.

The TGA data show similar second degradation patterns (weight loss) which can be seen again for PFDTNT-**P1**, PCDTNT-**P2** and PPADTNT-**P3** at 578, 591 and 616 °C, respectively. The loss of mass of all these polymers is gradual. This is probably due to the loss of aromatic units of the polymers.
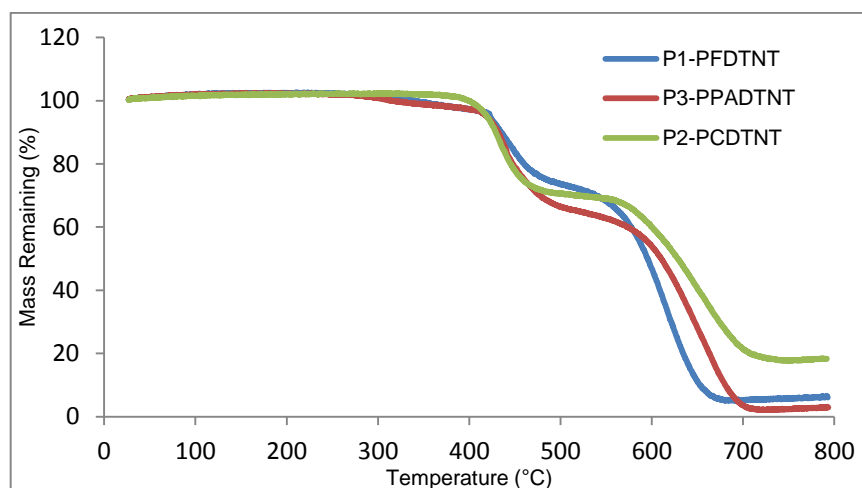
Figure 2-3: TGA plots of the resulting polymers with a heating rate of 10 °C/min under N$_2$.

After the second degradation step, the residual mass of PCDTNT-**P2** (17%) is higher than that of PPADTNT-**P3** (2%) and that of PFDTNT-**P1** (5%). This may be attributed to more carbonaceous residues [27] as a result of extra nitrogen heteroatoms on the carbazole-based polymer. Unfortunately, no comparison can be drawn between the resulting NT-based polymers and their BT analogues owing to a lack of thermal

analysis reported. The TGA analysis has confirmed that all polymers have presented a high thermal stability.

2.2.5 XRD studies

Powder X-ray diffraction (XRD) patterns of PFDTNT-**P1**, PCDTNT-**P2** and PPADTNT-**P3** were obtained (Figure 2-4) to investigate the polymer chain packing structures. It can be seen that PFDTNT-**P1** and PPADTNT-**P3** exhibit very weak broad peaks in the wide-angle region at 15.0 and 19.7° values, respectively. These peaks correspond to π-π stacking distances of 5.90 and 4.50 Å, respectively. However, PCDTNT-**P2** displayed a sharper, more intense peak in the same area at 2θ value of 20.5°. This peak reflects a more ordered packing of polymer main chains with a π-π stacking distance of 4.32 Å. On the whole, these results are consistent with the polymers in this series of materials (class 1) adopting an amorphous morphology; suggesting a lack of regular packing of polymer chains. This is probably due to steric hindrance between naphthothiadiazole repeat units and adjacent thiophene rings and the twisting out of planarity of the polymer main chains, resulting in a lack of close packing polymer chains. XRD pattern of PFDTNT-**P1** is comparable with its counterpart **PFDTBT** in a previous study.[28] Obviously, the results obtained from the XRD trends indicate that all polymers adopt an amorphous structure in the solid state.
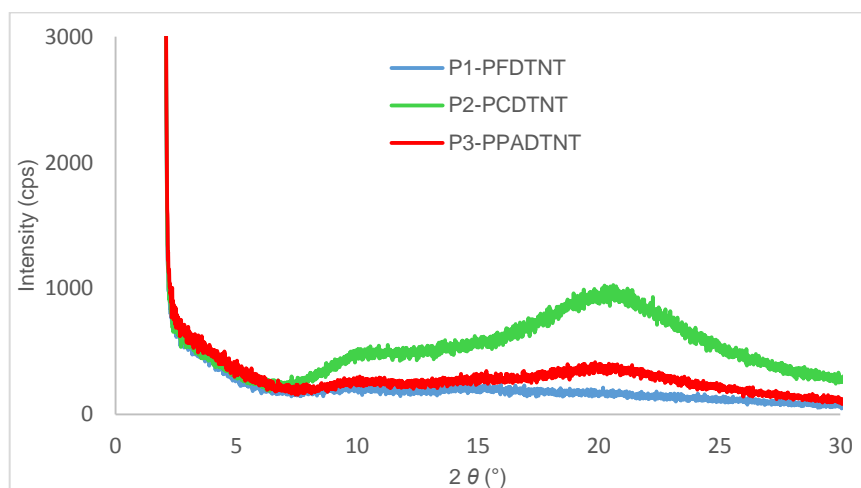
Figure 2-4: XRD patterns of PFDTNT-**P1**, PCDTNT-**P2** and PPADTNT-**P3**.

2.2.6 Photovoltaic Device Characterisation

BHJ solar cells using blends of the polymers as electron donors and $PC_{71}BM$ as acceptor with weight ratios of 1:4 were deposited by spin-casting on ITO/PEDOT:PSS anodes. A bilayer calcium/aluminum cathode (5 nm/100 nm) was used in these devices. The best results from the photovoltaic devices obtained in these studies are summarised in Table 2-4 and the J–V curves are shown in Figure 2-5. As shown on Table 2-4, all polymers displayed very good open-circuit voltages (V_{oc}) ranging from 0.94 to 1.02 V. In the case of the anthracene and carbazole-based polymers, the V_{oc} values are higher than those observed with the analogous polymers with BT rather than NT as the acceptor units. As an example devices using PPATNT-**P3** provide a V_{oc} of 0.94 V while **PPATBT**[21] which is the BT analogous polymer gave a V_{oc} of 0.59 V. The same observation is evident on comparing the V_{oc} of PCDTNT-**P2** to that of **PCDTBT** (1.01 V *vs.* 0.86 V [23] respectively). However, the V_{oc} of fluorene-based polymers are similar for both the NT-based polymer **PFDTNT** or its BT analogous polymer **PFDTBT** (1.02 V *vs* 1.03 V [22] respectively). It is well established that V_{oc} in BHJ solar cells is generally proportional to the energy difference between the HOMO level of the electron donor and the LUMO level of the electron acceptor in the active layer.[8,29] Such V_{oc} differences observed for both the anthracene and carbazole-based polymers in this study (PPATNT-**P3** and PCDTNT-**P2**) when compared to the V_{oc} values obtained from their BT analogues (**PPATBT** and **PCDTBT**) are not a result of differences of the HOMO levels of the two sets of polymers, but such differences in the V_{oc} values between the NT and BT polymers might be the result of differences in their molecular aggregations in blends.[30]

Table 2-4: Performance in bulk heterojunction photovoltaic devices under a simulated photovoltaic light with 100 mW cm^{-2} illumination (AM 1.5); cathode: 95%.

Polymer	Polymer:PC$_{71}$BM (weight ratio)	J_{sc}(mA cm^{-2})	V_{oc} (V)	FF (%)	PCE (%)
P1 [a]	1:4	-5.58	0.99	34.88	1.93
P1 [b]	1:4	-6.12	1.02	35.14	2.02
P2 [b]	1:4	-6.25	1.01	34.50	2.17
P3 [a]	1:4	-5.40	0.94	34.26	1.74

[a] Toluene fraction. [b] chloroform fraction of the polymers.

In Table 2-4, polymer PCDTNT-P2 exhibits the best performance with PCEs of 2.17 because it has high value of V_{oc} and J_{sc} compared to other polymers synthesised. Despite of it has shallower HOMO energy level than PFDTNT-P1 in toluene fraction.

However, the photovoltaic devices based on the polymer synthesised show the limiting fill factor of their photovoltaic performance compared to their counterparts polymers which based on BT units, this mainly causes the significantly lower FF and lacking at this stage. This is probably due to the unfavorable morphology between donor and acceptor because of a steric interaction between adjacent units of thiophene and NT units in donor in backbone of polymers. This leads to intrinsic low charge carrier mobility of these polymers. Apparently, UV-absorption spectra shows low intensity of ICT bands of the polymer, this is likely slightly impeding the effective ICT between the donor and acceptor blocks. All NT-based copolymers synthesised in this chapter demonstrate poorer efficiencies when compared to their analogous BT-based polymers.
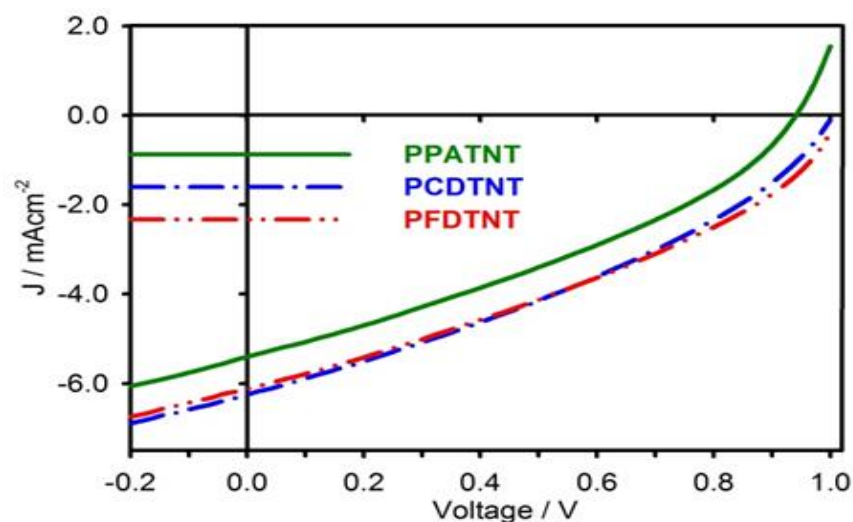
Figure 2-5: J-V characteristics of devices of polymers blended with $P_{70}CBM$ (1/4, w/w ratio). Device architecture: ITO/ PEDOT:PSS/ Active layer/ Ca (5 nm)/ Al (100 nm).

2.3 Conclusion

In conclusion, a series of low bandgap conjugated polymers comprising 4,9-linked 2,1,3-naphthothiadiazole units as electron accepting units and 2,7-linked fluorene, 2,7-linked carbazole or 2,6-linked anthracene alternate units flanked by thienyl units with alkoxy or alkyl substituents as donor units was successfully synthesised using the Suzuki coupling reactions. The physical, electrochemical, thermal, structural and photovoltaic properties of the resulting polymers were examined in order to ascertain the effect of replacing 2,1,3-benzothiadiazole (BT) with 2,1,3-naphthothiadiazole (NT) in this series of conjugated polymers. UV-vis spectroscopy showed that incorporation of NT units instead of BT results in red-shifted absorption maxima and lower bandgaps. This is explained by a more extended electronic delocalisation on the NT unit in virtue of an additional fused benzene ring in comparison with the BT unit. Moreover, replacing BT moieties with NT moieties over the main chain of polymers lead to polymers with increased molecular weights and solubilities. This is believed to be attributed to twisting of polymer chains out of planarity as a result of steric hindrance between naphthothiadiazole units and adjacent thiophene rings. The NT-based polymers display similar HOMO levels relative to their BT analogues. The LUMO levels of the NT and BT based polymers are also similar apart from the anthracene base polymers in which the NT-based polymer has a deeper LUMO level than its BT analogue. Photovoltaic devices with an active layer composed of thin films

(65-75 nm) of polymer/PC$_{71}$BM blends had power conversion efficiencies (PCEs) ranging from 1.74 to 2.17%. PCDTNT-**P2** displayed the best performance among this series of polymers (class 1). Comparison of the photovoltaic performance of the NT-based polymers to that of their BT analogues indicated a lower performance of the NT-based polymers, even though the latter polymers display lower bandgaps than the corresponding BT-counterparts, a result of significant low FF that leads to an overall low photovoltaic performance. We speculate that this may be attributed to the effect of the unfavourable morphology for given polymer/fullerene systems that did not yield efficient devices, this could have affected charge carrier motilities in devices. Taking the positions of energy levels and low bandgap of these polymers into account, there is possibility to design new categories of low bandgap polymers that could be applied as effective materials in photovoltaic devices when used with fullerene derivatives**.** Further investigations into the use of these new polymers in BHJs are currently ongoing.

References

1.   B. C. Thompson and J. M. Frechet, *Angewandte Chemie International Edition*, 2008, **47**, 58-77.

2.   H. Zhou, L. Yang and W. You, *Macromolecules*, 2012, **45**, 607-632.

3.   G. Yu, J. Gao, J. C. Hummelen, F. Wudl and A. J. Heeger, *Science-AAAS-Weekly Paper Edition*, 1995, **270**, 1789-1790.

4.   C. J. Brabec, C. Winder, M. C. Scharber, N. S. Sariciftci, J. C. Hummelen, M. Svensson and M. R. Andersson, *Journal of Chemical Physics*, 2001, **115**, 7235-7244.

5.   S. Günes, H. Neugebauer and N. S. Sariciftci, *Chemical Reviews*, 2007, **107**, 1324-1338.

6.   H. Shirakawa, A. McDiarmid and A. Heeger, *Chemical Communications*, 2003, **2003**, 1-4.

7.   H. Hoppe and N. S. Sariciftci, *Journal of Materials Research*, 2004, **19**, 1924-1945.

8.   M. C. Scharber, D. Muhlbacher, M. Koppe, P. Denk, C. Waldauf, A. J. Heeger and C. J. Brabec, *Advanced Materials-Deerfield Beach Then Weinheim-*, 2006, **18**, 789.

9. L. Dou, Y. Liu, Z. Hong, G. Li and Y. Yang, *Chemical Reviews*, 2015, **115**, 12633-12665.

10. Y. Deng, Y. Chen, X. Zhang, H. Tian, C. Bao, D. Yan, Y. Geng and F. Wang, *Macromolecules*, 2012, **45**, 8621-8627.

11. C. Kitamura, S. Tanaka and Y. Yamashita, *Chemistry of Materials*, 1996, **8**, 570-578.

12. P. M. Beaujuge, C. M. Amb and J. R. Reynolds, *Accounts of Chemical Research*, 2010, **43**, 1396-1407.

13. H.-Y. Chen, J. Hou, S. Zhang, Y. Liang, G. Yang, Y. Yang, L. Yu, Y. Wu and G. Li, *Nature Photonics*, 2009, **3**, 649-653.

14. P.-L. T. Boudreault, A. Najari and M. Leclerc, *Chemistry of Materials*, 2010, **23**, 456-469.

15. S. Sardar, P. Kar, H. Remita, B. Liu, P. Lemmens, S. K. Pal and S. Ghosh, *Scientific Reports*, 2015, **5**.

16. Y.-J. Cheng, S.-H. Yang and C.-S. Hsu, *Chemical Reviews*, 2009, **109**, 5868-5923.

17. S. H. Park, A. Roy, S. Beaupre, S. Cho, N. Coates, J. S. Moon, D. Moses, M. Leclerc, K. Lee and A. J. Heeger, *Nature Photonics*, 2009, **3**, 297-302.

18. M. Wang, X. Hu, P. Liu, W. Li, X. Gong, F. Huang and Y. Cao, *Journal of the American Chemical Society*, 2011, **133**, 9638-9641.

19. M. Karikomi, C. Kitamura, S. Tanaka and Y. Yamashita, *Journal of the American Chemical Society*, 1995, **117**, 6791-6792.

20. J. Kim, M. H. Yun, G.-H. Kim, J. Y. Kim and C. Yang, *Polymer Chemistry*, 2012, **3**, 3276-3281.

21. . H. Yi, M. S. Almeataq, S. Al-Faifi, A. A. Alghamdi, A. Iraqi, N. W. Scarratt, T. Wangc and D. G. Lidzey, *The Royal Society of Chemistry*, 2013, **49**, 2252--2254.

22. A. A. Alghamdi, D. C. Watters, H. Yi, S. Al-Faifi, M. S. Almeataq, D. Coles, J. Kingsley, D. G. Lidzey and A. Iraqi, *Journal of Materials Chemistry A*, 2013, **1**, 5165-5171.

23. H. Yi, S. Al-Faifi, A. Iraqi, D. C. Watters, J. Kingsley and D. G. Lidzey, *Journal of Materials Chemistry*, 2011, **21**, 13649-13656.

24. P. J. Brown, D. S. Thomas, A. Köhler, J. S. Wilson, J.-S. Kim, C. M. Ramsdale, H. Sirringhaus and R. H. Friend, *Physical Review B*, 2003, **67**, 064203.

25. S. C. Price, A. C. Stuart, L. Yang, H. Zhou and W. You, *Journal of the American Chemical Society*, 2011, **133**, 4625-4631.

26. P. Wei, L. Duan, D. Zhang, J. Qiao, L. Wang, R. Wang, G. Dong and Y. Qiu, *Journal of Materials Chemistry*, 2008, **18**, 806-818.

27. F. Bradner and J. Shapiro, *Polymer International*, 1991, **26**, 195-202.

28. L. Cartwright, A. Iraqi, Y. Zhang, T. Wang and D. G. Lidzey, *RSC Advances*, 2015, **5**, 46386-46394.

29. N. Blouin, A. Michaud, D. Gendron, S. Wakim, E. Blair, R. Neagu-Plesu, M. Belletête, G. Durocher, Y. Tao and M. Leclerc, *Journal of the American Chemical Society*, 2008, **130**, 732-742.

30. M. D. Perez, C. Borek, S. R. Forrest and M. E. Thompson, *Journal of the American Chemical Society*, 2009, **131**, 9281-9286.

Chapter 3

Synthesis and characterisation of a series of ethynylene and ethynylene-thiophene based alternating polymers containing 2,1,3-linked naphthothiadiazole units as acceptor with various linked donors.

Chapter 3

3.1 Introduction

In the last years, polymers solar cells (PSCs) have attracted increased attention because of their potential advantages over their inorganic semiconductor counterparts such as low manufacturing costs, mechanical flexibility of devices, light weight and large area fabrication.[1-5] Semiconducting polymers have been widely studied for electronic applications such as OLED and OPVs.[6-8] The ability to design conjugated polymers with a variety of optical and electrochemical properties makes them attractive candidates for electronic device applications.[9-11]

The chemical structure of polymers dictates their optical and electronic properties which determines their photovoltaic performance in devices.[1,12] It is well recognised that tuning of energy bandgaps and energy levels of conjugated polymers by tailoring their chemical structure is an effective way to achieve low bandgaps in polymers for high performance. One of the important approaches for the adjustment of these properties is to alternate electron rich-donor units with electron-deficient acceptor moieties over the polymer chain by copolymerisation.[13-18] This strategy optimises the intramolecular charge transfer (ICT) between the donor and acceptor building blocks, which enables control of the bandgap of the conjugated polymer *via* extending the π-delocalisation system and increasing rigidity of the structure of the polymer.[14,17,19] The introduction of fused aromatic rings within D-A polymer chains is considered as an effective strategy to reduce the bandgap of the resulting polymers and extend their absorption spectrum; a result of enhancing the rigidity and planarity of their backbone. Consequently, incorporation of various fused rings such as fluorene, carbazole and anthracene over π-conjugated systems presents good performances in OLED and OPV devices.[18] The push/pull D-π-A approach has been studied by the research community, not only to construct low bandgap polymers but also adjust the HOMO and LUMO energy levels in polymers to achieve promising performance in OSCs.[17,20] Further modulation of the energy levels of the alternating D-A polymer can be carried out through introducing solubilising chains of varying steric bulk. Attachment of alkyl chains on the electron donor and/or acceptor units of an alternating conjugated polymer enhances its solubility, molecular weight and adjusts non-covalent interchain interactions.[1,21,22] Thus, absorption of a broad part of the solar light spectrum for an

alternating polymer can be observed if there is efficient (ICT) between donor and acceptor units along polymer chains, resulting in a reduced bandgap of the polymer.[17] Moreover, it is believed that further changes in π-conjugated systems, delocalisation, energy levels and bandgap can be achieved using the linker units between the electron donor and acceptor moieties over the polymer chain.

Previous studies indicated that the linker effects between donor and acceptor moieties in D-π-A system plays a crucial role in determining the bandgap of the polymer, as a linker can affect the rigidity and planarity of polymer chains.[23,24] Incorporation of different spacers over the polymer chains results in significant differences in electronic delocalisation and rigidity of the backbone of the resulting polymers.[23] Zhang *et al.* compared the properties of thiophene-based polymers which consisted of thiophene homopolymers as well as alternating thiophene acetylene copolymers. This study showed the considerable influence of the introduction of the acetylene linker on the solubility and optoelectronic properties of the resulting polymer. This displayed much lower solubility and lower molecular weight compared with its analogue without acetylene linkers owing to higher rigidity and coplanar conformations of the polymer backbone.[18] However, other literature reports have found that the incorporation of the ethynylene units over polymer main chains does not have an effect on the solubility and molecular weight of the polymers obtained.[23] Du *et al.* also prepared a series of ethynylene-thiophene based polymers with either phenylene or carbazole units as electron donor units and benzothiadiazole (BT) as acceptor repeat units. The different positions of the ethynylene units and thiophene units between electron donor and acceptor units over the polymer chains exhibited differences in the optical, electronic and photovoltaic properties of these polymers. Insertion of ethynylene units between BT units and thiophene units displayed the best performance among these polymers, with a PCE of 1.6% for the carbazole-based polymer when fabricated with $PC_{71}BM$ in BHJ devices.[25] Incorporation of ethynylene units along the polymer backbone is a successful approach for attaining low HOMO levels in conjugated polymers and thus could potentially enhance the V_{oc} value of devices. In addition of a high V_{oc}, a lower HOMO level for the conjugated polymer also translates to a better oxidation stability of the polymer.[25]

In this chapter, we have decided to explore the use of ethynylene or ethynylene-thiophene spacers in alternate D-A polymers, comprising alternate naphthothiadiazole

electron accepting units and alternate electron donating units such as fluorene, carbazole and anthracene. The impact of ethynylene and thiophene units on the optoelectronic properties of the resulting polymers will be covered later in this chapter. Six conjugated polymers (Figure 3-1), which contain ethynylene units in the alternate D-A polymer backbone, have been synthesised successfully using the Sonogashira coupling reaction. In the class (2) polymers, the ethynylene units are located between the electron-deficient units and electron-rich units to yield three new copolymers PFDENT-**P4**, PCDENT-**P5** and PPADENT-**P6**. In the class (3) polymers, thiophene units are placed next to the electron donor units to be positioned between the ethynylene units and naphthothiadiazole electron-acceptor units to yield another three new polymers, PFDTENT-**P7**, PCDTENT-**P8** and PPADETNT-**P9**. The optical, electrochemical and thermal properties of the resulting polymers were investigated and compared. Our results displayed that ethynylene and thiophene-based polymers (class 3) showed lower bandgaps relative to their ethynylene counterparts (class 2). The series of polymers which have ethynylene and thiophene linkers between electron donor and acceptor units (class 3) exhibited red-shifted absorption spectra when compared with those of analogous polymers with ethynylene linkers (class 2). The synthesis and characterisation of these polymers will be discussed in this chapter along with a comparison of the properties of ethynylene-based polymers (class 2) with those of their thiophene counterparts (class 1) discussed in Chapter 2, as well as a comparison to the properties of the polymers with ethynylene-thiophene linkers (class 3).

Structure of polymers (class 2)   Structure of polymers (class 3)
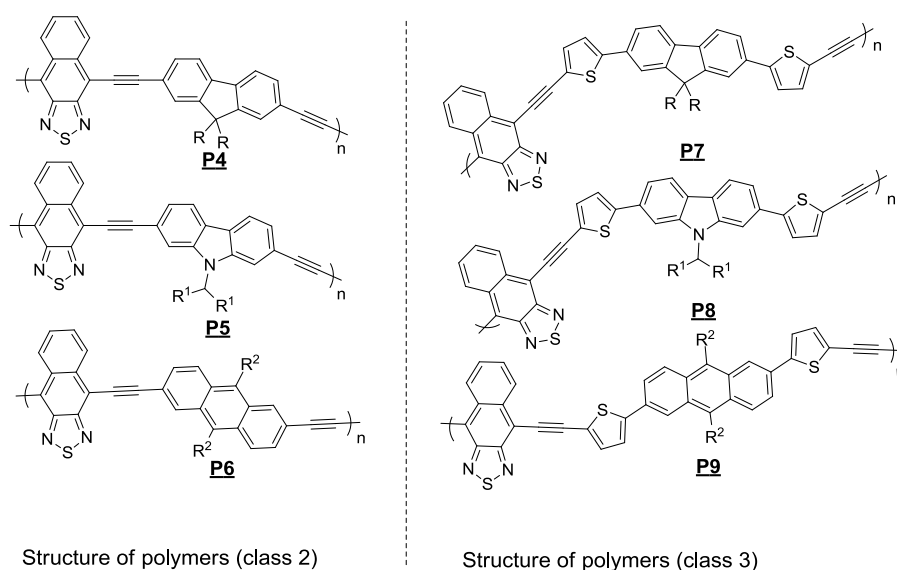
Figure 3-1: Structures of (class 2) and (class 3) polymers.

3.2 Result and discussion

3.2.1 Synthesis and characterisation

Polymers with ethynylene linkers between donor and acceptor units (class 2)

The general synthetic routes to prepare the intermediates monomers **M1-M3** and ethynylene-based polymers (class 2) **P4-P6** are outlined in Scheme 3-1. **M1** (9,9-dioctyl-2,7-diethynylfluorene) was synthesised from 9,9-dioctyl-2,7-dibromofluorene (**S3**) as starting material, this monomer requires to be kept at low temperature and in the dark before use. The first step in the monomer synthesis was a functionalisation of the 2,7-positions of fluorene with trimethylsilyl acetylene using a Sonogashira reaction, which gave compound (**4**) (9,9-dioctyl-2,7-[bis(2'-trimethysilyl)ethynyl)]fluorene) in a yield of 85%. The reaction was carried out in the presence of (Pd and CuI) as the catalysts with diisopropylamine/(THF, toluene) as the reaction media under an inert atmosphere. The procedure is well established in the literature.[26] The mechanism of the Sonogashira reaction has been covered in Scheme 1-5 - Chapter 1. The following step was the cleavage of the trimethyl silyl protecting groups of compound **4** that was carried out under base treatment to afford pure monomer **M1** in a yield of 96% after extraction without further purification. The method is well documented in the literature.[26]
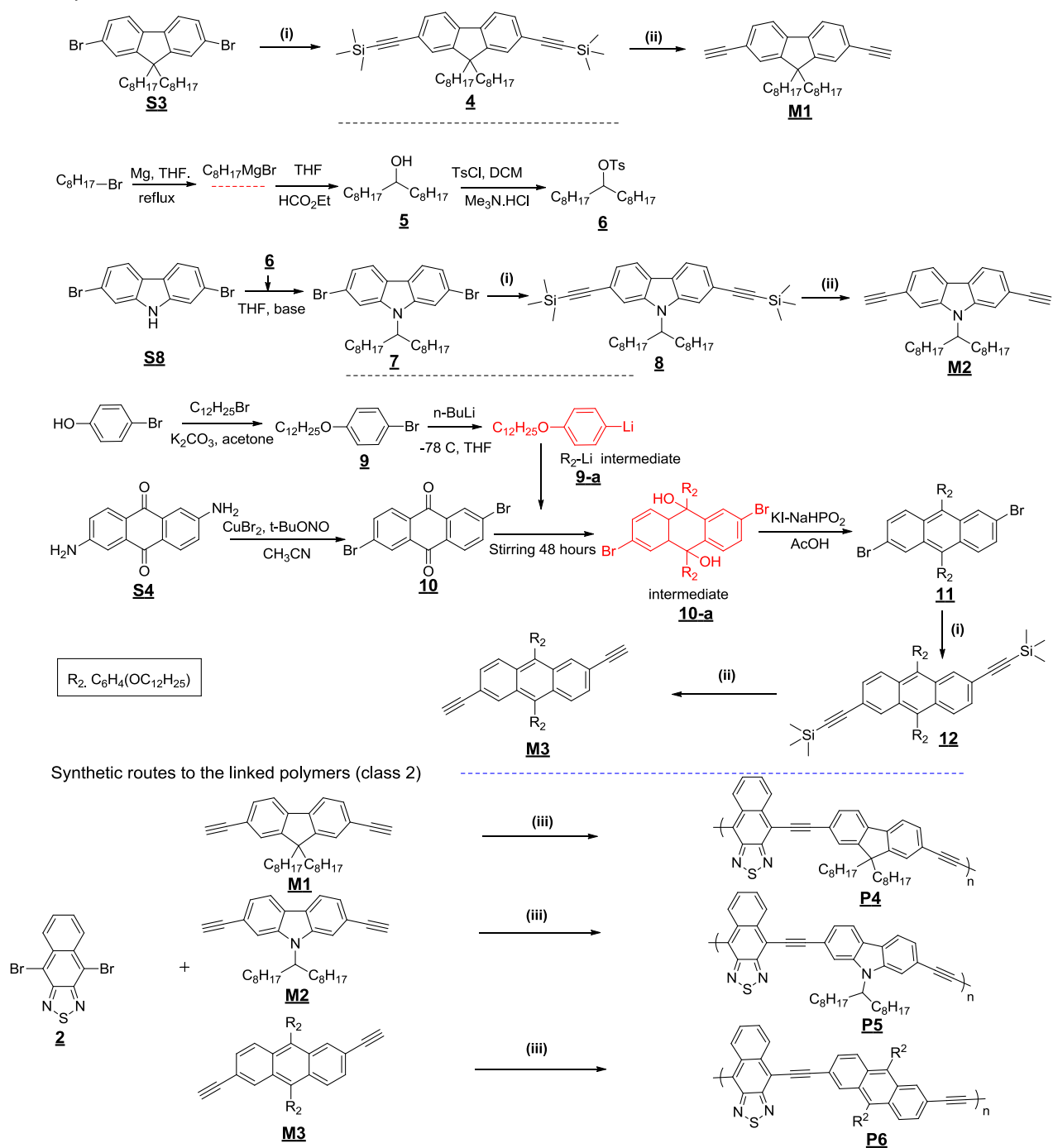
Scheme 3-1: Synthetic route towards monomers (**M1-M3**) and the resulting polymers (**P4-P6**).

The deprotection mechanism is illustrated in Scheme 3-2. It proceeds through two steps. Firstly, the protecting group is attacked by a nucleophile (methoxide) on the silicon atom under base treatment. Secondly, the resulting acetylide anion formed extracts a proton from the solvent used (methanol) to afford **M1**.
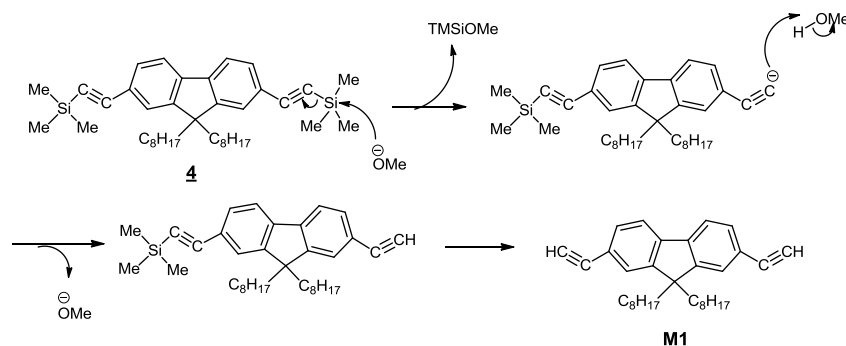
Scheme 3-2: Proposed mechanism for the formation of **M1**.

Similarly, the synthesis of **M2** involved three main steps including alkylation of carbazole, a Sonogashira reaction, followed by a cleavage reaction. Regarding to preparing the tosylate **6**, it was synthesised through two main reactions according to literature reports.[27] This involved the formation of a Grignard reagent prepared by the reaction between octyl bromide and magnesium in dry THF. Once the reagent was synthesised it was added to a suspension of ethyl formate in dry THF to yield alcohol compound **5** in good yield. The mechanism for this reaction is generally through a nucleophilic addition mechanism. Grignard reagents act well as nucleophile reacts with the electrophile carbon in a carbonyl group in ethyl formate, followed by formation of carbonyl again after pushing out the alcohol. The formed intermediate compound is subject to another nucleophilic attack to produce the target product **5** after hydrolysis (Scheme 3-3).
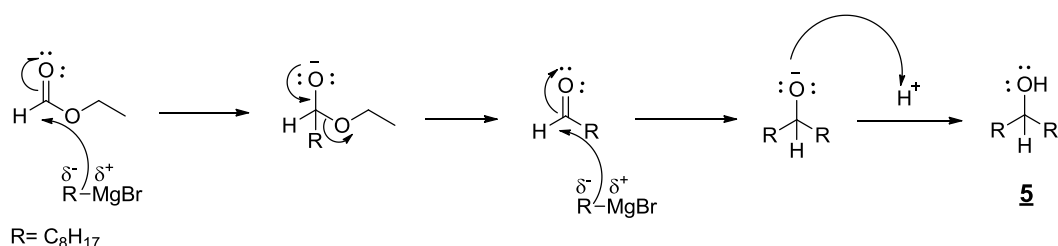
Scheme 3-3: The mechanism reaction of compound **5**.

The next step is a tosylation reaction using *p*-toluenesulfonyl chloride in dry DCM, trimethylamine hydrochloride as a catalyst which was added in the presence of the base under low temperature. The aim of this reaction is to transform the alcohol group into

the sulfonic ester using *para*-toluene sulfonyl chloride in order to produce organic tosyl ester **6**. The mechanism for formation **6** is depicted in Scheme 3-4. The suggested mechanism proceeds through the tosylation mechanism under basic conditions where, trimethylamine hydrochloride Me₃N•HCl generates trimethylamine Me₃N which reacts with *p*-toluenesulfonyl chloride TsCl to obtain a very strong tosylation reagent. The hydroxyl group in alcohol acts as good nucleophile that attacks the tosylate reagent to produce the desired product (tosyl ester) and Me₃N•HCl which converts back to Me₃N again.
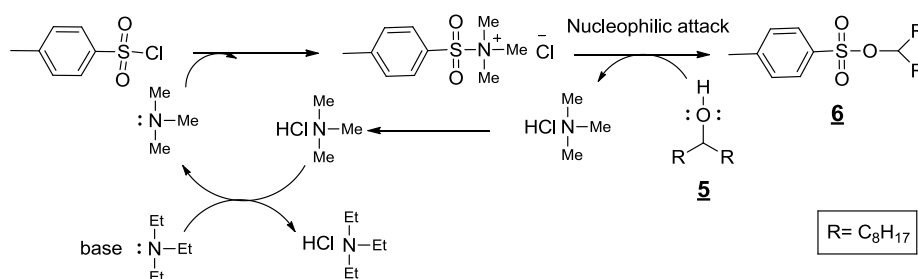
Scheme 3-4: The suggested mechanism for the formation of compound **6**.

After the tosyl ester was prepared it was reacted with 2,7-dibromo-carbazole (**S8**) at the nitrogen atom to produce the alkylated compound **7**. Attaching an alkyl chain this long is essential to promote solubility of the final desired product. It is worth mentioning that the yield of the alkylated compound using a DMSO-KOH system to produce the alkylated carbazole was low [27] due to low solubility of alkylation reagent (alkyl toluenesulfonate) in DMSO. To overcome this issue, dry THF was used successfully in the system to increase the solubility of the reaction mixture leading to a high yield of 84%. The mechanism of alkylation follows a nucleophilic substitution reaction including, deprotonation by the strong ion (OH⁻), followed by attack from of the carbazole anion on the tosyl ester yielding the desired product as depicted in Scheme 3-5.
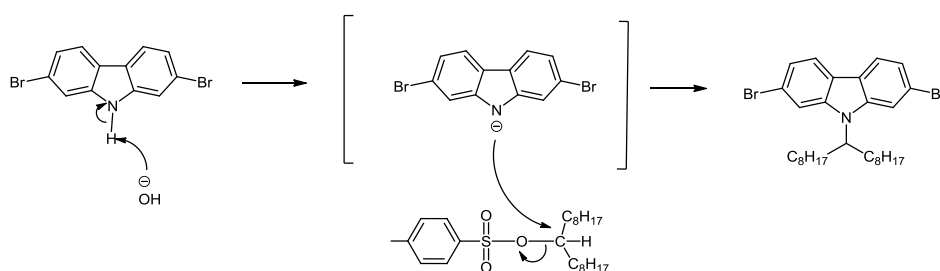
Scheme 3-5: Reaction mechanism for forming compound **7**.

The preparation of monomer **M3** follows similar steps to those to prepare monomers **M1** and **M2** from anthracene intermediate **11** as shown in Scheme 3-1. The preparation of **11** required first the preparation of 1-bromo-4-(dodecyloxy) benzene (**9**) from 4-bromo phenol as starting material under base treatment as catalyst.[28] The resulting product was treated with n-BuLi to generate the 1-lithio-4-dodecyloxybenzene intermediate. Once the lithiated compound was prepared it was added to 2,6-dibromo-anthraquinone (**10**) to produce its derivative compound (**11**). The mechanism for formation (**9**) proceeds *via* nucleophilic substitution reaction (S$_N$2) as presented in Scheme 3-6. Clearly, the mechanism begins the treatment with base, this was used to deprotonate the starting material to form a phenoxide intermediate, this attacks the alkyl halide in (S$_N$2), resulting in the formation of the target ether product (**9**).
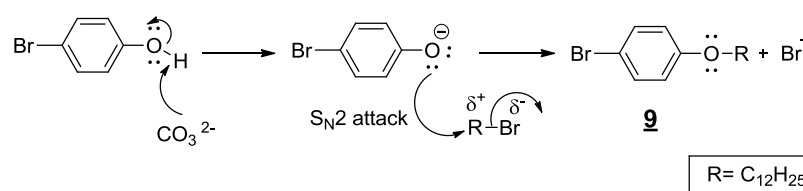
Scheme 3-6: The reaction mechanism for the formation of compound **9**.

The second reaction mechanism is the formation of the lithiated reagent (**9-a**) (Scheme 3-7). Organolithiums can exchange its lithium atom with a halide in an exchange reaction to form the corresponding organolithium derivative.
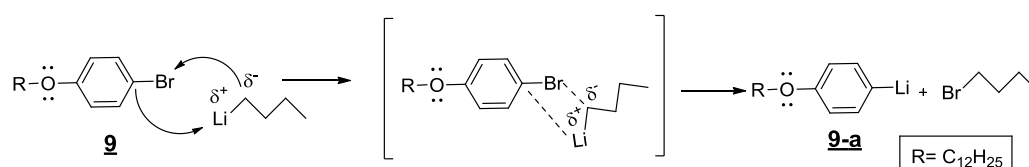
Scheme 3-7: Proposed mechanism for the formation of the lithated intermediate alkoxyphenyl (**9-a**).

2,6-Dibromoanthraquinone (**10**) was prepared from the corresponding 2,6-diamino-anthraquinone **S4** through a modified Sandmeyer-reaction to afford the desired product (yield = 86 %) using a well-documented procedure.[29] The general mechanism of modified Sandameyer-reaction is illustrated in Scheme 3-8.
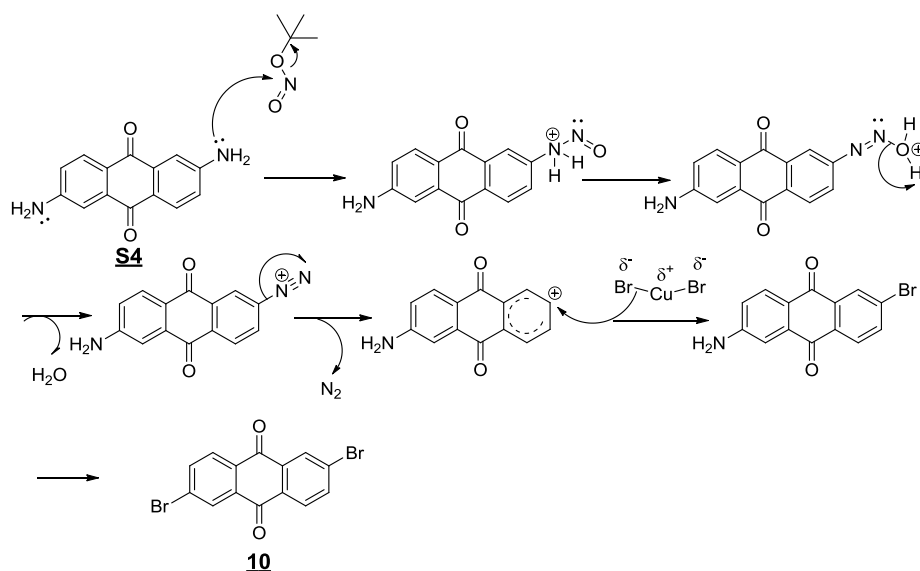
Scheme 3-8: Proposed mechanism of Sandameyer for forming compound **10**.

Once the lithiated-intermediate compound was synthesised it was added to a suspension of **10** in dry THF to afford a diol compound (**10-a**) as intermediate product. The resulting compound was reduced using KI–NaH-PO$_2$, the crude product was recrystallised from methanol to yield the anthracene intermediate (**11**) as a pure product (yield = 69 %),[30,31] Clearly, the addition of bulky groups at 9,10-positions of **11** increases the solubility of the resulting monomer in common organic solvents.

It is noteworthy to point out that incorporation of ethynylene units on the NT electron accepting moiety was achieved. However, the diyene compound was very unstable and immediately degraded while the ethynylene-linked electron donor units were more stable products during preparation and copolymerisation. The preparation of **2** has been covered in Chapter 2- P 49. The chemical structures of the final monomers were adequately characterised and confirmed by ^{1}H NMR as shown in (supplementary information), ^{13}C NMR, the mass spectra and elemental analysis.

Polymerisations of **2** with respectively **M1**, **M2** and **M3** by the Sonogashira reaction produced polymers PFDENT-**P4** (yield = 18 %), PCDENT-**P5** (yield = 15 %) and PPADENT-**P6** (yield = 35 %). These polymerisations were easily carried out in the presence of catalytic amount of (20%) Pd(PPh$_3$)$_2$Cl$_2$ and 14% (CuI) with diisopropylamine as the base media into a mixture of solvents (THF, toluene) under an inert atmosphere. Using excess of co-catalyst as modification is required to guarantee a successful reaction. It is observed that the polymerisation times varied between 1 to 5 hours with large quantities of polymer precipitates forming during the reactions. All the

74

resulting polymers were purified by successive Soxhlet extractions with different common organic solvents. It was observed that large amounts of the resulting polymers remained as intractable materials in the Soxhlet thimbles after extraction. The low solubilities of the resulting polymers explain the low yields observed from these polymerisations. The products obtained from the toluene and chloroform Soxhlet fractions (which are generally the fractions obtained on extraction of processable materials from most conjugated polymers) were soluble in common organic solvents. The chemical structures of these copolymers were verified by ^{1}H NMR and elemental analysis. Details of the synthesis of monomers **M1-M3**, polymers and their characterisations are described in the experimental section.

Gel permeation chromatography (GPC) analysis of these polymers against polystyrene standards estimated the number and weight-average molecular weights (M_n and M_w) using 1,2,4-trichlorobenzene (TCB) as the eluent at 140 °C (Table 3-1). GPC measurements of ethynylene-based polymers exhibit moderate molecular weights. These ethynylene-based polymers (class 2) were only obtained in their toluene fractions except PPADENT-**P6** which was obtained from its chloroform fraction. It was speculated that incorporation of the ethynylene units over the polymer chains results in a decrease in the torsion angle between alternate units along polymer chains, leading to aggregation of polymer chains as a result of their coplanar geometry.[32] This then limits accessibility to soluble high molecular weight polymers. Despite most of these ethynylene-based polymers being extracted in the toluene fractions, the polymers still displayed poor solubility with other organic solvents at high temperature. For comparison purposes, ethynylene-based polymers display a significant reduction in molecular weight relative to their thiophene analogous polymers previously synthesised (Chapter 2 - P 50-51), and where the thiophene units are replaced by ethynylene units. For example, GPC analysis estimated the M_n and M_w of PCDENT-**P5** to be 8,800 and 22,900 Da, respectively. While the M_n and M_w of its counterpart, PCDTNT-**P2** (Chapter 2), are 23,100 and 89,600 Da, respectively. It is hypothesised that the presence of ethynylene-spacer facilitates π-π interchain stacking and planarization, leading to reduced M_n and M_w values obtained for PCDENT-**P5** relative to that of its counterpart, PCDTNT-**P2**.

Table 3-1: GPC data and yields of the class2 polymers.

Polymer	Fraction	Yield %	M_n (Da) [a]	M_w(Da) [a]	PDI [b]
P4	toluene	18	10,000	30,200	3.0
P5	toluene	15	8,800	22,900	2.5
P6	toluene	25	7,900	16,000	2.0
	chloroform	10	9,200	17,700	1.9

[a] Measurements conducted on the toluene and chloroform fractions of polymers using a differential refractive index (DRI) detection method. [b] Polydispersity index.

Polymers with ethynylene-thiophene linkers between donor and acceptor units (class 3)

The synthetic routes to all three monomers **M4**-**M6** and the corresponding conjugated polymers **P7-P9** are outlined in Scheme 3-9. The final monomer **M4** could be obtained in four steps following modified procedures.[33,34] The first step used a Stille reaction between 2-(tributylstannyl)thiophene and 2,7-dibromo-9,9-dioctylfluorene (**S3**) to afford 2,7-dithienyl-9,9-dioctylfluorene (**13**). The reaction was carried out in chlorobenzene at 120 °C overnight using Pd$_2$(dba)$_3$ and tri(o-tolyl)phosphine as catalyst. In this reaction, choosing a high boiling point solvent helps the reaction to proceed to completion. The reaction was high yielding (91%) after purification of the product by column chromatography. The mechanism of this reaction proceeds through a catalytic cycle of the Stille coupling reaction as described in (Scheme 1-3-Chapter 1).

The second step is a bromination reaction, compound (**13**) was brominated at the 5,5 positions of thiophene units using NBS in a CHCl$_3$/AcOH solvent mixture to obtain the desired product 2,7-bis(5-bromothiophen-2-yl)-9,9-di-n-octylfluorene (**14**) in a high yield. Using a ratio of NBS:**13** of 1.98:1 eliminated concerns about the formation of tri and tetra brominated compounds that are difficult to be separate from the desired product. The mechanism for this reaction follows the same route as that presented in (Scheme 2-4 -Chapter 2).
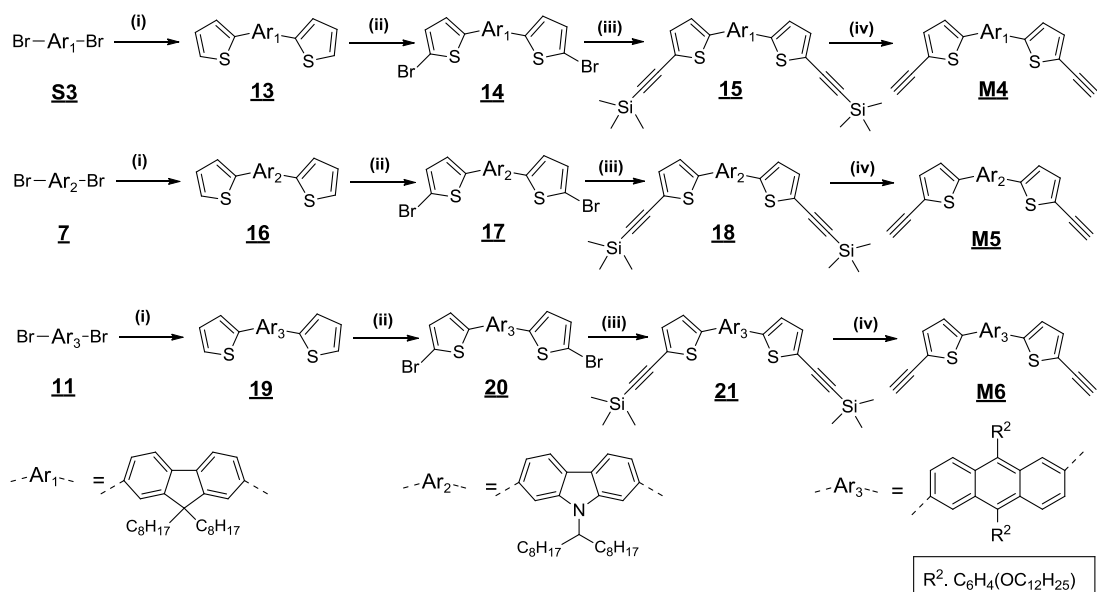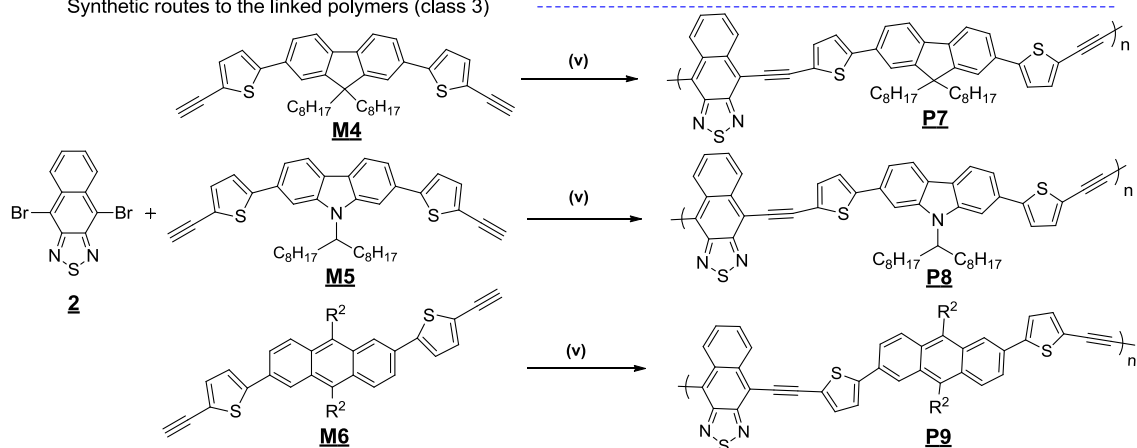
(i) $Pd_2(dba)_3$, P(o-tolyl)$_3$, $C_{16}H_{30}SSn$, CB, reflux. **(ii)** NBS, AcOH, CHCl$_3$. **(iii)** Pd(PPh$_3$)$_2$Cl$_2$, CuI, trimethylsilyl acetylene, diisopropylamine, toluene, reflux. **(iv)** KOH, THF, MeOH. **(v)** Pd(PPh$_3$)$_2$Cl$_2$, CuI, diisopropylamine, THF, toluene, reflux.

Scheme 3-9: The synthetic route to polymers and their monomers, conditions and reagents.

The following steps involved a Sonogashira reaction of dibromide **14** and trimethylsilyl acetylene using Pd/Cu catalyst and base to afford compound **15**. The crude product was purified *via* silica gel column chromatography to afford the desired product **15** in a high yield (85 %). The catalytic cycle for the Sonogashira reaction is depicted in (Scheme 1-5- Chapter 1). Compound **15** was then treated with potassium hydroxide solution in THF at room temperature. The resulting deprotected product **M4** was extracted with DCM, washed with water and dried to afford a brown coloured product. The mechanism for this cleavage reaction is presented above in Scheme 3-2.

M5 and **M6** were synthesised through similar steps, conditions and mechanisms as **M4**. The chemical structures of the resulting monomers were confirmed by ^{1}H NMR, as

described in supporting information, ^{13}C NMR, mass spectrometry and elemental analysis.

Polymerisations of **2** with respectively, **M4**, **M5**, and **M6** by the Sonogashira coupling reaction yielded PFDTENT-**P7**, PCDTENT-**P8** and PPADTENT-**P9**. These polymerisations were carried out with Pd/CuI as the catalyst precursors and mixed anhydrous solvents THF/toluene/diisopropylamine as the reaction media under inert atmosphere. All polymerisations were left for 1 hour or less with large quantities of the polymers that precipitated from the reaction media. The obtained crude polymers were separated by precipitation in methanol. They were then purified through Soxhlet extraction using different common organic solvents including methanol, acetone, hexane, toluene, CHCl$_3$ and chlorobenzene. Similarly to the previous class of polymers (class 2), only 15- 20 % of the resulting polymers was soluble in their toluene and chloroform fractions that can be able to processed for electronic applications. It can be noted that large amounts of resulting polymers remained as intractable materials in the Soxhlet thimbles. The low solubilities of these polymers explain the low yields of tractable materials from these polymers. The chemical structures of the obtained polymers were confirmed by ^{1}H NMR (Supplementary information) and elemental analysis. It is perhaps worth noting that the elemental analysis values for some monomers synthesised and class 2 and 3 polymers deviate from the expected values. This can be ascribed to the incomplete combustion of these polymers during analysis due to strong solvent retention inside polymer structure which effects on degradation reactions.[35] Details of the synthesis of the monomers, polymers and their characterisation are described in the experimental section.

GPC analysis using TCB as the eluent was undertaken against polystyrene standards at 140 °C. The GPC data of the three polymers **P7-P9** displays moderate molecular weights (Table 3-2). The M_n values of the toluene fractions of PFDTENT-**P7**, PCDTENT-**P8** and PPADTENT-**P9** are 11,500, 8,700 and 10,400 Da, respectively. The low yield of the resulting polymers (class 3 polymers) (20% yields or less) and their low solubilities are probably due to the incorporation of ethynylene units over the polymer chains which leads to their aggregation. This is a result of the planarity of the main chains of polymers, leading to low molecular weights in these materials as a result. The GPC results of these polymers (class 3) are in a good agreement with their ethynylene counterparts (class 2) that are considered as moderate molecular weights.

Table 3-2: A summary of the GPC data and yield for PFDTENT-**P7**, PCDTENT-**P8** and PPADTENT-**P9**.

Polymer	Fraction	Yield %	M_n (Da) [a]	M_w(Da) [a]	PDI [b]
P7	toluene	17	11,500	29,700	2.5
P8	toluene	16	8,700	17,000	1.9
P9	toluene	12	10,400	23,300	2.2
	chloroform	08	11,300	20,600	1.8

[a] Measurements conducted on the toluene and chloroform fractions of polymers using a differential refractive index (DRI) detection method. [b] Polydispersity index.

3.2.2 Optical properties

The optical properties of the polymers were measured in dilute chloroform solutions (Figure 3-2) and in thin films. The optical spectra in the solid state are presented in Figure 3-3. The results for both classes of polymers (class 2 and 3) are presented in Table 3-3. All resulting polymers displayed the same absorption pattern in their spectra. It can be seen that UV-vis absorption spectra of the polymers in the solid state exhibit two main distinct absorption bands in the region from (300-410 nm) and (460-700 nm). The shorter wavelength absorption peaks correspond to π-π* transitions of the conjugated structure of polymers. The absorption bands at longer wavelength can be attributed to the intramolecular charge transfer (ICT) bands between the donor and acceptor moieties along the D-A polymer backbones. Dilute solutions of ethylene-based polymers (class 2) (Figure 3-2-a) PFDENT-**P4**, PCDENT-**P5** and PPADENT-**P6** display ICT absorption bands at 585, 592 and 600 nm, respectively. When fabricated in films (Figure 3-3-a), the bands are red-shifted and observed at 608, 613 and 670 nm for PFDENT-**P4**, PCDENT-**P5** and PPADENT-**P6**, respectively. The bathochromic shift is mostly attributed to the ordered packing of polymer chains as well as their aggregation in the solid state.[36,37]

The optical bandgaps of ethynylene-based polymers (Table 3-3), as calculated from the onset of absorption wavelengths in solid films, were estimated to be 1.83, 1.81 and 1.67 eV for PFDENT-**P4**, PCDENT-**P5** and PPADENT-**P6**, respectively. Interestingly, PPADENT-**P6** in thin film is red-shifted up to 650 nm. While the values of absorption maxima of PFDENT-**P4** and PCDENT-**P5** is limited to (~610 nm). This can be explained by the fact that the backbone of polymer PPADENT-**P6** possesses a more

extended electronic delocalisation structure on anthracene moieties on **P6** compared to other donor moieties in other polymers. It is assumed that the anthracene-based polymer (PPADENT-**P6**) is able to provide a more planar arrangement of its polymer chains in the solid state (probably due to better π–π stacking) in comparison to its fluorene and carbazole counterparts (PFDENT-**P4** and PCDENT-**P5**), given the similar absorption wavelengths of all three polymers in solution but a larger difference of their absorption maxima in the solid state. This provides a lower optical bandgap for PPADENT-**P6** and increased ICT along its polymer chains. Furthermore, PPADENT-**P6** shows a shoulder peak at (~447 nm), indicating a high degree aggregation and intermolecular interactions of polymer main chains. The bandgap of PCDENT-**P5** (1.81 eV) is lower than for PFDENT-**P4** (1.83 eV). This can be attributed to the better electron donating properties of carbazole repeat units when compared to fluorene units, resulting in a more D-A character and low optical bandgap.

Table 3-3: A summary of absorption in solution and in films and HOMO and LUMO levels of the polymers.

Polymer	λ_{max} solution (nm)	ε [a] (M^{-1} cm^{-1})	λ_{max} film (nm)	$E_{g\ opt}$ [b](eV)	HOMO [c] (eV)	LUMO [d] (eV)
Class 2						
P4	585	29,600	608	1.83	-5.58	-3.59
P5	592	30,000	613	1.81	-5.55	-3.54
P6	600	42,500	670	1.67	-5.39	-3.68
Class 3						
P7	590	30,800	614	1.71	-5.46	-3.60
P8	599	31,400	620	1.68	-5.37	-3.59
P9	613	44,700	702	1.54	-5.32	-3.55

[a] Absorption coefficient measured at λ_{max} = 350 nm for **P6** and 375 nm for **P4** and **P5**, λ_{max} = 373 nm for **P9** and 402 nm for **P7** and **P8** in chloroform solutions. [b] Optical bandgaps determined from the onset of UV-vis absorption spectra on solid films. [c] HOMO position (*vs vacuum*) determined from the onset of oxidation. [d] LUMO position (*vs vacuum*) determined from the onset of reduction.

To ascertain the effect of ethynylene units on the optical properties of polymers, a further comparison was conducted between ethynylene-based polymers (class 2) and their thiophene analogues discussed in Chapter 2- P. 52-53. The intensity of (ICT) bands of PFDENT-P**4**, PCDENT-**P5** and PPADENT-**P6** are more pronounced relative to their thiophene equivalent polymers, PFDTNT-**P1**, PCDTNT-**P2** and PPADTNT-**P3**

(Chapter 2- P 53-54); suggesting that incorporation of acetylene-spacers instead of thiophene repeat units next to the NT units reduces steric hindrance between these and adjacent units and enhance intramolecular charge transfer and π-overlap as well as the planarity of polymer chains. As a result, the absorption maxima for PFDENT-**P4** and PCDENT-**P5** and PPADENT-**P6** are red-shifted compared to their analogous, PFDTNT-**P1**, PCDTNT-**P2** and PPADTNT-**P3**. This would extend the absorption spectrum of the polymers synthesised although the presence of acetylene units may localise π-electron wave function on ethynylene spacers, thus, this decreases the electronic delocalisation between the electron acceptor and donor segments.[23]

Figure 3-2: Normalised UV-vis absorption spectra of resulting polymers, (a) ethynylene-based polymers, (b) ethynylene-thiophene based polymers in chloroform solutions.

The optical bandgap of PPADENT-**P6** was estimated to be 1.67 eV, which is lower than that of its thiophene counterpart, PPADTNT-**P3** (1.75 eV). However, the optical bandgap of PFDENT-**P4** and PCDENT-**P5** were calculated to be 1.83 and 1.81 eV, respectively. These bandgap values are wider than their polymer analogous, PFDTNT-

P1 and PCDTNT-**P2** (1.76, 1.74 eV, respectively), despite having broader absorption spectra. Incorporation of acetylene units in fluorene and carbazole-based alternate polymers (PFDENT-**P4** and PCDENT-**P5**) display red-shifted absorption maxima compared to those of their analogous polymers, PFDTNT-**P1** and PCDTNT-**P2**. However, it does not result in a lower optical bandgap. This can be attributed to the presence of acetylene units in the polymer chains, which adopt ordered structures and would show sharper absorption peaks owing to improved electronic delocalisation.

The absorption maxima of PFDTENT-**P7**, PCDTENT-**P8** and PPADETNT-**P9** in the solid state (Figure 3-3-b) are located at 614, 620 and 702 nm, respectively. The red-shifted spectra from solution to solid state can be attributed to more planar structures in films. The optical bandgaps (E_g) of PFDTENT-**P7**, PCDTENT-**P8** and PPADETNT-**P9** from these spectra are estimated to be 1.71, 1.68 and 1.54 eV. The lowest optical bandgap for PPADETNT-**P9** indicates a more extended electronic delocalisation on the anthracene-donor moieties compared to other donor units of the polymers, PFDTENT-**P7**, PCDTENT-**P8**. Interestingly, PPADETNT-**P9** displays shoulder absorption peaks in solution and solid state. We tentatively ascribe this to pure vibrational-electronic transitions. It is assumed that the anthracene-based polymer PPADETNT-**P9** is able to provide a more planar arrangement of its polymer chains in the solid state due to better $\pi-\pi$ stacking in comparison to its fluorene and carbazole counterparts (PFDTENT-**P7** and PCDTENT-**P8**), given the similar absorption wavelengths of all three polymers in solution but a larger difference of their absorption maxima in the solid state (Table 3-3). The same observation was made on comparing the optical properties of polymers of class 2, and where anthracene-based polymer PPADENT-**P6** has much extended electronic delocalisation than its carbazole and fluorene-based polymers PFDENT-**P4** and PCDENT-**P5**.
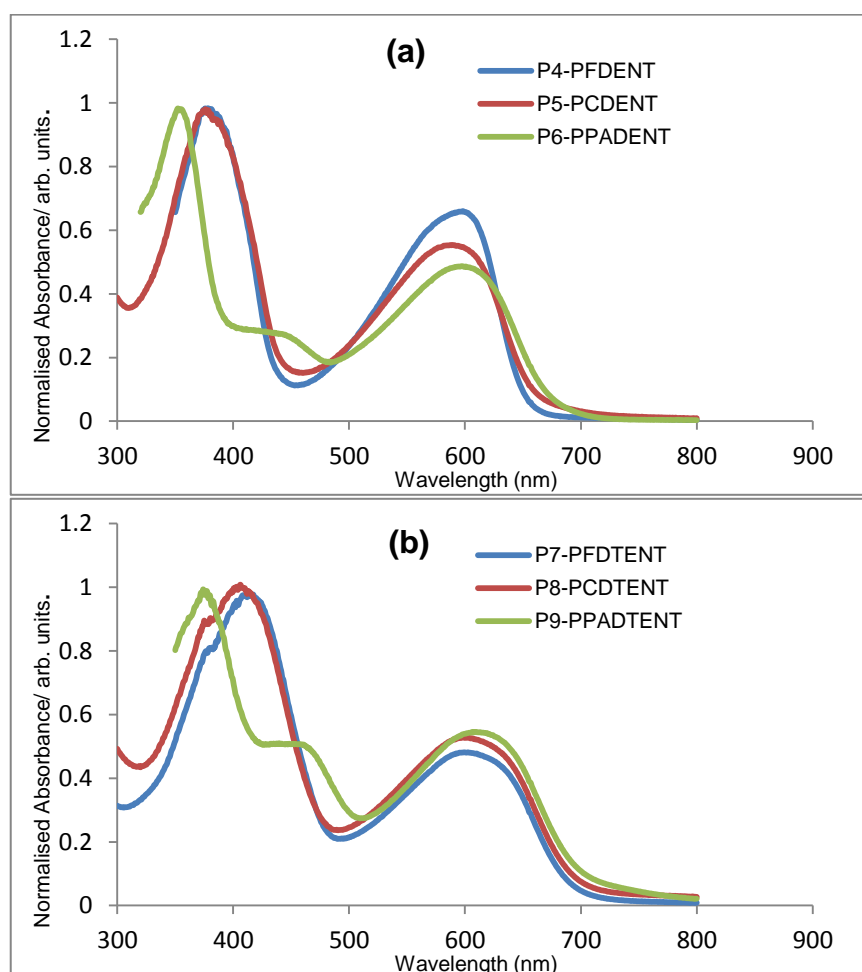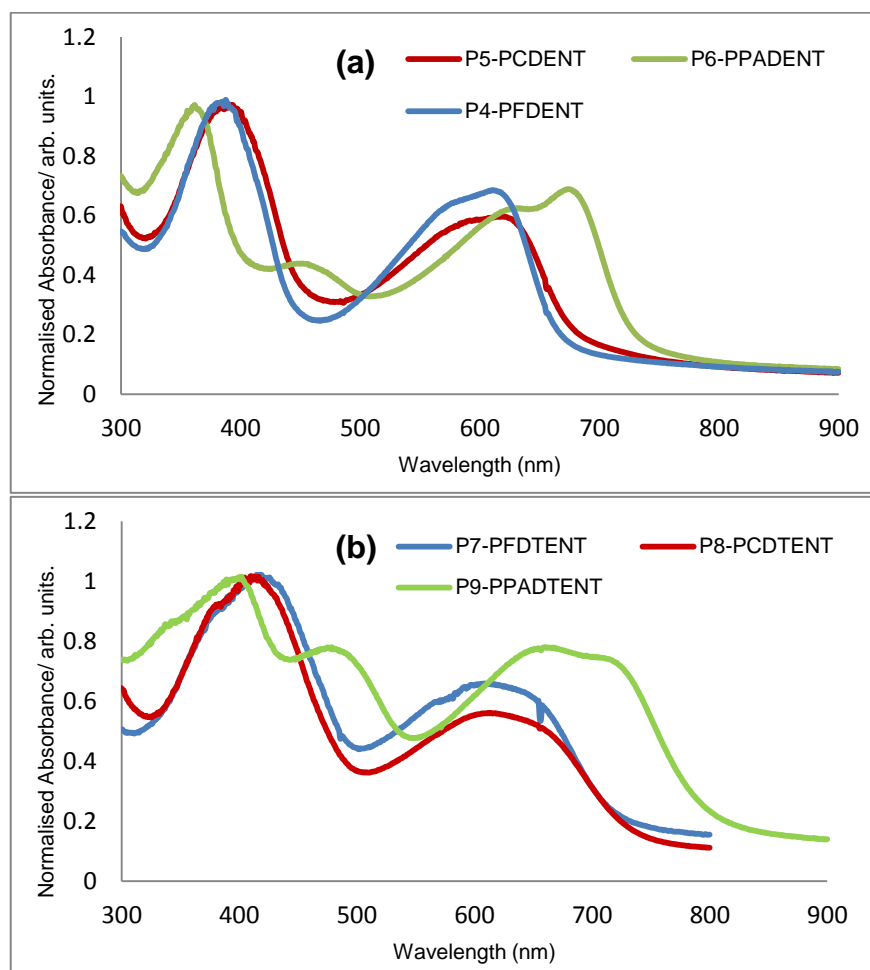
Figure 3-3: Normalised UV-vis absorption spectra of resulting polymers, (a) ethynylene-based polymers, (b) ethynylene-thiophene based polymers in solid films

The ethynylene-thiophene based polymers, PFDTENT-**P7**, PCDTENT-**P8** and PPADETNT-**P9** (class 3) display red-shifted absorption maxima and reduced bandgaps, relative to their respective analogous, PFDENT-**P4**, PCDENT-**P5** and PPADENT-**P6** (class 2). The absorption maxima of the anthracene-based polymer PPADTENT-**P9** (702 nm) is red-shifted relative to that of its anthracene analogue PPADENT-**P6** (670 nm). The optical bandgap of PPADTENT-**P9** is 0.13 eV lower than its analogue, PPADENT-**P6**.

Another example, PCDTENT-**P8**, which has carbazole as donor moiety, has lower bandgap (E_g = 1.68 eV) relative to its carbazole analogue polymer PCDENT-**P5** (E_g = 1.81 eV). It is speculated that the absorption maxima of class 3 polymers, which have ethynylene-thiophene linkers, are higher than their ethynylene counterparts (class 2) owing to incorporation of additional thiophene units in the polymer chains. The additional electron rich thiophene units leads to overall stronger electron donating segments in class 3 polymers compared to class 2 polymers and as a result of stronger

ICT along polymer chains resulting in reduced bandgaps. A recent study by Ozel *et al.* has shown that incorporation of phenylene-acetylene units as spacers in D-A polymers does not add any extension of π-conjugation over polymer chains; suggesting that how the electron donating properties of thiophene are key in leading to the reduction of the band gaps of class 3 polymers compared to class 2 polymers.[38]

The absorption coefficients of all resulting polymers (class 2, 3) in chloroform solutions are in the range 2.9×10^4 to 4.4×10^4 and all data are presented in Table 3-3. Clearly, the molar absorption of polymers with ethynylene-thiophene units is slightly higher compared to their ethynylene counterparts. This is probably because the electron donating ability of donor moieties into polymers (class 3) is stronger than their corresponding polymers without thiophene units.

3.2.3 Electrochemical properties

The electrochemical behaviour of the polymers was investigated by cyclic voltammetry (CV). The measurements were conducted using drop-cast polymer films in acetonitrile solutions with tetrabutylammonium perchlorate as an electrolyte. The cyclic voltammograms are presented in Figure 3-4. They show that most polymers present irreversible oxidation peaks and reversible reduction potential peaks.

Details of the measurements are given in the experimental section. The frontier energy levels (*vs. vacuum*) of the polymers were calculated from their first onset of oxidation and reduction waves as summarised in Table 3-3.

In the series of polymers (class 2), the potentials of first onsets of oxidation waves were estimated to be at 0.86, 0.83 and 0.67 V for PFDENT-**P4**, PCDENT-**P5** and PPADENT-**P6**, respectively, which correspond to HOMO energy levels of -5.58, -5.55 and -5.39 eV, respectively. The onsets of reduction potentials for PFDENT-**P4**, PCDENT-**P5** and PPADENT-**P6** were observed at -1.13, -1.18 and -1.04 V respectively and corresponding to LUMO energy levels of -3.59, -3.54 and -3.68 eV, respectively. Obviously, PPADENT-**P6** with HOMO energy level (-5.39 eV) and LUMO energy level (-3.68 eV) displays less-positive oxidation and less-negative reduction potential compared to the other two polymers. The shallower HOMO level of PPADENT-**P6**, relative to both PFDENT-**P4**, PCDENT-**P5**, is a result of the increased electronic delocalisation in the anthracene-based polymer compared to the fluorene and carbazole-based polymers. Moreover, it can be seen from Table 3-3 that the change of

the electron donor moieties impacts the LUMO energy levels of this series of polymers to a greater extent. The LUMO level of PPADENT-**P6** is deeper than the other two polymers in this series of polymers, despite all polymers having the same electron acceptor moiety. It is speculated that varying the electronic properties of donating ability of donor units can also disturb the electron accepting nature of the polymer main chains in this series.

Comparison of the electrochemical properties of ethynylene-based polymers (class 2) to those of their corresponding thiophene-based polymers (class 1- Chapter 2), revealed that the ethynylene-based polymers have lower lying HOMO energy levels relative to the thiophene-based polymers. Indeed thiophene-based polymers, PFDTNT-**P1**, PCDTNT-**P2** and PPADTNT-**P3** (Chapter 2- P 55) display HOMO/LUMO level of -5.36/-3.50 eV, -5.34/-3.44 eV and -5.40/-3.47 eV, respectively. As observed for example by comparing PFDENT-P**4** and its thiophene-analogue PFDTNT-**P1**. The HOMO of the ethynylene polymer PFDENT-P**4** is -5.58 eV while the HOMO of its thiophene counterpart, PFDTNT-**P1** is -5.36 eV. It is hypothesised that the acetylene linkers on polymer chains in class 2 polymers, which incorporate sp-hybridised carbons, have a weakly electron withdrawing character when compared to the electron rich thiophene units on the polymer chains in class 1 polymers, which explains the shallower HOMO energy levels of the thiophene-based polymers. This is consistent with previous literature reported that has shown decreased HOMO and LUMO energy levels with incorporation of acetylene units over the polymer main chain.[25] These findings indicates how the incorporation of ethynylene units induces intermolecular interactions and increase the planarity of the polymer chains while changing the electronic properties of this series of the resulting polymers and increasing their electrochemical energy bandgaps.

The frontier HOMO energy levels (*vs vacuum*) of PFDTENT-**P7**, PCDTENT-**P8** and PPADTENT-**P9**, as calculated from the onset of oxidation waves, were estimated to be at -5.46, -5.37 and -5.32 eV while the corresponding LUMO energy levels were determined to be at -3.60, -3.59 and -3.55 eV, respectively. Notably, the anthracene-based polymer PPADTENT-**P9** displays the shallowest HOMO energy level (closest to the *vacuum* level) compare to the other two polymers in the class 3 series of polymers; a consequence of more enhanced electronic conjugation compared to the fluorene and carbazole-based polymers.
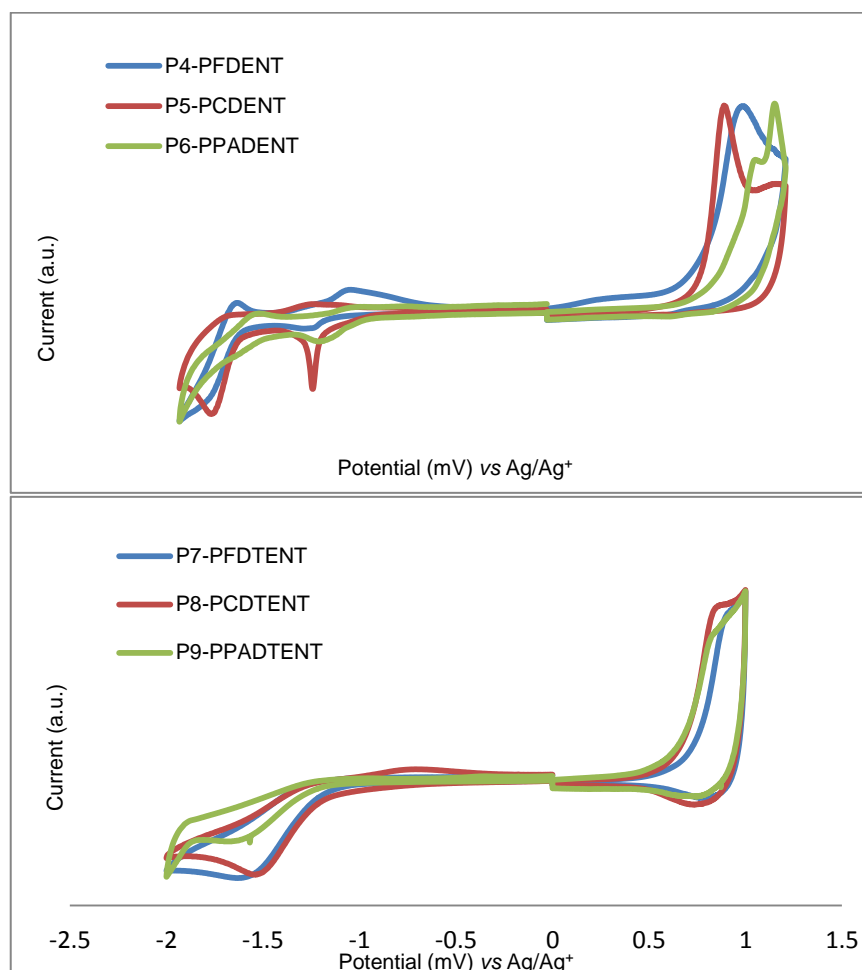
Figure 3-4: Cyclic voltammetry curves of polymers (class 2 and 3) in 0.1 M a solution of tetrabutylammonium percolate with acetonitrile at a scan rate of 100 mV s^{-1} under argon atmosphere.

A comparison of the electrochemical properties (Table 3-3) of the resulting polymers (class 3), PFDTENT-**P7**, PCDTENT-**P8** and PPADTENT-**P9** with their ethynylene analogues (class 2) reveals considerable increasing of the HOMO energy levels of the ethynylene-thiophene based polymers, resulting in lower bandgap polymers when compared to their ethynylene counterparts. It is believed that incorporation of thiophene units as electron-donating units in the main chain of conjugated polymers is responsible for lifting the HOMO energy levels of the resulting polymers in this series (class 3), upon increasing the electron donating ability of the donor segments on the polymer chains. Eventually, this leads to the decreased bandgap polymers. As an example, the HOMO energy level of ethynylene-thiophene based polymer PCDTENT-**P8** is -5.37 eV while its ethynylene counterpart has a HOMO energy level at -5.55 eV. These results indicated that how the combined thiophene units could increase the electron donating ability on donor moieties of polymer chains, leading to change the positions of HOMO energy levels.

3.2.4 Thermal properties

The thermal properties of the resulting polymers were measured by thermogravimetric analysis (TGA) (Figure 3-5). The TGA curves (a) indicate that the ethynylene-based polymers have thermal stability with decomposition temperatures, defined as the 5% weight-loss temperature, T_d above 300 °C in a N_2 atmosphere at heating rate of 10 °C/min, suggesting their excellent thermal stability. The first onset of thermal degradation temperatures for PFDENT-**P4**, PCDENT-**P5** and PPADENT-**P6** were determined to be respectively at 328 °C, 316 °C and 303 °C. For all polymer synthesised in this series, the first weight loss in the degradation can be attributed to elimination of alkyl and alkoxy substituents from the electron donor moieties in the conjugated polymers. Above 500 °C, degradation of the polymer chains follows with a total weight loss of 94%, 96% and 94%, respectively for PFDENT-**P4**, PCDENT-**P5** and PPADENT-**P6**, that is observed when temperature above 590 °C. These results indicated that PPADENT-**P6** displays a high thermal stability with one step degradation, while PFDENT-**P4** and PCDENT-**P5** exhibited the same thermal profile with two main step degradation processes. It is theorised that the different thermal behaviours of this series of polymer (class 2) correspond to varying electron donor moieties over the polymer main chains.

These findings indicated that the thermal stabilities of the ethynylene-based polymers are adequate for their application in solar cells and other electronic devices. It can be noted that the thiophene-based polymers PFDTNT-**P1**, PCDTNT-**P2** and PPADTNT-**P3** synthesised (Chapter 2- P 56-57), exhibited higher decomposition temperature (~ 400 °C) relative to their ethenylene analogues, PFDENT-**P4**, PCDENT-**P5** and PPADENT-**P6** (class 2). We speculate that the high molecular weight of thiophene-based polymers (class 1) decreased the molecular mobility and promotes chain entanglements, resulting in increased degradation temperature of polymers. These results are consistent with previous studies that show the relationship between molecular weight of polymers and degradation kinetics.[39]
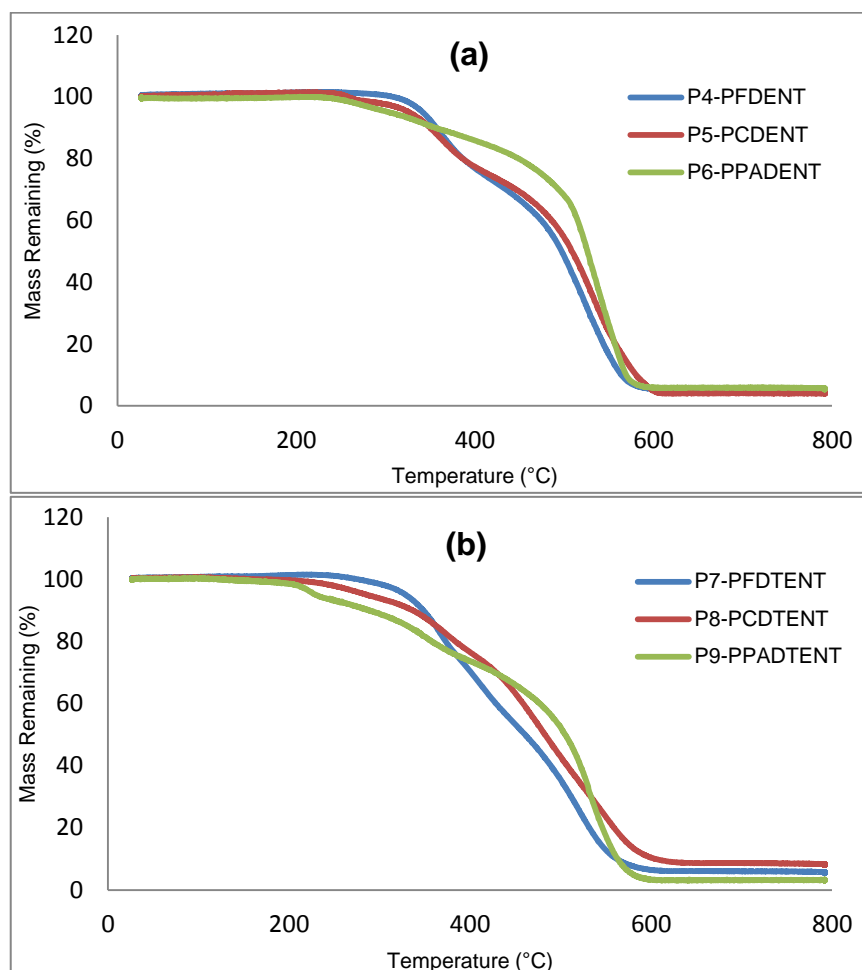
Figure 3-5: (TGA) plots of ethynylene (a) and ethynylene-thiophene (b) linked
polymers with a heating rate of 10 °C/min under N_2.

Figure 3-5, (b) shows the TGA curves of the thermal degradation of the ethynylene-
thiophene based polymers (class 3). TGA analysis of PFDTENT-**P7**, PCDTENT-**P8**
and PPADTENT-**P9** revealed that all polymers display moderate thermal stabilities
with decomposition temperature (T_d) above 230 °C. The T_d values were determined to
be respectively at 329 °C, 285 °C and 230 °C. For all polymers, the first step in the
degradation is observed ranging from 230 °C to 500 °C, corresponding to the
elimination of alkyl and alkoxy chains from the electron donor moieties of the
polymers. Decomposition of the polymer chains follows with a total loss of 94%, 91%
and 97% respectively for PFDTENT-**P7**, PCDTENT-**P8** and PPADTENT-**P9** that is
observed when the temperature is above 550 °C.

The thermal results of all synthesised polymers confirm that the polymers possess good
thermal properties. Compared with the ethynylene counterparts (class 2), ethynylene-
based polymers (class 2) undergo degradation at higher temperature compared to their

ethynylene-thiophene counterparts. No further comparison can be drawn between ethynylene polymers and their analogues because of a lack of thermal analysis reported.

3.2.5 Powder x-ray diffraction studies

Figure 3-6 displays powder X-ray diffractions (XRD) of all resulting polymers. The XRD profile was studied to examine the molecular packing of polymer chains. PFDENT-**P4**, PCDENT-**P5** and PPADENT-**P6** displayed broad peaks in the wide-angle region respectively at 2θ values of 19.95, 20.02 and 20.39°, corresponding to distances of 4.45, 4.43 and 4.35 Å, respectively. These broad peaks in this area revealed that ethynylene-based polymers adopt amorphous structures in solid states. However, PPADENT-**P6** exhibited a more ordered molecular packing *via* more pronounced peak, which appeared in wide-angle region with a distance of 4.35 Å compared to the other two polymers**.** It is assumed that there is improved π–π stacking between the main chains of **P6** as a consequence of the intermolecular interactions brought about by using planar anthracene-donor moieties. Generally, these results are consistent with previous results in the literature concerning the effect of ethynylene-spacers on the packing of polymer chains.[40]

In comparison, it is interesting to compare the XRD studies of ethynylene-based polymers in this series (class 2) and their thiophene analogous polymer synthesised (Chapter 2- P 58). PFDTNT-**P1**, PCDTNT-**P2** and PPADTNT-**P3** did not show any pronounced diffraction peaks in this wide-angle region compared to PFDENT-**P4**, PCDENT-**P5** and PPADENT-**P6**. We speculate that incorporation of acetylene units along the main chains of polymers slightly promote the packing of polymer chain *via* improving the coplanar interactions owing to decreased torsion angle between the electron donor and acceptor moieties.
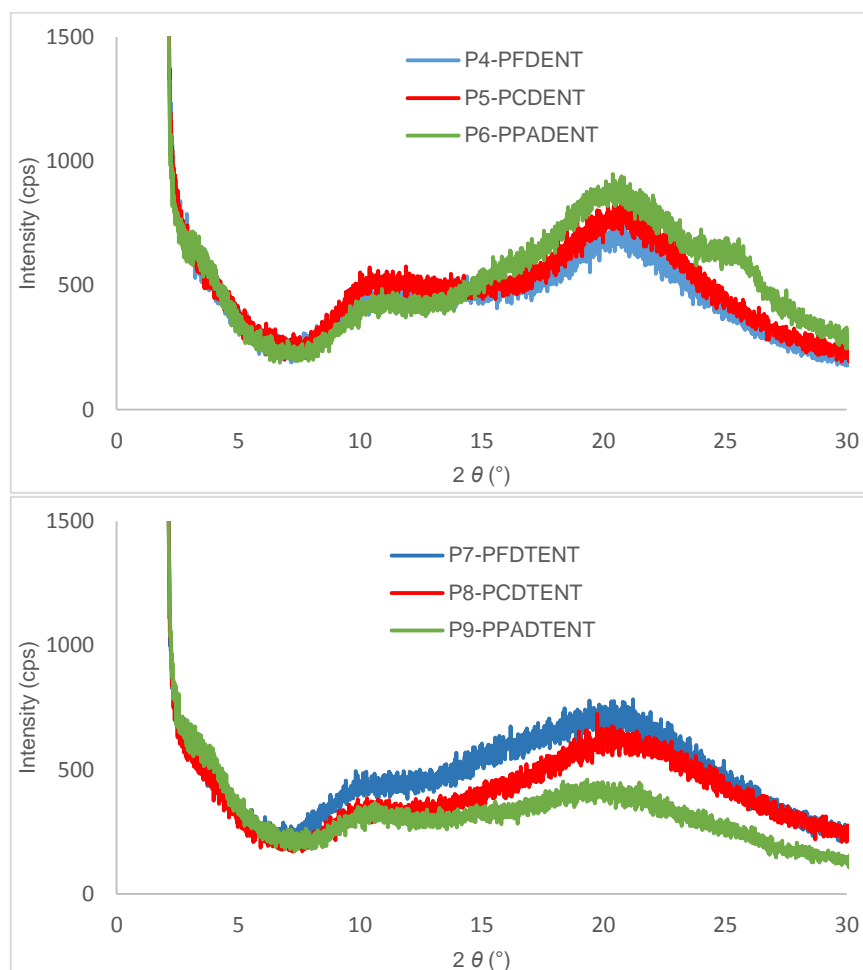
Figure 3-6: Powder (XRD) patterns of PFDENT-**P4**, PCDENT-**P5**, PPADENT-**P6**, PFDTENT-**P7**, PCDTENT-**P8** and PPADTENT-**P9**.

Powder XRD pattern of ethynylene-thiophene based polymers (class 3) revealed that the broad peaks of PFDTENT-**P7**, PCDTENT-**P8** and PPADTENT-**P9** appeared respectively at values of 20.51, 20.58 and 20.11°. A comparison with the ethynylene analogue polymers synthesised, PFDENT-**P4**, PCDENT-**P5** and PPADENT-**P6** indicate a little change in the XRD pattern. However, the ethynylene counterparts (class 2) show more pronounced peaks in the wide-angle region compared to thiophene-ethylene based polymers (class 3). It is assumed that incorporation thiophene-spacers with ethynylene results in an increased torsion angle and therefore, an indication of the polymers amorphous conformations. Unfortunately, further comparison cannot be drawn owing to a lack of XRD studies reported as supporting evidence.

3.3 Conclusion

In this chapter, two series of acetylene-based polymers were synthesised using Sonogashira coupling reactions. The first series of conjugated polymers PFDENT-**P4**, PCDENT-**P5** and PPADENT-**P6** contains ethynylene units positioned between 2,1,3 naphthothiadiazole (NT) repeat units as electron acceptor moieties and 2,7-linked fluorene, 2,7-linked-carbazole or 2,6-linked anthracene alternate units as electron donor moieties. Their optical, electrochemical, thermal and chemical structures were investigated. Clearly, the ethynylene-based polymers were obtained in low yields as they have low solubilities in common organic solvents. We tentatively attribute this low solubility to the incorporation of acetylene-spacers over the polymer main chains, which results in aggregation of polymer chains and formation much rigid polymers. PPADENT-**P6** displays the lowest optical bandgap (1.67 eV) in this series of alternating polymers with ethynylene linkers. This is probably due to the extension of the conjugation length of the 9,10-functionilised anthracene polymer compared to fluorene and carbazole-based polymers. The HOMO/LUMO frontier energy levels of PFDENT-**P4**, PCDENT-**P5** and PPADENT-**P6** were estimated to be -5.58/-3.59 eV, -5.55/-3.54 eV and -5.39/-3.68 eV, respectively. It can be seen that the change of the electron donor repeat units in this series of polymers affects the HOMO energy levels of the polymers to good extent. PFDENT-**P4** displayed the deepest HOMO level in this series; suggesting that the fluorene repeat unit is the weakest electron donor unit relative to the other two donor moieties (carbazole and anthracene repeat units).

The properties of this series of polymers (class 2) were compared with the first series of polymers described in Chapter 2 of this thesis (class 1), and which have thiophene linkers between NT repeat units and donor units to ascertain the effects of the acetylene units on the properties of the resulting polymers. UV-visible absorption spectroscopy revealed that (ICT) bands of PFDENT-**P4**, PCDENT-**P5** and PPADENT-**P6** are more pronounced and red-shifted when compared to their thiophene analogues polymers (Chapter 2), PFDTNT-**P1**, PCDTNT-**P2** and PPADTNT-**P3.** It is believed that the insertion of acetylene π-linkers along the D-A polymers reduces the steric hindrance between electron accepting naphthothiadiazole repeat units and electron donors repeat units. This increases their aggregation and planarity due to promoting π-π interactions. Despite ethynylene-based polymers exhibiting a red-shifted and vibrational structure compared to their thiophene analogues, the optical bandgaps of this series are larger

with the exception of PPADENT-**P6**. This is attributed to the electronic effect of ethynylene spacers as weak electron withdrawing units, which may decrease the pull-push character and ICT over polymer chains. The HOMO energy levels of ethynylene-based polymers are deeper compared to their thiophene analogous polymers synthesised (class 1). It is ascribed that the incorporation of ethynylene units as weak electron acceptor units in the polymer chains instead of thiophene as electron donating units results in lowering the HOMO energy levels of the resulting polymers; a result of decreasing the electron donating ability of donor units along the polymer chains. The thermal properties were studied *via* TGA and showed that ethynylene-based polymers possess good thermal stability with decomposition temperature in excess of 300 °C. X-ray diffraction studies revealed that PFDENT-**P4**, PCDENT-**P5** and PPADENT-**P6** exhibit a certain degree of molecular ordering as a result of π–π stacking.

The second series of polymers described in this chapter (class 3) includes three alternating polymers, comprising ethynylene-thiophene spacers between 2,1,3 naphthothiadiazole (NT) electron accepting units and functionalised-fluorene, carbazole or anthracene electron donor alternate moieties. The novel conjugated polymers were synthesised *via* the Sonogashira coupling reactions to yield this series of polymers, PFDTENT-**P7**, PCDTENT-**P8** and PPADTENT-**P9**. The resulting polymers were obtained in low yields as they have low solubilities and as result have moderate molecular weights which are comparable in their values to those of their ethynylene analogous polymers (class 2). Unsurprisingly, UV-visible absorption spectroscopy showed that PPADTENT-**P9** showed the lowest optical bandgap in this series of polymer at value of 1.54 eV, which is expected to be efficient in harvesting solar light in bulk heterojunction devices. The optical bandgaps of this series of polymers (class 3) are lower compared to their corresponding ethynylene counterparts (class 2). We hypothesised that this is a result of incorporation of additional thiophene as electron donor units over the main chains of polymers, which increases delocalisation and the donating ability of the donor segments on the resulting polymers, resulting in the reduced bandgaps of polymers. TGA measurement revealed that ethynylene-thiophene based polymers have low onset of decomposition compared to their ethynylene counterparts. X-ray diffraction patterns revealed that PFDTENT-**P7**, PCDTENT-**P8** and PPADTENT-**P9**.showed broad and weak peaks in ranging of (15-25 °), an indication the polymers possessed an amorphous structure in solid state.

References

1.   H. Zhou, L. Yang and W. You, *Macromolecules*, 2012, **45**, 607-632.

2.   C. J. Brabec, *Solar Energy Materials and Solar Cells*, 2004, **83**, 273-292.

3.   R. Service, *Science (New York, NY)*, 2011, **332**, 293.

4.   G. Yu, J. Gao, J. C. Hummelen, F. Wudl and A. J. Heeger, *Science-AAAS-Weekly Paper Edition*, 1995, **270**, 1789-1790.

5.   S. Günes, H. Neugebauer and N. S. Sariciftci, *Chemical Reviews*, 2007, **107**, 1324-1338.

6.   A. Banerji, M. W. Tausch and U. Scherf, *Educación Química*, 2013, **24**, 17-22.

7.   R. Tipnis, D. Laird and M. Mathai, *Material Matters*, 2008, **3**, 92-96.

8.   M. K. Siddiki, J. Li, D. Galipeau and Q. Qiao, *Energy & Environmental Science*, 2010, **3**, 867-883.

9.   A. Yassar, F. Garnier, H. Jaafari, N. Rebiere-Galy, M. Frigoli, C. Moustrou, A. Samat and R. Guglielmetti, *Applied Physics Letters*, 2002, **80**, 4297-4299.

10.   P. M. Beaujuge and J. R. Reynolds, *Chemical Reviews*, 2010, **110**, 268-320.

11.   R. S. Ashraf, I. Meager, M. Nikolka, M. Kirkus, M. Planells, B. C. Schroeder, S. Holliday, M. Hurhangee, C. B. Nielsen and H. Sirringhaus, *Journal of the American Chemical Society*, 2015, **137**, 1314-1321.

12.   J. Kim, M. H. Yun, G.-H. Kim, J. Lee, S. M. Lee, S.-J. Ko, Y. Kim, G. K. Dutta, M. Moon and S. Y. Park, *ACS Applied Materials & Interfaces*, 2014, **6**, 7523-7534.

13.   I. Osaka, *Polymer Journal*, 2015, **47**, 18-25.

14.   M. Wang, X. Hu, P. Liu, W. Li, X. Gong, F. Huang and Y. Cao, *Journal of the American Chemical Society*, 2011, **133**, 9638-9641.

15.   L. Zhang, K. Pei, M. Yu, Y. Huang, H. Zhao, M. Zeng, Y. Wang and J. Gao, *The Journal of Physical Chemistry C*, 2012, **116**, 26154-26161.

16.   S. H. Park, A. Roy, S. Beaupre, S. Cho, N. Coates, J. S. Moon, D. Moses, M. Leclerc, K. Lee and A. J. Heeger, *Nature Photonics*, 2009, **3**, 297-302.

17.   S. L. Hsu, C. M. Chen and K. H. Wei, *Journal of Polymer Science Part A: Polymer Chemistry*, 2010, **48**, 5126-5134.

18.   S. Zhang, H. Fan, Y. Liu, G. Zhao, Q. Li, Y. Li and X. Zhan, *Journal of Polymer Science Part A: Polymer Chemistry*, 2009, **47**, 2843-2852.

19.   Q. T. Zhang and J. M. Tour, *Journal of the American Chemical Society*, 1998, **120**, 5355-5362.

20. R. Kroon, M. Lenes, J. C. Hummelen, P. W. Blom and B. De Boer, *Polymer Reviews*, 2008, **48**, 531-582.

21. Y. Zhang, S.-C. Chien, K.-S. Chen, H.-L. Yip, Y. Sun, J. A. Davies, F.-C. Chen and A. K.-Y. Jen, *Chemical Communications*, 2011, **47**, 11026-11028.

22. T. Umeyama, Y. Watanabe, E. Douvogianni and H. Imahori, *Journal of Physical Chemistry C*, 2013, **117**, 21148-21157.

23. B. Liu, W.-L. Yu, J. Pei, S.-Y. Liu, Y.-H. Lai and W. Huang, *Macromolecules*, 2001, **34**, 7932-7940.

24. J. Li, M. Yan, Y. Xie and Q. Qiao, *Energy & Environmental Science*, 2011, **4**, 4276-4283.

25. C. Du, W. Li, C. Li and Z. Bo, *Journal of Polymer Science Part A: Polymer Chemistry*, 2013, **51**, 383-393.

26. S. Liu, K. Zhang, J. Lu, J. Zhang, H.-L. Yip, F. Huang and Y. Cao, *Journal of the American Chemical Society*, 2013, **135**, 15326-15329.

27. A. Saeki, S. Yoshikawa, M. Tsuji, Y. Koizumi, M. Ide, C. Vijayakumar and S. Seki, *Journal of the American Chemical Society*, 2012, **134**, 19035-19042.

28. Y. Wang, Y. Liu, J. Luo, H. Qi, X. Li, M. Nin, M. Liu, D. Shi, W. Zhu and Y. Cao, *Dalton Transactions*, 2011, **40**, 5046-5051.

29. S. K. Lee, W. J. Yang, J. J. Choi, C. H. Kim, S.-J. Jeon and B. R. Cho, *Organic Letters*, 2005, **7**, 323-326.

30. K. Danel, T.-H. Huang, J. T. Lin, Y.-T. Tao and C.-H. Chuen, *Chemistry of Materials*, 2002, **14**, 3860-3865.

31. Y. Zhang, Y. Jin, R. Bai, Z. Yu, B. Hu, M. Ouyang, J. Sun, C. Yu, J. Liu and C. Zhang, *Journal of Photochemistry and Photobiology A: Chemistry*, 2012, **227**, 59-64.

32. R. Tarsang, V. Promarak, T. Sudyoadsuk, S. Namuangruk, N. Kungwan, P. Khongpracha and S. Jungsuttiwong, *RSC Advances*, 2015, **5**, 38130-38140.

33. L. Liu, C. L. Ho, W. Y. Wong, K. Y. Cheung, M. K. Fung, W. T. Lam, A. B. Djurišić and W. K. Chan, *Advanced Functional Materials*, 2008, **18**, 2824-2833.

34. P.-T. Wu, T. Bull, F. S. Kim, C. K. Luscombe and S. A. Jenekhe, *Macromolecules*, 2009, **42**, 671-681.

35. H. R. Kricheldorf, *Handbook of Polymer Synthesis*, CRC Press, 1991.

36. P. J. Brown, D. S. Thomas, A. Köhler, J. S. Wilson, J.-S. Kim, C. M. Ramsdale, H. Sirringhaus and R. H. Friend, *Physical Review B*, 2003, **67**, 064203.

37. S. C. Price, A. C. Stuart, L. Yang, H. Zhou and W. You, *Journal of the American Chemical Society*, 2011, **133**, 4625-4631.

38. M. Ozel, I. Osken and T. Ozturk, *Phosphorus, Sulfur, and Silicon and the Related Elements*, 2015, **190**, 1216-1218.

39. S. Yoshioka and Y. Aso, *Journal of pharmaceutical sciences*, 2007, **96**, 960-981.

40. C. W. Ge, C. Y. Mei, J. Ling, J. T. Wang, F. G. Zhao, L. Liang, H. J. Li, Y. S. Xie and W. S. Li, *Journal of Polymer Science Part A: Polymer Chemistry*, 2014, **52**, 1200-1215.

Chapter 4

Impact of ethynylene linkers on the optoelectronic properties of benzothiadiazole based alternate conjugated polymers.

Chapter 4

4.1 Introduction

Solar cell technology is one of the potential methods to solve global energy needs. Considerable progress in plastic electronics technology, such as organic semiconducting materials used as main active layers in bulk heterojunction BHJ solar cells, would assist to reduce the cost of manufacture of such devices.[1-4] Over the past decade, solution processed BHJ polymer solar cells (PSCs) have received increasing attention in the research community as a result of its potential advantages such as light weight, high flexibility, low manufacturing costs and ease of synthesis of the polymers.[5,6]

Great success has been made with such PSC devices with efficiencies ranging from 1% to 12%.[7] It is imperative for the conjugated polymers used in this area to absorb a broad part of the solar light spectrum in order to obtain high power conversion efficiencies (PCE). Consequently, a variety of conjugated polymers have been developed which have low energy bandgaps in order to efficiently harvest energy from sunlight.[8,9] At the molecular level, the bandgap (E_g) and the HOMO and LUMO energy levels can be effectively tuned to achieve high performance in such organic polymer solar cells (OPSCs).[10,11] One of the effective approaches in designing conjugated polymers with suitable energy bandgaps is to prepare polymers with alternating electron-releasing units and electron-withdrawing units over the same conjugated polymeric chain.[8,12] It is well established that benzothiadiazole (BT) is one of the most commonly used electron acceptor units for the construction of low bandgap polymers, this is a result of its strong electron withdrawing ability in D-A systems.[13] In previous reports, BT-based conjugated polymers have exhibited high performance (PCE) in solar cells up to 6% when these polymers are fabricated with fullerene derivatives as an acceptor in OPSC device. Iraqi *et al.* explored a series of D-A polymers (Figure 4-1) with alternating 2,7-linked carbazole or fluorene units flanked by thiophene as electron donor units and BT units as electron acceptors. These polymers displayed good efficiencies ranging from 3.34 to 5.41% when used with fullerene derivatives in BHJ solar cells.[14,15] Recently, Kuznetsov *et al.* reported that the PCE of PSCs based on polymers with alternate BT-acceptor units reached up to 6% by the introduction of solubilising groups on thiophene units between donor and acceptor moieties.[16]
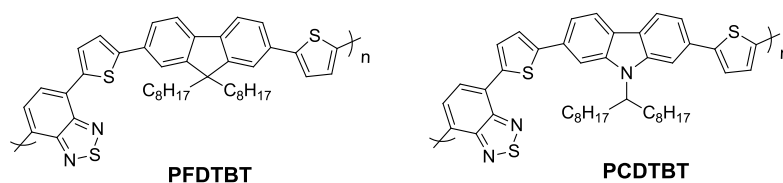
Figure 4-1: Structures of **PFDTBT** and **PCDTBT**.

However, it was observed that BT-acceptor units lead to large twist angles between the BT units and their adjacent units in the resulting polymer, resulting in decreased packing and conjugation length in the D-A systems. Thus, this effect still remains as a challenge to improve the efficiency of D-A conjugated polymers.[17]

In order to enhance the packing and rigidity of polymer chains, a linker is often employed between the electron donor and acceptor units along the conjugated polymer backbone. Previous reports have shown that the incorporation of an ethynylene unit (weak electron withdrawing unit) into the main chain of conjugated polymers generally enlarges their electronic bandgaps and lowers their HOMO energy levels.[18,19] Furthermore, some theoretical studies showed that ethynylene units along the conjugated polymer chains would reduce the barrier energy of rotation, resulting in low fluorescence quantum yields.[20] Cremer *et al*. incorporated ethynylene units in a thiophene-based polymer. They found that ethynylene units lead to a polymer with a deeper HOMO level (~ 0.3 eV) but a slightly higher bandgap (~ 0.15 eV) than poly(3-hexylthiophene) (P3HT). The ethynylene-based polymer showed a higher V_{oc} value than that of P3HT (1.01 V *vs*. 0.62 V) in BHJ devices, it had a lower PCE than that of P3HT. This was explained by low charge mobility in devices as a result of a lower aggregation of polymer chains in blends with PCBM for the ethynylene-based polymer, even though it showed good aggregation of polymer chains in pristine films.[21]

In this part of the thesis, we have decided to investigate the use of the ethynylene linker in alternate D-A polymers comprising alternate electron donating units such as carbazole, fluorene or anthracene units together with alternate BT units. The role of the ethynylene linker on the physical properties of the resulting polymers including their energy bandgaps and energy levels will be discussed. Three conjugated polymers have been synthesised in this part of the project using the Sonogashira coupling reaction. The structures of the new copolymers, PFDEBT-**P10**, PCDEBT-**P11** and PPADEBT-**P12**, are shown in Figure 4-2. The optical, electrochemical and thermal properties of these polymers which contain ethynylene linkers between donor and acceptor moieties

were investigated. Our results showed that the anthracene-based polymer **P12** showed the lowest bandgap (E_g) at 2.18 eV relative to the other two polymers **P10** and **P11** in this series of polymers. On comparing this series of polymers which have ethynylene units between the donor and acceptor units (class 4) with analogous polymers with thiophene linkers, a blue shift of their peak absorptions was observed. The preparation of this series of ethynylene-based polymers along with a discussion of their properties and a comparison to the properties of analogous polymers with thiophene units is presented.
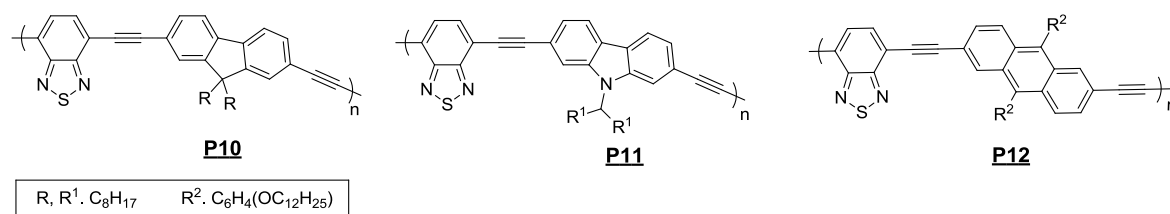
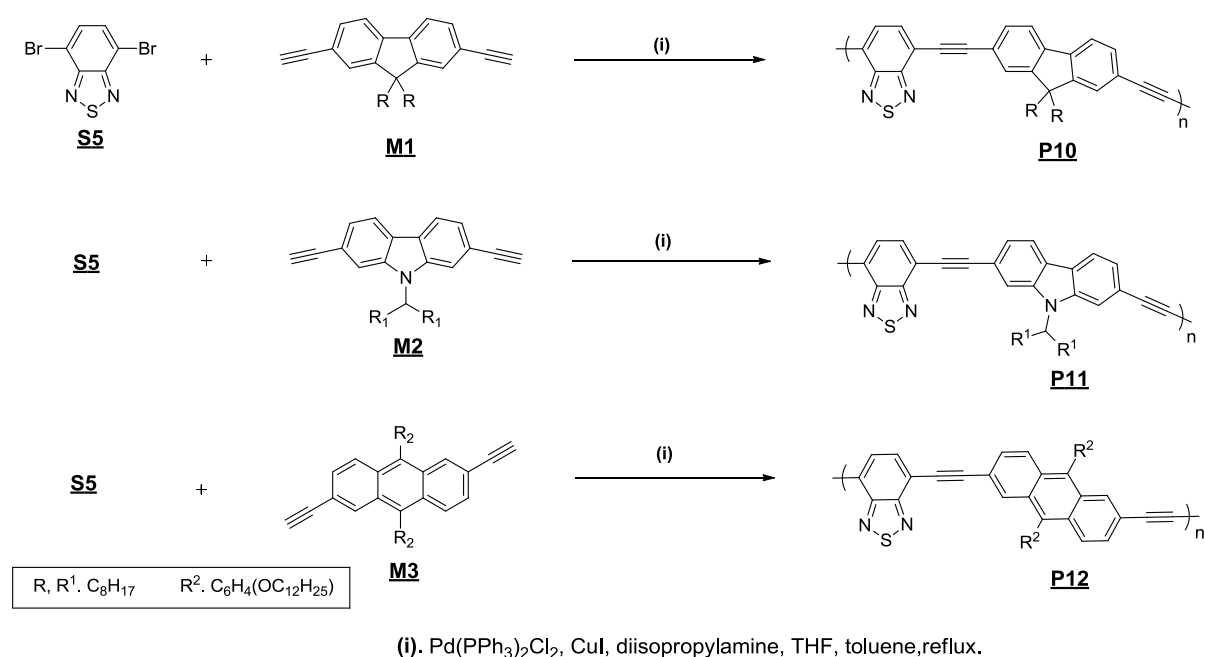Structure of polymers (class 4)

Figure 4-2: Structures of PFDEBT -**P10**, PCDEBT -**P11** and PPADEBT-**P12**.

4.2 Result and discussion

4.2.1 Synthesis and characterisation

The synthetic routes for the preparation of the three conjugated polymers **P10**-**P12** are outlined in Scheme 4-1. 4,7-Dibromobenzo[c]-1,2,5-thiadiazole (BT) (**S5**) is used as the electron-acceptor unit in the polymerisations. Polymerisations of **S5** with respectively **M1**, **M2** and **M3** by the Sonogashira coupling reaction produced polymers PFDEBT-**P10** (yield = 17 %), PCDEBT-**P11** (yield = 8 %) and PPADEBT-**P12** (yield = 21 %). The Sonogashira polymerisations were carried out using $Pd(PPh_3)_2Cl_2$ as the catalyst and CuI as co-catalyst, along with diisopropylamine as the base in a mixture of anhydrous THF/toluene solvent under inert atmosphere. All polymerisations were conducted until precipitates of the polymers were observed. The time of polymerisation reactions varied between 3 to 12 hours. The obtained crude products formed were separated by precipitation in methanol then cleaned with different organic solvents using a Soxhlet apparatus in order to remove the catalyst impurities, unreacted monomers and low molecular weight oligomers. It was observed that the polymers displayed limited solubilities and only their toluene fractions were separated, and used for further analysis with large fractions of the product remaining behind in the thimbles

of Soxhlet apparatus. This explains the low yields observed from these polymerisations. The products obtained from the Soxhlet fractions were soluble in most common organic solvents such as chloroform and dichlorobenzene. The chemical structures of these polymers were confirmed by ^{1}H NMR and elemental analysis. It should be noted that the deviations between actual values and expected values of the elemental analysis can be attributed to the incomplete combustion of the samples during analysis due to strong solvent retention inside sample structure which effects on degradation reactions.[22] The mechanisms of these polymerisations proceed through the Sonogashira reaction scheme as described in (Scheme 1-5 –Chapter 1). Details of the synthesis of the polymers and their characterisation are given in the experimental section.

(i). Pd(PPh$_3$)$_2$Cl$_2$, CuI, diisopropylamine, THF, toluene,reflux.

Structure of polymers (class 4)

Scheme 4-1: The synthetic route toward polymers PFDEBT-**P10**, PCDEBT-**P11** and PPADEBT-**P12**.

Gel permeation chromatography (GPC) data of all polymers is summarised in Table 4-1 with their number-average molecular weights (M_n), weight-average molecular weights (M_w) and polydispersity index (PDI) against polystyrene standards using 1,2,4-trichlorobenzene (TCB) as the eluent at 140 °C. These ethynylene-based polymers (class 4) were only separated in 20% yields or less from their toluene fractions. These toluene polymer fractions are the portions of the polymers that are soluble but at the limit of their processability. It is believed that incorporation of ethynylene units along the polymer chains results in their aggregation as a consequence

of more planar polymer conformations. This leads to a limit of their molecular weights and a lack of solubility of the portions with higher molecular weights. The M_n of PPADEBT-**P12** was estimated to be 8,700 Da with a polydispersity of 2.5. These values are lower compared to those of PFDEBT-**P10** and PCDEBT-**P11** owing to the effect of a more extended conjugation and also the planarity of the anthracene repeat units.

Table 4-1: The summary of the GPC analysis of PFDEBT-**P10**, PCDEBT-**P11** and PPADEBT-**P12**.

Polymer	Fraction	Yield %	M_n (Da)	M_w(Da)	PDI
P10	toluene	17	11,600	29,300	2.5
P11	toluene	08	25,000	80,400	3.2
P12	toluene	21	8,700	21,800	2.5

Measurements conducted on the toluene fractions of polymers using a differential refractive index (DRI) detection method.

4.2.2 Optical properties

The optical properties of all polymers were measured by UV-vis absorption spectroscopy in dilute chloroform solutions and in thin solid films (drop cast from chloroform solution). The optical spectra as depicted in Figure 4-3. All the optical data of ethynylene-based polymers are summarised in Table 4-2. The values of the bandgap polymers are determined from their onsets of absorption in the solid state.

Table 4-2: A summary of the optical and electrochemical data for PFDEBT-**P10**, PCDEBT-**P11** and PPADEBT-**P12**.

Polymer	λ_{max} solution (nm)	λ_{max} film (nm)	ε [a] (M^{-1} cm^{-1})	$E_{g\ opt}$ [b] (eV)	HOMO [c] (eV)	LUMO [d] (eV)	$E_{g\ elec}$ [e] (eV)
P10	468	481	25,100	2.31	-5.72	-3.21	2.51
P11	480	492	27,900	2.22	-5.66	-3.31	2.35
P12	491	510	40,000	2.14	-5.68	-3.34	2.34

[a] Absorption coefficient measured (ε) at λ_{max} = 324 for **P12** and 358 for **P10** and **P11** nm in chloroform solutions. [b] Optical energy bandgap determined from the onset of absorption band in thin film. [c] HOMO position (*vs. vacuum*) determined from the onset of oxidation. [d] LUMO position (*vs. vacuum*) determined from the onset of oxidation. [e] Electrochemical bandgap.

All polymers revealed two absorption bands in chloroform solutions in the range of 300-380 nm and 400-550 nm. The shorter wavelength absorption bands can be attributed to π-π* transitions, whereas the longer wavelength bands can be ascribed to the intramolecular charge transfer (ICT) bands between donor and acceptor moieties along the D-A polymer backbones. The thin films (Figure 4-3-b) displayed red-shifted absorption bands relative to those observed in solutions (Figure 4-3-a). This phenomenon is caused by stronger π-π interactions and increased polymer chain aggregation in the solid state, which increases their planarity. Interestingly, the small bathochromic shift (~20 nm) from dilute solution to solid state indicates that these polymers (ethynylene linked polymers) adopt relatively similar conformations whether in solutions or as films. Polymer PPADEBT-**P12** displays an absorption maximum at 491 nm in solution and 510 nm films with shoulder absorption peaks in both states. The shoulder absorption comes from stacking and aggregation of polymer chains in dilute solution and when cast in films. The optical bandgaps, as determined from the onset of the film absorption, are 2.31, 2.22 and 2.14 eV for PFDEBT-**P10**, PCDEBT-**P11** and PPADEBT-**P12**, respectively. It is evident from these results that the magnitude of the molecular weights of these polymers has no significant effects on their optical properties and absorption spectra.

In comparison, the values of the absorption maxima of PPADEBT-**P12** both in solution and in thin films are red-shifted compared to those of PFDEBT-**P10** and PCDEBT-**P11**. PPADEBT-**P12** has also a lower bandgap than those of PFDEBT-**P10** and PCDEBT-**P11**. This is probably due to a more extended electronic delocalisation on the anthracene moieties on **P12** relative to other donor units in other polymers. Furthermore, incorporation of anthracene unit on ethynylene-based polymer leads to enhance coplanarity of polymer chains compared to the other two polymers synthesised. However, the intensity of the ICT band of PPADEBT-**P12** is observed to be lower than the other two absorption bands for PFDEBT-**P10** and PCDEBT-**P11**. It was hypothesised that the alkoxy bulky substituents, which were grafted onto the anthracene, effectively affected the ICT between the anthracene unit and the BT unit due to large twisting of the phenyl rings at the position 9,10 of anthracene that slightly impeding ICT. A wider bandgap of fluorene-based polymer **P10** in comparison to the carbazole-based polymer **P11** is attributed to the more electron donating nature of carbazole moiety than fluorene units; this would help in increasing the electron delocalisation in PCDEBT- **P11** when compared to that in PFDEBT- **P10**.
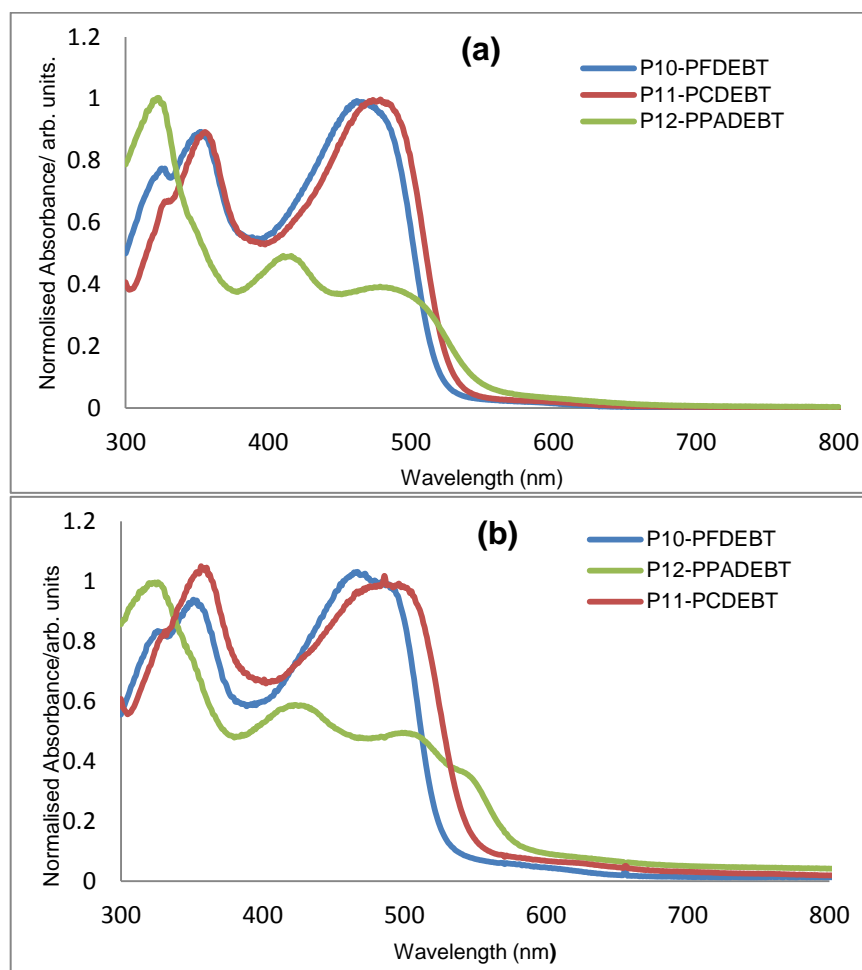
Figure 4-3: Normalised absorption spectra of polymers (a) in solution and (b) as thin films.

It is interesting to compare the optical properties of ethynylene-based polymers which incorporate acetylene unit as linker and their thiophene analogues; this will help to ascertain the effect of ethynylene units on the properties of polymers. The thiophene counterparts of these polymers, **PFDTBT**, **PCDTBT** and **PPADTBT** have been synthesised by Iraqi group and exhibit remarkable hypochromic shifts [14,15,23] in comparison with ethynylene-based polymers. As an example, ethynylene-based polymer PFDEBT-**P10** displays a significant blue shift at $\lambda_{max} = 481$ nm in film while its thiophene counterpart, **PFDTBT**[14] has a $\lambda_{max} = 592$ nm in drop cast films. Consequently, the optical bandgap of 2.31 eV for PFDEBT-**P10** is wider than that of its thiophene analogue (1.86 eV).[14] The same pattern is observed with other polymers for PCDEBT-**P11** and PPADEBT-**P12** by comparison with their thiophene equivalent polymers. We attribute the blue shift in the absorption of the resulting polymers in this series of polymers to a decrease of electron delocalisation and conjugation length between donor and acceptor moieties caused by the ethynylene linker.[24,25] These results indicate that the acetylene π-spacers between alternating units have a profound effect

103

on the backbone of conjugated polymers and their properties. The ethynylene unit has slightly π-accepting properties as a result of the sp hybridization of its carbon centres, which reduce the overall ICT between the strong π-accepting benzothiadiazole repeat units and the arylene units flanked by the ethynylene spacers along the polymer chains in these polymers.

The absorption coefficient data of the three polymers is summarised in Table 4-2. Obviously, PPADEBT-**P12** reveals high molar absorption coefficient (ε) of 40,000 M^{-1} cm^{-1} relative to PFDEBT-**P10** and PCDEBT-**P11**. This phenomenon is probably due to the extension of the conjugation length of anthracene donor moiety compared to fluorene and carbazole systems.

4.2.3 Electrochemical properties

Cyclic voltammetry (CV) studies were used to investigate the electrochemical properties of the polymers. The CV measurements were conducted on the polymers using drop-cast films in acetonitrile with tetrabutylammonium perchlorate as the electrolyte at scan rate of 100 mV/s under inert conditions. The cyclic voltammograms are shown in Figure 4-4 and the HOMO and LUMO energy levels (*vs vacuum*) of the polymers, as calculated from their first onset of oxidation or reduction waves, are summarised in Table 4-2. PPADEBT-**P12** displayed a HOMO energy level of -5.68 eV which is comparable in value to that of PCDEBT-**P11**; suggesting comparable electron donating ability of the 2,6-linked anthracene units and the 2,7-linked carbazole repeat units. PFDEBT-**P10** displays a slightly lower lying HOMO energy level relative to the other two polymers at -5.72 eV due to the reduced electron donating properties of the fluorene repeat units. However, the variation in the position of the HOMO levels of this series of polymers is not majorly affected by the nature of their electron donating moieties. It can be seen from Table 4-2.that the change of donor moieties affects the LUMO energy levels of the polymers to a greater extent. The LUMO level of PFDEBT-**P10** (-3.21 eV) is about 0.1 eV closer to the *vacuum* level than the other two polymers in this series of polymers (class 4). PCDEBT-**P11** and PPADEBT-**P12** display similar LUMO levels at -3.31 and -3.34 eV, respectively although this series of polymers possess the same acceptor (BT). These results indicate that varying the electron donor units can also perturb the electron accepting ability of the main chain of polymers in this series.
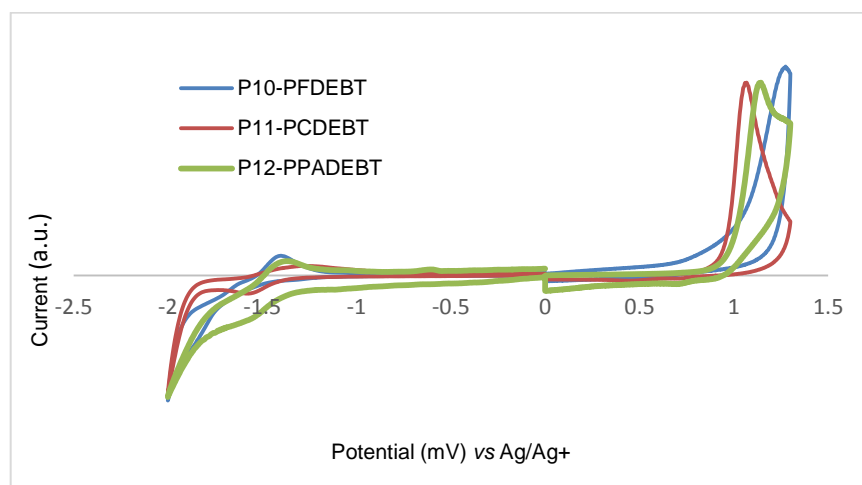
Figure 4-4: Cyclic voltammograms of the polymer films.

A comparison of the electrochemical properties of the resulting polymers (class4), PFDEBT-**P10**, PFDEBT-**P11** and PPADEBT-**P12** with their thiophene analogues reveals considerable lowering of the HOMO energy levels of the ethynylene-based polymers, resulting in wider bandgap polymers when compared to their thiophene counterparts. Indeed, a series of thiophene analogues, **PFDTBT**, **PCDTBT** and **PPADTBT** reported by Iraqi *et al*. display shallower HOMO energy levels and smaller bandgap polymers [14,15,23] relative to the new synthesised ethynylene polymers in this series. It is believed that incorporation of ethynylene units as weak electron-withdrawing units in the main chain of conjugated polymers instead of the electron donating thiophene units is responsible for lowering the HOMO energy levels of the resulting polymers. This is a result of decreasing the electron donating ability of the donor segments on the polymer chains,[24] resulting in an enlarged bandgap. As an example, the HOMO level of the ethynylene polymer PFDEBT-**P10** is -5.72 eV while the HOMO of its thiophene analogue **PFDTBT** is at -5.34 eV.[14] A similar comparison indicates that the HOMO level of PPADEBT-**P12** is at -5.68 eV while its corresponding thiophene analogue **PPADTBT** has a HOMO level at -5.44 eV.[23] These findings indicate how the ethynylene units could increase the planarity of polymer chains while at the same time changing the electronic properties of the resulting polymers and increasing their energy bandgaps.

4.2.4 Thermal properties and XRD studies

Thermogravimetric analysis (TGA) studies were performed on the polymers under a N_2 atmosphere at a heating rate of 10 °C/min. The TGA plots (Figure 4-5) suggest that these polymers possess good thermal stability with decomposition temperature (T_d)

(5% weight loss) over 240 °C. The TGA curves reveal that the 5% weight loss temperature (T_d) for PFDEBT-**P10**, PCDEBT-**P11** and PPADEBT-**P12** were found to be respectively at 240 °C, 249°C and 330 °C,. For all polymers, the first step in the degradation can be ascribed to loss of alkyl and alkoxy chains from the donor moieties of the polymers. Above 500 °C, degradation of the polymer chains follows with a total weight loss of about 92%, 89% and 93% respectively for PFDEBT-**P10**, PCDEBT-**P11** and PPADEBT-**P12**, that is observed when the temperature is above 600 °C. The high thermal stability of these polymers is probably due to the high thermal stability of BT units in the resulting polymers. For the purpose of comparison, PPADEBT-**P12** exhibited a higher thermal stability with two step degradations, while PFDEBT-**P10** and PCDEBT-**P11** showed an apparent three step degradation process. It was hypothesised that the different thermal behaviours of these polymers come from varying electro donor moieties of these polymers. Generally, these thermal stabilities of synthesised polymers are adequate for their applications in solar cells and other electronic devices.
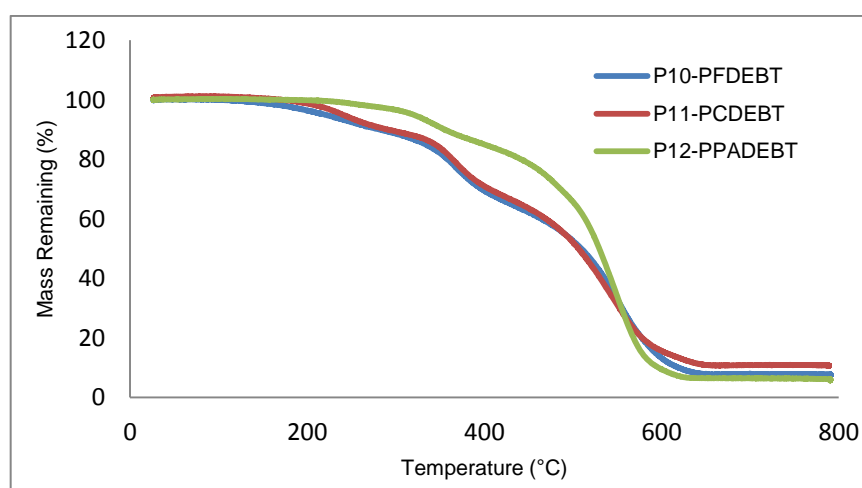
Figure 4-5: TGA plots of the resulting polymers with a heating rate of 10 °C/min under N₂.

Powder X-ray diffraction profiles of polymers PFDEBT-**P10**, PCDEBT-**P11** and PPADEBT-**P12** were recorded (Figure 4-6). A more pronounced diffraction peak appeared at 2θ value of 20.6° for PPADEBT-**P12**; suggesting the polymer adopt a more ordered structure in the solid state compared to the other two polymers. This corresponds to a π-π distance of 4.30 Å between polymer chains. PFDEBT-**P10** and PCDEBT-**P11** display weak and broad peaks in the wide-angle region at 2θ values of 20.7° and 20.8°, respectively. Clearly the low intensity of these diffraction peaks indicate that these two polymers adopt more amorphous structures with a distance of

4.29 and 4.27 Å between polymer chains for PFDEBT-**P10**, PCDEBT-**P11**, respectively. Interestingly, all polymers do not display any apparent peaks in the low-angle region. It can be seen that introduction of the anthracene-donor moiety in this series of polymers leads to more π-π stacking in the polymer backbones by increasing intermolecular interactions, thus increasing the planarity of polymer chains and reducing the bandgap of polymers. Improved molecular packing of polymer chains is required for efficient charge carriers in BHJ devices. Thus, we believe that device fabricated from PPADEBT-**P12** should provide improved charge carrier transportation and J_{sc} value as a result of the enhanced π-π stacking of polymer chains.
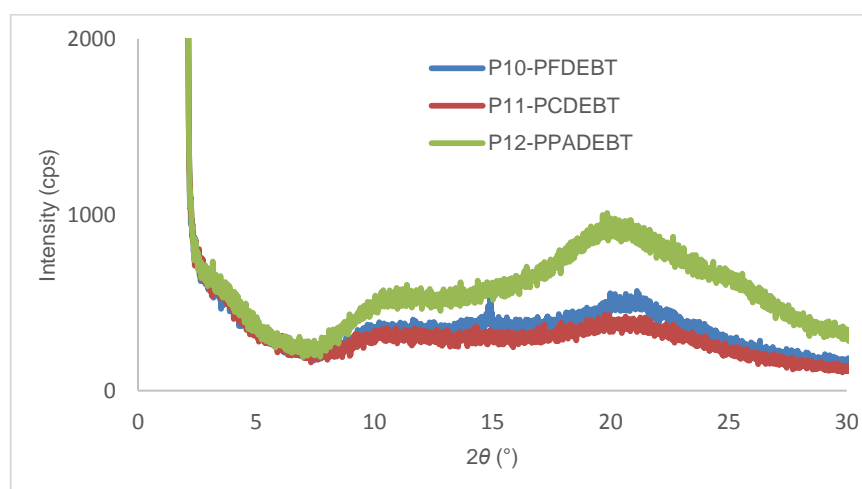
Figure 4-6: Powder XRD profiles of the target polymers.

4.3   Conclusion

In this study, a series of new D-A conjugated polymers PFDEBT-**P10**, PCDEBT-**P11** and PPADEBT-**P12** containing acetylene π-spacers in the main backbone of conjugated polymers were synthesised based on 2,7-linked fluorene, 2,7-linked carbazole or 2,6-linked anthracene repeat units as donor moieties and 1,2,5-benzothiadiazole (BT) alternate repeat units as acceptor moieties. The polymers were successfully prepared by Sonogashira coupling reactions. Moreover, their optical, electrochemical, thermal and structure properties were investigated systematically. The resulting polymers were obtained in low yields as they have low solubilities. The introduction of ethynylene units over the main chains of polymers results in their aggregation and formation of much rigid polymeric chains. Compared with the thiophene-based polymers, the ethynylene-based polymers displayed more pronounced blue-shifted absorption spectra and larger bandgaps owing to the incorporation of acetylene π-spacers into the alternate D-A polymers. It was speculated that this phenomenon is probably due to electronic

effects. The ethynelene units can be considered as weak electron acceptors and as they are incorporated between various electron donors and the strong electron accepting BT repeat units; they lead to lower intramolecular charge transfer along polymer chains and as a result to higher bandgap polymers. PPADEBT-**P12** exhibits a lower bandgap relative to the other two polymers. It also exhibits the wider absorption bands and absorption shoulders owing to extended conjugated system in the anthracene-based polymer. Interestingly, the higher M_n values of the fluorene and carbazole-based polymers do not influence the optical and electrochemical properties. In spite of the further lowering the HOMO and LUMO level of the resulting polymers with incorporation of ethynylene units, the high photovoltaic performance could be expected through optimised morphology of these polymers with fullerene in BHJ. Further investigations into the use of this new class of polymers in BHJs are currently ongoing.

References

1. C. J. Brabec, C. Winder, M. C. Scharber, N. S. Sariciftci, J. C. Hummelen, M. Svensson and M. R. Andersson, *Journal of Chemical Physics*, 2001, **115**, 7235-7244.

2. H. Hoppe and N. S. Sariciftci, *Journal of Materials Research*, 2004, **19**, 1924-1945.

3. K. M. Coakley and M. D. McGehee, *Chemistry of Materials*, 2004, **16**, 4533-4542.

4. S. Günes, H. Neugebauer and N. S. Sariciftci, *Chemical Reviews*, 2007, **107**, 1324-1338.

5. P.-L. T. Boudreault, A. Najari and M. Leclerc, *Chemistry of Materials*, 2010, **23**, 456-469.

6. M. A. Naik and S. Patil, *Journal of Polymer Science Part A: Polymer Chemistry*, 2013, **51**, 4241-4260.

7. M. Peach, *Optics. Org: the Business of Photonics*, 2013.

8. C. Du, W. Li, C. Li and Z. Bo, *Journal of Polymer Science Part A: Polymer Chemistry*, 2013, **51**, 383-393.

9. S. Sardar, P. Kar, H. Remita, B. Liu, P. Lemmens, S. K. Pal and S. Ghosh, *Scientific Reports*, 2015, **5**.

10. J. Roncali, *Chemical Reviews*, 1997, **97**, 173-206.

11. Y. M. Yang, W. Chen, L. Dou, W.-H. Chang, H.-S. Duan, B. Bob, G. Li and Y. Yang, *Nature Photonics*, 2015.

12. Y.-J. Cheng, S.-H. Yang and C.-S. Hsu, *Chemical Reviews*, 2009, **109**, 5868-5923.

13. H. Zhou, L. Yang and W. You, *Macromolecules*, 2012, **45**, 607-632.

14. A. A. Alghamdi, D. C. Watters, H. Yi, S. Al-Faifi, M. S. Almeataq, D. Coles, J. Kingsley, D. G. Lidzey and A. Iraqi, *Journal of Materials Chemistry A*, 2013, **1**, 5165-5171.

15. H. Yi, S. Al-Faifi, A. Iraqi, D. C. Watters, J. Kingsley and D. G. Lidzey, *Journal of Materials Chemistry*, 2011, **21**, 13649-13656.

16. I. E. Kuznetsov, A. V. Akkuratow, D. K. Susarova, D. V. Anokhin, Y. L. Moskvin, M. V. Kluyev, A. S. Peregudov and P. A. Troshin, *Chemical Communications*, 2015, **51**, 7562-7564.

17. P. Anant, N. T. Lucas and J. Jacob, *Organic Letters*, 2008, **10**, 5533-5536.

18. B. Liu, W.-L. Yu, J. Pei, S.-Y. Liu, Y.-H. Lai and W. Huang, *Macromolecules*, 2001, **34**, 7932-7940.

19. S. Zhang, H. Fan, Y. Liu, G. Zhao, Q. Li, Y. Li and X. Zhan, *Journal of Polymer Science Part A: Polymer Chemistry*, 2009, **47**, 2843-2852.

20. K. Okuyama, T. Hasegawa, M. Ito and N. Mikami, *Journal of Physical Chemistry*, 1984, **88**, 1711-1716.

21. J. Cremer, P. Bäuerle, M. M. Wienk and R. A. Janssen, *Chemistry of Materials*, 2006, **18**, 5832-5834.

22. H. R. Kricheldorf, *Handbook of Polymer Synthesis*, CRC Press, 1991.

23. H. Yi. M. S. Almeataq, S. Al-Faifi, A. A.. Alghamdi, A. Iraqi, N. W. Scarratt, T. Wangc and D. G. Lidzey, *The Royal Society of Chemistry*, 2013, **49**, 2252--2254.

24. J. Li, M. Yan, Y. Xie and Q. Qiao, *Energy & Environmental Science*, 2011, **4**, 4276-4283.

25. W.-Y. Wong, L. Liu, S.-Y. Poon, K.-H. Choi, K.-W. Cheah and J.-X. Shi, *Macromolecules*, 2004, **37**, 4496-4504.

Chapter 5

Conclusions and Future Work.

Chapter 5

5.1 Conclusions

A range of new electron donor-acceptor alternating conjugated polymers were successfully designed, prepared and characterised in this project. The polymers synthesised comprise either napthothiadiazole (NT) or benzothiadiazole (BT) as electron accepting units with 2,7-linked fluorene, 2,7-linked carbazole or 2,6-linked anthracene as donor repeat units flanked by thiophene, ethynylene or both as spacer units. These multiple classes of donor-acceptor copolymers were prepared for use in organic solar cell devices. The impacts of ethynylene and thiophene linkers over the polymer main backbones have been extensively discussed in this dissertation. Changing the linkers used in these D-A polymers have been investigated systematically on the optical, electrochemical and solubilities of the polymers. Attaching bulky alkyl chains on the donor moieties was aimed at increasing the solubility and molecular weights of the polymers synthesised. The main findings of characterisations of multiple families for each chapter are summarised and compared with other classes of polymers from both the literature as well as those from other chapters in this work.

Chapter 2 describes the preparation of three NT-based D-A conjugated polymers PFDTNT-**P1**, PCDTNT-**P2** and PPADTNT-**P3**, which were successfully synthesised using the Suzuki coupling reactions. The impact of replacing BT units with NT moieties in this series of polymers on the solubilities, optical, electrochemical and photovoltaic properties was investigated. The series of NT-based polymers were compared with their BT counterparts to help understand the effect of replacing their electron acceptor repeat units. BT-based polymers, which were synthesised by Iraqi group, are analogous polymers whose difference lies in the acceptor moiety. The BT equivalent polymers have shown a great promise with high efficiencies being achieved in solar cells. It was assumed that replacing 2,1,3-benzothiadiazole (BT) with 2,1,3-naphthothiadiazole (NT) in this series of conjugated polymers would result in red-shifted absorption maxima and narrow optical bandgaps, this hypothesis was proved correct. The donor moieties in these D-A alternating polymers were decorated with large alkoxy or alkyl chains to facilitate processability and allow the formation of higher molecular weight polymers. The optical bandgaps of PFDTNT-**P1**, PCDTNT-**P2** and PPADTNT-**P3** were estimated to be 1.76, 1.74 and 1.75 eV. The lower optical bandgaps of the NT-based polymers were attributed to a more extended electronic

delocalisation on the NT units by virtue of an additional fused benzene ring. We find the incorporation of NT units decreases the intensity of intramolecular charge transfer bands in the visible absorption; a result of steric hindrance over the main backbones between adjacent units. The NT-based polymers displayed excellent solubility in common organic solvents relative to that of their BT analogues; a consequence of twisting of polymer chains out of planarity upon steric hindrance between NT units and adjacent thiophene rings. Furthermore, GPC showed that the NT based polymers prepared in this study had higher molecular weights than their BT analogues. PFDTNT-**P1** displays an M_n = 41,100 Da, while that of **PFDTBT** analogue which has a much limited solubility was M_n = 5,300. The HOMO levels of NT-based polymers are comparable relative to their BT analogues.

The LUMO levels of polymers synthesised, with the exception of PPADTNT-**P3**, are however little shallower than their BT counterparts. In theory, NT moieties should be stronger acceptors owing to the fused ring on the thiadiazole system. However, the steric hindrance between thiophene unit and NT electron accepting unit results in a distorted main chain, which effectively reduces the electron withdrawing ability of the NT unit. Thermogravimetric analysis revealed that the onset of decomposition of these polymers are above 400 °C and display similar patterns, in spite of them containing different donor moieties. Powder X-ray diffraction studies revealed that all polymers adopt an amorphous structure in the solid state; suggesting a lack of regular packing of polymer chains as a result of steric hindrance between acceptor repeat units and adjacent thiophene rings which leads to a lack of close packing of polymer chains. Regrading to photovoltaic properties, organic photovoltaic devices based on NT-based polymer/ $PC_{71}BM$ blend films spin coated from co-solvents were investigated. The power conversion efficiencies (PCEs) varied from 1.74 to 2.17%. PCDTNT-**P2** showed the best performance among this series of polymers with a V_{oc} of 1.01 V, a J_{sc} of -6.25 mA/cm^2, an FF of 34.50, and a PCE of 2.17%. Comparison of the PCEs of the NT-based polymers synthesised in this chapter to those of their BT equivalent polymers, indicated that the NT-based conjugated polymers displayed a lower performance even though the latter polymers showed lower bandgaps than the corresponding BT-counterparts; a result of significant low FF that leads to an overall low photovoltaic performance. This may be attributed to the effect of the unfavourable morphology for given polymer/fullerene systems that did not yield efficient devices; this could have affected charge carrier motilities in devices.

In Chapter 3 two series of ethynylene-based polymers were synthesised using Sonogashira coupling reactions. It was hypothesised that incorporation of acetylene units over the main chains of polymers, relative to their analogues (Chapter 2), would promote the backbone planarity as a result of minimised steric hindrance, resulting in the formation of stronger π-π interchain stacking. In class 2 polymers (Chapter 3), the thiophene spacers used between donor and acceptor moieties in chapter 2 were substituted for ethynylene linkers; this has led to extremely planar conjugate polymers with strong π-π stacking between polymer chains in the solid state. Three ethynylene-based polymers which were synthesised by copolymerising NT units with either 2,7-linked diethynyl fluorene, 2,7-linked diethynyl carbazole or 2,6-linked diethynyl anthracene units yielded PFDENT-**P4**, PCDENT-**P5** and PPADENT-**P6**, respectively. It was speculated that the extended conjugated π-system of anthracene, relative to fluorene and carbazole systems, would enhance the planarity of main chains resulting in increased electronic conjugation and charge transportation. Unsurprisingly, the yields of these polymers were low; a consequence of having acetylene groups as spacer units resulting in aggregation of polymer chains and formation of much rigid polymers. Consequently, certain polymers demonstrated poor solubility in common organic solvents even at elevated temperature.

Comparing ethynylene-based polymers with polymers synthesised (Chapter 2) would help to ascertain the effects of ethynylene spacers on the properties of the resulting polymers. GPC analysis revealed that ethynylene-based polymers possessed moderate molecular weights; a consequence of having aggregations as a result of π-π stacking between polymer main chains. Despite their moderate molecular weights, PPADENT-**P6** displays the lowest optical bandgap (1.67 eV) and shows vibrational structure in its electronic spectra, a result that we interpret in terms of improved molecular ordering in the anthracene-based polymer. Both PFDENT-**P4** and PCDENT-**P5** display larger optical bandgaps (1.83 and 1.81 eV respectively). This is probably due to the extension of the conjugation length of the 9,10-functionalised anthracene polymer compared to fluorene and carbazole-based polymers. When comparing these polymers (class 2) to their analogous polymers in chapter 2 (class 1), ethynylene-based polymers displayed more pronounced ICT bands relative to their thiophene equivalent polymers. This suggests that incorporation of acetylene-spacers instead of thiophene repeat units next to the NT repeat units reduces steric hindrance between these and adjacent units, resulting in enhanced intramolecular charge transfer and π-overlap. However the UV-

vis spectra of the polymers (class 2) display wider optical bandgaps than their thiophene analogous (class 1). It is speculated that this a consequence of their low molecular weights and the electronic effect of ethynylene spacers as weak electron withdrawing groups may decrease the pull-push character in this series of polymers. CV results revealed that the HOMO/LUMO frontier energy levels of PFDENT-**P4**, PCDENT-**P5** and PPADENT-**P6** were estimated to be -5.58/-3.59 eV, -5.55/-3.54 eV and -5.39/-3.68 eV, respectively. Obviously, changing the electron donor repeat units over the polymer chains has an impact on the energy levels of the resulting polymers to a good extent. In comparison, the lower HOMO levels of ethynylene-based polymers, relative to their thiophene corresponding polymers, are a consequence of incorporation of ethynylene units as weak electron acceptor units in the polymer chains instead of thiophene as electron donating units, resulting in decreasing the electron donating ability of donor units along the polymer chains.

The thermal properties of the ethynylene-based polymers were investigated *via* TGA. PPADENT-**P6** displays the lowest thermal degradation temperature as a result of incorporating octyloxy chains on the anthracene moieties. The ethynylene-based polymers did still demonstrate good thermal stability with degradation temperatures in excess of 300 °C. XRD studies confirmed that the introduction of acetylene groups exhibit a certain degree of molecular ordering as a result of π-π stacking in solid state. However, the effect is more pronounced in PPADENT-**P6** relative to PFDENT-**P4**, PCDENT-**P5**; a consequence of having stronger intermolecular interactions brought about by the planar anthracene-donor moieties. All polymers show XRD peaks in wide-angle area which corresponds to π-π stacking between polymer main chains. Clearly, XRD patterns revealed that polymers synthesised in chapter 2 did not show any pronounced diffraction peaks in this wide-angle region compared to their ethynylene counterparts; a consequence of decreased torsion angle and better π-π stacking between the electron donor and acceptor moieties. PPADENT-**P6** shows more pronounced diffraction peak in wide-angle region compared to other polymers, which should benefit its charge transportation properties.

The physical and electrochemical properties of the conjugated polymers in (class 2) have been further improved *via* adding thiophene units to the ethynylene linkers over the main chains of polymers. In the new series of polymers synthesised (class 3), the ethynylene used as linkers in class 2 were replaced for ethynylene-thiophene as spacer

units. Incorporation of additional thiophene as electron donor units increases the electron donating ability of the donor segments and results in narrower optical and electrochemical bandgaps. PFDTENT-**P7**, PCDTENT-**P8** and PPADTENT-**P9** in this chapter were synthesised *via* Sonogashira coupling reactions. This series of polymers displayed more desirable optical properties. The optical bandgaps of PFDTENT-**P7**, PCDTENT-**P8** and PPADTENT-**P9** were estimated to be 1.71, 1.68 and 1.54 eV, respectively. It is hypothesised that the significant lower optical bandgaps of this series, relative to their ethynylene counterparts (class 2), is a consequence of utilising additional thiophene units in the polymer chains. The additional electron rich thiophene units lead to stronger electron donating segments over the main chains. Consequently, polymers (class 3) should be highly efficient in solar cells as they should harvest a wider portion of the solar spectrum. PPADTENT-**P9** has the lowest optical bandgap (1.54 eV) in all classes of polymers thus prepared in this project. It was speculated that this is a consequence of having extended conjugated anthracene units as donors with dodecyloxy phenyl on anthracene moiety. Furthermore, additional thiophene linkers used promote conjugation system over the polymer chains. GPC revealed that ethynylene-thiophene based polymers possessed moderate molecular weights ranging from 8,700 to 11, 500 Da, which are comparable to values of their ethynylene counterparts in this chapter. The HOMO levels of polymers (class 3) were shallower, relative to those polymers in class 2 series. It is expected that the introduction of additional thiophene as spacers increases the electron donating ability of the donor segments resulting in a shallower HOMO level. Consequently this should impact the oxidative stability of the resulting polymers. It is possible that this will negatively influence on the oxidative stability of the polymers synthesised (class 3). We find that varying of electronic properties of donating ability of donor units can also disturb the electron accepting nature resulting in an impact on the LUMO energy positions of the polymer main chains. X-ray diffraction patterns revealed that PFDTENT-**P7**, PCDTENT-**P8** and PPADTENT-**P9**.showed broad and weak peaks in the range 15 to 25°, an indication that the polymers possessed an amorphous structure in the solid state; a consequence of incorporation of additional thiophene spacers which disrupts the stacking interactions between polymer chains.

Finally, the polymers synthesised in chapter 4 used acetylene π-spacers and BT acceptor moieties in the main backbone of conjugated polymers. The impact of ethynylene linker units on the molecular, optical and electrochemical properties of the

resulting polymers, which incorporated 2,7-linked fluorene, 2,7-linked carbazole or 2,6-linked anthracene donor units, was investigated. The preparation of three ethynylene-based polymers (class 4) was undertaken by copolymerising dibromo[1,2,5]-benzothiadiazile (BT) with either 2,7-diethynylene fluorene, 2,7-diethynylene carbazole or 2,6-diethynylene anthracene to obtain PFDEBT-**P10**, PCDEBT-**P11** and PPADEBT-**P12**, respectively. **PFDTBT**, **PCDTBT** and **PPADTBT** are analogous polymers with thiophene linkers rather than acetylene linkers. The latter polymers were synthesised by Iraqi group and have shown great promise with high efficiencies being achieved in solar cells. It was believed that the use of ethynylene-donor moieties being weak donor units should display a higher V_{oc} and oxidative stability of the resulting polymers. GPC analysis revealed that PPADEBT-**P12** possessed the lowest molecular weight upon a more extended conjugation and also the planarity of the anthracene repeat units. Despite its low molecular weight, anthracene-based polymer exhibited the lowest optical bandgap (2.14 eV) and vibrionic resolution. However, PFDEBT-**P10** and PCDEBT-**P11** showed higher molecular weights of 11,600 and 25,000 Da, respectively, compared to PPADEBT-**P12.** Although both PFDEBT-**P10** and PCDEBT-**P11** having wider optical bandgaps of 2.31 and 2.22 eV. It is hypothesised that the molecular weights of these polymers has no effects on their optical properties and absorption spectra. The poor physical properties displayed by all polymers synthesised is a result of incorporation ethynylene units as spacer units between alternating moieties. When compared polymers in chapter 4, ethynylene-based polymers exhibited significant blue shifts and wider bandgaps, relative to their thiophene analogous. This is a consequence of decrease of electron delocalisation and conjugation length between donor and acceptor moieties caused by the ethynylene linker. XRD studies revealed that PPADEBT-**P12** displays a more pronounced diffraction peak in the wide-angle region, relative to other polymers; suggesting anthracene-based polymer possesses improved molecular packing of polymer chains *via* more π-π stacking in the polymer backbones. CV analysis revealed that the HOMO/LUMO levels of PFDEBT-**P10**, PCDEBT-**P11** and PPADEBT-**P12** were estimated to be -5.72/-3.21 eV, -5.66/-3.31 eV and -5.68/-3.4 eV, respectively. It can be seen that varying the electron donor units has little impact on the resulting energy levels. The lower HOMO level of resulting polymers (class 4), relative to their thiophene counterparts, is a consequence of incorporation ethynylene linkers instead of thiophene units, resulting in decreased electron donating ability over the main chains of

polymers. All polymers demonstrated good thermal stability with decomposition temperatures in excess of 240 °C.

In conclusion, a variety of electron donor moieties has been used to improve the physical and electrochemical properties of the resulting polymers. We found that the optical and molecular ordering properties of anthracene moiety with alkoxy phenyl substituents were the best. This is due to extended electronic delocalisation and planarity of polymers structures with anthracene units. Moreover, changing spacers used between alternating donor and acceptor repeat units has successfully improved the optical properties of the backbone polymer. Replacing thiophene with ethynylene units in conjugated polymers improved intermolecular charge transfer and minimised the steric hindrance between adjacent units. Moreover, using acetylene groups in alternating D-A polymers adopt more favoured and planar structures upon strong π-π interchain interactions. However, the aggregation and planarity of these polymers decreased the molecular weights and solubilities of the polymers synthesised. In addition, the optical bandgaps were relatively large as a result of incorporating ethynylene spacers as weak electron-withdrawing units. This decreased the electron donating ability over polymer backbone, which reduced the D-A character. Thus, acetylene linkers were changed for ethynylene-thiophene spacers to improve the electronic delocalisation in conjugated polymers. Additional thiophene units as linkers displayed excellent optical properties with low optical bandgaps for the resulting polymers. Presumably, this is a result of incorporation thiophene as donor units, which increased the donor ability of segments and extended electronic conjugation of the π-system. Therefore ethynylene-thiophene based anthracene polymer (**P9**) displayed the lowest optical bandgap of all resulting polymers in this dissertation. The polymer has desirable properties for use in organic photovoltaic devices as it has excellent sunlight harvesting ability in virtue of its low bandgap and it should also have good charge transportation properties. The BT-polymers showed poor physical properties owing to incorporation BT acceptor units beside ethynylne spacers that decreased the electronic delocalisation over polymeric chains. In spite of poor optical properties of the polymers synthesised, a good photovoltaic performance could be expected from this series of polymers through an optimised study for their use in BHJ cells with fullerene acceptors. Further investigations into the use of this new class of polymers in BHJs are currently ongoing.

5.2 Future Work

Considerable efforts have been achieved in this project to develop new polymers for application in organic solar cells. The photovoltaic results obtained on the polymers synthesised in Chapter 2 revealed that PCDTNT-**P2** displays the highest power conversion efficiency (2.17%). Both PFDTNT-**P1** and PPADTNT-**P3** display power conversion efficiencies of 2.02% and 1.74%, respectively. In actuality, these performances of the polymer synthesised in BHJ devices are limited compared to of their BT analogous. It is recommended that a series of fluorinated selenophene-naphthothiadiazole-*alt*-carbazole copolymers are synthesised as outlined in Figure 5-1. It is hypothesised that using selenophene rings into conjugated polymers would result in good optical and electrochemical properties of resulting polymers; suggesting that ionisation potential of the selenium atom is smaller relative to sulphur atom in its polymer counterpart. Furthermore, the polarisability of selenium is higher than that of the sulphur atom. Incorporation of fluorine substituents on the acceptor moiety aims to enhanced π-π stacking and intermolecular interactions brought about by the incorporation of fluorine, resulting in adopt more crystalline structures in solid state. This planarity of conformation facilitates delocalisation and reduces the bandgap. Increasing the regioregularity of polymers promotes the charge transportation properties and conductivity in BHJ device. Carbazole moieties into conjugated polymers should be attached by different size of alkyl chains to assist the formation of processable polymers with high molecular weights.
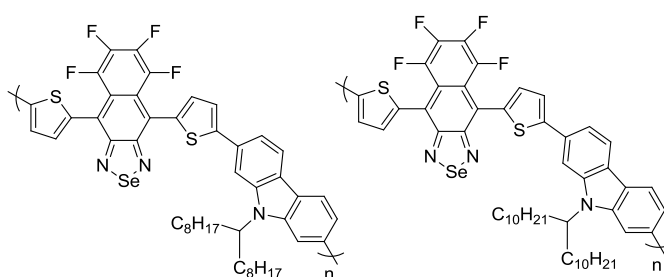
Figure 5-1: Structures of suggested polymers that should be investigated.

Relative to applications, a series of polymers (class 2 and 3) that were synthesised in Chapter 3, need to be fabricated into BHJ devices. It is worth mentioning that no research has been conducted on this type of polymer families. It is theorised that solubility of these polymers especially polymers class 3 can be significantly enhanced if alkyl chains are grafted on thiophene linkers as depicted in Figure 5-2. The

introduction of alkyl chains should help to address the limited molecular weights of these polymers.
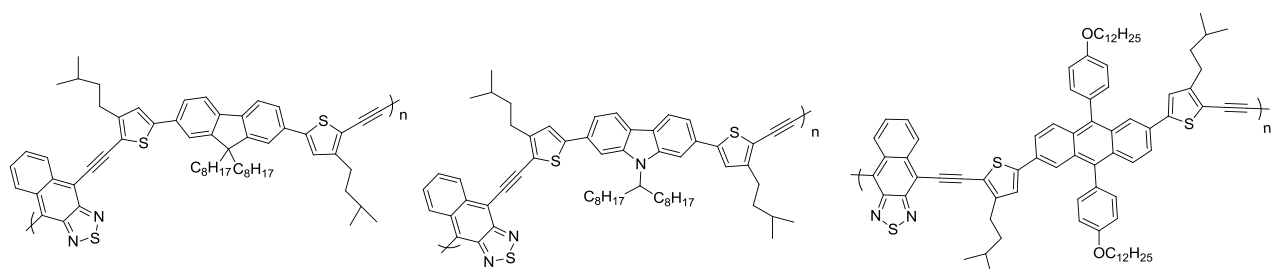
Figure 5-2: Structures of suggested ethynylene-thiophene based polymers that should be investigated.

Chapter 4 involved that preparation of ethynylene-based polymers with BT acceptor units. Clearly, these polymers displayed significant large optical and electrochemical bandgaps owing to incorporation of ethynylene spacer units as weak withdrawing segment. Moreover, the resulting polymers demonstrated limited solubilities which can negatively effect on devices fabricated. It is recommended larger alkyl chains need to be used in order to promote processability and obtain high molecular weight polymers (Figure 5-3). Moreover, fluorination of the benzothiadiazole moiety is required to promote molecular ordering of the polymer backbones resulting in good photovoltaic performance when fabricated into BHJ devices. Previous works have shown that fluorinated BT-based polymers possessed strong π-π stacking and aggregation of polymer chains, leading to limited solubility and molecular weight polymers. Therefore, attaching large solubilising groups should help to address this issue.
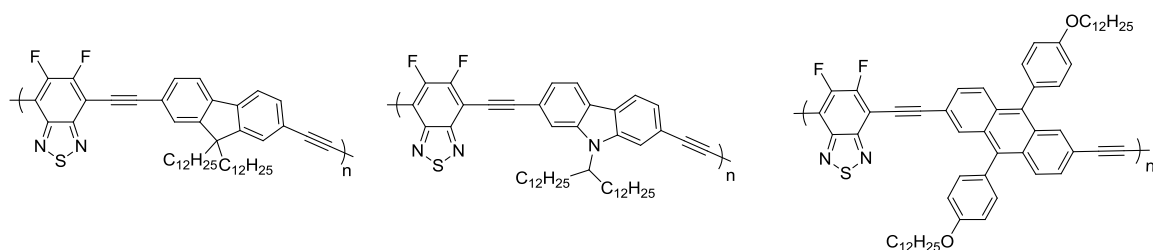
Figure 5-3: Structures of suggested BT-based polymers that should be investigated.

Chapter 6

Experimental Section.

Chapter 6

6.1 Materials

All the chemicals were purchased from Aldrich, Alfa Aesar and Fisher Ltd and used as received without further purification. All reagent grade common organic solvents were obtained from internal chemical stores. Dry solvents such as toluene, chloroform and dichloromethane (DCM) were used for reactions unless otherwise stated. Tetrahydrofuran (THF) was distilled and dried over sodium benzophenone under an inert nitrogen atmosphere. Toluene was dried and distilled over sodium under an inert atmosphere. Acetonitrile was dried and distilled over phosphorus pentoxide under an inert argon atmosphere, then stored over molecular sieves (3 Å).

2,3-Diaminonaphthalene (**S1**), 9,9-dioctylfluorene-2,7-diboronic acid bis(1,3-propanediol) ester (**S2**), 2,7-dibromo-9,9-dioctylfluorene (**S3**), 2,6-diaminoanthracene-9,10-dione (**S4**) and dibromobenzo[c]-1,2,5-thiadiazole (**S5**) (Figure 6-1) were purchased from commercial suppliers and used as received without further purification.
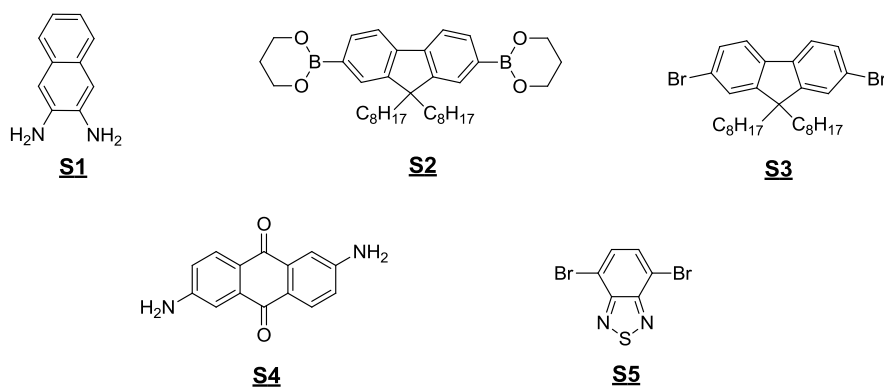
Figure 6-1: Structures of purchased chemicals.

9-(Heptadecan-9-yl)-2,7-bis(4,4,5,5-tetramethyl-1,3,2-dioxaborolan-2-yl)-9H-carbazole (**S6**) and 2,6-bis-(4,4,5,5-tetramethyl-[1,3,2]dioxaborolan-2-yl)-9,10-bis(4-(dodecyloxy)phenyl) anthracene (**S7**) (Figure 6-2) were synthesised by the Iraqi group according to a modified procedure by Blouin et al.[1] and Zhang et al,[2] respectively. Furthermore, 2,7-dibromo-9H-carbazole (**S8**) was prepared by Iraqi group according to a modified procedure by Sonntag et al.[3]
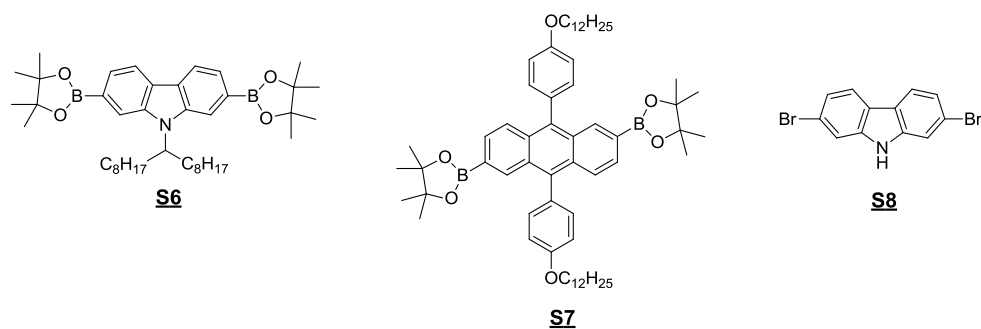
Figure 6-2: Chemical structures of monomers synthesised by the Iraqi group.

6.2 Measurement

^{1}H and ^{13}C nuclear magnetic resonance (NMR) spectra were recorded using on Bruker Avance 400 (MHz) NMR spectrometers at ambient temperature using chloroform-d (CDCl$_3$) with tetramethylsilane (TMS) as an internal standard. The NMR shifts are described by using following abbreviations: singlet (s), doublet (d), double doublet (dd), triplet (t), multiple (m) and broad (br). Moreover, coupling constants (*J*) are calculated in Hertz (Hz) and chemical shifts in part per million (ppm). CHN analyses were performed on the Perkin Elmer 2400 CHN Elemental Analyzer. In addition, the flask combustion method was used for the analysis of halides and sulfur. Mass spectra of monomers were recorded on a Perkin Elmer Turbomass Mass Spectrometer equipped with auto system XL GC. It has ability to operate in both chemical ionization (CI) and electron ionization (EI) modes. GPC measurements were conducted on polymer solutions using chloroform or 1,2,4-trichlorobenzene (TCB) as eluents at a flow rate of 1 cm^3 mintue^{-1}. The system was calibrated against a series of narrow polystyrene standards (polymer laboratories) using a 1037 Differential Refractive Detector. UV-visible absorption spectra were performed using a Hitachi U-2010 Double Beam UV/Visible Spectrophotometer. Solution samples of polymers in CHCl$_3$ were measured by using rectangular quartz cuvettes (light path = 10 mm). Thin films of the polymers were prepared for UV-visible absorption spectra measurements by dip coating quartz plates into approximately 1 mg cm^{-3} solutions in chloroform, then drying at room temperature. Measurements were performed under ordinary laboratory condition. The measurements of CV were obtained from a Princeton Applied Research Model 263A Potentiostat/Galvanostat. The electrochemical data was conducted under an inert pure argon atmosphere in a standard three-electrode cell system using (0.1 M)

tetrabutylammonium perchlorate in dry acetonitrile as the electrolyte solution. The electro system used consists of a platinum (Pt) disk as the working electrode, Pt wire as counter electrode and an Ag/Ag$^+$ (0.01 M in dry acetonitrile) reference electrode containing silver wire inside the capillary electrode. Polymer thin films were formed by drop casting (1.0 mg.cm^{-3}) in chloroform (HPLC graded) onto the Pt disk, and then dried in air. All three electrodes were immersed in the electrolyte solution. The experiments were calibrated with ferrocene, a reference redox system according to IUPACs recommendation.[4] Thermogravimetric analyses (TGAs) were recorded using a Perkin Elmer TGA-1 Thermogravimetric analyzer at a scan rate of 10 °C min^{-1} under inert conditions. Powder X-ray diffraction profiles of polymers were obtained using a Bruker D8 advance diffractometer with a CuK-α radiation source (1.5418 Å, rated as 1.6 kW). The scanning angle was performed over the range (2-40°).

6.3 Preparation of the monomers and polymers (class 1)- Chapter 2

6.3.1 1,4-Dibromo-2,3-diaminonaphthalene (1).[5]
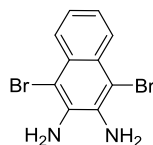
A solution of bromine (3.47 ml, 10.80 g, 67.50 mmol) in glacial acetic acid (90 ml) was added dropwise into a solution of 2,3-diaminonaphthalene (**S1**) (5.00 g, 31.60 mmol) in acetic acid (140 ml) under vigorous stirring at 5 °C for 0.5 hour, then stirred for 4 hours at room temperature. The precipitate was filtered off and washed with glacial acetic acid (50 ml) and 2% sodium carbonate solution (500 ml) respectively. The product was obtained as a brown precipitate (**1**) (8.20 g, 26.03 mmol, 82 %) then used in the next step without further purification despite the crude having a little trace of bromine.

^{1}H NMR (400 MHz, CDCl$_3$) (δ/ppm): 8.35 (dd, J = 7.0 and J = 3.0 Hz, 2H), 7.42 (dd, J = 7.0 and J = 3.0 Hz, 2H), 4.32 (s, 4H).

^{13}C NMR (400 MHz, CDCl$_3$) (δ/ppm): 135.37, 126.72, 124.80, 124.19, 102.12.

Mass (EI+): (m/z) (M$^{\bullet+}$) 315 (50%), 316 (100%), 319 (50%).

Elemental analysis calculated for C$_{10}$H$_8$Br$_2$N$_2$: C, 38.01; H, 2.55; Br, 50.57; N, 8.87; found: C, 38.61; H, 2.56; N, 8.54; Br, 49.43 %.

6.3.2 4,9-Dibromo-2,1,3-naphthothiadiazole (2).[6]
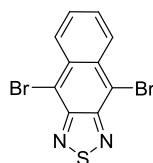
A mixture of thionyl chloride (12.7 ml, 20.8 g, 174.8 mmol), anhydrous CHCl$_3$ (80 ml), pyridine (30 ml) was added dropwise into a solution of compound (**1**) (8.10 g, 25.63 mmol) in anhydrous CHCl$_3$ (280 ml) with vigorous stirring in an ice-water bath. After the dropwise addition, the mixture heated to reflux overnight. Upon completion, the reaction mixture was quenched with water. The product was extracted with DCM (3 × 300 ml), washed with saturated brine (4 × 300 ml), dried (MgSO$_4$) and the solvent

evaporated *in vacuo*. The crude product was purified using column chromatography on silica gel and eluted with toluene:petroleum ether (70: 30%). Further purification was carried out by recrystallisation from ethanol to afford orange solid crystals (**2**) (4.31 g, 12.52 mmol, 49 % yield). The product gave a single spot on TLC plate ($R_f = 0.5$) (toluene: petroleum ether. 70: 30%).

^{1}H NMR (400 MHz, CDCl$_3$) (δ/ppm): 8.44 (dd, $J = 7.0$ and $J = 3.0$ Hz, 2H), 7.63 (dd, $J = 7.0$ Hz and $J = 3.0$ Hz, 2H).

^{13}C NMR (400 MHz, CDCl$_3$) (δ/ppm): 150.50, 133.26, 128.68, 127.86, 112.64.

Mass (EI+): (m/z) (M$^{\bullet +}$) 342 (50%), 344 (100%), 346 (50%).

Elemental analysis calculated for C$_{10}$H$_4$Br$_2$N$_2$S: C, 34.91; H, 1.17; Br, 46.45; N, 8.14; S, 9.32; found: C, 34.66; H, 0.96; Br, 46.42; N, 7.90; S, 9.20%.

6.3.3   4,9-Di-2'-thienyl-2,1,3-naphthothiadiazole (3).[7]
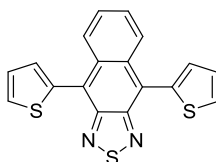
A mixture of dibromo compound (**2**) (2.50 g, 7.26 mmol) and 2-(tributylstannyl)thiophene (3.6 ml, 5.99 g, 16.05 mmol) was dissolved in a mixture of dry toluene (65 ml) and DMF (14 ml) under an inert atmosphere of argon and then degassed. Tris(di benzylideneacetone)dipalladium(0) Pd$_2$(dba)$_3$ (0.167 g, 0.181 mmol) and tri-*o*-tolyl phosphine (0.441 g, 1.45 mmole) were added and the reaction mixture was degassed again. The mixture reaction was heated to reflux with vigorous stirring overnight. After being cooled to room temperature, the product was extracted with DCM (3 × 200 ml), washed with water (2 × 200 ml), dried over (MgSO$_4$) and the solvent was removed *in vacuo* to yield the crude product. The crude material was purified over silica gel column chromatography, eluted with 4:6 (petroleum ether: toluene) then recrystallised from ethanol to obtain dark purple crystals (**3**) (1.39 g, 3.97 mmol, 55 % yield). This gave one dark spot on the TLC plate ($R_f = 0.26$) in petroleum ether: toluene. (40: 60 %).

^{1}H NMR (400 MHz, CDCl$_3$) (δ/ppm): 8.32 (dd, J = 7.0 and J = 3.0 Hz, 2H), 7.71 (dd, J = 5.0 and J = 2.0 Hz, 2H), 7.49 (dd, J = 4.0 and J = 2.0 Hz, 2H), 7.46 (dd, J = 7.0 and J = 3.0 Hz, 2H), 7.36 (dd, J = 5.0 and J = 4.0 Hz, 2H).

^{13}C NMR (400 MHz, CDCl$_3$) (δ/ppm): 151.35, 136.42, 133.00, 130.34, 127.91, 127.26, 127.01, 126.97, 123.59.

Mass (EI+): (m/z) (M•$^+$) 350.

Elemental analysis calculated for C$_{18}$H$_{10}$N$_2$S$_3$: C, 61.69; H, 2.88; N, 7.99; S, 27.44; found: C, 61.50; H, 2.47; N, 7.87; S, 25.58 %.

6.3.4 4,9-Di(2-bromothienyl-5-yl)-2,1,3-naphthothiadiazole (M).[6]
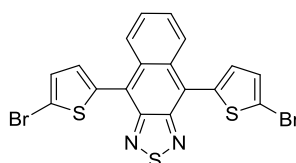
Dithienyl-NT compound (**3**) (1.30 g, 3.71 mmol) was dissolved in chlorobenzene (CB) (50 ml). A portion of N-bromosuccinimide (NBS) (1.30 g, 7.35 mmol) was added to the solution then the reaction system was degassed and placed under an inert atmosphere. The mixture was heated slowly to 55 °C with stirring for 3 hours, resulting in the formation of slurry as the reaction progressed. The mixture was heated up to 130°C until all solids were dissolved. The mixture was cooled down to room temperature and the resulting precipitate was filtered off and washed with methanol. The crude product was purified *via* silica gel column chromatography and eluted with 40-60 petroleum ether:toluene (30:70%) to obtain red crystals (**M**) (1.2 g, 63 %). This gave a dark red spot on TLC plate (R$_f$ = 0.66), (toluene: petroleum ether. 70: 30%).

^{1}H NMR (400 MHz, CDCl$_3$) (δ/ppm): 8.34 (dd, J = 7.0 and J = 3.0 Hz, 2H), 7.49 (dd, J = 7.0 and J = 3.0 Hz, 2H), 7.31 (d, J = 4.0 Hz, 2H), 7.24 (d, J = 4.0 Hz, 2H).

^{13}C NMR (400 MHz, CDCl$_3$) (δ/ppm): 151.35, 137.85, 132.84, 130.81, 130.20, 127.43, 126.72, 122.80, 115.08.

Mass (EI+): (m/z) (M•$^+$) 506 (50%), 508 (100%), 510 (50%).

Elemental analysis calculated for C$_{18}$H$_8$Br$_2$N$_2$S$_3$: C, 42.54; H, 1.59; Br, 31.44; N, 5.51; S, 18.92 found: C, 42.75; H, 1.37, N, 5.36; Br, 31.20; S, 18.46 %.

6.3.5 Poly(2,7-(9,9-dioctyl-fluorene)-*alt*-5,5(4,9-di-2-thienyl-2,1,3-naphthothiadiazole) PFDTNT-P1.[8]
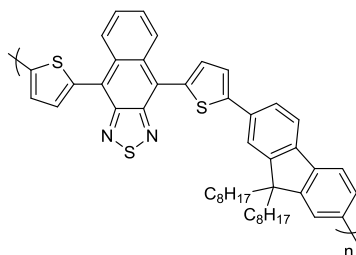
A single neck 100 ml round bottom flask under argon containing monomer (**M**) (0.186 g, 0.36 mmol) and monomer (**S2**) (0.204 g, 0.36 mmol) in dry THF (9 ml) was degassed using standard Schlenk link techniques. To the mixture, a saturated solution of sodium bicarbonate (2.1 ml, 2.85 mmol) was added and the system degassed again. The flask was charged with a mixture of tri-o-tolyl phosphine (0.017 g, 0.056 mmol) and Pd(OAc)$_2$ (0.0063 g, 0.028 mmol), the reaction system was degassed again and then heated to reflux for 24 hours. After cooling the reaction mixture to room temperature, 1-bromobenzene (0.1 ml, 0.94 mmol) and dry THF (5 ml) were added to the reaction solution for end-capping. The mixture was heated to 90 °C for 1 hour and then cooled to room temperature. Phenyl boronic acid (0.15 mg, 1.23 mmol) was added and the mixture was stirred at 90 °C for 3 hours. The mixture was then cooled to room temperature and poured into a mixture of CHCl$_3$ (200 ml) and an ammonium hydroxide solution (28 % in H$_2$O, 50 ml) then stirred vigorously overnight. The organic layer was separated *via* a separating funnel and washed with water, concentrated to roughly 20 ml *in vacuo* and poured into degassed methanol (300 ml). This mixture was stirred overnight and then filtered through a membrane filter. The obtained solid was fractionated using a Soxhlet extraction with organic solvents: methanol (300 ml), acetone (300 ml), hexane (300 ml), toluene (300 ml), chloroform (300 ml) and CB (300 ml). The chloroform fraction was concentrated to 50 ml and then poured into degassed methanol (200 ml). The resulting mixture was stirred overnight and the solid was collected by filtration through a membrane filter to afford the product as a dark purple powder.

Toluene fraction (29 % yield) GPC in CHCl$_3$ at 40 °C (M_n = 9,900), (M_w = 16,800), (PDI = 1.7)

Chloroform fraction (43 % yield) GPC in CHCl$_3$ at 40 °C (M_n = 41,100), (M_w = 79,500), (PDI = 1.93).

^{1}H NMR (400 MHz, CDCl$_3$) (δ/ppm): 8.54 (m, 2H), 7.80 (br, 4H), 7.74 (br, 2H), 7.67 (br, 2H), 7.55 (br, 4H), 2.11 (br, 4H), 1.26-1.06 (br, 20H), 0.85- 0.68 (m, 10H).

Elemental Analysis calculated for C$_{49}$H$_{54}$N$_2$S$_3$: C, 76.71; H, 7.09; N, 3.65; S, 12.54%. Found: C, 76.40; H, 6.27; N, 3.73; S, 12.55%.

6.3.6   Poly(N-9-hepta-decanyl-2,7-carbazole-*alt*-5,5-(4,9-di-2-thienyl-2,1,3-naphthothiadiazole) PCDTNT-P2.[8]
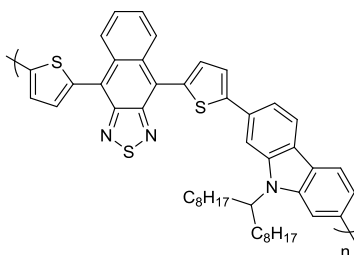
A mixture of monomer (**M**) (0.186 g, 0.36 mmol) and compound (**S6**) (0.241 g, 0.36 mmol) was added to a single neck 100 ml round bottom flask and placed under argon using standard Schlenk link techniques. Dry THF (9 ml) and degassed solution of sodium bicarbonate (2.1 ml, 2.85 mmol) were added and degassed again. To this solution, tri-o-tolyl phosphine (0.017 g, 0.056 mmol) and Pd(OAc)$_2$ (0.0063 g, 0.028 mmol) were added, degassed and heated to 90 °C for 48 hour. The mixture was cooled to room temperature and then 1-bromobenzene (0.1 ml, 0.94 mmol) was added, degassed and heated at 90 °C for 1 hour. The mixture was cooled to room temperature and phenylboronic acid (0.15 mg, 1.23 mmol) was added, degassed and heated to reflux for 3 hours. The mixture was poured into a mixture of CHCl$_3$ (200 ml) and an ammonium hydroxide solution (28 % in H$_2$O, 50 ml) then stirred vigorously overnight. The organic layer was separated using a separating funnel and washed with distilled water, concentrated to roughly 20 ml *in vacuo* and poured into degassed methanol (300 ml) under stirring. The mixture was then filtered through a membrane filter. The precipitate was cleaned using Soxhlet extraction with solvents in the order; methanol (300 ml), acetone (300 ml), hexane (300 ml), toluene (300 ml), chloroform (300 ml) and CB (300 ml). The chloroform fraction was concentrated (50 ml) and then poured into degassed methanol (300 ml). The resulting mixture was stirred overnight and the

solid was collected by filtration through a membrane filter to afford the product as a dark purple powder.

Chloroform fraction (67 % yield) GPC in CHCl$_3$ at 40 °C (M_n = 23,100), (M_w = 89,600), (PDI =3.8)

^{1}H NMR (400 MHz, CDCl$_3$) (δ/ppm): 8.56 (m, 2H), 8.18 (br, 2H), 7.95 (br, 1H), 7.78 (br, 1H), 7.68 (br, 4H), 7.60-7.51 (br, 4H), 4.70 (br, 1H), 2.42 (br, 2H), 2.02 (br, 2H), 1.4-1.10 (br, 24H), 0.83-0.77 (m, 6H).

Elemental Analysis calculated for C$_{49}$H$_{55}$N$_3$S$_3$: C, 75.24; H, 7.09; N, 5.37; S, 12.30%. Found: C, 74.58; H, 6.29; N, 5.45; S, 12.51%.

6.3.7 Poly(9,10-bis (4-dodecyloxy) phenyl) anthracene-2,6-diyl-*alt*-(4,9-dithiophen-2-yl)-2,1,3-naphthothiadiazole-5,5-diyl) PPATNT-P3.[8]
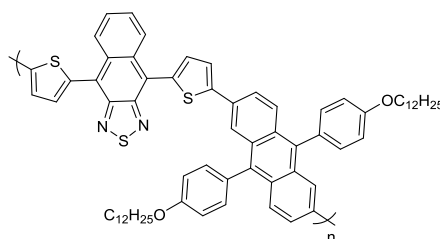
A solution of (**M**) (0.186 g, 0.36 mmol) and (**S7**) (0.350 g, 0.36 mmol) in dry toluene (9 ml) was added to a single neck 100 ml round bottom flask and placed under argon using standard Schlenk link techniques. A 20% w/w aqueous hydroxide solution of tetraethylammonium hydroxide (2.1 ml, 2.85 mmol, degassed) was added and degassed under an inert atmosphere. Pd(OAc)$_2$ (0.006 g, 0.028 mmol) and tri-o-tolyl phosphine (0.017 g, 0.056 mmol) were added to the mixture then the reaction system was degassed and heated up to 90 °C for 24 hours. After cooling to room temperature, 1-bromobenzene (0.1 ml, 0.94 mmol) was added to end-cap and the solution was heated to reflux for 1 hour before cool to room temperature. Phenyl boronic acid (0.15 mg, 1.23 mmol) was added to the reaction components and heated to 90 °C for 3 hours. After cooling the mixture to room temperature, the organic content was dissolved in CHCl$_3$ (200 ml) and added to an ammonium hydroxide solution (28 % in H$_2$O, 50 ml), followed by vigorous stirring overnight. The organic layer was separated and washed with distilled water then concentrated to about 20 ml *in vacuo*. The mixture was poured slowly into degassed methanol (300 ml) and stirred overnight. The resulting precipitate

was filtered off by membrane filter. The precipitate obtained was sequentially purified by Soxhlet apparatus with different solvents in the following order: methanol (300 ml), acetone (300 ml), hexane (300 ml), toluene (300 ml), chloroform (300 ml) and CB (300 ml). The toluene and chlorobenzene fractions were concentrated to about 50 ml *in vacuo* and then separately poured into degassed methanol (200 ml). After stirring overnight, the precipitate was collected separately by membrane filtration and dried *in vacuo* to afford dark red-coloured powders.

Toluene fraction (32 % yield) GPC in CHCl$_3$ at 40 °C (M_n = 10,900), (M_w = 23,100), (PDI = 2.1).

^{1}H NMR (400 MHz, CDCl$_3$) (δ/ppm): 8.42 (br, 2H), 8.12, (br, 2H), 7.85-7.73 (br, 4H), 7.56-7.37 (br, 8H), 7.22-7.13 (br, 6H), 4.18-4.12 (br, 4H), 2.37 (s, 1H), 2.19 (s, 1H), 1.95-1.82 (br, 4H), 1.71-1.19 (br, 36H), 0.88 (t, *J*= 6.0, 6H).

Elemental Analysis calculated for C$_{70}$H$_{78}$N$_2$O$_2$S$_3$: C, 78.17; H, 7.31; N, 2.60; S, 8.94%. Found: C, 77.30; H, 6.89; N, 2.50; S, 8.10%.

6.4 Preparation of the monomers and polymers (class 2 and 3)-Chapter 3

6.4.1 9,9-Dioctyl-2,7-[bis(2'-trimethysilyl)ethynyl)] fluorene (4).[9]
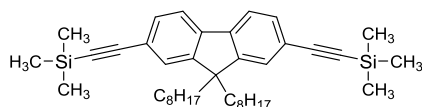
A two-neck 100 ml round bottom flask containing a solution of 2,7-dibromo-9,9-dioctylfluorene (**S3**) (1.10 g, 2.01 mmol) in dry toluene (20 ml) and diisopropylamine (6 ml, degassed) was stirred and placed under an inert atmosphere. Copper (I) iodide (CuI) (0.016 g, 5%) and bis(triphenylphosphine) palladium(II) dichloride $Pd(PPh_3)_2Cl_2$ (0.052 g, 4%) were added to the solution reaction then the system was degassed. After stirring for 0.5 hour, a solution of trimethylsilyl acetylene (0.43 g, 0.62 ml, 4.40 mmol, d = 0.695 g/ml) in disopropylamine (4.0 ml, degassed) was added *via* syringe to the suspension. Purging of the inert gas was continued during and after the addition. The mixture was degassed and then heated to reflux overnight to give a reddish brown suspension. The reaction was monitored by TLC to verify the completion of the reaction. After cooling the mixture to room temperature, the solvent was removed *in vacuo* to produce a crude product. The material was purified *via* chromatography over silica gel using petroleum ether as eluent to give a pure product as white crystals (1.10 g, 1.88 mmol, 94 %). The purity of the product was confirmed by TLC (single spot Rf = 0.5) in petroleum ether.

^{1}H NMR (400 MHz, CDCl$_3$) (δ/ppm): 7.61 (d, *J* = 8.0 Hz, 2H), 7.47 (dd, *J* = 8.0 and *J* = 2.0 Hz, 2H), 7.43 (s, 2H), 1.94 (m, 4H), 1.27-1.0 (m, 20H), 0.84 (t, *J* = 7.0 Hz, 6H), 0.57-0.48 (br, 4H), 0.30 (s, 18H).

^{13}C NMR (400 MHz, CDCl$_3$) (δ/ppm): 150.93, 140.85, 131.22, 126.21, 121.73, 119.83, 106.07, 94.25, 55.23, 40.34, 31.79, 29.89, 29.24, 23.59, 22.60, 14.10, -0.06.

Mass (EI+): (m/z) (M$\bullet^+$) 582.

Elemental analysis calculated for $C_{39}H_{58}Si_2$: C, 80.34; H, 10.03 found; C, 79.83; H, 9.82.

6.4.2 9,9-Dioctyl -2,7-diethynylfluorene (M1).[9]
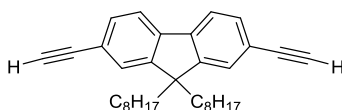
A solution of compound (**4**) (1.00 g, 1.71 mmol) in dry THF (15 ml) was stirred under degassed conditions. KOH aqueous solution (2.5 ml, 25% wt) in methanol (10 ml) was slowly added to the above reaction mixture under an inert atmosphere. The reaction was left at room temperature for 2 hours. The mixture reaction was extracted with DCM (3 × 200 ml), washed with brine (2 × 200 ml) and dried over (MgSO₄). The solvent was evaporated *in vacuo* to obtain white-yellow crystals as pure product (0.72 g, 1.64 mmol, 96 %). The product gave a single spot on TLC (Rf = 0.36) in 100% hexane.

^{1}H NMR (400 MHz, CDCl$_3$) (δ/ppm): 7.65 (d, J = 8.0 Hz, 2H) 7.50 (dd, J = 8.0 and J = 2.0 Hz, 2H), 7.48 (s, 2H), 3.17 (s, 2H), 1.97-1.93 (m, 4H), 1.27-1.05 (m, 20H), 0.84(t, J = 7.0, 6H), 0.60-0.53 (br, 4H).

^{13}C NMR (400 MHz, CDCl$_3$) (δ/ppm): 151.05, 141.01, 131.25, 126.55, 120.84, 119.98, 84.53, 55.22, 40.21, 31.77, 29.94, 29.20, 23.65, 22.59, 14.08.

Mass (EI+): (m/z) (M•$^+$). 438.

Elemental analysis calculated for C$_{33}$H$_{42}$; C, 90.35; H, 9.65, found; C, 89.23; H, 9.59.

6.4.3 Heptadecan-9-ol (5).[10]
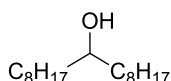
A two-neck 500 ml round bottom flask was charged with a fresh solution of octyl magnesium bromide, which was prepared from a reaction between 1-bromooctane (48.20 g, 250 mmol) and fresh magnesium (6.68 g) in dry THF (80 ml) at 0 °C under inert condition. The resulting mixture was heated to reflux for 2 hours to obtain octylmagnesium bromide as a grey solution (Grignard solution). The reagent was added dropwise to another flask containing a solution of ethyl formate (6.69 ml, 83.35 mmol) in dry THF (130 ml) at -78 °C. The reaction mixture was allowed to stir at -78 °C for 1 hour then the suspension mixture was warmed to room temperature and stirred

overnight. Upon completion, the reaction was quenched by the addition of MeOH, followed by saturated aqueous NH_4Cl was added. The product was extracted with diethyl ether (3 × 200 ml), washed with brine solution (2 × 200 ml) and dried over ($MgSO_4$). After removal of the solvent *in vacuo*, the crude product was subjected to silica gel column chromatography using petroleum ether: ethyl acetate (13:1) to yield (1b) as white crystals (19.61 g, 76.60 mmol, 92 %). The purity of the product was confirmed by TLC (single spot Rf = 0.68) in 100% hexane.

^{1}H NMR (400 MHz, $CDCl_3$) (δ/ppm): 3.64-3.56 (br, 1H), 1.50-1.25 (br, 29H), 0.90 (t, *J* = 7.0 Hz, 6H).

^{13}C NMR (400 MHz, $CDCl_3$) (δ/ppm): 72.03, 37.50, 31.88, 29.72, 29.60, 29.28, 25.66, 22.67, 14.09.

Mass (EI+): (m/z) (M•[+]) 256.

Elemental analysis calculated for $C_{17}H_{36}O$; C, 79.61; H, 14.15, found; C, 79.69; H, 14.14.

6.4.4   9-Heptadecane p-toluenesulfonate.(6).[11]
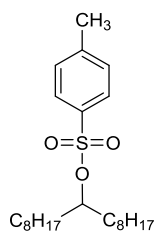
A two-necked flask was charged with a mixture of heptadecan-9-ol (**5**) (10.18 g, 39.69 mmol), triethylamine Et_3N (20 ml) and $Me_3N.HCl$ (2.13 g, 22.28 mmol) in DCM (50 ml). The mixture was stirred at 0 °C, followed by solution of p-toluenesulfonyl chloride (13.82 g, 72.52 mmol) in DCM (50 ml) was added dropwise. The reaction mixture was stirred for 1.5 hour. Upon completion, water was added to quench the reaction. The product was extracted with DCM (3 x 200 ml), washed with brine (2 × 200 ml) and dried over ($MgSO_4$). The solvent was evaporated *in vacuo* to produce a crude product. The resulting precipitate was purified through silica gel column chromatography and eluted with petroleum ether: ethyl acetate (90: 10%). The material was then recrystallised from methanol affording the compound (**6**) as white crystals (13.85 g,

33.73 mmol, 85 % yield). The progress of the reaction and the purity of the product were monitored by TLC (Rf = 0.57) in petroleum ether: ethyl acetate (90:10 %).

^{1}H NMR (400 MHz, CDCl$_3$) (δ/ppm): 7.81 (d, J = 8.0 Hz, 2H), 7.34 (d, J = 8.0 Hz, 2H), 4.56 (m, 1H), 2.46 (s, 3H), 1.64-1.50 (m, 4H), 1.34-1.13 (m, 24H), 0.90 (t, J = 7.0 Hz, 6H).

^{13}C NMR (400 MHz, CDCl$_3$) (δ/ppm): 144.24, 129.60, 127.72, 84.65, 34.13, 31.83, 29.35, 29.29, 29.15, 24.68, 22.64, 21.57, 14.08.

Mass (EI+): (m/z) (M$^{\bullet+}$). 410.

Elemental analysis calculated for C$_{24}$H$_{42}$O$_3$S, C, 70.20; H, 10.31; S, 7.81, found; C, 70.33; H, 10.34; S, 7.71.

6.4.5 2,7-Dibromo-9-(heptadecan-9-yl)-9H-carbazole.(7).[12]
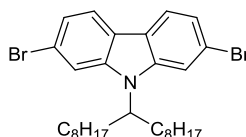
A solution of 9-heptadecane *p*-toluenesulfonate (**6**) (4.84 g, 11.80 mmol) in dry THF (10 ml) was slowly added to a suspension containing 2,7-dibromo -9H-carbazole (**S8**) (1.92 g, 5.91 mmol) and a fresh powder of KOH (2.97 g, 53.1 mmol) in dry THF (17 ml) under vigorous stirring. The reaction mixture was degassed and placed under an inert atmosphere. The reaction was left overnight at ambient temperature. Upon completion, the mixture was slowly poured into iced water (200 ml) to quench the reaction. The aqueous solution was extracted with hexane (3 x 200 ml), washed with brine solution (2 × 200 ml) and dried over (MgSO$_4$). The solvent was evaporated *in vacuo* to obtain a crude product. The precipitate was chromatographed *via* silica gel, eluting with petroleum ether to obtain the pure product as white crystals (2.81 g, 4.98 mmol, 85% yield). The purity of the product was confirmed by TLC (single spot. Rf = 0.45) in 100 % petroleum ether.

^{1}H NMR (400 MHz, CDCl$_3$, (δ/ppm): 7.75 (m, 2H); 7.71 (s, 1H); 7.55 (s, 1H), 7.35 (m, 2H), 4.43 (m, 1H); 2.27-2.16 (m, 2H), 2.06-1.86 (m, 2H); 1.37-1.09 (m, 20H); 1.04-0.93 (br, 4H); 0.85 (t, J = 7.0 Hz, 6H).

^{13}C NMR (400 MHz, CDCl$_3$) (δ/ppm): 122.32, 121.48, 121.23, 114.53, 112.16, 56.96, 33.48, 31.74, 29.28, 29.27, 29.12, 26.73, 22.60, 14.07.

Mass (EI+): (m/z) (M•$^+$) 561 (50%), 563 (100%), 565 (50%).

Elemental analysis calculated for C$_{29}$H$_{41}$Br$_2$N; C, 61.82; H, 7.33; N, 2.49; Br, 28.36, found; C, 63.08; H, 7.73; N, 2.49; Br, 27.16.

6.4.6 9-(Heptadecan-9-yl)-2,7-bis((trimethylsilyl)ethynyl)-9H-carbazole.(8).
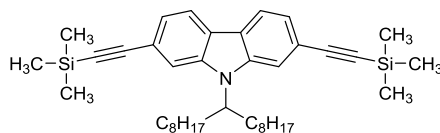
A single neck 100 ml round bottom flask containing compound (**7**) (0.50 g, 0.88 mmol), CuI (0.008 g, 5%) and Pd(PPh$_3$)$_2$Cl$_2$ (0.031 g, 4%) in dry toluene (10 ml), followed by diisopropylamine (6 ml, degassed) was added and placed under an inert condition. To this mixture, a solution of trimethylsilyl acetylene (0.19 g, 0.27 ml, 1.95 mmol, d = 0.695 g/ml) in disopropylamine (4.0 ml, degassed) was slowly added *via* syringe to the reaction mixture. The mixture was then degassed again and heated at 70 °C overnight. The reaction was monitored by TLC to verify the completion of the reaction. Upon completion, the mixture was cooled to room temperature and the solvent removed *in vacuo* to the crude product. The precipitate was purified over column chromatography using silica gel as the column material and petroleum ether as the eluent to yield the product (**8**) as a yellow powder (0.50 g, 0.83 mmol, 95 %). The product gave a single spot on TLC (Rf = 0.40) in 100 % petroleum ether.

^{1}H NMR (400 MHz, CDCl$_3$) (δ/ppm): 7.98 (m, 2H); 7.67 (s, 1H); 7.53 (s, 1H), 7.34 (br, 2H)., 4.51 (m, 1H); 2.31-2.20 (m, 2H), 1.98-1.87 (m, 2H); 1.30-1.08 (br, 20H); 1.04-0.93 (br, 4H); 0.85 (t, *J* = 7.0 Hz, 6H); 0.32 (s, 18H).

^{13}C NMR (400 MHz, CDCl$_3$) (δ/ppm): 142.08, 138.64, 123.69, 123.18, 122.99, 122.25, 120.32, 120.09, 119.82, 115.04, 112.62, 106.63, 93.55, 56.85, 33.67, 31.72, 29.37, 29.30, 29.12, 26.84, 22.57, 14.03, -0.08.

Mass (EI+): (m/z) (M•$^+$). 597.

Elemental analysis calculated for C$_{39}$H$_{59}$NSi$_2$, C, 78.32; H, 9.94; N, 2.34; found; C, 78.30; H, 10.14; N, 2.09.

6.4.7 2,7-Diethynyl-9-(heptadecan-9-yl)-9H-carbazole. (M2).
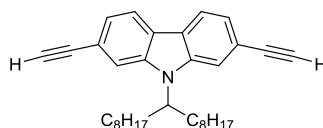
An aqueous solution of KOH (2.5 ml, 25% wt) in methanol (4 ml) was added dropwise to a single neck 100 ml flask containing compound (**8**) (0.44 g, 0.73 mmol) in dry THF (10 ml) under argon atmosphere. The reaction system was degassed and stirred at ambient temperature for 3 hours. The progress of reaction was monitored by TLC to confirm the completion. Upon completion, the mixture was extracted with DCM (3 × 200 ml), washed with water (2 × 200 ml) and dried over (MgSO$_4$). The solvent was removed *in vacuo* to yield pure product (**M2**) as yellow viscous oil (0.31 g, 0.68 mmol, 92 %). The product gave a single spot on TLC (Rf = 0.45) in petroleum ether.

^{1}H NMR (400 MHz, CDCl$_3$) (δ/ppm): 8.02 (br, 2H); 7.74 (s, 1H); 7.58 (s, 1H), 7.38 (br, 2H)., 4.51 (m, 1H); 3.19 (s, 2H); 2.31-2.20 (m, 2H), 1.98-1.89 (m, 2H); 1.29-1.09 (m, 20H); 1.04-0.93 (br, 4H); 0.85 (t, J = 7.0 Hz, 6H).

^{13}C NMR (400 MHz, CDCl$_3$) (δ/ppm): 142.31, 138.62, 123.88, 123.05, 122.98, 122.44, 120.59, 120.31, 119.93, 118.84, 115.46, 112.97, 85.07, 56.85, 33.63, 31.74, 29.32, 29.28, 29.13, 26.80, 22.60, 14.07.

Mass (EI+): (m/z) (M•$^+$).453.

Elemental analysis calculated for C$_{33}$H$_{43}$N, C, 87.36; H, 9.55; N, 3.09; found; C, 87.31; H, 9.62; N, 3.05.

6.4.8 1-Bromo-4-(dodecyloxy) benzene (9).[13]
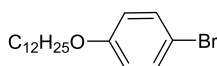
Under an inert condition, 4-bromo-phenol (5.00 g, 28.90 mmol) and K$_2$CO$_3$ (11.98 g, 8.67 mmol) in dry acetone (50 ml) were added to two-neck 100 ml flask. A solution of 1-bromododecane (8.71 g, 34.9 mmol) in dry acetone (15 ml) was slowly added. After addition, the mixture was stirred at ambient temperature for 0.5 hour. The suspended mixture was then degassed and heated to reflux overnight. The mixture was cooled to room temperature and filtered off, the filtrate was concentrated *in vacuo*. The resulting

residue was subjected to silica flash column chromatography using petroleum ether: DCM (1:1) as eluent to afford white crystals as the pure product (9.66 g, 28.32 mmol, 98 %).

^{1}H NMR (400 MHz, CDCl$_3$) (δ/ppm): 7.37 (d, J = 9.0 Hz, 2H); 6.79 (d, J = 9.0 Hz, 2H), 3.94 (t, J = 7.0 Hz, 2H), 1.78 (m, 2H); 1.50-1.23 (br, 18H); 0.90 (t, J = 14.0 Hz, 3H).

^{13}C NMR (400 MHz, CDCl$_3$) (δ/ppm): 158.26, 132.19, 116.30, 112.55, 68.28, 34.08, 32.87, 31.93, 29.67, 29.65, 29.60, 29.58, 29.46, 29.37, 29.18, 28.79, 28.20, 26.01, 22.71, 14.14.

Mass (EI+): (m/z) (M•$^+$). 340 (50%), 342 (50%).

Elemental analysis calculated for C$_{18}$H$_{29}$BrO, C, 63.34; H, 8.56, Br, 23.41, found; C, 63.27; H, 8.57; Br, 24.69.

6.4.9 2,6-Dibromoanthracene-9,10-dione (10).[14]
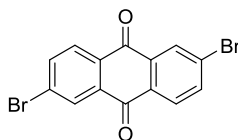
Under an inert condition, 2,6-diaminoanthracene-9,10-dione (**S4**) (9.60 g, 40 mmol), anhydrous copper (II) bromide CuBr$_2$ (17.8 g, 80 mmol), and tert-butyl nitrite t-BuONO (11.89 ml, 100 mmol) in dry acetonitrile CH$_3$CN (200 ml) were added to a two neck 500 ml round bottom flask. The reaction mixture was heated to 65 °C for 3 hours. Upon completion, the reaction mixture was cooled to room temperature and HCl aq (100 ml, 20%) was slowly added to quench the reaction, followed by water was added to produce light brown precipitate. The product was filtered and washed with water (3 × 200 ml) and CH$_3$CN (3 × 200 ml). The crude product was purified over a flash column of silica gel with CHCl$_3$ as the eluent and then recrystallised from hot toluene as the solvent to obtain a pure product (**10**) as shiny yellow crystals (12.59 g, 34.40 mmol, 86 %).

^{1}H NMR (400 MHz, CDCl$_3$) (δ/ppm): 8.46 (br, 2H), 8.19 (d, J = 8.0 Hz, 2H), 7.96 (dd, J = 8.0 and J = 2.0 Hz, 2H).

Mass (EI+): (m/z) (M•$^+$). 364 (50%), 366 (100%), 368 (50%).

Elemental analysis calculated for $C_{14}H_6Br_2O_2$, C, 45.94; H, 1.65, Br; 43.66, found; C, 46.01; H, 1.69, Br; 43.74.

6.4.10 2,6-Dibromo-9,10-bis(4-(dodecyloxy)phenyl)anthracene (11).[15]
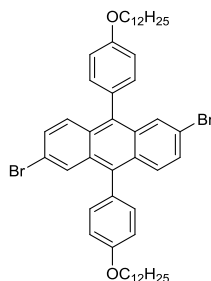
A two neck 500 ml round bottom flask containing a solution of 1-bromo-4-(dodecyloxy)benzene (**9**) (2.80 g, 8.21 mmol) in dry THF (50 ml) was cooled to −78 °C under vigorous stirring. The reaction was degassed and placed under an inert condition. N-butyl lithium (3.2 ml, 8.21 mmol) was added dropwise a using syringe then the reaction was left to stir for 3 hours, 2,6-dibromoanthracene-9,10-dione (**10**) (1 g, 2.37 mmol) was added as one portion to the above suspension mixture. The mixture was then allowed to warm to room temperature and left to stir for 48 hours. The resulting mixture was poured into water (200 ml) and extracted with diethyl ether (3 × 200 ml). The organic phases were combined, washed with brine (2 × 200 ml), dried over (MgSO$_4$) and the solvent removed *in vacuo*. The brownish residue was obtained as crude product and starting material for next reduction step. A mixture of the resulting material (2.53 g, 2.63 mmol), potassium iodide KI (3.77 g, 22.74 mmol) and sodium hypophosphite NaHPO$_2$ (2.65 g, 30.71 mmol) in acetic acid (30 ml) was stirred vigorously. The reaction mixture was refluxed at 120 °C for 24 hours. Upon completion, the solution was allowed to cool to ambient temperature and the solvent removed *in vacuo*. The organic precipitate was dissolved with DCM (200 ml), washed with brine (2 × 200 ml) and dried (MgSO$_4$). The solvent was removed *in vacuo* and recrystallised from methanol to afford the product as a yellow powder with a reasonable yield: (1.58 g, 1.82 mmol, 69 %).

^{1}H NMR (400 MHz, CDCl$_3$) (δ/ppm): 7.89 (br, 2H), 7.61 (d, J = 9.0 Hz, 2H), 7.38 (dd, J = 9.0 and J = 2.0 Hz, 2H), 7.33 (d, J = 9.0 Hz, 4H), 7.15 (d, J = 9.0 Hz, 4H), 4.14 (t, J = 7.0 Hz, 4H), 1.92 (m, 4H); 1.61-1.25 (br, 36H); 0.91 (t, J = 14.0 Hz, 6H).

^{13}C NMR (400 MHz, CDCl$_3$) (δ, ppm): 158.98, 136.59, 132.21, 131.28, 129.48, 129.20, 129.05, 128.95, 128.82, 128.40, 126.66, 120.05, 114.67, 68.20, 31.95, 29.72, 29.66, 29.55, 92.43, 29.39, 26.20, 22.72, 14.15.

Mass (EI+): (m/z) (M•$^+$) 854 (50%), 856 (100%), 858 (50%).

Elemental analysis calculated for C$_{50}$H$_{64}$Br$_2$O$_2$, C, 70.09; H, 7.53; Br, 18.65 found; C, 71.16; H, 7.78; Br, 17.91.

6.4.11 ((9,10-Bis(4-(dodecyloxy)phenyl)anthracene-2,6-diyl)-bis(ethyne-2,1-diyl-bis (trimethylsilane)) (12).
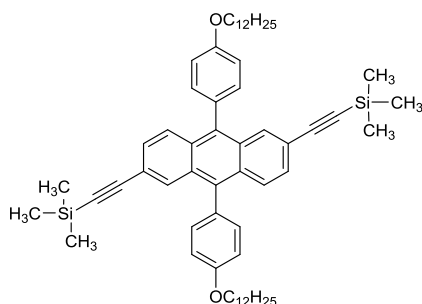
A single neck 100 ml round bottom flask was charged with compound (**11**) (0.40 g, 0.46 mmol), CuI (0.005 g, 5%) and Pd(PPh$_3$)$_2$Cl$_2$ (0.018 g, 4%) in dry toluene (20 ml), followed by diisopropylamine (6 ml, degassed) were degassed and placed under an inert atmosphere for 0.5 hour. To this solution, trimethylsilyl acetylene (0.99 g, 0.14 ml, 1.0 mmol, d = 0.695 g/ml) in disopropylamine (4.0 ml, degassed) was added. The system was degassed again and then refluxed at 70 °C for 48 hours. The reaction was monitored by spot TLC to verify the completion of the reaction. Upon completion, the solvent was removed from the reaction mixture *in vacuo* to obtain a crude product. The product was purified *via* silica gel chromatography column using petroleum ether: toluene (80: 20%) as eluent to yield a pure product **12** as a yellow precipitate (0.39 g, 0.43 mmol, 95 %). The product gave a single spot on TLC (Rf = 0.5) in petroleum ether: toluene (80: 20%).

^{1}H NMR (400 MHz, CDCl$_3$) (δ/ppm): 7.89 (br, 2H), 7.64 (d, J = 9.0 Hz, 2H), 7.35 (d, J = 9.0 Hz, 4H), 7.31 (dd, J= 9.0 and J = 2.0 Hz, 2H), 7.16 (d, J = 9.0 Hz, 4H), 4.14 (t, J = 7.0 Hz, 4H), 1.92 (m, 4H); 1.62-1.25 (br, 36H); 0.91 (t, J = 7.0 Hz, 6H), 0.26 (s, 18H).

^{13}C NMR (400 MHz, CDCl$_3$) (δ/ppm): 158.79, 137.01, 132.42, 131.13, 130.22, 129.96, 129.86, 127.69, 127.25, 119.84, 114.53, 105.85, 95.47, 88.94, 68.20, 31.95, 29.71, 29.66, 29.51, 92.45, 29.39, 26.20, 22.72, 14.15, -0.05.

Mass (EI+): (m/z) (M•$^+$) 891.

Elemental analysis calculated for C$_{60}$H$_{82}$O$_2$Si$_2$, C, 80.84; H, 9.27, found; C, 77.15; H, 8.76%.

6.4.12 9,10-Bis(4-(dodecyloxy)phenyl)-2,6-diethynyl anthracene (M3).
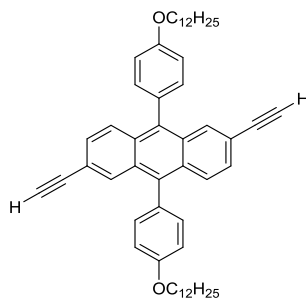
Under an inert condition, a solution of compound (**12**) (0.34 g, 0.38 mmol) in dry THF (15 ml) was stirred vigorously. KOH (2.5 ml, 25 % wt, aqueous solution) in methanol (4 ml) was slowly added and the reaction system was degassed again. The resulting mixture was stirred at ambient temperature for 4 hours; the mixture was then extracted with DCM (3 × 200 ml), washed with water (2 × 200 ml) and dried over (MgSO$_4$). The solvent was removed *in vacuo* to obtain the crude product. The material was purified *via* silica gel chromatography column using petroleum ether: toluene (80:20 %) as eluent to afford a pure product (M3) as yellow crystals (0.22 g, 0.29 mmol, 77 %). The product provided a single spot on TLC (Rf = 0.45) in petroleum ether: toluene (80: 20 %).

^{1}H NMR (400 MHz, CDCl$_3$) (δ/ppm): 7.94 (br, 2H), 7.69 (d, *J* = 9.0 Hz, 2H), 7.36-7.32 (br, 6H), 7.15 (d, *J* = 9.0 Hz, 4H), 4.13 (t, *J* = 7.0 Hz, 4H), 3.13 (s, 2H), 1.91 (m, 4H); 1.62-1.25 (br, 36H); 0.91 (t, *J* = 7.0 Hz, 6H).

^{13}C NMR (400 MHz, CDCl$_3$) (δ/ppm): 158.89, 137.18, 132.29, 131.85, 130.25, 129.95, 129.72, 127.50, 127.41, 118.84, 114.57, 84.43, 78.14, 68.18, 31.95, 29.72, 29.66, 29.50, 29.43, 29.39, 26.19, 22.72, 14.15.

Mass (EI+): (m/z) (M•$^+$) 746.

Elemental analysis calculated for $C_{54}H_{66}O_2$, C, 86.81; H, 8.90, found; C, 85.22; H, 8.78%.

6.4.13 Poly((9,9-dioctyl-fluorene)-2,7-diethynylene-*alt*-4,9-2,1,3-naphthothiadiazole) PFDENT-P4.[16]
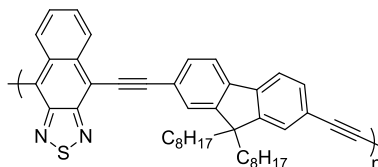
4,9-Dibromo-2,1,3-naphthothiadiazole (**2**) (0.120 g, 0.35 mmol) and monomer (**M1**) (0.153 g, 0.35 mmol) were added to single-neck 100 ml round bottom flask and placed under argon. Dry THF (2 ml), toluene (4 ml), followed by diisopropylamine (3 ml, degassed) were added and the system degassed. To this mixture, $Pd(PPh_3)_2Cl_2$ (0.035 g, 0.049 mmol, 14%) and CuI (0.015 g, 0.078 mmol, 23%) were added, degassed and refluxed at 75 °C for 5 hours. Upon completion, the reaction mixture was cooled to room temperature and precipitated in degassed methanol (300 ml), the polymer solution was then left to stir overnight. The solution was filtered through a membrane and cleaned using a Soxhlet extraction with different organic solvents in the following order: methanol, acetone, hexane and toluene for 24 hours. The toluene fraction was concentrated to 10 ml *in vacuo* and the solution precipitated in degassed methanol (300 ml). The resulting precipitate was stirred overnight and the bright dark purple product collected by a membrane filter.

^{1}H NMR (400 MHz, CDCl$_3$) (δ/ppm): 8.78-8.71 (br, 2H), 7.92-7.65 (br, 6H), 7.92-7.65 (br, 2H), 2.23-1.96 (br, 4H), 1.31-1.01 (br, 20H), 0.89-0.57 (br, 10H).

Toluene fraction (18 % yield) GPC in TCB at 140 °C (M_n = 10,000), (M_w = 30,200), (PDI = 3.0)

Elemental Analysis calculated for $C_{43}H_{44}N_2S$: C, 83.18; H, 7.14; N, 4.51; S, 5.16. Found: C, 78.30; H, 6.98; N, 3.62; S, 3.38%.

6.4.14 Poly(9-(heptadecan-9-yl)-9H-carbazole-2,7-diethynylene-*alt*-4,9-2,1,3-naphthothiadiazole) PCDENT-P5.[16]
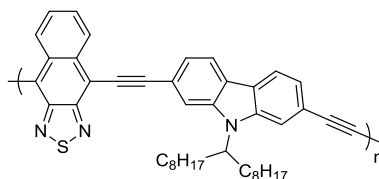
PCDENT-**P5** was prepared according to the polymerisation method in PFDENT-**P4.** (**M2**) (0.13 g, 0.30 mmol) and (**2**) (0.10 g, 0.30 mmol) were added to a single neck 100 ml round bottom flask under an inert condition. Dry THF (2 ml) and toluene (4 ml), followed by diisopropylamine (3 ml, degassed) were added and degassed. Pd(PPh$_3$)$_2$Cl$_2$ (0.029, 0.042 mmol, 14%) and CuI (0.013 g, 0.068 mmol, 23%) were then added, degassed and heated to reflux under for 5 hours. After carrying out the workup of the reaction mixture, the polymer was only obtained in the toluene fraction as a dark blue precipitate.

^{1}H NMR (400 MHz, CDCl$_3$) (δ/ppm): 8.82-8.73 (br, 2H), 8.27-7.64 (br, 4H), 7.79-7.64 (br, 2H), 7.51-7.42 (br, 2H), 4.71 (br, 1H), 2.49-2.26 (br, 2H), 2.13-1.94 (br, 2H) 1.40-1.00 (br, 24H), 0.93-0.74 (br, 6H).

Toluene fraction (15 % yield) GPC in TCB at 140 °C (M_n = 8,800), (M_w = 22,900), (PDI = 2.5).

Elemental Analysis calculated for C$_{43}$H$_{45}$N$_3$S: C, 81.22; H, 7.13; N, 6.61; S, 5.04%. Found: C, 75.49; H, 8.18; N, 4.64; S, 3.14%.

6.4.15 Poly(9,10-bis(4-(dodecyloxy)phenyl)anthracene-2,7-diethynylene-*alt*-4,9- 2,1,3-naphthothiadiazole) PPADENT-P6.[16]
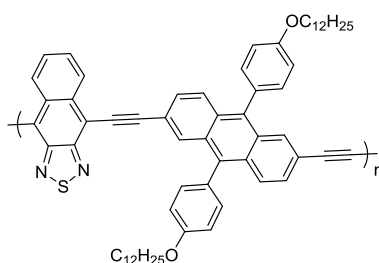
PPADENT-**P6** was synthesised according to the polymerisation method in PFBENT-**P4**. Under inert atmosphere, (**M3**) (0.168 g, 0.25 mmol) and (**2**) (0.086 g, 0.25 mmol)

were added to single neck 100 ml round bottom flask. Dry THF (2 ml) and toluene (4 ml), followed by diisopropylamine (3 ml, degassed) were added and degassed under vigorous stirring. Pd(PPh$_3$)$_2$Cl$_2$ (0.024 g, 0.035 mmol, 14%) and CuI (0.011 g, 0.057 mmol, 23%) were added and the system was degassed again. The polymerisation was left for 1 hour. Upon completion, the workup of the reaction was carried out; the polymer was then obtained in the toluene and chloroform fraction as a dark blue and green product, respectively.

^{1}H NMR (400 MHz, CDCl$_3$) (δ/ppm): 8.64-8.54 (br, 2H), 8.28-8.22 (br, 2H), 8.05-7.04 (br, 10H), 4.21-4.10 (br, 4H), 1.99-1.86 (br, 4H) 1.50-1.07 (br, 36H), 0.89 (br, 6H). Toluene fraction (25 % yield) GPC in TCB at 140 °C (M_n = 7,900), (M_w = 16,000), (PDI = 2.0).

Chloroform fraction (10 % yield) GPC in TCB at 140 °C (M_n = 9,200), (M_w =17,700), (PDI = 1.9).

Elemental Analysis calculated for C$_{64}$H$_{68}$N$_2$O$_2$S: C, 82.72; H, 7.38; N, 3.01; S, 3.45%. Found: C, 75.87; H, 7.17; N, 2.19; S, 2.40%.

6.4.16 2,7-Dithienyl-9,9-dioctylfluoroene (13).[17]
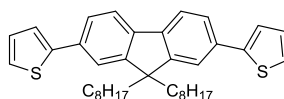
2,7-Dibromo-9,9-dioctylfluorene (S3) (0.50 g, 0.91 mmol) was dissolved in dry CB (8 ml). 2-(Tributylstannyl)thiophene (0.85 g, 0.72 ml, 2.27 mmol), Pd$_2$(dba)$_3$ (0) (0.042 g, 5 %) and tri(o-tolyl)phosphine (0.028 g, 10 %) were added to the solution and refluxed at 120 °C under an inert atmosphere overnight. Upon completion, the mixture was cooled to room temperature the reaction, diethyl ether (100 ml) was added to the reaction mixture. The organic phases were combined, washed with brine (2 × 200 ml) and dried over (MgSO$_4$). The solvent was removed *in vacuo*, the crude product was then purified *via* silica gel column chromatography using petroleum ether: DCM (13:1) to yield a pure product (13) as a faint blue oily material (0.46 g, 0.82 mmol, 91%).

¹H NMR (400 MHz, CDCl₃) (δ/ppm): 7.70 (d, *J* = 8.0 Hz, 2H), 7.63 (d, *J* = 8.0 Hz, 2H), 7.58 (s, 2H), 7.41 (d, *J* = 4.0 Hz, 2H), 7.32 (d, *J* = 5.0 Hz, 2H), 7.14 (t, *J* = 4.0 Hz, 2H), 2.06-2.00 (m, 4H), 1.28-1.04 (m, 20H), 0.81(t, *J* = 7.0, 6H), 0.73-0.64 (br, 4H).

¹³C NMR (400 MHz, CDCl₃) (δ/ppm): 151.71, 145.17, 140.22, 133.28, 128.07, 124.98, 124.54, 122.90, 120.17, 120.09, 55.30, 40.42, 31.79, 30.00, 29.22, 29.19, 23.76, 22.60, 14.07.

Mass (EI+): (m/z) (M•⁺) 554.

Elemental analysis calculated for C₃₇H₄₆S₂; C, 80.09; H, 8.36, S, 11.56, found; C, 79.05; H, 8.14, S, 11.03%.

6.4.17 2,7-Bis(5-bromothiophen-2-yl)-9,9-di-n-octylfluorene (14).[18]
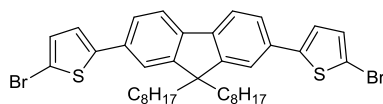
A solution of compound (**13**) (0.43 g, 0.77 mmol) in CHCl₃ (10 ml) and glacial acetic acid (10 ml) was shielded from light and stirred. NBS (0.27 g, 1.53 mmol, freshly purified by recrystallisation from water) in CHCl₃ (2 ml) and glacial acetic acid (2 ml) was slowly added. After addition, the mixture was refluxed at 70 °C for 2 hours; the progress of reaction was monitored by TLC plate. Upon completion, water (200 ml) was added and the organic layer was extracted with DCM (2 × 200 ml), dried (MgSO₄) and the solvent evaporated *in vacuo*. The crude product was purified *via* column chromatography using petroleum ether as eluent to yield the product (**14**) as a yellow sticky product (0.47 g, 0.66 mmol, 85 %). The product gave a single spot on TLC (Rf = 0.45) in 100% hexane.

¹H NMR (400 MHz, CDCl₃) (δ/ppm): 7.69 (d, *J* = 8.0 Hz, 2H), 7.53 (d, *J* = 8.0 Hz, 2H), 7.47 (s, 2H), 7.14 (d, *J* = 4.0 Hz, 2H), 7.07 (d, *J* = 4.0 Hz, 2H), 2.07-1.98 (m, 4H), 1.28-1.04 (m, 20H), 0.82 (t, *J* =7.0, 6H), 0.73-0.64 (br, 4H).

¹³C NMR (400 MHz, CDCl₃) (δ/ppm): 151.84, 146.51, 140.41, 132.36, 130.88, 124.67, 123.06, 120.31, 119.80, 111.12, 55.31, 40.32, 31.80, 29.93, 29.22, 29.16, 23.72, 22.62, 14.10.

Mass (EI+): (m/z) (M•⁺), 710 (50%), 712 (100%), 714 (50%).

Elemental analysis calculated for $C_{37}H_{44}Br_2S_2$; C, 62.36; H, 6.22, Br, 22.42, S, 9.00, found; C, 61.12; H, 6.14, Br, 23.61 S, 8.04%.

6.4.18 [5,5'-(9,9-Dioctyl-9H-fluorene-2,7-diyl)bis(thiophene-5,2diyl))bis(ethyne-2,1-diyl)] bis(trimethylsilane) (15). [19]
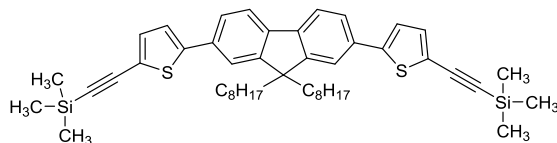
Compound (**14**) (0.40 g, 0.56 mmol), CuI (0.007 g, 5%) and Pd(PPh$_3$)$_2$Cl$_2$ (0.015 g, 4%) in dry toluene (20 ml), followed by diisopropylamine (6 ml, degassed) were added to a single neck flask and stirred under an inert atmosphere for 0.5 hour, followed by trimethylsilyl acetylene (0.12 g, 0.17 ml, 1.23 mmol, d = 0.695 g/ml) in disopropylamine (4.0 ml) was added. The system was degassed and refluxed at 70 °C for 24 hours. The reaction was monitored by spot TLC to verify the completion of the reaction. After cooling to room temperature, the solvent was removed from the reaction mixture *in vacuo* to yield a crude product. The material was purified *via* column chromatography over silica gel using petroleum ether as the eluent to obtain the desired product (**15**) as a yellow oil product (0.37 g, 0.47 mmol, 85 %).

^{1}H NMR (400 MHz, CDCl$_3$) (δ/ppm): 7.69 (d, *J* = 8.0 Hz, 2H), 7.57 (d, *J* = 8.0 Hz, 2H), 7.53 (s, 2H), 7.28-7.22 (m, 4H), 2.04-1.95 (m, 4H), 1.29-1.02 (m, 20H), 0.81 (t, *J* = 7.0, 6H), 0.72-0.64 (br, 4H), 0.29 (s, 18H).

^{13}C NMR (400 MHz, CDCl$_3$) (δ/ppm): 151.88, 146.52, 140.56, 133.67, 132.72, 124.98, 122.64, 122.10, 120.27, 120.14, 99.67, 97.79, 55.31, 40.27, 31.75, 29.91, 29.16, 29.11, 23.73, 22.57, 14.02, -0.12.

Mass (EI+): (m/z) (M•$^+$) 746.

Elemental analysis calculated for $C_{47}H_{62}Si_2S_2$; C, 75.45; H, 8.36, S, 8.58, Si, 7.52, found; C, 75.52; H, 8.24, S, 8.37%.

6.4.19 5,5'-(9,9-Dioctyl-fluorene-2,7-diyl)bis(2-ethynylthiophene) (M4). [19,20]
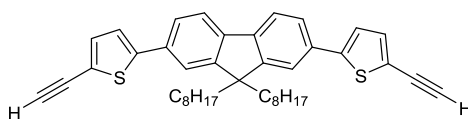
To a solution of compound (**15**) (0.30 g, 0.40 mmol) in dry THF (10 ml), an aqueous KOH (0.7 ml, 25 % wt) in methanol (4 ml) was slowly added and stirred at ambient temperature under an inert atmosphere. The mixture was degassed and left for 3 hours. The reaction was monitored by TLC to confirm the completion of the reaction. Upon completion, the mixture was extracted using a DCM (3 × 100) and washed with water (2 × 100 ml). The organic layers were combined, dried (MgSO$_4$) and the solvent removed *in vacuo*. The desired product (**M4**) was obtained as a brown sticky product (0.22 g, 0.36 mmol, 91 %) which gave a single spot on the TLC plate in 100% petroleum ether.

^{1}H NMR (400 MHz, CDCl$_3$) (δ/ppm): 7.70 (d, J = 8.0 Hz, 2H), 7.59 (d, J = 8.0 Hz, 2H), 7.54 (s, 2H), 7.31-7.25 (m, 4H), 3.43 (s, 2H), 2.04-1.99 (br, 4H), 1.29-1.02 (m, 20H), 0.81 (t, J = 7.0, 6H), 0.72-0.64 (br, 4H).

^{13}C NMR (400 MHz, CDCl$_3$) (δ/ppm): 151.91, 146.85, 140.66, 134.21, 132.62, 125.09, 122.67, 120.84, 120.35, 120.16, 81.97, 77.23, 55.37, 40.30, 31.78, 29.93, 29.19, 29.15, 23.74, 22.60, 14.06.

Mass (EI+): (m/z) (M•$^+$) 603.

Elemental analysis calculated for C$_{41}$H$_{46}$S$_2$; C, 81.67; H, 7.69, S, 10.64, Si, 7.52, found; C, 80.68; H, 7.53, S, 10.43 %.

6.4.20 2,7-Dithienyl-N-9'-heptadecanylcarbazole (16).[17]
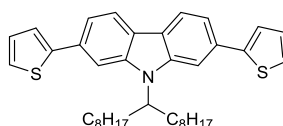
A mixture of 2,7-dibromo-9-(heptadecan-9-yl)-9H-carbazole.(**7**) (1.50 g, 2.66 mmol), Pd$_2$(dba)$_3$ (0) (0.122 g, 5 %) and tri(o-tolyl)phosphine (0.081 g, 10 %) in dry CB (10 ml) were stirred and degassed under argon. 2-(Tributylstannyl) thiophene (2.48 g, 2.1 ml, 6.7 mmol) was added by syringe and the system degassed again. The reaction mixture was heated to reflux overnight. After cooling to room temperature, diethyl ether (100 ml) was added to the reaction suspension and washed with brine (2 × 200 ml). The combined organic phase was extracted, dried over (MgSO$_4$) and the solvent was removed *in vacuo*. The crude product was purified *via* silica gel column chromatography and eluted using petroleum ether: DCM (13:1) to obtain the desired

product (**16**) as a colourless sticky material (1.32 g, 2.31 mmol 87 %). The product gave a single spot on TLC (Rf = 0.55) in petroleum ether: DCM (13:1).

^{1}H NMR (400 MHz, CDCl$_3$) (δ/ppm): 8.02 (br, 2H); 7.81 (s, 1H); 7.62 (s, 1H), 7.52 (d, J = 8.0, 2H), 7.43 (br, 2H), 7.33 (dd, J = 5.0 and J = 1.0 Hz, 2H), 7.16 (dd, J = 5.0 and J = 4.0 Hz, 2H), 4.63 (m, 1H); 2.42-2.31 (br, 2H), 2.04-1.94 (m, 2H); 1.34-1.03 (m, 24H); 0.83 (t, J = 7.0 Hz, 6H).

^{13}C NMR (400 MHz, CDCl$_3$) (δ/ppm): 145.83, 142.98, 139.63, 132.17, 131.67, 128.07, 124.56, 123.23, 123.02, 121.85, 120.69, 120.46, 117.71, 108.95, 106.26, 56.47, 33.79, 31.76, 29.41, 29.31, 29.19, 26.79, 22.60, 14.06.

Mass (EI+): (m/z) (M•$^+$) 569.

Elemental analysis calculated for C$_{37}$H$_{47}$NS$_2$, C, 77.98; H, 8.31; N, 2.46; S, 11.25, found; C, 78.18; H, 8.42. ; N, 2.46; S, 11.02%.

6.4.21 2,7-Bis(5-bromothiophen-2-yl)-9-(heptadecan-9-yl)-9H-carbazole (17).[18]
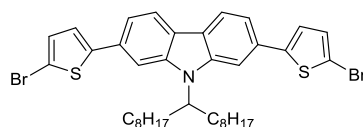
To a solution of compound (**16**) (1.18 g, 2.07 mmol) in chloroform (10 ml) and glacial acetic acid (10 ml), NBS (0.27 g, 1.53 mmol) in 12 ml (1:1 CHCl$_3$, glacial acetic acid) was slowly added under dark conditions. After addition, the reaction mixture was refluxed at 70 °C for 3 hours. Upon completion, the mixture was extracted with DCM (3 × 200 ml), washed with brine solution (2 × 30 ml) and dried (MgSO$_4$). The organic solvent was evaporated *in vacuo* to yield the crude product. The resulting crude solid was purified *via* column chromatography using petroleum ether: DCM (13:1) as eluent to obtain the pure product (**17**) as yellow sticky product (1.32 g, 1.81 mmol, 87%). The product gave a single spot on the TLC (Rf = 0.45) in petroleum ether: DCM (13:1).

^{1}H NMR (400 MHz, CDCl$_3$) (δ/ppm): 8.06 (br, 2H); 7.68 (s, 1H); 7.50 (s, 1H), 7.41 (d, J = 8.0, 2H), 7.15 (br, 2H), 7.09 (d, J = 4.0 Hz, 2H), 4.59 (m, 1H); 2.37-2.26 (m, 2H), 2.02-1.92 (m, 2H); 1.32-1.01 (m, 24H); 0.82 (t, J = 7.0 Hz, 6H).

^{13}C NMR (400 MHz, CDCl$_3$) (δ/ppm): 147.91, 142.96, 136.61, 131.35, 131.05, 130.90, 123.41, 123.17, 122.05, 120.91, 120.68, 117.32, 111.05, 108.67, 105.99, 56.55, 33.74, 31.76, 29.37, 29.29, 29.18, 26.76, 22.61, 14.06.

Mass (EI+): (m/z) (M$^{•+}$) 725 (50%), 727 (100%), 729 (50%).

Elemental analysis calculated for C$_{37}$H$_{45}$Br$_2$NS$_2$, C, 61.07; H, 6.23; N, 1.92; Br, 21.96; S, 8.81, found; C, 59.93; H, 6.15; N, 1.67; Br, 21.96; S, 8.47%.

6.4.22 9-(Heptadecan-9-yl)-2,7-bis(5-((trimethylsilyl)ethynyl)thiophen-2-yl)-9H-carbazole (18).
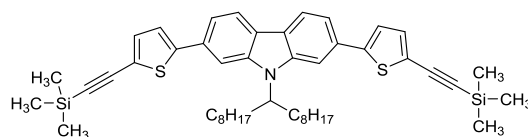
To dried 100 ml round bottom flask, attached with condenser, was added compound (**17**) (1.03 g, 1.41 mmol), dry toluene (40 ml) and diisopropylamine (15 ml, degassed). The mixture was degassed and placed under an inert atmosphere using standard Schlenk line technique. CuI (0.013 g, 5%) and Pd(PPh$_3$)$_2$Cl$_2$ (0.040 g, 4%) were then added above the reaction mixture, followed by trimethylsilyl acetylene (0.30 g, 0.43 ml, 3.10 mmol, d = 0.695 g/ml) in disopropylamine (7.0 ml) was added. The mixture was degassed again under an inert condition and refluxed at 70 °C for 24 hours. The reaction was monitored by spot TLC to verify the completion of reaction. After cooling the reaction to room temperature, the organic solvent was evaporated *in vacuo* to obtain a crude product. The product was purified over silica gel chromatography using petroleum ether: toluene (10:1) as the eluent. The solvent was removed *in vacuo* to yield the pure product (**18**) as a yellow sticky precipitate (0.95 g, 1.24 mmol, 88%). The product gave a single spot on TLC (Rf = 0.3) in petroleum ether: toluene (10:1).

^{1}H NMR (400 MHz, CDCl$_3$) (δ/ppm): 8.06 (br, 2H); 7.75 (s, 1H); 7.57 (s, 1H), 7.48 (br, 2H), 7.29-7.24 (br, 4H), 4.59 (m, 1H); 2.39-2.27 (m, 2H), 2.02-1.92 (m, 2H); 1.31-1.02 (m, 24H); 0.83 (t, *J* = 7.0 Hz, 6H), 0.31 (t, *J* = 4.0 Hz, 18H).

^{13}C NMR (400 MHz, CDCl$_3$) (δ/ppm): 147.21, 142.98, 139.64, 133.78, 131.57, 131.06, 123.54, 122.77, 122.18, 122.03, 120.89, 120.66, 117.54, 108.92, 106.23, 99.60, 97.84, 56.55, 33.74, 31.75, 29.36, 29.29, 29.17, 26.77, 22.61, 14.06, -0.08.

Mass (EI+): (m/z) (M$^{•+}$) 762.

Elemental analysis calculated for $C_{47}H_{63}NS_2Si_2$, C, 74.05; H, 8.33, S, 8.41, N, 1.84, found; C, 73.03; H, 7.90, S, 8.59, N, 1.63%.

6.4.23 2,7-Bis(5-ethynylthiophen-2-yl)-9-(heptadecan-9-yl)-9H-carbazole (M5).
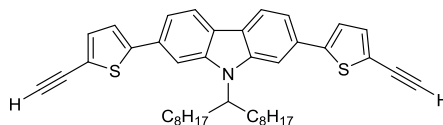
Compound (**18**) (0.80 g, 1.05 mmol) was dissolved in dry THF (20 ml). The reaction system was degassed and an aqueous solution of KOH (3 ml, 25% wt) in methanol (4 ml) was added dropwise. After addition, the suspension reaction was stirred, degassed and placed under an inert atmosphere at ambient temperature for 3 hours. The reaction was monitored by TLC to confirm the completion of the reaction. Upon completion, the mixture was extracted with DCM (3 × 200 ml), washed with water (2 × 200 ml) and dried (MgSO$_4$). The organic layer was evaporated *in vacuo* to yield the brown sticky product (**M5**) (0.59 g, 0.95 mmol, 91 %). It gave single spot on TLC plate. (Rf = 0.2) in petroleum ether.

^{1}H NMR (400 MHz, CDCl$_3$) (δ/ppm): 8.07 (br, 2H); 7.76 (s, 1H); 7.57 (s, 1H), 7.48 (br, 2H), 7.31 (d, J = 4.0 Hz, 2H), 7.29-7.26 (br, 2H), 4.60 (m, 1H), 3.44 (s, 2H), 2.38-2.27 (m, 2H), 2.03-1.93 (m, 2H); 1.33-1.02 (m, 24H); 0.82 (t, J = 7.0 Hz, 6H).

^{13}C NMR (400 MHz, CDCl$_3$) (δ/ppm): 147.55, 134.25, 122.76, 120.95, 120.85, 120.72, 117.67, 108.99, 106.31, 81.90, 77.27, 56.57, 33.76, 31.75, 29.36, 29.29, 29.18, 26.76, 22.61, 14.06.

Mass (EI+): (m/z) (M•+) 617.

Elemental analysis calculated for $C_{41}H_{47}NS_2$, C, 79.68; H, 7.67, S, 10.38, N, 2.27, found; C, 79.65; H, 7.73, S, 10.28, N, 2.21%.

6.4.24 2,2'-(9,10-Bis(4-(dodecyloxy)phenyl) anthracene-2,6-diyl)dithiophene (19).
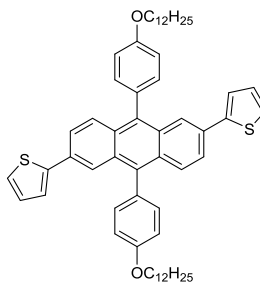
To solution of 2,6-dibromo-9,10-bis(4-(dodecyloxy)phenyl)anthracene (**11**) (1.30 g, 1.50 mmol), in dry CB (13 ml), Pd$_2$(dba)$_3$ (0) (0.096 g, 5 %) and tri(o-tolyl)phosphine (0.054 g, 10 %) were then added and the reaction mixture was degassed. 2-(Tributylstannyl)thiophene (1.39 g, 1.19 ml, 3.75 mmol) was slowly added by syringe then the system was degassed three times and placed under an inert atmosphere. The reaction mixture was heated to reflux for overnight. Upon completion, the mixture was cooled to room temperature and diethyl ether (100 ml) was added. The reaction suspension was washed with brine solution (2 × 200 ml), dried over (MgSO$_4$) and the solvent removed *in vacuo*. The resulting precipitate was purified by a silica gel chromatography column using petroleum ether: toluene (80:20%) as the eluent to obtain a yellow powder (**19**) (1.20 g, 1.39 mmol, 93 %). The product provided a single spot on TLC (Rf = 0.6) in petroleum ether: toluene) (80: 20%).

^{1}H NMR (400 MHz, CDCl$_3$) (δ/ppm): 7.98 (br, 2H), 7.78 (d, *J* = 9.0 Hz, 2H), 7.61 (dd, *J* = 9.0 and *J* = 2.0 Hz, 2H), 7.43 (d, *J* = 9.0 Hz, 4H), 7.30 (dd, *J* = 4.0 and *J* = 1.0 Hz, 2H), 7.27 (dd, *J* = 6.0 and *J* = 5.0 Hz, 2H), 7.18 (d, *J* = 9.0 Hz, 4H), 7.09 (dd, *J* = 5.0 and *J* = 4.0 Hz, 2H) 4.15 (t, *J* = 7.0 Hz, 4H), 1.93 (m, 4H); 1.63-1.26 (br, 36H); 0.92 (t, *J* = 7.0 Hz, 6H).

^{13}C NMR (400 MHz, CDCl$_3$) (δ/ppm): 158.73, 144.72, 137.01, 132.44, 130.64, 130.50, 130.37, 130.04, 128.10, 127.89, 125.09, 124.11, 123.53, 123.10, 114.51, 68.21, 31.96, 29.73, 29.68, 29.54, 29.47, 29.40, 26.21, 22.73, 14.16.

Mass (EI+): (m/z) (M•$^+$) 863.

Elemental analysis calculated for C$_{58}$H$_{70}$O$_2$S$_2$, C, 80.69; H, 8.17; S, 7.43, found; C, 79.20; H, 8.02; S, 7.02%.

6.4.25 5,5'-(9,10-Bis(4-(dodecyloxy)phenyl)anthracene-2,6-diyl)bis(2-bromothiophene) (20).
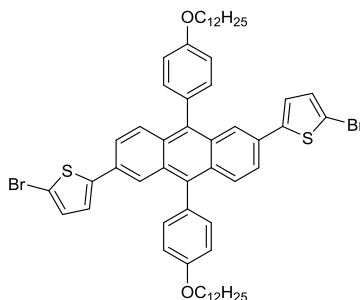
A two neck round bottom flask was charged with compound (**19**) (1.00 g, 1.15 mmol), $CHCl_3$ (13 ml) and glacial acetic acid (13 ml) was stirred and shielded from light at room temperature. NBS (0.27 g, 1.53 mmol) in $CHCl_3$ (12 ml) and glacial acetic acid (12 ml) was added dropwise. After addition, the reaction mixture was refluxed at 70 °C for 3 hours. After cooling to room temperature, the reaction mixture was extracted with DCM (3 × 200 ml), washed with brine (2 × 200 ml) and dried ($MgSO_4$). The organic solvent was evaporated *in vacuo* to produce the crude material. The crude product was recrystallised from methanol to yield a yellow powder (**20**) (1.10 g, 1.07 mmol, 93 %).

^{1}H NMR (400 MHz, $CDCl_3$) (δ/ppm): 7.86 (br, 2H), 7.76 (d, J = 9.0 Hz, 2H), 7.50 (dd, J = 9.0 and J = 2.0 Hz, 2H), 7.39 (d, J = 9.0 Hz, 4H), 7.17 (d, J= 9.0 Hz, 4H), 7.05-7.01 (br, 4H), 4.16 (t, J = 7.0 Hz, 4H), 1.93 (m, 4H); 1.63-1.26 (br, 36H); 0.91 (t, J = 7.0 Hz, 6H).

^{13}C NMR (400 MHz, $CDCl_3$) (δ/ppm): 158.82, 146.08, 137.22, 132.35, 130.94, 130.49, 130.12, 130.03, 129.98, 128.14, 123.68, 123.83, 123.01, 114.56, 111.76, 68.22, 31.96, 29.73, 29.68, 29.54, 29.46, 29.40, 26.20, 22.72, 14.15.

Mass (EI+): (m/z) (M•[+]) 1018 (40%), 1021 (100%), 1022 (60%).

Elemental analysis calculated for $C_{58}H_{68}Br_2O_2S_2$, C, 68.22; H, 6.71; S, 6.28; Br, 15.65, found; C, 68.04; H, 7.40; S, 4.92; Br, 11.03%.

6.4.26 ((5,5'-(9,10-Bis(4-(dodecyloxy)phenyl)anthracene-2,6-diyl)bis(thiophene-5,2-diyl))bis(eyhyne-2,1-diyl))bis(trimethylsilane) (21).
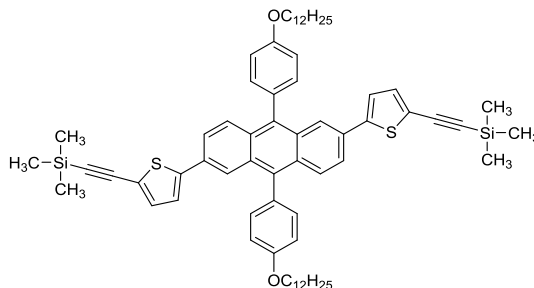
A single neck 100 ml round bottom flask was charged with compound (**20**) (0.62 g, 0.60 mmol), CuI (0.005 g, 5%), Pd(PPh$_3$)$_2$Cl$_2$ (0.021 g, 5 %). Dry toluene (20 ml) and diisopropylamine (7 ml, degassed) were stirred and degassed under an inert atmosphere. Trimethylsilyl acetylene (0.13 g, 0.18 ml, 1.30 mmol, d = 0.695 g/ml) in disopropylamine (4.0 ml) was added, degassed and refluxed at 70 °C for 48 hours. The reaction was monitored by spot TLC to confirm the completion of reaction. Upon completion, the reaction mixture was cooled to room temperature. The organic solvent was removed *in vacuo* to produce a crude product. The resulting product was then purified through a silica gel chromatography column using petroleum ether: DCM (90:10 %) as the eluent to yield a brown sticky product (**21**) (0.53 g, 0.50 mmol, 84 %). The product gave a single spot on TLC (Rf = 0.25) in petroleum ether: DCM (90:10 %).

^{1}H NMR (400 MHz, CDCl$_3$) (δ/ppm): 7.94 (br, 2H), 7.76 (d, J = 9.0 Hz, 2H), 7.55 (dd, J = 9.0 and J = 2.0 Hz, 2H), 7.40 (d, J = 9.0 Hz, 4H), 7.19-7.14 (br, 8H), 4.16 (t, J = 7.0 Hz, 4H), 1.93 (m, 4H); 1.63-1.26 (br, 36H), 0.91 (t, J = 7.0 Hz, 6H), 0.27 (s, 18H).

^{13}C NMR (400 MHz, CDCl$_3$) (δ/ppm): 158.82, 146.03, 137.29, 133.82, 132.36, 130.53, 130.20, 130.05, 128.10, 123.61, 123.83, 123.37, 123.30, 122.54, 114.56, 99.91, 97.75, 68.22, 31.96, 29.73, 29.67, 29.54, 29.48, 29.40, 26.21, 22.72, 14.15. -0.12.

Mass (EI+): (m/z) (M•$^+$) 1054.

Elemental analysis calculated for C$_{68}$H$_{86}$O$_2$S$_2$Si$_2$, C, 77.36; H, 8.21; S, 6.07, found; C, 71.26; H, 7.65; S, 5.19%.

6.4.27 5,5'-(9,10-Bis(4-(dodecyloxy)phenyl)anthracene-2,6-diyl)bis(2-ethynylthiophene) (M6).
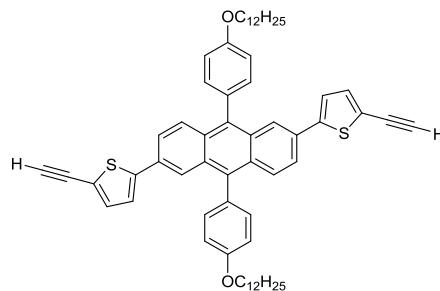
Under an inert atmosphere, a solution of compound (**21**) (0.34 g, 0.32 mmol) in dry THF (15 ml) was stirred and degassed at room temperature. To this mixture, an aqueous solution KOH (2.0 ml, 25% wt) in methanol (4 ml) was added dropwise and the system degassed again. The reaction was left to stir at ambient temperature for 3 hours. Upon completion, the reaction mixture was extracted with DCM (3×200 ml), washed with water (2×200 ml) dried over (MgSO$_4$). The solvent was removed *in vacuo* to produce dark brown solid. The crude product was purified *via* silica gel chromatography column using petroleum ether as the eluent to obtain a brown sticky product (**M6**) (0.25 g, 0.27 mmol, 85 %). The product gave a single spot on TLC (Rf = 0.5) in 100% petroleum ether.

^{1}H NMR (400 MHz, CDCl$_3$) (δ/ppm): 7.94 (br, 2H), 7.77 (d, J = 9.0 Hz, 2H), 7.55 (dd, J = 9.0 and J = 2.0 Hz, 2H), 7.40 (d, J = 9.0 Hz, 4H), 7.23 (d, J = 4.0 Hz, 2H), 7.19-7.15 (br, 6H), 4.15 (t, J = 7.0 Hz, 4H), 3.42 (s, 2H), 1.93 (m, 4H); 1.63-1.26 (br, 36H); 0.91 (t, J = 7.0 Hz, 6H).

^{13}C NMR (400 MHz, CDCl$_3$) (δ/ppm): 158.83, 146.38, 137.35, 134.25, 132.37, 130.54, 130.21, 129.96, 128.16, 123.62, 123.55, 123.27, 121.29, 114.56, 82.15, 77.19, 68.20, 31.97, 29.74, 29.69, 29.56, 29.47, 29.42, 26.22, 22.74, 14.18.

Mass (EI+): (m/z) (M$\bullet^+$) 910.

Elemental analysis calculated for C$_{62}$H$_{70}$O$_2$S$_2$: C, 81.71; H, 7.74; S, 7.04, found; C, 76.42; H, 7.65; S, 6.08%.

6.4.28 Poly(5,5'-(9,9-dioctyl-fluorene-2,7-diyl)bis(ethynyl-2-thienyl)-*alt*-4,9-(2,1,3-naphthothiadiazole) PFDTENT-P7.[16]
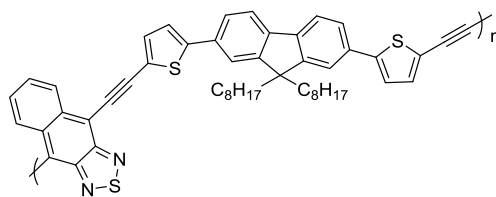
PFDTENT-**P7** was prepared according to the polymerisation method in PFDENT-**P4**. A single neck 100 ml round bottom flask was charged with (**M4**) (0.180 g, 0.30 mmol) and (**2**) (0.103 g, 0.30 mmol) under inert atmosphere. Dry THF (2 ml) and toluene (4 ml), followed by diisopropylamine (3 ml, degassed) were added and degassed at ambient temperature. To this mixture, Pd(PPh$_3$)$_2$Cl$_2$ (0.029 g, 0.042 mmol, 14%) and CuI (0.013 g, 0.068 mmol, 23%) were added and the system was degassed again. The mixture was refluxed at 75 °C for 1 hour. After carrying out the extraction and purification using different organic solvents, the polymer was only obtained in toluene fraction to afford dark green product.

^{1}H NMR (400 MHz, CDCl$_3$) (δ/ppm): 8.64-8.58 (br, 2H), 7.80-7.37(br, 12H), 2.14-1.99 (br, 4H), 1.31-1.06 (br, 20H), 0.86-0.68 (br, 10H).

Toluene fraction (17 % yield) GPC in TCB at 140 °C (M_n = 11,500), (M_w = 29,700), (PDI = 2.5).

Elemental Analysis calculated for C$_{51}$H$_{48}$N$_2$S$_3$: C, 78.02; H, 6.16; N, 3.57; S, 12.25%. Found: C, 72.91; H, 6.14; N, 2.46; S, 10.25%.

6.4.29 Poly(5,5'-(9-(heptadecan-9-yl)-9H-carbazole-2,7-diyl)bis(ethynyl-2-thienyl)-*alt*-4,9-(2,1,3-naphthothiadiazole) PCDTENT-P8.[16]
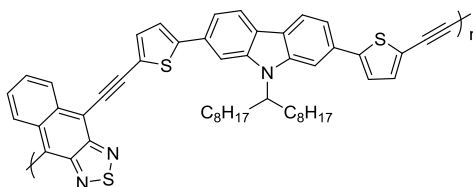
PCDTENT-**P8** was synthesised according to the polymerisation method in PFDENT-**P4**. A single neck 100 ml round bottom flask was charged with (**M5**) (0.136 g, 0.30 mmol) and (**2**) (0.103 g, 0.3 mmol) under an inert atmosphere using standard Schlenk

line techniques. Dry THF (2 ml), toluene (4 ml), followed by diisopropylamine (3 ml, degassed) were added and degassed. To this mixture, Pd(PPh$_3$)$_2$Cl$_2$ (0.029 g, 0.042 mmol, 14%) and CuI (0.013 g, 0.068 mmol, 23%) were added and the system was degassed again. The mixture was heated to reflux for 0.5 hour. Upon completion, the mixture was cooled to room temperature. After carrying out the extraction and purification using different organic solvents, the desired polymer was only obtained in the toluene fraction, where it was present as a dark green product.

^{1}H NMR (400 MHz, CDCl$_3$) (δ/ppm): 8.65-8.60 (br, 2H), 8.16-8.03 (br, 2H), 7.90-7.18 (br, 8H), 7.10 (m, 2H), 4.66 (br, 1H), 2.47-2.30 (br, 2H), 2.13-1.96 (br, 2H) 1.40-1.01 (br, 24H), 0.93-0.71 (br, 6H).

Toluene fraction (16 % yield) GPC in TCB at 140 °C (M_n = 8,700), (M_w = 17,000), (PDI = 1.9).

Elemental Analysis calculated for C$_{51}$H$_{49}$N$_3$S$_3$: C, 76.56; H, 6.17; N, 5.25; S, 12.02%. Found: C, 65.76; H, 6.23; N, 3.31; S, 6.83%.

6.4.30 Poly(5,5'-(9,10-bis(4-(dodecyloxy)phenyl)anthracene-2,6-diyl)bis(ethynyl-2-thienyl)-*alt*-4,9-(2,1,3-naphthothiadiazole) PPADTENT-P9.[16]
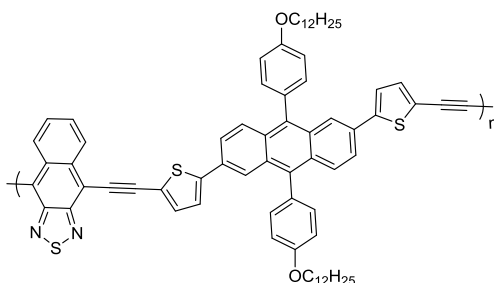
PPADTENT-**P9** was synthesised according to the polymerisation method in PFDENT-**P4**. A single neck 100 ml round bottom flask was charged with monomer (**M6**) (0.182 g, 0.20 mmol) and (**2**) (0.068 g, 0.20 mmol) was placed under an inert atmosphere. Dry THF (2 ml) and toluene (4 ml), followed by diisopropylamine (3 ml, degassed) were added and the system was degassed at ambient temperature. Pd(PPh$_3$)$_2$Cl$_2$ (0.019 g, 0.027 mmol, 14%) and CuI (0.008 g, 0.042 mmol, 23%) were added and the system degassed a further three times and placed under an inert atmosphere. After addition, the reaction mixture was heated to reflux for 15 minutes. Upon completion, the polymer

solution was cooled to room temperature. The extraction and purification of polymer using different organic solvents were carried out sequentially. The final polymer was obtained in the toluene and chloroform fraction to afford dark green products.

^{1}H NMR (400 MHz, CDCl$_3$) (δ/ppm): 8.62-8.49 (br, 2H), 8.08-7.93 (br, 2H), 7.85-7.04 (br, 18H), 4.25-4.09 (br, 4H), 2.02-1.87 (br, 4H) 1.51-1.14 (br, 36H), 0.90 (br, 6H). Toluene fraction (12 % yield) GPC in TCB at 140 °C (M_n = 10,400), (M_w = 23,300), (PDI = 2.2).

Chloroform fraction (8 % yield) GPC in TCB at 140 °C (M_n = 11,300), (M_w = 20,600), (PDI = 1.8).

Elemental Analysis calculated for C$_{72}$H$_{72}$N$_2$O$_2$S$_3$: C, 79.08; H, 6.64; N, 2.56; S, 8.08%. Found: C, 67.43; H, 7.54; N, 1.46; S, 5.18%.

6.5 Preparation of polymers (class 4)-Chapter 4

6.5.1 Poly(9,9-dioctyl-2,7-diethynylene fluorene-*alt*-4,7-benzo[c]-1,2,5-thiadiazole) PFDEBT-P10.[16]
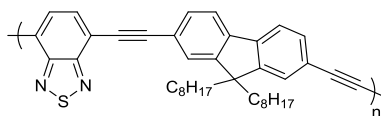
PFDEBT-P**10** was synthesised according to the polymerisation method outlined in PFDENT-**P4**. A mixture of 4,7-dibromobenzo[c]-1,2,5-thiadiazole (**S5)** (0.058 g, 0.20 mmol), 9,9-dioctyl -2,7-diethynylfluorene (**M1)** (0.087 g, 0.20 mmol), bis(triphenylphosphine) palladium(II) dichloride Pd(PPh$_3$)$_2$Cl$_2$ (0.019 g, 0.027 mmol, 14%) and copper (I) iodide CuI (0.009 g, 0.046 mmol, 23%) were added to a 100 ml one neck flask containing anhydrous THF (2 ml), toluene (4 ml) and diisopropylamine (3 ml, degassed) under inert conditions. The solution was stirred at reflux temperature (75 °C) in an oil bath for 6 hours. The reaction was stopped then the mixture allowed cooling to room temperature, then it was slowly added into degassed methanol (300 ml) before being stirred overnight to give a precipitate. The solid precipitate was collected through a membrane filter. Then it was cleaned using a Soxhlet extraction with different organic solvents in the following order: methanol, acetone, hexane, toluene, chloroform and chlorobenzene. The toluene fraction was obtained and concentrated to 10 ml *in vacuo* then poured into degassed methanol (300 ml). The resulting solution was stirred overnight then the precipitate collected through membrane filtration to afford the final polymer as a dark orange colour product.

^{1}H NMR (400 MHz, CDCl$_3$) (δ/ppm): 7.89 (br, 2H), 7.80-7.54 (br, 6H), 2.13-1.97 (br, 4H), 1.28-1.03 (br, 20H), 0.87-0.80 (br, 6H), 0.70-0.58 (br, 4H).

Toluene fraction (17 % yield) GPC in TCB at 140 °C (M_n = 11,600), (M_w = 29300), (PDI = 2.5).

Elemental Analysis calculated for C$_{39}$H$_{42}$N$_2$S: C, 82.06; H, 7.42; N, 4.91; S, 5.62%. Found: C, 76.13; H, 7.63; N, 3.83; S, 4.11%.

6.5.2 Poly((9-(heptadecan-9-yl)-9H-2,7-diethynylene carbazole)-*alt*-4,7-benzo[c]-1,2,5-thiadiazole) PCDEBT-P11.[16]
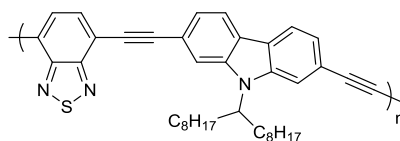
PCDEBT-**P11** was synthesised according to the polymerisation method in PFDENT-**P4**. 7,7-Dibromobenzo[c]-1,2,5-thiadiazole (**S5**) (0.058 g, 0.20 mmol) and 2,7-diethynyl-9-(heptadecan-9-yl)-9H-carbazole (**M2**) (0.090 g, 0.20 mmol) were added to a single neck 100 ml round bottom flask and placed under argon using standard Schlenk line techniques. Dry co-solvents toluene (4 ml) and THF (2 ml), followed by diisopropylamine (3 ml, degassed) were added and the internal system was degassed again. Then $Pd(PPh_3)_2Cl_2$ (0.019 g, 0.027 mmol,14%) and CuI (0.009 g, 0.046 mmol, 23%) were added to the degassed solution and heated to 75 °C for 4 hours. Upon completion, the reaction was cooled to room temperature; then the mixture was added dropwise into degassed methanol (300 ml) and stirred overnight to give a precipitate. The solid precipitate was collected through a membrane filter. Then it was cleaned using a Soxhlet extraction with different organic solvents in the following order: methanol, acetone, hexane, toluene, chloroform and chlorobenzene. The toluene fraction was obtained and concentrated to 10 ml *in vacuo* then poured into degassed methanol (300 ml). The resulting mixture was stirred overnight and the polymer collected by filtration as an orange powder.

^{1}H NMR (400 MHz, CDCl$_3$) (δ/ppm): 8.20-8.06 (br, 2H), 7.96-7.75 (br, 4H), 7.65-7.40 (br, 2H), 4.70-4.53 (br, 1H), 2.42-2.26 (br, 2H), 2.09-1.94 (br, 2H) 1.36-0.98 (br, 24H), 0.84 (t, J = 7.0, 6H).

Toluene fraction (8 % yield) GPC in TCB at 140 °C (M_n = 25,000), (M_w = 80,400), (PDI = 3.2).

Elemental Analysis calculated for $C_{39}H_{43}N_3S$: C, 79.96; H, 7.40; N, 7.17; S, 5.47%. Found: C, 76.85; H, 8.52; N, 4.23; S, 3.02%.

6.5.3 Poly((9,10-bis(4-(dodecyloxy)phenyl-2,6-diethynylene anthracene)-*alt*-4,7-benzo[c]-1,2,5-thiadiazole) PPADEBT-P12.[16]
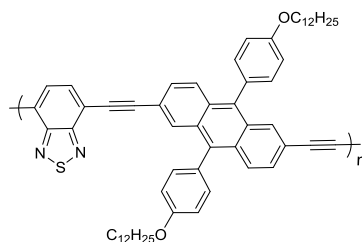
PPADEBT-P12 was synthesised according to the polymerisation method in PFDENT-**P4**. A single neck 100 ml round bottom flask under argon was charged with 4,7-dibromobenzo[c]-1,2,5-thiadiazole (**S5**) (0.058 g, 0.20 mmol) and 2,6-diethynyl-9,10-bis(4-(dodecyloxy)phenyl)anthracene (**M3**) (0182 g, 0.20 mmol) in dry toluene (4 ml) and THF (2 ml), followed by diisopropylamine (3 ml, degassed) were added and degassed. To this mixture, Pd(PPh$_3$)$_2$Cl$_2$ (0.019 g, 0.027 mmol, 14%) and copper (I) iodide CuI (0.009 g, 0.046 mmol, 23%) were added. After addition, the solution was stirred at reflux temperature (75 °C) in an oil bath for 3 hours. The reaction was stopped then the mixture allowed cooling to room temperature, then it was slowly added into degassed methanol (300 ml) before being stirred overnight to give a precipitate. The solid precipitate was collected through a membrane filter. Then it was cleaned using a Soxhlet extraction with different organic solvents in the following order: methanol, acetone, hexane, toluene, chloroform and chlorobenzene. The toluene fraction was obtained and concentrated to 10 ml *in vacuo* then poured into degassed methanol (300 ml). The resulting mixture was stirred overnight and the solid was collected by filtration through a membrane filter. The final polymer was obtained as a dark red powder after drying.

^{1}H NMR (400 MHz, CDCl$_3$) (δ/ppm): 8.14-7.96 (br, 2H), 7.85-7.34 (br, 10H), 7.20 (t, *J* = 8.0, 4H), 4.20-4.10 (br, 4H), 1.97-1.87 (br, 4H) 1.50-1.19 (br, 36H), 0.93-0.86 (br, 6H).

Toluene fraction (21 % yield) GPC in TCB at 140 °C (M_n = 8,700), (M_w = 21800), (PDI = 2.5).

Elemental Analysis calculated for C$_{60}$H$_{66}$N$_2$O$_2$S: C, 81.96; H, 7.57; N, 3.19; S, 3.657%. Found: C, 70.80; H, 7.22; N, 2.14; S, 2.17%.

References

1. N. Blouin, A. Michaud and M. Leclerc, *Advanced Materials*, 2007, **19**, 2295-2300.

2. Z.-G. Zhang, Y.-L. Liu, Y. Yang, K. Hou, B. Peng, G. Zhao, M. Zhang, X. Guo, E.-T. Kang and Y. Li, *Macromolecules*, 2010, **43**, 9376-9383.

3. M. Sonntag and P. Strohriegl, *Chemistry of Materials*, 2004, **16**, 4736-4742.

4. G. Gritzner, *Pure and Applied Chemistry*, 1990, **62**, 1839-1858.

5. K. Johansson, Ö. Andersson and Å. Olin, *Analyst*, 1995, **120**, 423-429.

6. J. Kim, M. H. Yun, G.-H. Kim, J. Y. Kim and C. Yang, *Polymer Chemistry*, 2012, **3**, 3276-3281.

7. C. Kitamura, S. Tanaka and Y. Yamashita, *Chemistry of Materials*, 1996, **8**, 570-578.

8. H. Yi, S. Al-Faifi, A. Iraqi, D. C. Watters, J. Kingsley and D. G. Lidzey, *Journal of Materials Chemistry*, 2011, **21**, 13649-13656.

9. S. Liu, K. Zhang, J. Lu, J. Zhang, H.-L. Yip, F. Huang and Y. Cao, *Journal of the American Chemical Society*, 2013, **135**, 15326-15329.

10. D. Sahu, H. Padhy, D. Patra, J.-F. Yin, Y.-C. Hsu, K.-L. Lu, K.-H. Wei and H.-C. Lin, *Tetrahedron*, 2011, **67**, 303-311.

11. G. y. Chen, S. c. Lan, P. y. Lin, C. w. Chu and K. h. Wei, *Journal of Polymer Science Part A: Polymer Chemistry*, 2010, **48**, 4456-4464.

12. A. Saeki, S. Yoshikawa, M. Tsuji, Y. Koizumi, M. Ide, C. Vijayakumar and S. Seki, *Journal of the American Chemical Society*, 2012, **134**, 19035-19042.

13. Y. Wang, Y. Liu, J. Luo, H. Qi, X. Li, M. Nin, M. Liu, D. Shi, W. Zhu and Y. Cao, *Dalton Transactions*, 2011, **40**, 5046-5051.

14. S. K. Lee, W. J. Yang, J. J. Choi, C. H. Kim, S.-J. Jeon and B. R. Cho, *Organic Letters*, 2005, **7**, 323-326.

15. K. Danel, T.-H. Huang, J. T. Lin, Y.-T. Tao and C.-H. Chuen, *Chemistry of Materials*, 2002, **14**, 3860-3865.

16. F. He, X. Ren, X. Shen and Q.-H. Xu, *Macromolecules*, 2011, **44**, 5373-5380.

17. M.-J. Baek, W. Jang, S.-H. Lee and Y.-S. Lee, *Synthetic Metals*, 2012, **161**, 2785-2791.

18. M. O'neill, S. Kelly, A. Contoret and G. Richards, Google Patents, 2001.

19. P.-T. Wu, T. Bull, F. S. Kim, C. K. Luscombe and S. A. Jenekhe, *Macromolecules*, 2009, **42**, 671-681.

20. L. Liu, C. L. Ho, W. Y. Wong, K. Y. Cheung, M. K. Fung, W. T. Lam, A. B. Djurišić and W. K. Chan, *Advanced Functional Materials*, 2008, **18**, 2824-2833.

Chapter 7

Supplementary Information.

Chapter 7

7.1 Supplementary Information
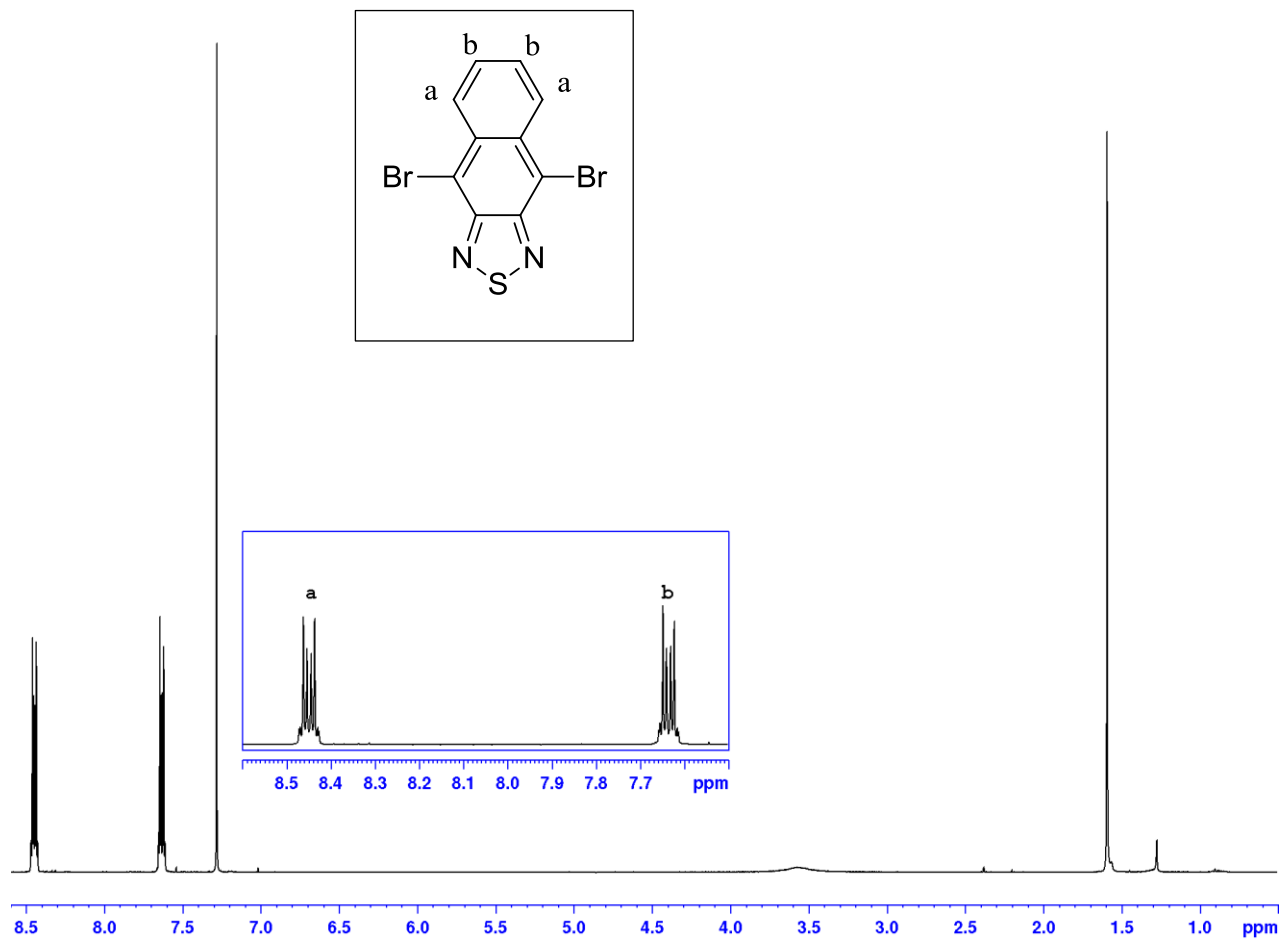
Figure 7-1: ^{1}H NMR of 4,9-dibromo-2,1,3-naphthothiadiazole (**2**)
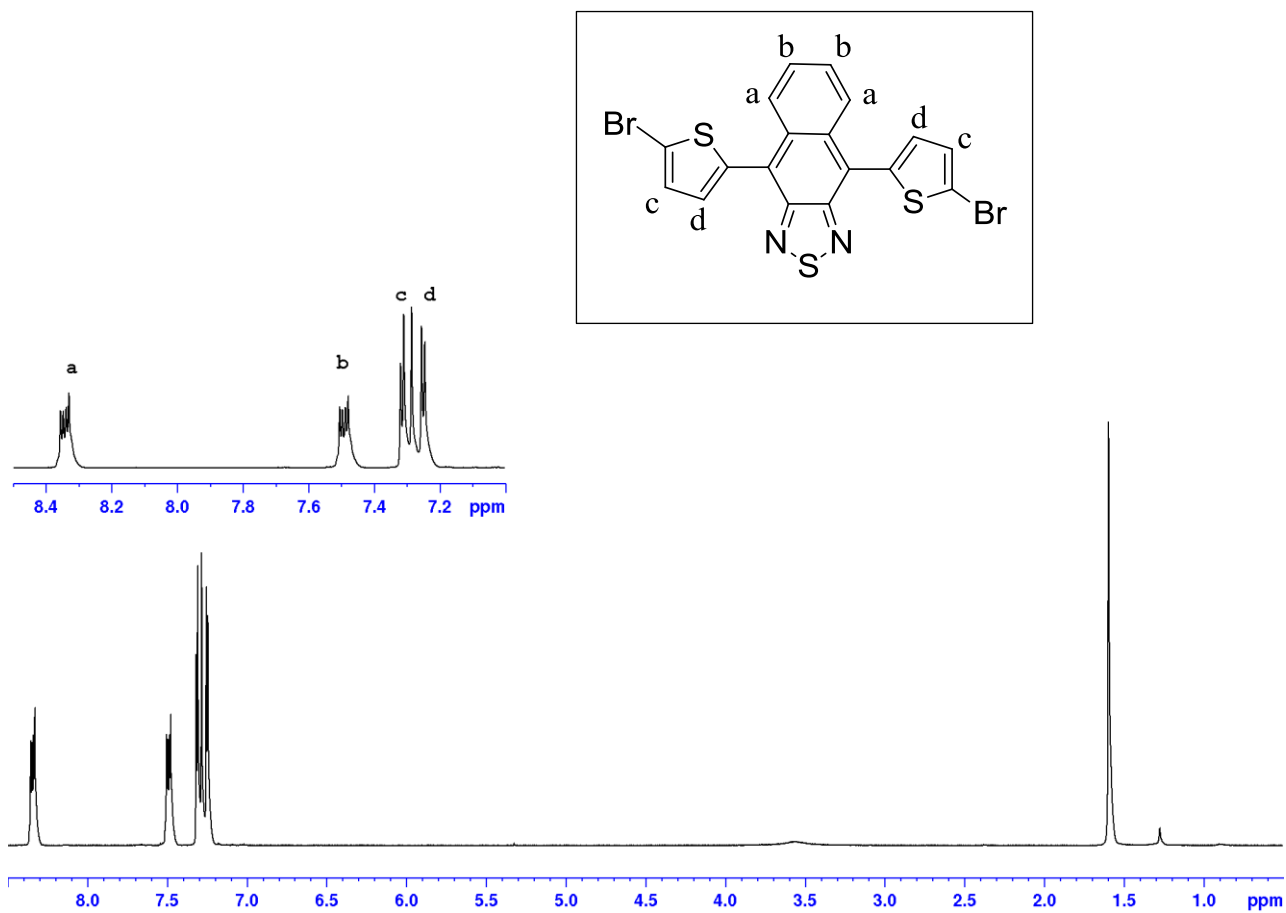
Figure 7-2: ^{1}H NMR of 4,9-di(2-bromothienyl-5-yl)-2,1,3-naphthothiadiazole (**M**)
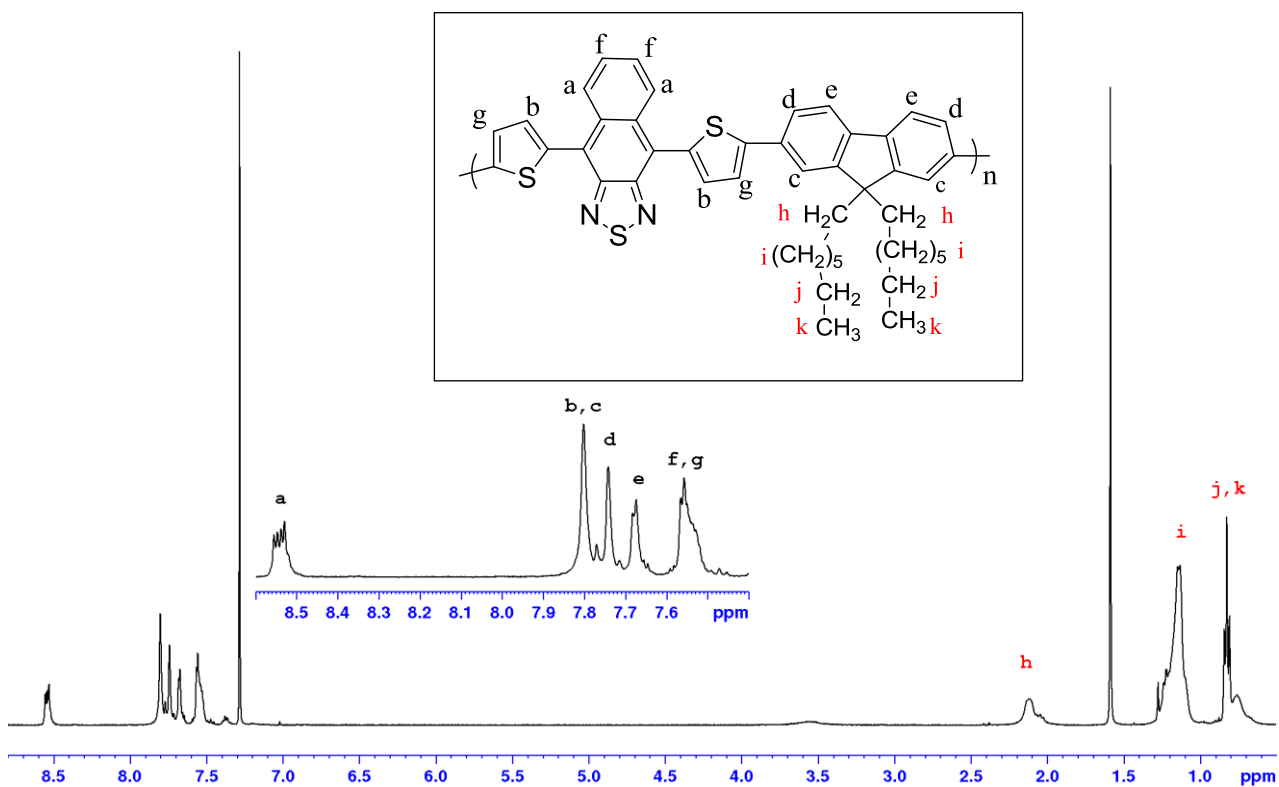
Figure 7-3: ^{1}H NMR spectra of PFDTNT-**P1** in CDCl$_3$ at R.T
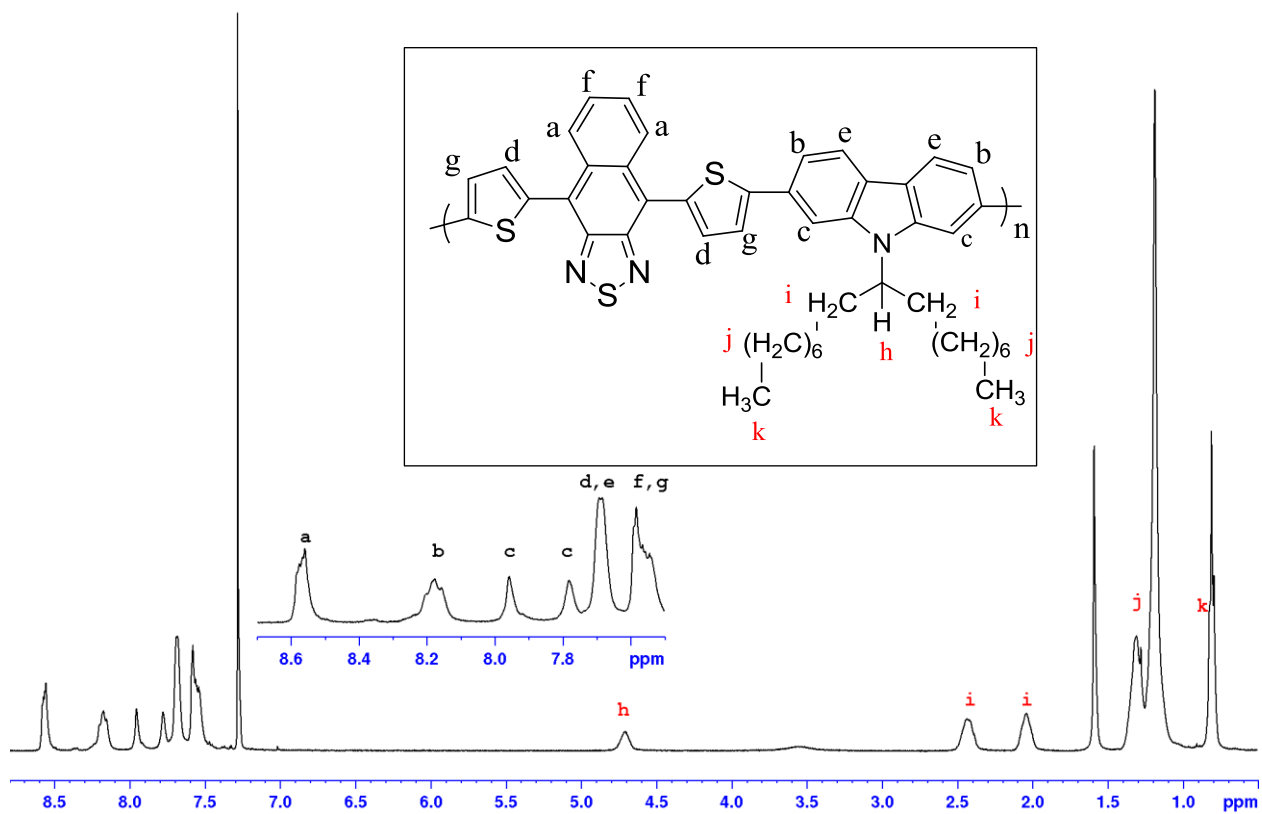
Figure 7-4: ^{1}H NMR spectra of PCDTNT-**P2** in CDCl$_3$ at R.T
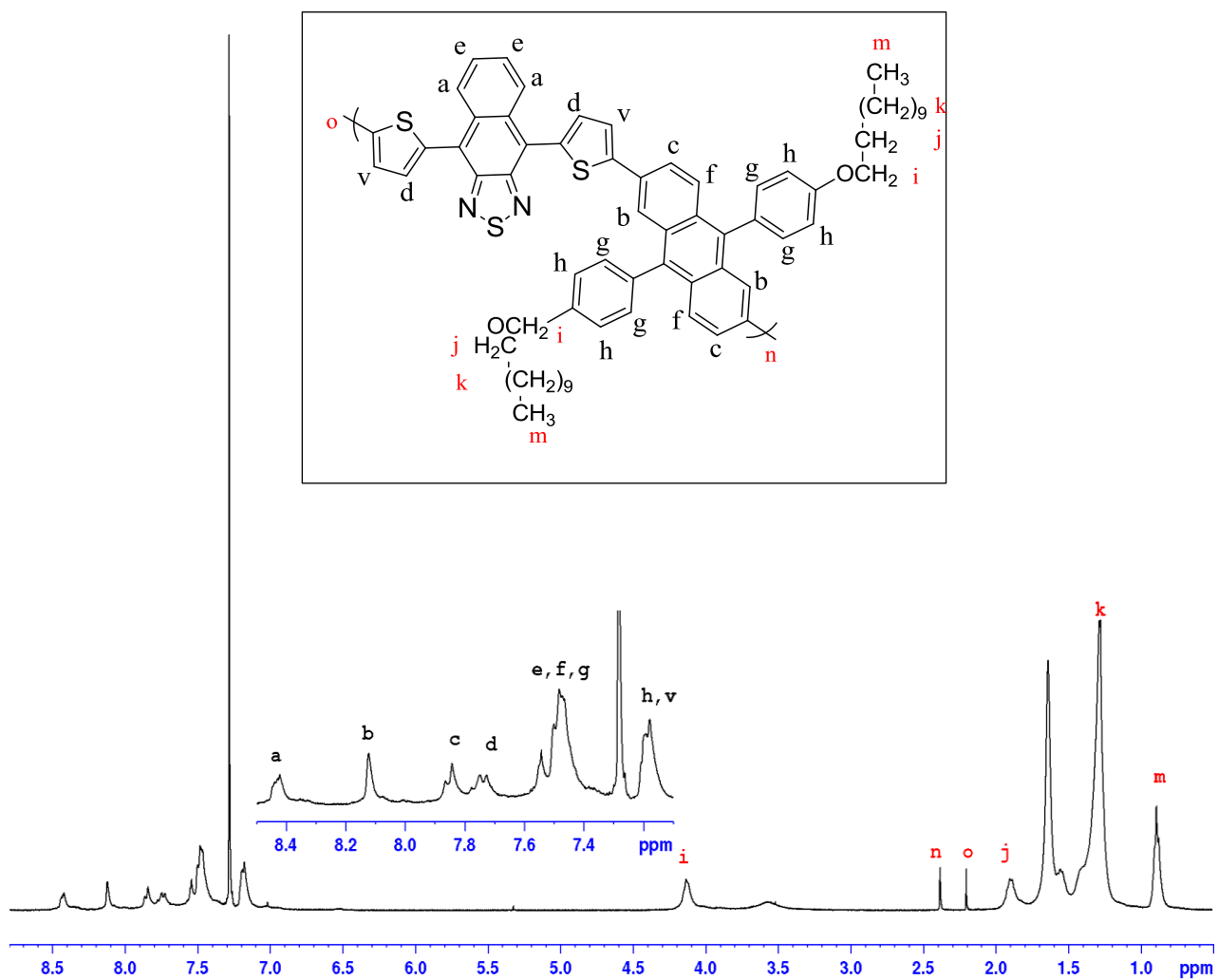
Figure 7-5: ^{1}H NMR spectra of PPADTNT-**P3** in CDCl$_3$ at R.T
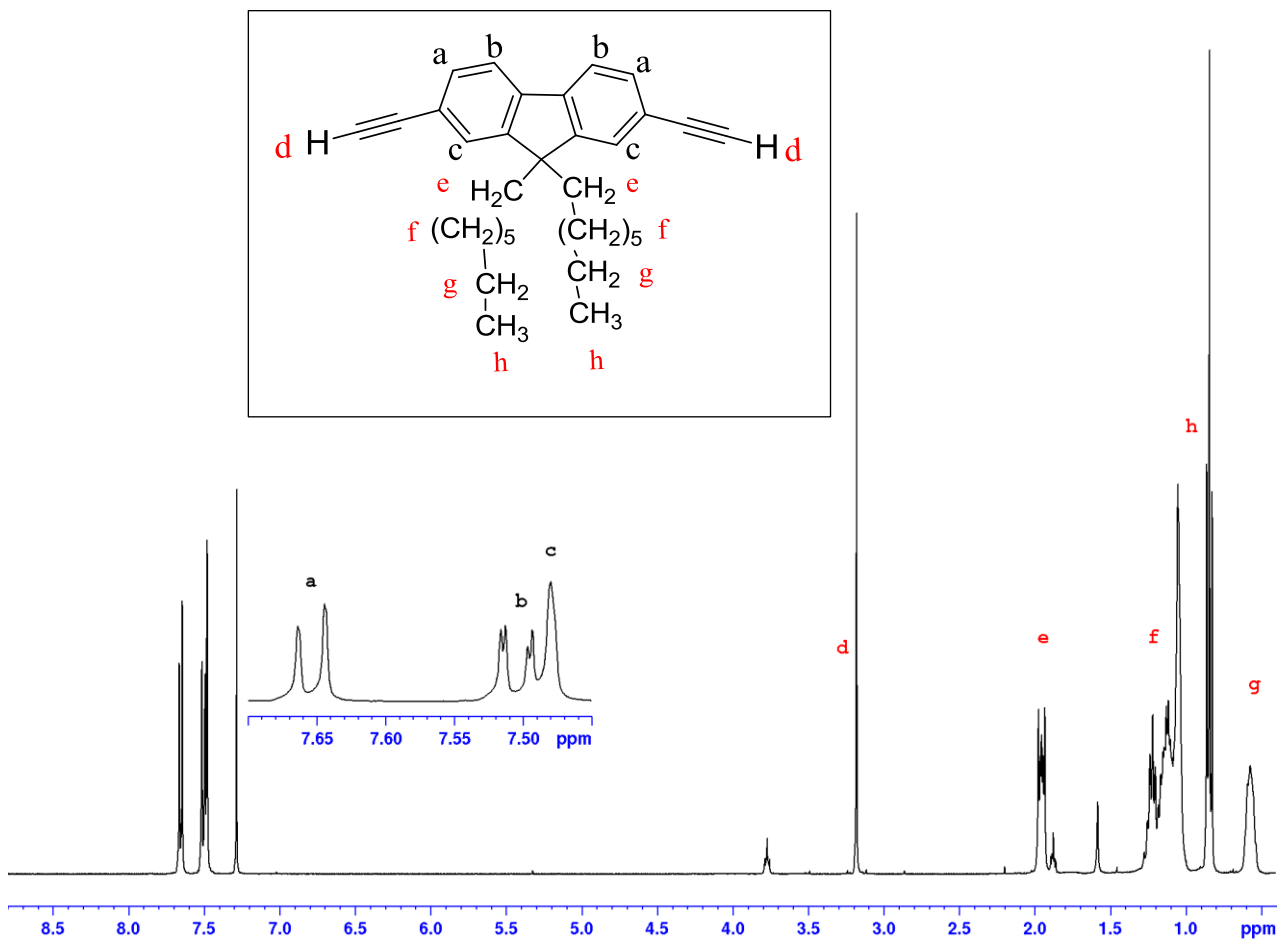
Figure 7-6: ^{1}H NMR spectra of 9,9-dioctyl -2,7-diethynylfluorene (**M1**)
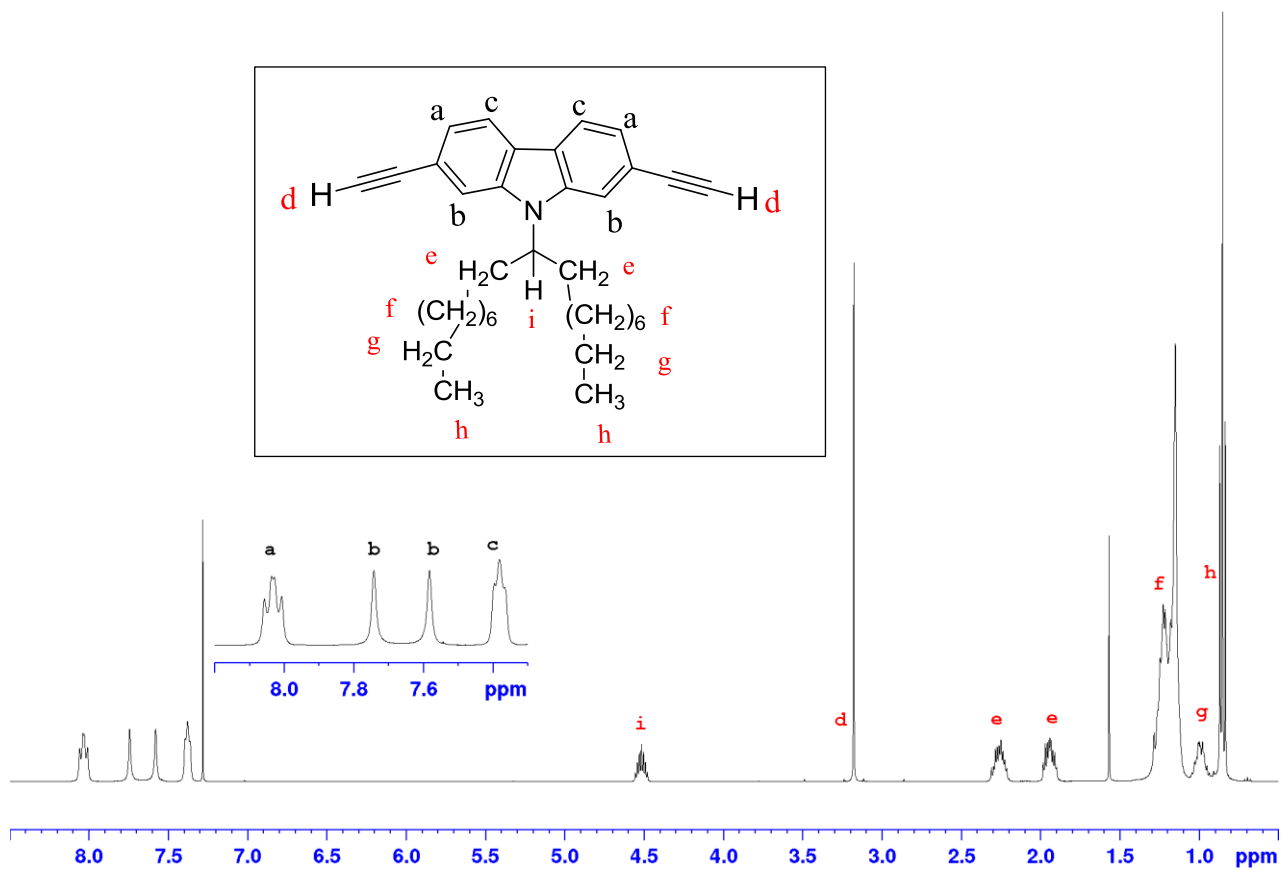
Figure 7-7: ^{1}H NMR spectra of 2,7-diethynyl-9-(heptadecan-9-yl)-9H-carbazole (**M2**)
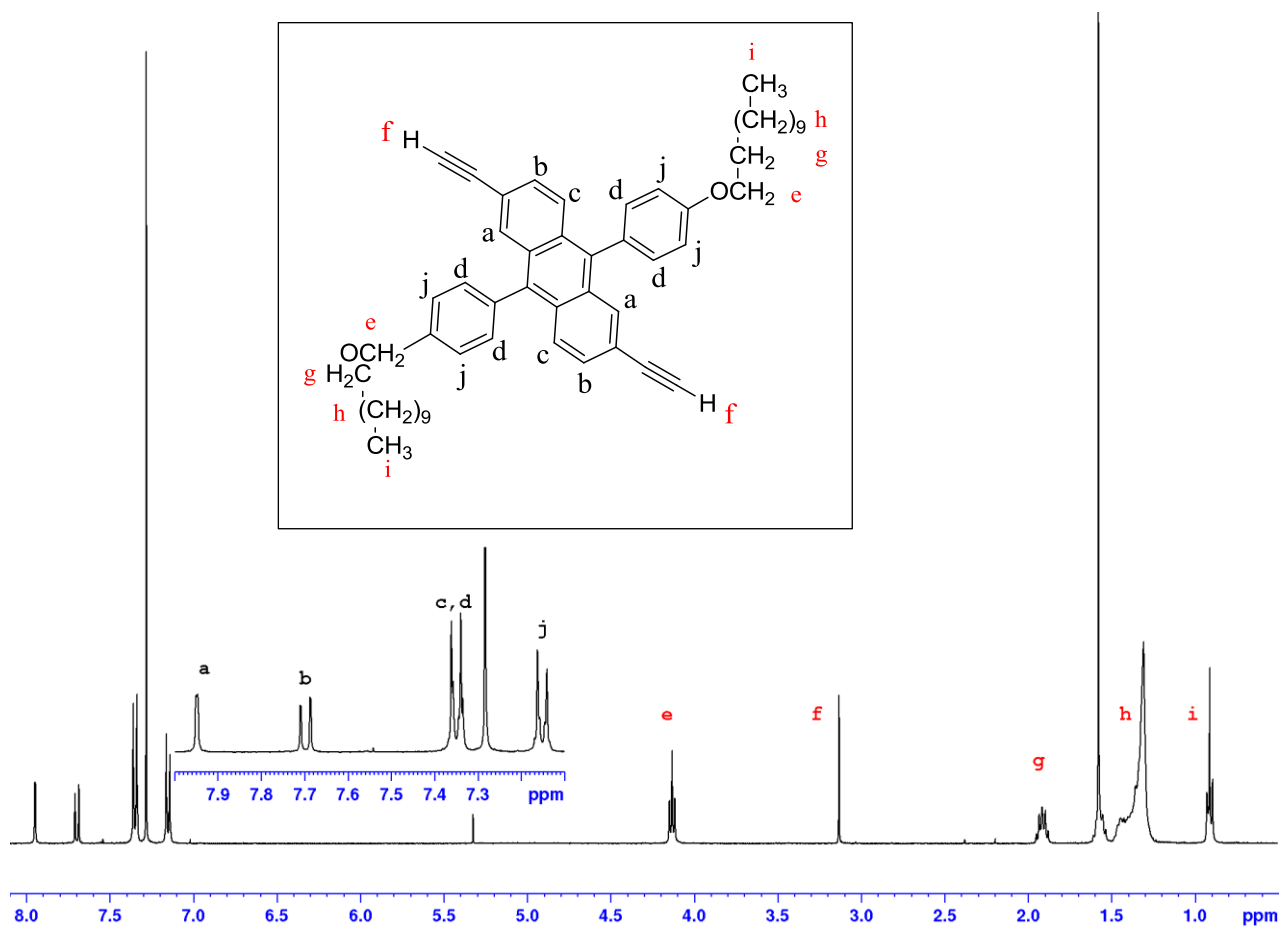
Figure 7-8: ^{1}H NMR spectra of 9,10-bis (4-(dodecyloxy)phenyl)-2,6-diethynyl anthracene (**M3**)
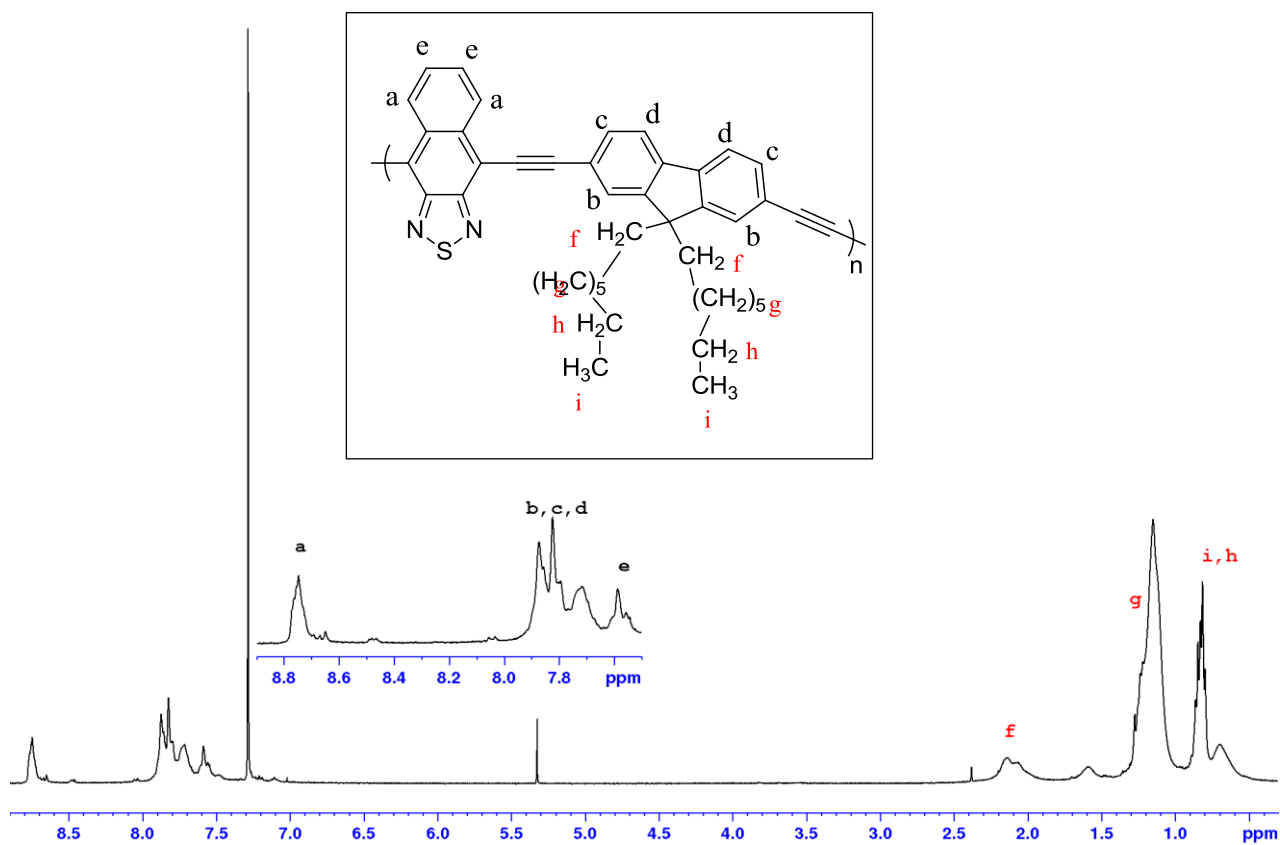
Figure 7-9: ^{1}H NMR spectra of PFDENT-**P4** in CDCl$_3$ at R.T
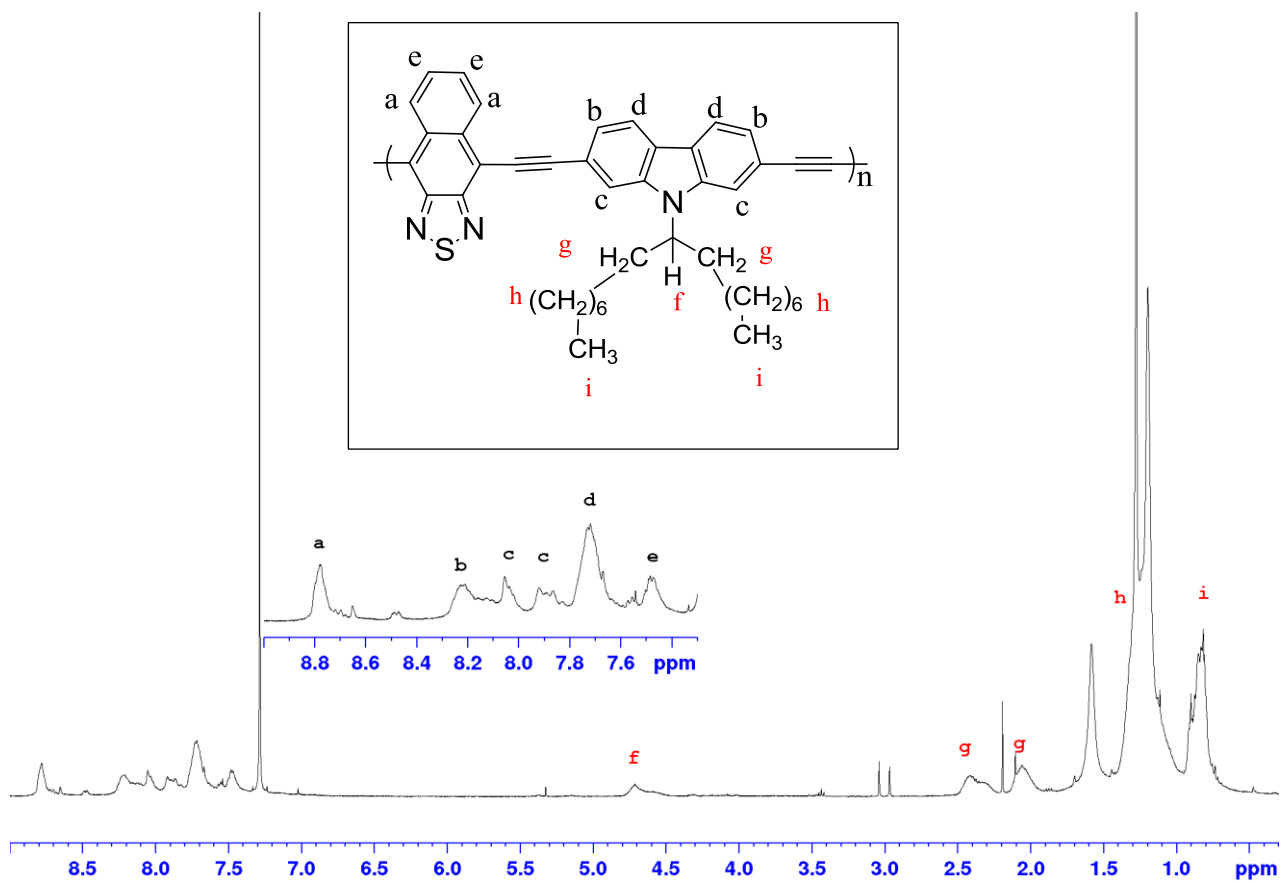
Figure 7-10: ^{1}H NMR spectra of PCDENT-**P5** in CDCl$_3$ at R.T
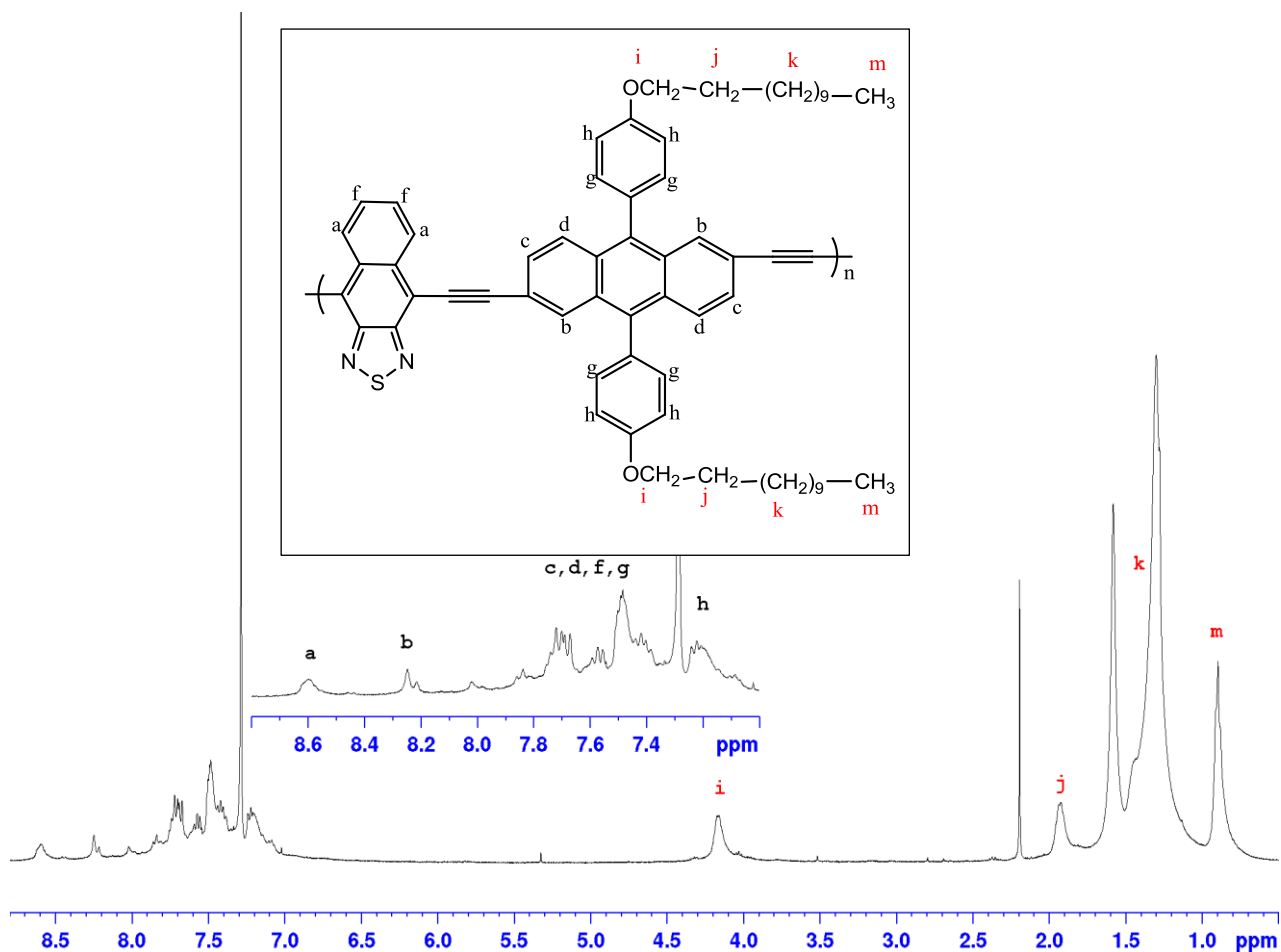
Figure 7-11: ^{1}H NMR spectra of PPADENT-**P6** in CDCl$_3$ at R.T
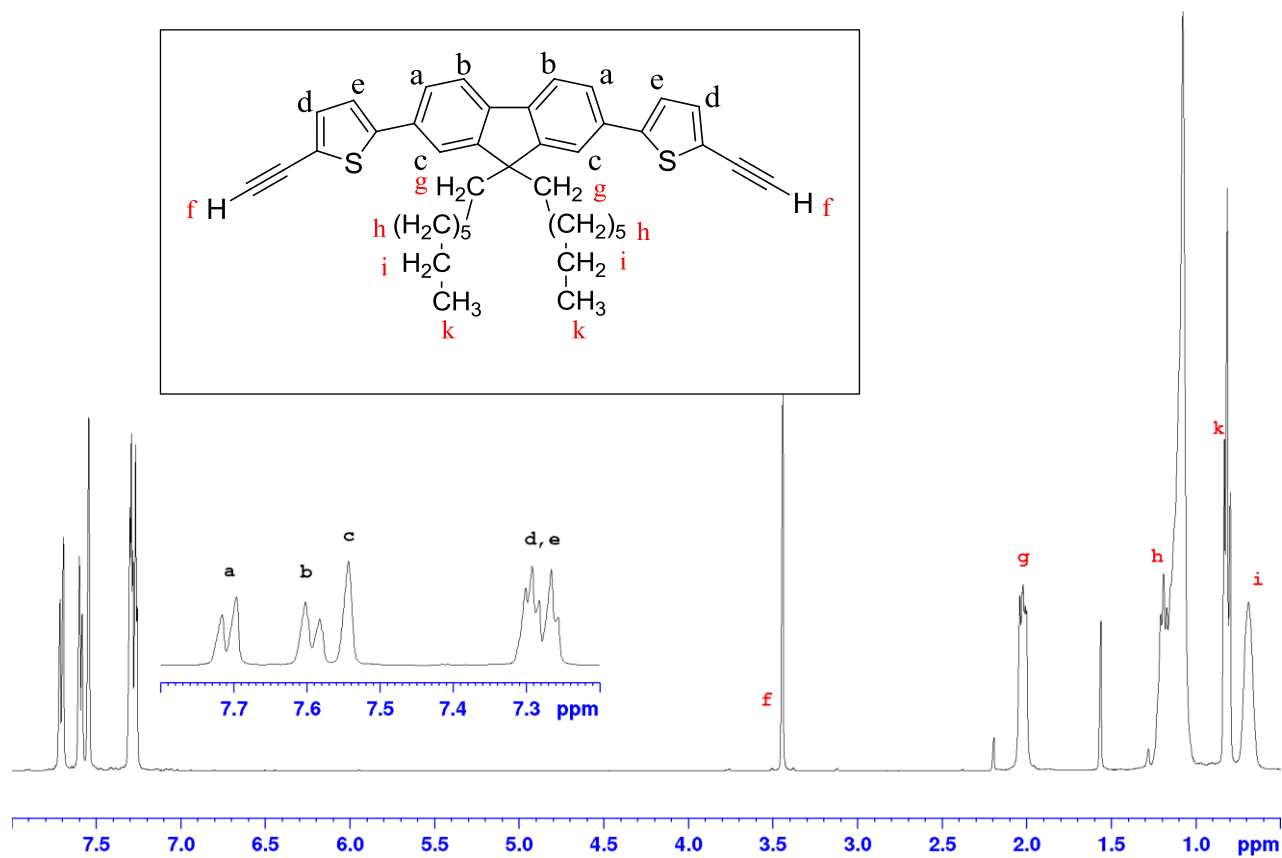
Figure 7-12: ^{1}H NMR spectra of 5,5'-(9,9-dioctyl-fluorene-2,7-diyl)bis(2-ethynyl thiophene) (**M4**) in CDCl$_3$ at R.T.
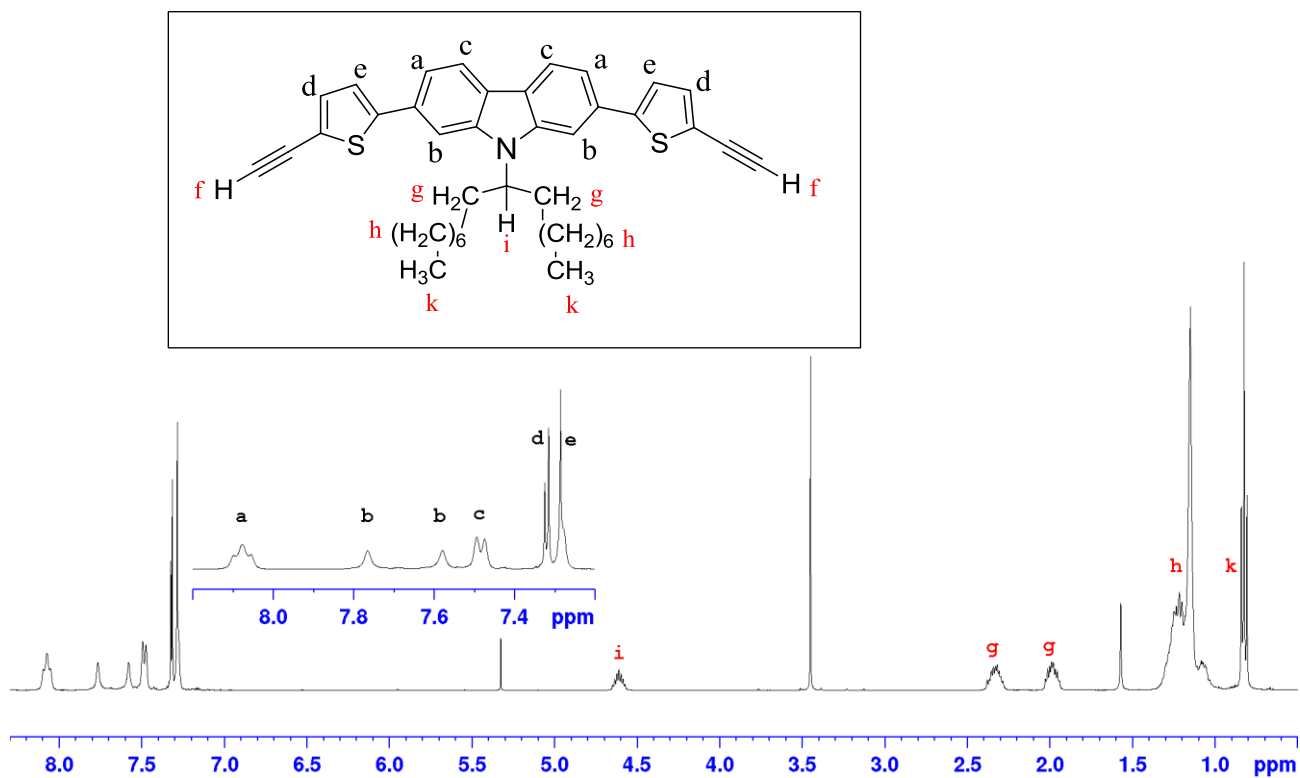
Figure 7-13: ^{1}H NMR spectra of 2,7-bis (5-ethynylthiophene-2-yl)-9-(heptadecan-9-yl)-9H-carbazole (**M5**) in CDCl3 at R.T
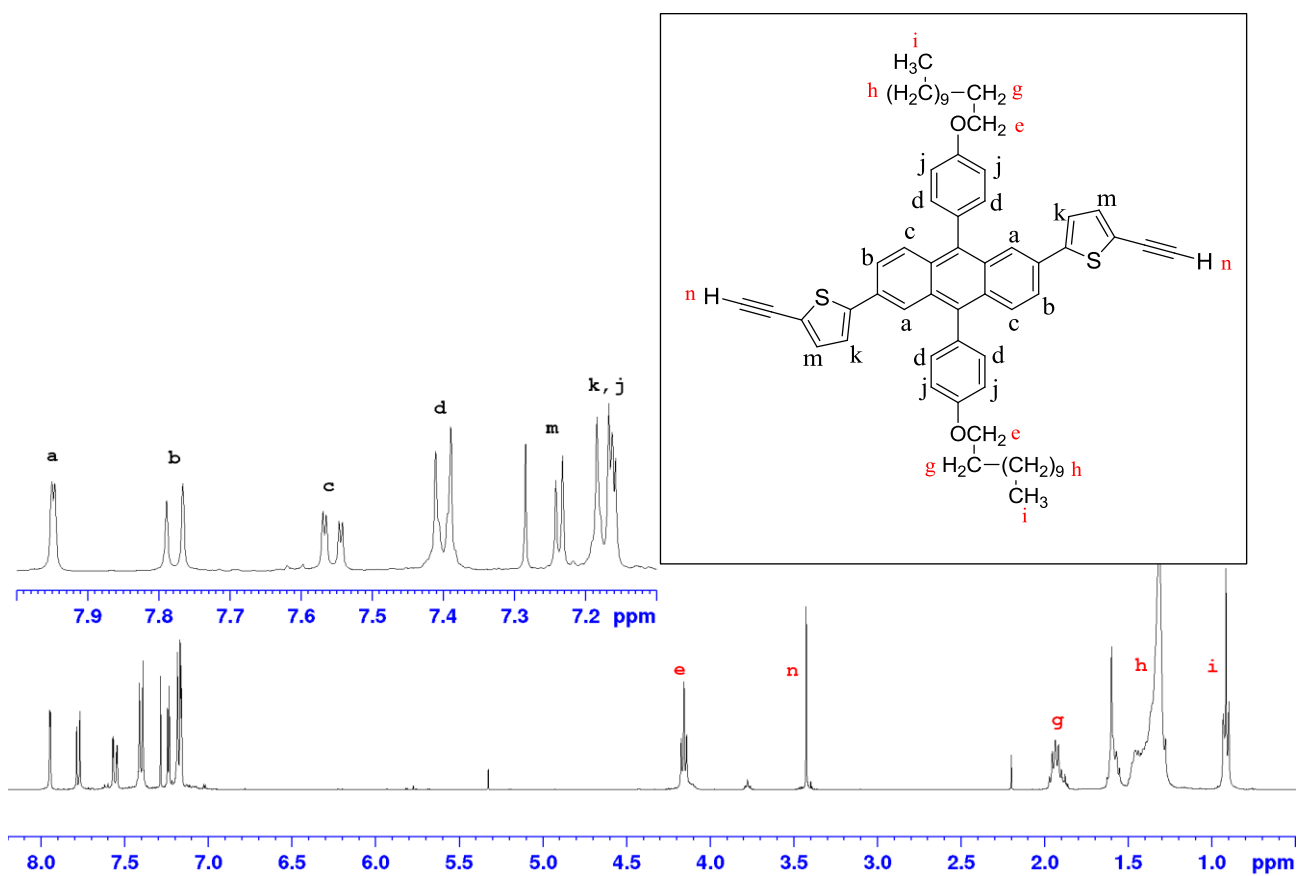
Figure 7-14: ^{1}H NMR spectra of 5,5'-(9,10-bis (4-(dodecyloxy)phenyl) anthracene-2,6-diyl)bis(2-ethynylthiophene) (**M6**) in CDCl$_3$ at R.T
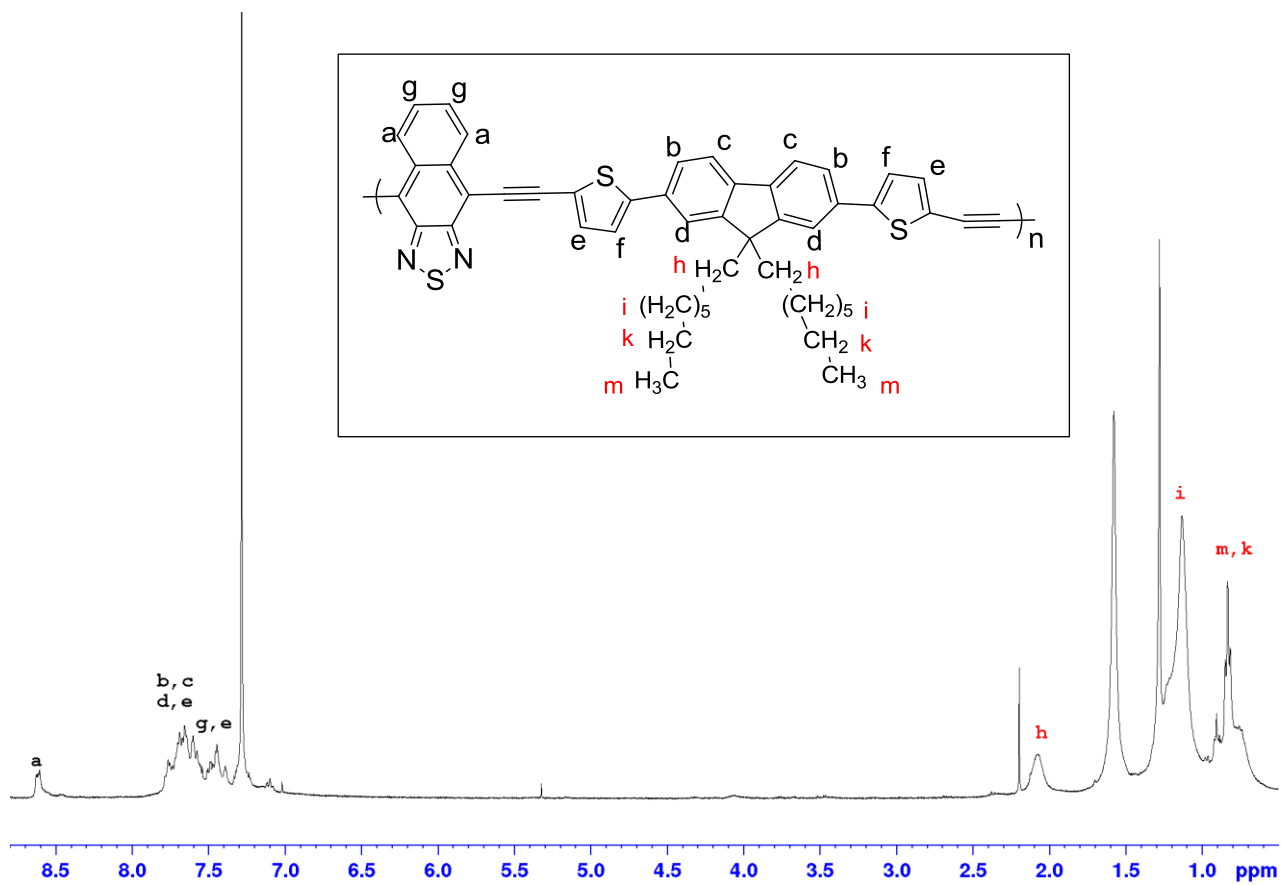
Figure 7-15: ^{1}H NMR spectra of PFDTENT-**P7** in CDCl$_3$ at R.T
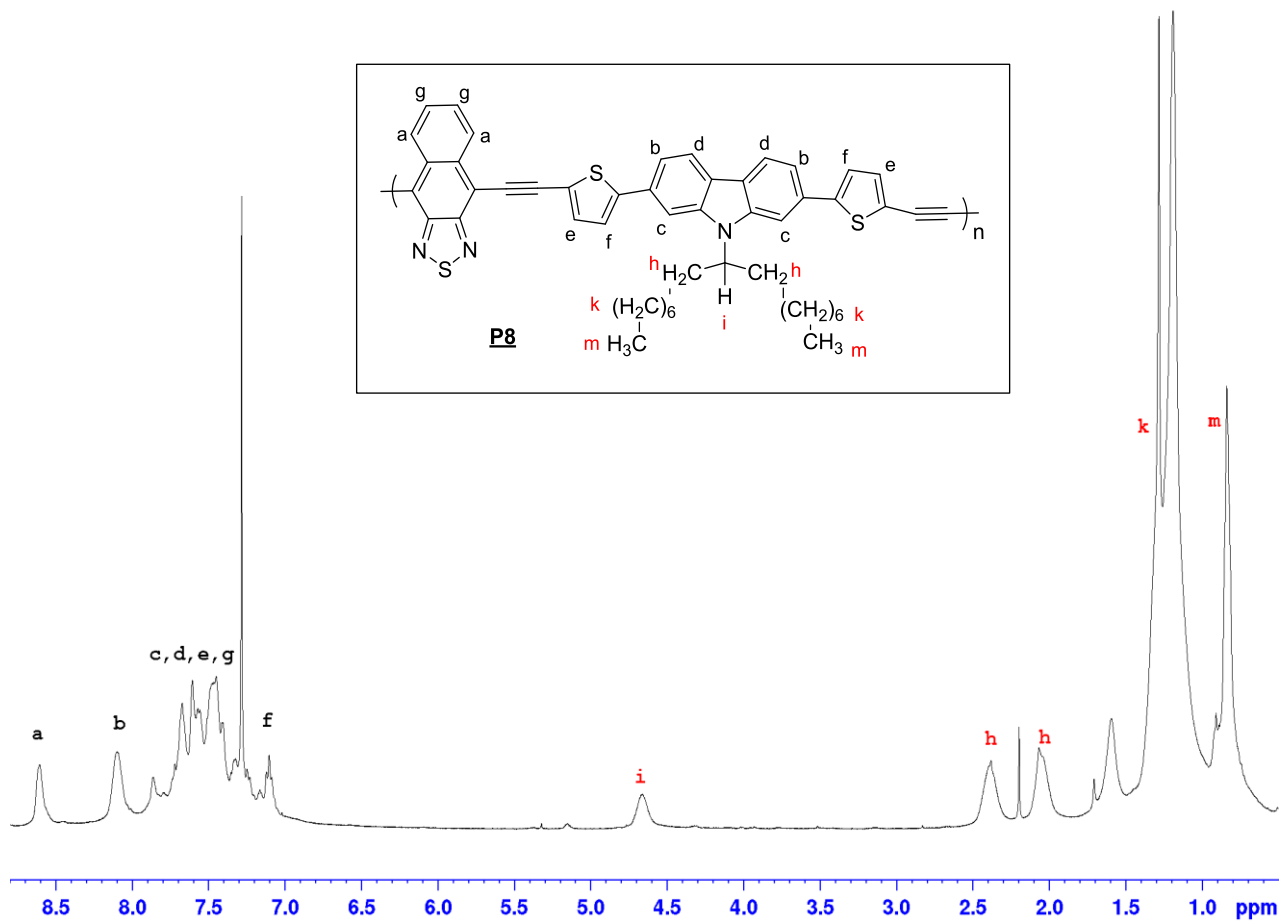
Figure 7-16: ^{1}H NMR spectra of PCDTENT-**P8** in CDCl$_3$ at R.T
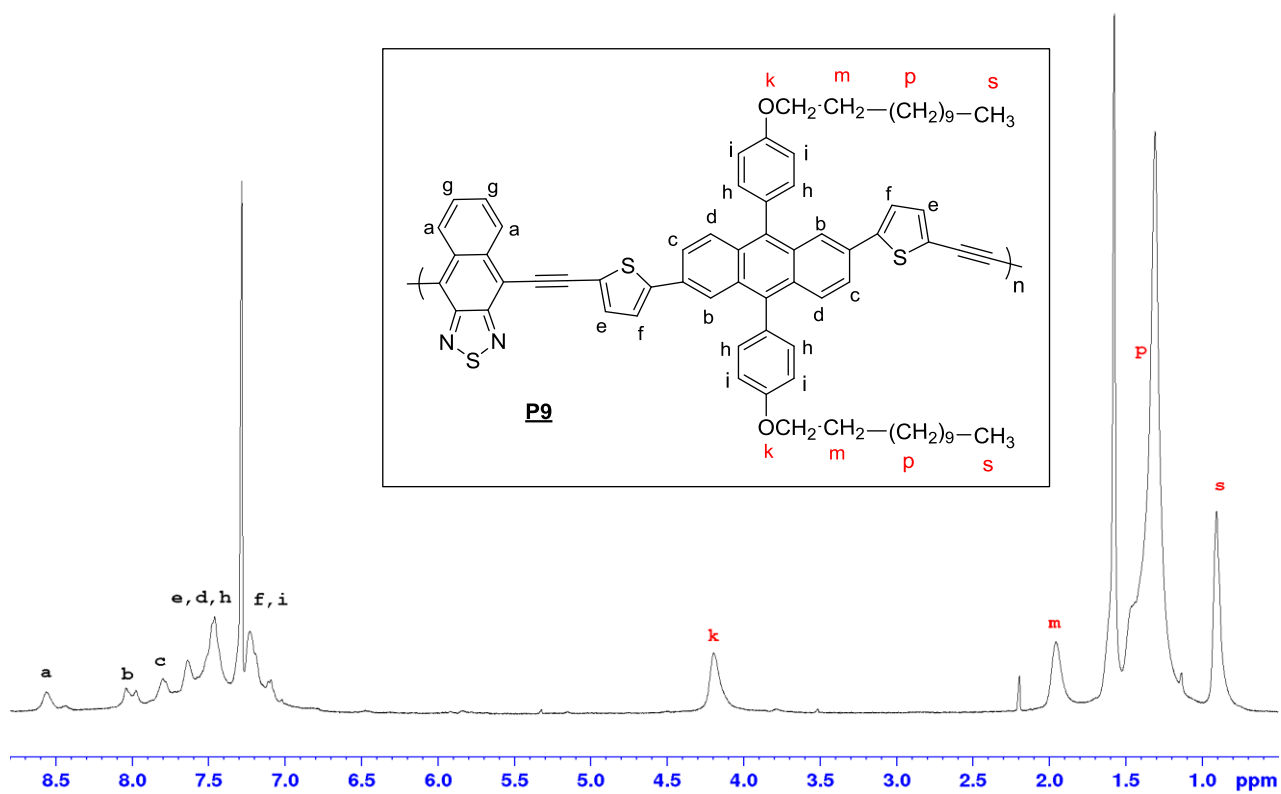
Figure 7-17: ^{1}H NMR spectra of PPADTENT-**P9** in CDCl$_3$ at R.T
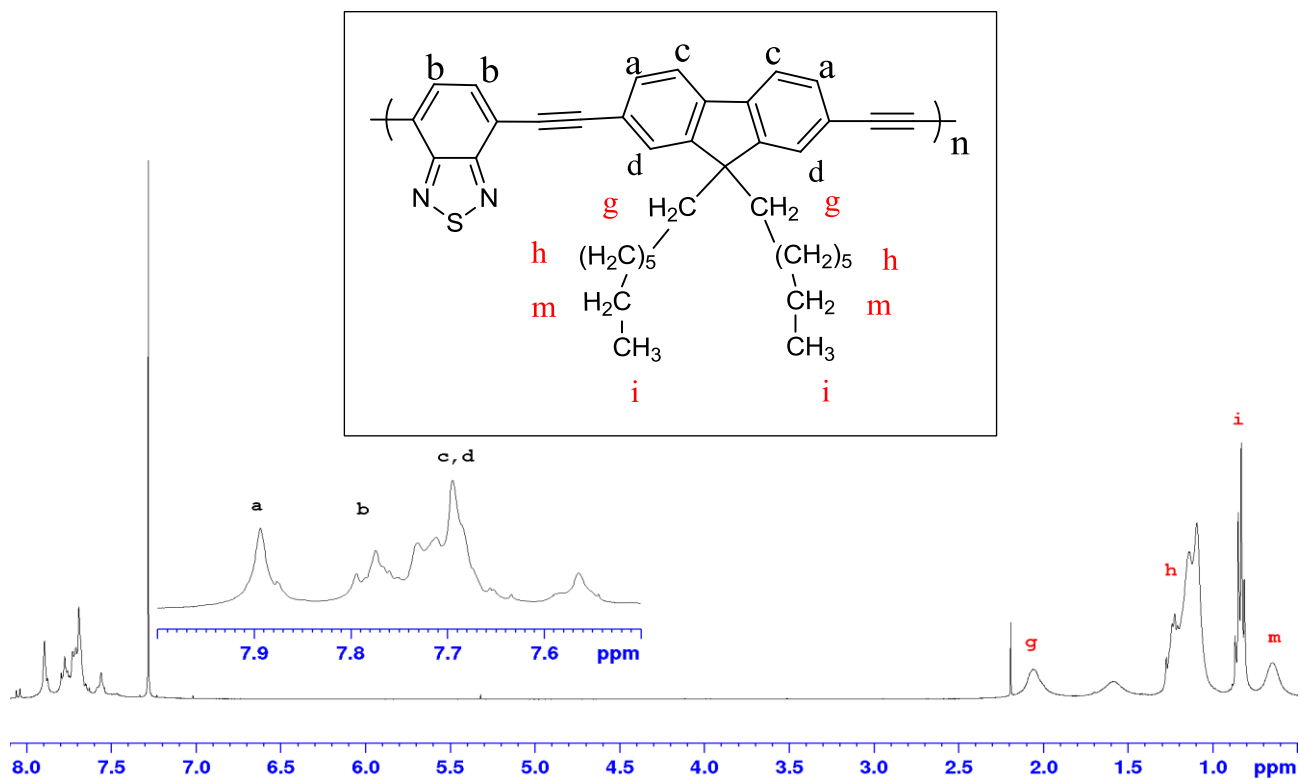
Figure 7-18: ^{1}H NMR spectra of PFDEBT-**P10** in CDCl$_3$ at R.T

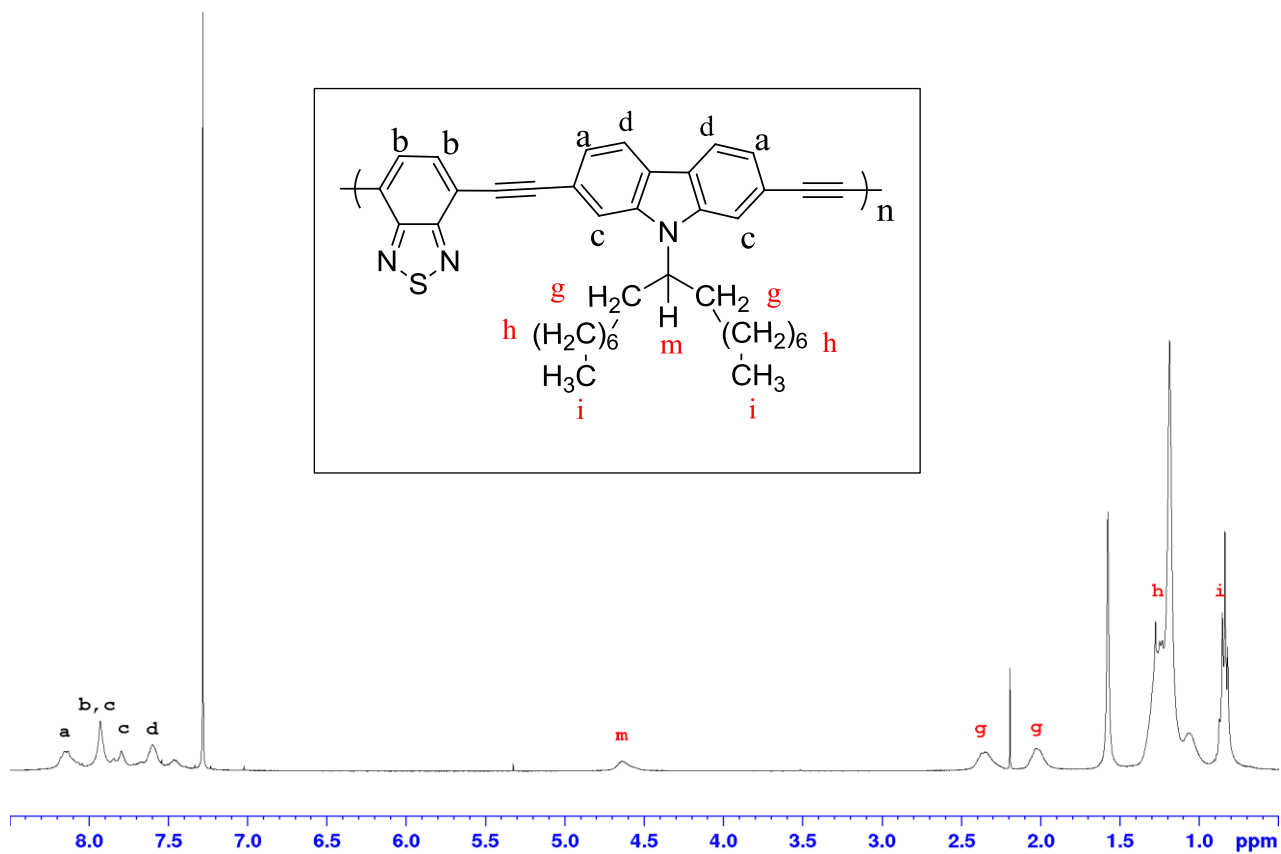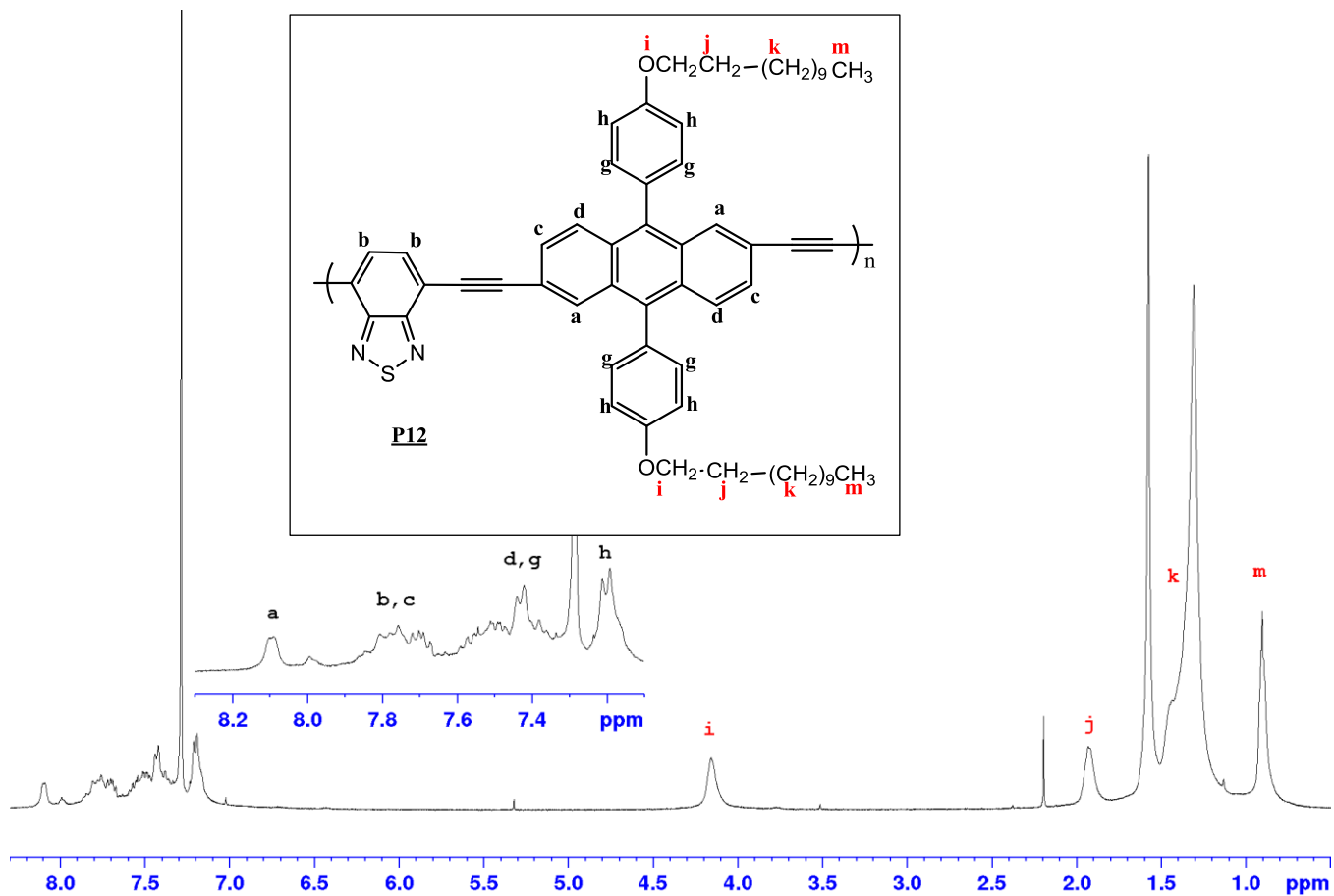Figure 7-19: ^{1}H NMR spectra of PCDEBT-**P11** in CDCl$_3$ at R.T

Figure 7-20: ^{1}H NMR spectra of PPADEBT-**P12** in CDCl$_3$ at R.T